Plasma Electrolytic Oxidation (PEO) Coatings on a Mg Alloy from Particle Containing Electrolytes

Dissertation

zur Erlangung des akademischen Grades

Doktor der Ingenieurwissenschaften

(Dr.-Ing.)

der Technischen Fakultät

der Christian-Albrechts-Universität zu Kiel

Xiaopeng Lu

aus

Shandong, VR China

Kiel 2017

Gutachtern der Dissertation:

1. Gutachter: Prof. Dr. Mikhail Zheludkevich

2. Gutachter: Prof. Dr. rer. nat. Franz Faupel

3. Gutachter: Prof. Dr.-Ing. Karl Ulrich Kainer

4. Gutachter: Prof. Dr.-Ing. Daniela Zander

Vorsitzender des Promotionsausschusses:

Prof. Dr.-Ing. Eckhard Quandt

Tag der mündlichen Prüfung:

9th Jan 2017

Erklärung

Hiermit erkläre ich, dass die beigefügte Dissertation, abgesehen von der Beratung durch die Betreuer, nach Inhalt und Form meine eigene Arbeit ist.

Die Arbeit, ganz oder zum Teil, wurde nie schon einer anderen Stelle im Rahmen eines Prüfungsverfahrens vorgelegt und ist abgesehen, von den im Anhang angegebenen Veröffentlichungen, nicht anderweitig zur Veröffentlichung vorgelegt worden.

Außerdem ist die Arbeit unter Einhaltung der Regeln guter wissenschaftlicher Praxis der Deutschen Forschungsgemeinschaft entstanden.

Geesthacht, den 07.10.2016

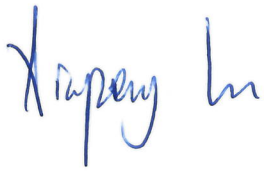

Abstract

Plasma electrolytic oxidation (PEO) processing for Mg alloy is known for decades and has been established as a well-known industrial surface treatment offering a reasonable wear and corrosion protection. However the long-term protection is often limited by the intrinsic porosity and limited phase compositions in the PEO layer. A novel optimization approach is to introduce particles to the PEO electrolyte, aiming at their in-situ incorporation into PEO coatings during growth. The idea is that with the help of particles the defects can be sealed, and the composition range and the functionalities of produced coatings can be enhanced.

The thesis reports the influence of particle addition on PEO processing, how the particle up-take can be controlled and how the morphology, microstructure, phase composition, and properties of PEO coating on Mg alloy are influenced. The mechanisms of uptake and incorporation of particles into PEO layers as well as the coating growth mechanisms are also discussed. It was found that addition of particles cannot avoid/seal fully the high porosity of PEO coatings. Moreover, the growth rate of the coatings is reduced in the presence of particles. The nature of particle itself, together with electrical and electrolyte parameters during the process determine the way and efficiency of particle uptake and incorporation into PEO coatings. The uptake of particles takes place primarily via the open pores and melt pools in the coating surface. The size of the particles has an effect on the uptake mode. Uptake of the small-sized particles can more easily occur via the open pores and discharge channels in comparison to the relatively large-sized particles which can only stick to melt pools around discharges. Thus, uptake of the particles can be controlled by the electrical parameters applied during the treatment. Longer pulse duration and higher voltage applied during PEO treatment result in uptake of more particles into the coating. The final incorporation of the particles into the coating can range from inert to reactive, which can also be controlled by modifying the processing parameters. Although the corrosion resistance of the coating cannot be significantly improved by the particles, it is feasible to control and modify the biodegradability and compatibility of the coating via addition of particles. Furthermore, multifunctional coatings with anti-wear and photocatalytic properties were produced and it was demonstrated that particle properties can be transferred directly to the coatings.

Zusammenfassung

Die Beschichtung von Mg-Legierungen mit Hilfe der plasmaelektrolytischen Oxidation (PEO) ist seit Jahrzehnten bekannt und ist inzwischen als industrielle Oberflächenbehandlung etabliert. Sie bietet dabei einen hinreichend guten Verschleiß- und Korrosionsschutz. Allerdings ist der Langzeitschutz häufig durch die intrinsische Porosität und eine eingeschränkte Schichtzusammensetzung begrenzt. Ein neuer Optimierungsansatz ist die Zugabe von Partikeln in die PEO-Elektrolyten und deren In-situ Einbau in die PEO-Schichten während des Schichtwachstums. Mit Hilfe der Partikel sollen Defekte versiegelt, Schichtzusammensetzungen modifiziert und die Funktionalitäten der erzeugten Beschichtungen erweitert werden.

Die vorliegende Arbeit untersucht sowohl den Einfluss der Partikelzugabe auf die PEO Behandlung, die Möglichkeiten die Partikelaufnahme zu kontrollieren, als auch die Morphologie, Mikrostruktur, Phasenzusammensetzung und Eigenschaften der PEO-Beschichtungen auf der Mg-Legierung. Die Mechanismen der Aufnahme und des Einbaus von Partikeln in PEO-Schichten sowie die Schichtwachstumsmechanismen werden ebenfalls diskutiert. Durch die Zugabe von Partikeln gelingt es nicht vollständig, die hohe Porosität der PEO-Beschichtungen zu vermeiden. Zusätzlich wird die Wachstumsgeschwindigkeit der Schichten durch die Anwesenheit von Partikeln im Elektrolyten verringert. Die Eigenschaften der Partikel in Kombination mit der Elektrolytzusammensetzung und den elektrischen Prozessparametern (Energieeintrag), bestimmen den Weg und die Effizienz der Partikelaufnahme und deren Einbau in die PEO-Beschichtungen. Die Aufnahme der Partikel erfolgt in erster Linie über die Poren und Schmelzbäder in/auf der Beschichtungsoberfläche. Die Größe der Teilchen wirkt sich dabei auf den Aufnahmemechanismus aus. Während die kleinen Partikel über die offenen Poren und Entladungskanäle aufgenommen werden können, können die großen Partikel nur über ein Anhaften an die Schmelzbäder aufgenommen werden. Somit kann die Aufnahme der Partikel über die elektrischen Prozessparameter kontrolliert werden. Eine längere Pulsdauer und höhere Spannungen, führen zur Aufnahme von mehr Partikeln in die Beschichtung. Der endgültige Einbau der Teilchen in die Beschichtung kann dabei von inert bis reaktiv reichen und kann durch die Prozessparameter gesteuert werden.

Obwohl die Korrosionsbeständigkeit durch die Teilchen nicht signifikant verbessert werden kann, ist es möglich, die biologische Abbaubarkeit und Verträglichkeit der Beschichtung durch Zugabe

von Teilchen zu kontrollieren und zu modifizieren. Weiterhin konnten multifunktionelle Beschichtungen mit erhöhtem Verschleißschutz und photokatalytischen Eigenschaften hergestellt werden und es konnte gezeigt werden, dass sich Partikeleigenschaften direkt auf die Beschichtungen übertragen lassen.

Table of Contents

1 Introduction

Plasma electrolytic oxidation (PEO), also often referred to microarc oxidation (MAO), is a promising process derived from conventional anodizing to form ceramic-like coatings on light metals and their alloys (Al, Mg, Ti and Zr). The main advantages of PEO coatings are enhanced wear and corrosion performance together with other features such as improved biocompatibility, biodegradability, thermal stability and dielectric properties [1-6]. PEO usually employs eco-friendly alkaline electrolytes and the coatings are formed under high voltage, when short-lived discharges occur locally on the coating surface leading to a conversion of the surface to an oxide based layer. Metals or alloys are normally treated in silicate, phosphate, fluoride or aluminate containing electrolytes, resulting in coatings consisting of amorphous and/or crystalline phases stemming from the substrate and electrolyte components. The formation mechanisms of the PEO coatings are complex due to the involvement of electro-, thermal-, and plasma-chemical reactions at metal/electrolyte interface [7]. In the case of Mg and its alloys, a two- or three-layer structure is typically observed with a characteristic thin barrier layer directly on the substrate surface, and an outer porous layer which can be utilized for post treatments such as paints or other polymer coatings providing good adhesion [3, 8]. The coatings are generally composed by mixtures of MgO, Mg_2SiO_4, MgF_2, $Mg_3(PO_4)_2$ and Mg_2AlO_4 phases depending on the electrolyte composition and applied electrical parameters.

However, high porosity, limited range of chemical compositions and high energy consumption are the main restrictions for PEO coatings to achieve a wider range of applications and desirable properties such as long-term corrosion protection without post treatments. In general, the properties of PEO coatings mainly depend on their microstructure and composition, which are determined by the process and electrolyte parameters as well as the substrate. The major strategy to gain improved properties for PEO coating is to optimize the process parameters and electrolyte compositions. In the case of process parameters, various investigations have been performed to optimize the electrical parameters of PEO processing, such as applied voltage/current magnitude, mode, frequency and duty cycle [9-11]. Changing the electrical parameters can change the PEO process characteristics, including the breakdown voltage and the discharge events, both in terms of discharge intensity and density, which in turn have a profound effect on the coating microstructure and properties. Nevertheless, it is unlikely to avoid high porosity for PEO coatings,

especially for Mg alloys, and also the coating properties are confined due to the limited influence of the electrical properties on coating composition.

Altering the electrolyte composition is another effective way to optimize the microstructure and to improve properties of PEO coatings [12, 13], since the composition of the electrolyte plays a decisive role in the formation of coating microstructure and its composition which finally determine the coating properties. Recent developments in this area are focused on the addition of particles into the electrolyte, aiming to achieve in-situ incorporation or sealing of the porous PEO coatings, and also endowing the coatings with more functionality. The addition of particles into the electrolyte influences the PEO processing since it can change the fundamental electrolyte properties, i.e. pH value, conductivity, viscosity and discharge conditions. The involvement of the particles in the growing coating will change the coating morphology and properties. If particles are incorporated without reaction or no new phase formation, it is considered as an inert incorporation. The second possibility is reactive or partly reactive incorporation, since the particles can be melted by the high-energy discharges during the PEO processing leading to formation of a new phase.

This PhD thesis work focuses on development of new particle-containing PEO coatings with enhanced functionality and on deeper understanding of the role of particles in the PEO process as well as their effect on the basic properties of formed ceramic layers.

2 Literature review

2.1 Particles used in PEO coatings: characteristics and requirements

In vast majority of the studies, particles are directly added in the form of powder or sol to the electrolyte, since it is more flexible and confers more alternatives than particles originating from the substrate, e.g., the particle reinforcement in metal matrix composites. Additionally, in-situ particle formation can occur in the electrolyte intentionally or if the solubility of certain compounds is exceeded during PEO processing. Such systems can also be considered as particle-containing electrolytes. A challenge is to obtain uniform dispersion of particles in the PEO electrolyte. Zeta potential is used to evaluate the surface charge of the particles and their dispersion stability in a certain solution [14]. The magnitude of the zeta potential indicates the degree of electrostatic repulsion between the adjacent particles in the solution. Particles with higher absolute value of zeta potential are more stable, resulting in inhibiting agglomeration and

settling in PEO electrolyte. A high zeta potential (absolute value) is desirable in electrophoretic process as this enhances the rate of particle movement under a given electrical field [15]. It was found that most of the particles are negatively charged and demonstrate negative zeta potential in the commonly used alkaline electrolytes. The negative zeta potential could facilitate the incorporation of particles since the substrate and the coating on top of it serves as anode during DC or positive pulses under AC conditions. In particular, the absolute value of zeta potential increases with the pH value of the PEO electrolyte (Figure 2-1) [16, 17]. The properties of the particles (e.g., size and density) also determine their stability in the electrolyte. For instance, it is likely that there is a limitation of the particle size, since the majority of the studies have used particles which are less than 10 μm. Consequently, external forces are generally utilized to avoid sedimentation and agglomeration of the particles, e.g., mechanical stirring, gas bubbling, electrolyte pumping and ultrasonic agitation. In some cases, nonionic and anionic surfactants are utilized to improve dispersion stability of the particles, e.g., PTFE, MnO_2 and NiO [18, 19]. Another approach is to use in-situ formed sol suspensions. However, organic solvents (e.g., ethanol) or specific complexants are often used to synthesize such sols [20-22]. They often act as unwanted additives in the electrolyte and might have an adverse effect on PEO coatings. Table 2-1 summarizes various particles that have been introduced to the PEO electrolyte aiming to obtain enhanced properties and providing new functionalities for PEO coatings.

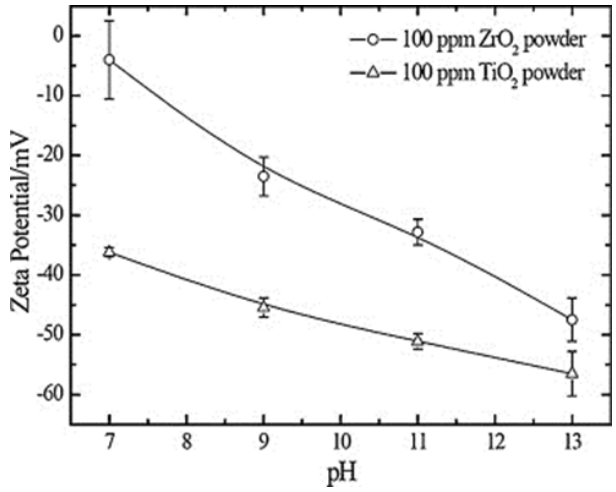

Figure 2-1 Zeta potentials of ZrO_2 and TiO_2 powders at different pH levels in alkaline fluoride based electrolyte *(with permission from Elsevier [16]).*

Table 2-1 Particles applied in PEO processing

Particle	Properties, activities and field of applications	Melting point	Reference
Polytetrafluoroethylene (PTFE)	lower friction coefficient, chemical inertness and hydrophobicity	326.8 °C	[23]
Ag	antibacterial properties	961.8 °C	[24]
Hydroxyapatite (HA)	major component of natural bone	1100 °C	[25]
Montmorillonite (clay)	filler material for polymer applications	1000 -1200 °C	[26]
ZrO_2	refractory ceramic	monoclinic <1170 °C, tetragonal 1170-2370 °C, and cubic >2370 °C	[27, 28]
SiO_2	high heat and chemical resistance	1600 °C	[29, 30]
TiO_2	chemical stability and heat resistance	1843 °C	[31]
Al_2O_3	insulator and low conductivity	2072 °C	[31]
CeO_2	optics catalyst chemistry, superconductors and sensors	2400 °C	[32, 33]
SiC	high mechanical strength, chemical inertness, high-temperature stability	2730 °C	[34, 35]

2.2 Influence of particle addition on PEO processing

Generally, addition of new components into the electrolyte can have an effect on the electrical response of PEO process. It was demonstrated that addition of particles can slow down the voltage ramp during PEO treatment [14, 17, 36, 37]. Li et al. [36] reported that the voltage ramp was delayed in the presence of Al_2O_3 particles (Figure 2-2). Lim et al. [37] claimed that addition of CeO_2 particles in the electrolyte have decreased the final voltage for PEO processing. However, controversial results about the voltage response and final voltage were found by other researchers [38, 39]. Wang et al. [39] have found that addition of Al_2O_3 nanoparticles enables PEO coatings to grow faster and reach higher final voltage. It was also reported that there is no significant influence of particles addition on PEO processing [16, 40-43]. The addition of zirconia particles had only minor influence on the coating growth rate and voltage response during PEO treatment [44, 45]. This discrepancy is probably ascribed to the different power supplies and electrical

parameters utilized during PEO process, as the pH and conductivity of the electrolyte are not greatly altered after particle addition. However, the addition of particles in form of alco-sol to the electrolyte has a larger influence on the electrical response of PEO process [46, 47]. This is probably caused by the main solvent of the alco-sol, ethanol, which decreases the conductivity of the electrolyte (Figure 2-3) [46, 48-50]. It was found that the breakdown potential, final voltage and the layer growth rate significantly increased with the sol concentration in the electrolyte [22, 46, 48, 51]. However, it was also reported that addition of such a sol to the electrolyte can delay the coating growth. Breakdown and final voltage were much lower when adding alumina sol to the electrolyte [21].

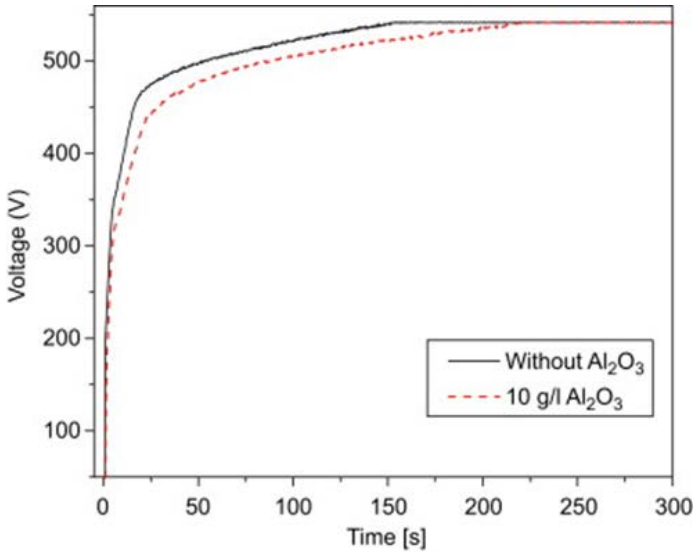

Figure 2-2 Voltage-time response of coatings produced from aluminate based electrolyte with and without 10g/L Al_2O_3 particles on AM60B Mg alloy *(with permission from Elsevier* [36]).

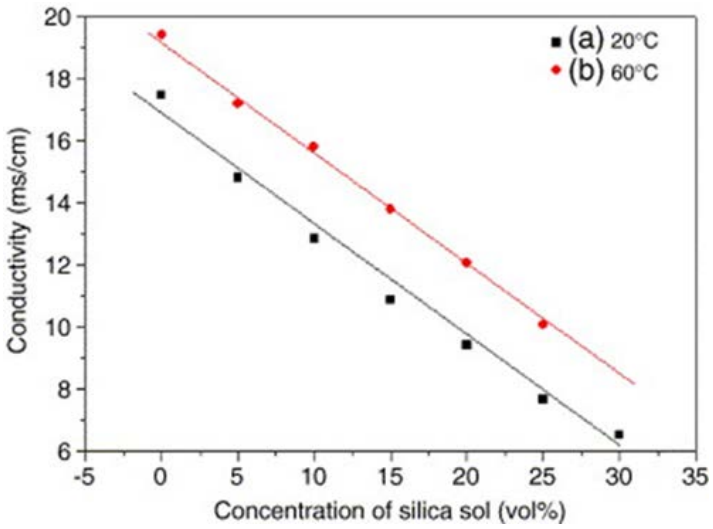

Figure 2-3 The conductivity of an 1.0 M Na_2SiO_3 electrolyte with addition of different concentrations of silica sol at (a) 20 °C; (b) 60 °C *(with permission from Elsevier* [46]).

Summarizing, it can be stated that the effect of particle addition to the electrolyte via the sol route causes more influences on the electrical response of PEO process than the addition of powders. This is associated with the change of the composition, conductivity and viscosity of the electrolyte by the organic additives, which plays an important role in the electrical response of PEO process. Apart from that the influence depends very much on the base electrolyte, substrate, properties of the particles (type and size), power source as well as the electrical parameters applied during PEO treatment, so that no clear picture exists.

2.3 Uptake of particles and incorporation mechanisms

The mechanisms of particle uptake and incorporation into PEO coatings were discussed in a number of recent studies. The pores on the coating surface were considered as uptake paths for particles to enter into the coating, since the pores are normally filled with particles after PEO treatment [41]. It was confirmed by Seyfoori et al. [52] that the accumulation of nanoparticles in the vicinity and inside the pores was higher than in the other zones. Arrabal et al. [40, 53] assumed that the particles were transferred to the interface between the inner and outer layer through short-circuit paths in the outer layer. Necula et al. [54] proposed that the mechanism of incorporation of Ag nanoparticles into the coating was a result of three main steps: delivery of particles to the sites of coating growth, entrapment of particles at the sites of coating growth and preservation of the embedded particles during layer growth. According to Lee et al. [41],

electrophoretic deposition and mechanical mixing were the main factors leading to the incorporation of particles into the coatings on Mg alloy.

Particles can achieve either reactive or inert incorporation into the coating, depending on the applied electrical parameters, electrolyte composition, substrate as well as the size, melting point and chemical stability of the particles, as shown in Table 2-2. Alteration of the electrical parameters can influence the incorporation mode [40], which is mainly related to the change of energy of the discharges. Inert and reactive incorporation into the coating have been observed for ZrO_2 particles when using the same electrical conditions but various electrolytes [53]. Particles with low melting point experience more easily reactive incorporation [16, 26, 55]. Low melting point particles can also achieve inert incorporation into the coating when they have relatively high chemical stability [18]. In some cases solid state sintering can occur [56], resulting in fusion of particle boundaries with the surrounding oxide material. For other particles, e.g. ZrO_2, phase transformation was observed if they have different lattice modifications at different temperatures [53]. In short, it still needs more investigations to find out the uptake and incorporation mechanisms of particles, specifically particles with different sizes and melting points, during PEO treatment under different treatment conditions.

2.4 Influence of particle addition on composition, microstructure and morphology of PEO coatings

The composition of the PEO electrolyte is one key factor to determine the composition, microstructure and morphology of PEO coatings. Thus introduction of particles to the electrolyte will modify the coatings, such as phase composition, pore characteristic, thickness and compactness of the layer. The detailed information of the substrate, type and size of the particles, electrolyte composition and incorporation mode of the particles is shown in Table 2-2.

Table 2-2 Detailed information of the substrate, type and size of the particles, electrolyte composition, phase composition of the coatings and incorporation mode of the particles.

Substrate	Type and size of the particles	Electrolyte composition	Phase composition	Incorporation mode	Reference
pure Mg	2 g/L m-zirconia, 150-300 nm	5.3 g/L $Na_2SiO_3 \cdot 5H_2O$ + 2.8 g/L KOH; 9.5 g/L $Na_3PO_4 \cdot 12H_2O$ +	MgO, Mg_2SiO_4, m-ZrO_2, t-ZrO_2; MgO, $Mg_3(PO_4)_2$, m-ZrO_2, t- ZrO_2, $Mg_2Zr_5O_{12}$	Inert and partly reactive incorporation	[53]

		52.5 g/L NH_4OH			
pure Mg	10 g/L m-zirconia, 150-300 nm	5.3 g/L $Na_2SiO_3 \cdot 5H_2O$, 2.8 g/L KOH	MgO, Mg_2SiO_4, m-ZrO_2, $Mg_2Zr_5O_{12}$	Partly reactive incorporation	[40]
AZ91 Mg	9 g/L zirconia, 200-400 nm	5 g/L KOH, 3 g/L KF, 3 g/L $K_4P_2O_7$	MgO, t-ZrO_2, $Mg_3(PO_4)_2$	Inert incorporation	[41]
AZ91 Mg	9 g/L zirconia, 150-200 nm	5 g/L KOH, 2.9 g/L KF, 3.3 g/L $K_4P_2O_7$	MgO, t-ZrO_2	Inert incorporation	[16]
AZ91D Mg	5 vol.% zirconia sol	10 g/L Na_2SiO_3, 10 g/L KOH	MgO, Mg_2SiO_4, $Mg_2Zr_5O_{12}$	Reactive incorporation	[57]
Mg-Li alloy	1 vol.% silica sol	10 g/L Na_2SiO_3, 3 g/L NaOH	MgO, SiO_2 Mg_2SiO_4	Partly reactive incorporation	[51]
AM50 Mg	10 g/L clay, avg. 12 μm	10 g/L Na_3PO_4, 10 g/L Na_2SiO_3 1 g/L KOH	Amorphous	Reactive incorporation	[26]
AM50 Mg	5 g/L clay, avg. 12 μm	10 g/L Na_3PO_4, 1 g/L KOH	Amorphous, MgO, Mg_2SiO_4, $Mg_3(PO_4)_2$	Reactive incorporation	[55]
AM50 Mg	10 g/L halloysite nanotubes, 1 to 15 μm in length and 10-100 nm inner diameter	12 g/L Na_2SiO_3, 2 g/L KOH, 4 g/L NaF	Amorphous, Mg_2SiO_4, halloysite	Inert incorporation	[43]
AZ91D Mg	5, 10, 15 g/L of Al_2O_3, 30 nm	1 g/L KOH, 10 g/L $NaAlO_2$	MgO, Al_2O_3, $MgAl_2O_4$	Partly reactive incorporation	[39]
AZ91D Mg	2 vol% of alumina sol	15 g/L $NaAlO_2$, 1.2 g/L KOH	MgO, $MgAl_2O_4$	Partly reactive incorporation	[21]
AM60B Mg	10 g/L of Al_2O_3, 1 μm	18 g/L $NaAlO_2$, 0.5 g/L KOH, 6 g/L $Na_5P_3O_{10}$, 8 g/L glycerin	MgO, $MgAl_2O_4$	Reactive incorporation	[36]
AZ31 Mg	10 g/L Al_2O_3, 500 nm	120 g/L Na_2SiO_3, 5 g/L NaOH	MgO, Mg_2SiO_4, Al_2O_3	Inert incorporation	[58]
AM60B Mg	4 vol. % TiO_2	10 g/L Na_3PO_4, 1 g/L KOH	MgO, $MgAl_2O_4$, rutile, anatase	Inert incorporation	[20]
Mg-Li alloy	4 vol. % TiO_2	10 g/L Na_2SiO_3, 3 g/L NaOH, 0.6 g/L K_2ZrF_6	MgO, Mg_2SiO_4	Inert incorporation	[59]
AZ91D Mg	5 and 10 vol.% titania sol	15 g/L Na_2SiO_3, 10 g/L NaOH, 8 g/L KF	MgO, Mg_2SiO_4, amorphous	Undefined	[60]
AZ91D Mg	2, 4, 6 g/L TiO_2 nanoparticles	6 g/L $(NaPO_3)_6$, 3 g/L NaOH	MgO, $MgAl_2O_4$, $Mg_3(PO_4)_2$, rutile, anatase, Mg_2TiO_4	Partly reactive incorporation	[38]
Mg-Ca alloy	4 g/L and 8 g/L TiO_2 nanoparticles	2 g/L KOH and 10 g/L $NaAlO_2$	MgO, $MgAl_2O_4$, rutile, anatase	Inert incorporation	[61]
AZ91D Mg	2 g/L SiC, 400 nm	20 g/L $NaAlO_2$ 3 g/L NaOH	MgO, $MgAl_2O_4$	Inert incorporation	[62]

AZ31 Mg	2 g/L SiC, 50 nm	12 g/L $Na_2SiO_3 \cdot 9H_2O$ 15 g/L $(NaPO_3)_6$	MgO, Mg_2SiO_4, SiC	Inert incorporation	[63]
AZ31 Mg	5 g/L SiC, 30 nm	2 g/L $NaAlO_2$ + 2 g/L Na_2SiO_3 + 1.5 g/L KOH; 4 g/L Na_3PO_4 + 1.5 g/L KOH	MgO, $MgAl_2O_4$ and Mg_2SiO_4	Undefined	[42]
SiCw/AZ91 MMC	20 vol.% SiC whisker, 0.1-1 μm in diameter and 30-100 μm in length	15 g/L Na_2SiO_3, 8 g/L KF, 8 g/L KOH	MgO	Undefined	[64]
SiC_p/AZ31 MMC	6 vol.% SiC, 10 μm	4 g/L Na_3PO_4, 4 g/L KOH, 4 g/L NaF	MgO, MgF_2, $Mg_3(PO_4)_2$, Mg_2SiO_4	Partly reactive incorporation	[65]
ZC71 Mg, MMC	12 vol.% SiC, 2-20 μm	10.6 g/L $Na_2SiO_3.5H_2O$, 5.6 g/L KOH	MgO, SiC, Mg_2SiO_4	Inert incorporation	[66]
AZ31 Mg	10, 20, 30 g/L CeO_2, <5 μm	10 g/L Na_2SiO_3 3 g/L KF	Mg_2SiO_4, CeO_2	Inert incorporation	[37]
AM50 Mg	3, 10 g/L CeO_2, <5 μm	10 g/L Na_2SiO_3 2 g/L KOH	CeO_2, MgO, Mg_2SiO_4	Inert incorporation	[67]
AM60B Mg	3 vol. % PTFE, 170-270 nm	10 g/L Na_3PO_4 1 g/L KOH, 1-2 vol.% octylphenol polyoxyethylene ether, 2-4 vol.% sodium dodecyl sulfonate	MgO, $MgAl_2O_4$, PTFE	Inert incorporation	[18]
AZ31 Mg	5 g/L HA, 60 to 70 nm in length and 15 to 20 nm in width	5 g/L $Na_3PO_4 \cdot 12H_2O$, 3 g/L KOH	MgO, HA	Inert incorporation	[68]
ZK60 Mg	1, 3 and 5 g/L HA	3 g/L $(NaPO_3)_6$, 8 g/L $KF \cdot 2\ H_2O$	MgO, MgF_2, HA	Inert incorporation	[69]
AZ31 Mg	10 g/L HA	7 g/L Na_2SiO_3, 5 g/L NaF 2 g/L KOH	HA, Mg_2SiO_4,whitlockite	Partly reactive incorporation	[52]
Mg-2 Zn-0.24 Ca alloy	2 g/L HA, 5 μm	54 g/L $Na_3PO_4 \cdot 12H_2O$, 5 g/L $KF \cdot 2H_2O$, 0.56 g/L KOH	HA, $Mg_3(PO_4)_2$, $Ca_3(PO_4)_2$ (TCP)	Partly reactive incorporation	[70]
Mg-Zn-Zr-RE alloy	1, 3, 5 g/L Ag, 39 nm	Low concentrated alkaline solution	MgO Ag	Inert incorporation	[14]

2.4.1 Oxide ceramic particles

Various oxide particles have been used to modify PEO coatings on Mg and its alloys. In general, oxide particles with low melting point can experience reactive incorporation more easily in comparison to high melting point particles. For instance, clay particles (< 1200 °C) have achieved fully reactive incorporation into PEO coatings on AM50 Mg alloy [26, 55]. In the presence of particles, the main fraction of the coating in the top and center region has been transformed from crystalline phase to amorphous phase (Figure 2-4). It was reported that the particle-containing amorphous layer was close to commercial bio-glasses [26]. Other oxide particles (ZrO_2, TiO_2 and Al_2O_3) with higher melting point were generally found to achieve inert incorporation [16, 20, 37, 41, 58-60, 67, 71] or partly reactive incorporation, resulting in formation of $Mg_2Zr_5O_{12}$, Mg_2TiO_4 and $MgAl_2O_4$ phases in the coatings [21, 36, 38-40, 53, 57, 72, 73].

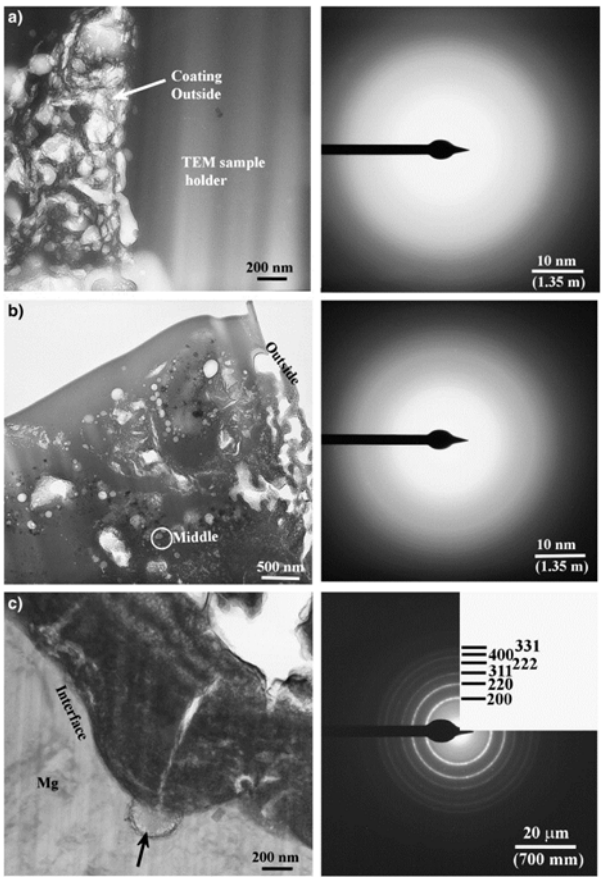

Figure 2-4 TEM micrographs and corresponding diffraction pattern from various regions of the coating with clay particle addition (a) top surface region, (b) center region and (c) interface region *(with permission from Elsevier* [26]).

The applied electrical and electrolyte conditions also determine the incorporation mode of the particles as well as the coating composition. For example, it was claimed that the incorporation of ZrO_2 particles into the coating can range from inert incorporation [16, 41] to partly reactive incorporation [40, 53, 57] under different treatment conditions. The $Mg_2Zr_5O_{12}$ reaction phase was only observed in the coating produced from phosphate electrolyte and not from the silicate-based one [53]. However, the ZrO_2 particles achieved reactive incorporation in the same silicate electrolyte under AC instead of DC regime [40]. The crystallinity of the layer increased with the energy input (current density/voltage) during PEO treatment [55]. Furthermore the incorporation mode of the introduced particles can be considered as an indirect evidence for the plasma temperature during PEO treatment. It was found that the monoclinic zirconia transformed to tetragonal phase, indicating that the local temperature reached at least 1513 K [16, 53]. According to Lee et al. [16], it can be assumed that the temperature of the plasma was between 2116-2643 K, which are the melting temperatures of TiO_2 and ZrO_2 particles, since Mg_2TiO_4 was detected while ZrO_2 particles were inertly incorporated into the coating.

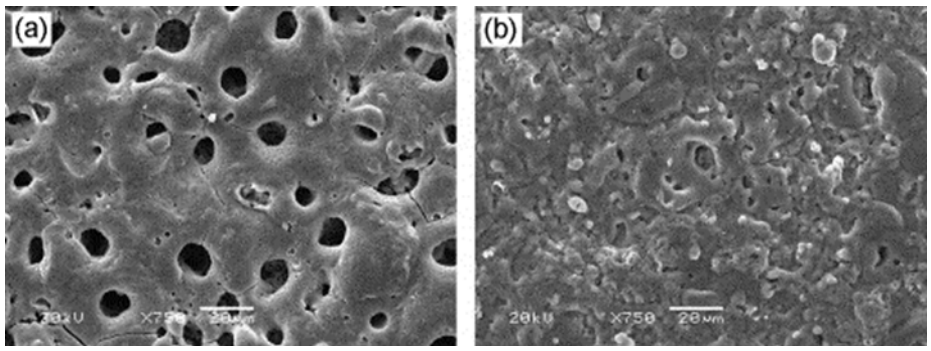

Figure 2-5 Surface morphologies of oxide film formed in an alkaline phosphate bath without (a) and with (b) addition of 4 vol% titania sol *(with permission from Elsevier* [20]).

Introduction of particles has an effect on the microstructure and morphology of PEO coatings, e.g., pore characteristic, thickness and compactness of the layer. Addition of oxide particles to the electrolytes can reduce the number and/or size of the pores on the coating surface [20, 21, 26, 41, 43, 51, 58, 71]. For instance, the surface of coatings with inertly incorporated titania sol was much less porous (Figure 2-5) [20]. Normally sealing of the surface is more effective when adding sols to the electrolyte and/or in the case of reactive incorporation. However, it was also claimed that the coating surface was not influenced too much [37, 67] or became more porous when oxide particles were added to the electrolytes [39]. The compactness and thickness of the

layer can be altered or enhanced in the presence of oxide particles. It was reported that the outer layer of the coating became more compact and uniform compared with the coatings formed in particle-free electrolytes [21, 37, 40, 51, 57, 67]. There is no clear trend for the influence of particle addition on the coating thickness. It was found that oxide particles were not effective to increase coating thickness, since the coatings generally demonstrated similar thickness [16, 37, 41] or even became thinner [67] with addition of particles. In contrast, some reports claimed that the particle-containing coatings were slightly thicker than particle-free coatings [38, 39, 57, 58]. The change of the thickness of the particle-containing coatings is associated with the altered voltage/current evolution during PEO processing.

2.4.2 Non-oxide ceramic, organic and metallic particles

It was reported that non-oxide particles, e.g., PTFE, Ag and hydroxyapatite, are generally inertly incorporated into the PEO layers [14, 18, 68, 69]. In some cases, partly reactive incorporation can also be observed for HA and SiC particles [52, 63, 70]. For instance, the coatings produced from HA particles containing electrolyte were composed of hydroxyapatite and whitlockite (TCP) [52]. This discrepancy is probably ascribed to the different substrates, base electrolytes and electrical parameters utilized during PEO process. Inert incorporated particles are often reported to decrease the porosity of PEO coatings [18, 52, 68, 69]. For example, the pores on the coating surface were smaller and more homogenous after incorporation of PTFE particles [18]. The coating morphology has also been modified in the presence of particles. The cross section of the coating was reported to be denser, as through-going pores and defects were hardly detected in the particle-containing coatings [18, 70]. In terms of coating thickness, thicker coatings were formed in SiC nanoparticles containing electrolyte under constant current regime [63]. The increment of the coating thickness depends on the applied current density. It is larger when using lower current density (Δ thickness=12 μm) in comparison to Δ thickness=5 μm at higher current density. It was also found that the thickness of the coatings decreased from 15 to 13 μm with addition of PTFE particles [18]. This is probably caused by the different incorporation modes and applied electrical parameters.

Additionally, the substrate can serve as source of particles or fibers for PEO coatings if metal matrix composites are used. SiC is usually used as reinforcement in metal matrix composites [64, 66]. It was found that SiC particles were partly reactively incorporated into PEO coatings, as

some particles were oxidized and then reacted with MgO to synthesize Mg_2SiO_4 phase (Figure 2-6) [65]. However, such a strong oxidation was not confirmed by Arrabal et al. [66, 74], which might be attributed to the large-sized embedded particles in the latter case. SiC particles were distributed throughout the layer and only a thin layer of reaction product, possibly silica, was formed at the particle/coating interface. The coating thickness was reduced by the particles, while the surface morphology was not significantly influenced in this case.

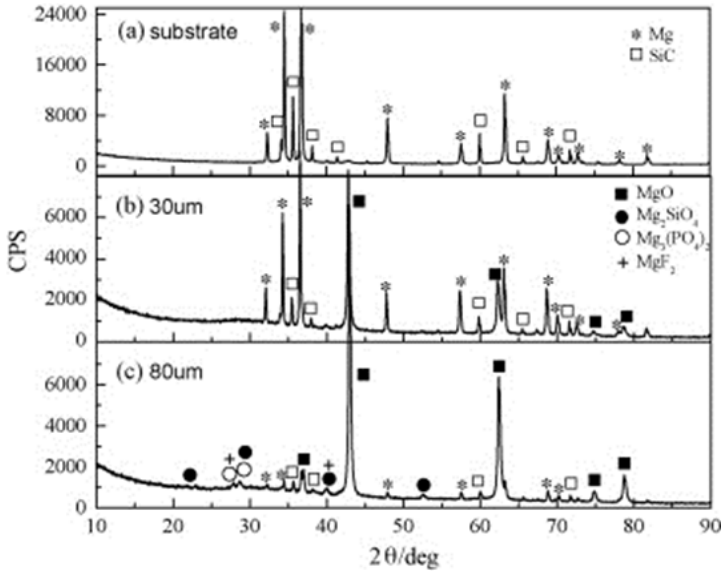

Figure 2-6 XRD patterns for (a) SiCP/AZ31 composite substrate, (b) 30 μm coating, and (c) 80 μm coating *(with permission from Elsevier* [65]).

In summary, the composition of the coating is related to the incorporation mode of the particles. Oxide particles can more easily achieve reactive incorporation into the coating in comparison to non-oxide ceramic, organic and metallic particles. The electrical parameters applied during PEO treatment play a vital role in the coating composition as well. Introduction of particles cannot fully seal the porosity of PEO coatings. The influence of particle addition on the coating thickness/growth rate is non-significant in comparison to the coating composition, which mainly depends on the evolution of voltage and current density during PEO process. Moreover, additional particles can colorize PEO coatings. For instance, addition of TiO_2 particles to the electrolyte produced blue PEO coatings [38, 73] and the white-grey coatings became darker after incorporation of Ag nanoparticles [14].

2.5 Influence of particle addition on coating properties

The demand of modern technological society for Mg alloys emphasizes a combination of good corrosion resistance with wear resistance and functionalized surfaces. The applications range from structural and transport components to bioengineering. Regardless of the final application, improved tailored surfaces are required to prolong service life and reduce long-term costs. The influence of particles addition on the properties of PEO coatings is addressed below as well as in Table 2-3.

Table 2-3 Influence of particle addition on coating properties.

Substrate and particle	Test condition	Property changes	Reference
AZ91 Mg, 9 g/L zirconia, 200-400 nm	Corrosion test: 3.5 wt. % NaCl solution, vs Ag/AgCl	Corrosion current density decreased from 7.3×10^{-7} to 7.0×10^{-8} A/cm^2, corrosion potential increased from -1.4 to -1.3 V, polarization resistance increased from 3.1×10^5 to 1.8×10^6 Ω cm^2	[41]
AZ91D Mg, 5 vol.% zirconia sol	Corrosion test: 10 min in 3.5 wt.% NaCl solution, vs SCE	Corrosion current density decreased from 5.3×10^{-7} to 1.4×10^{-8} mA/cm^2, corrosion potential increased from -1.5 to -1.2 V	[57]
Mg-Li alloy, 1 vol.% silica sol	Corrosion test: 5 min in 3.5 wt.% NaCl solution, vs SCE	Corrosion current density decreased from 6.3×10^{-7} to 1.0×10^{-7} A/cm^2, polarization resistance increased from 3.9×10^4 to 1.8×10^5 Ω	[51]
AZ91D Mg, 2 vol% of alumina sol	Corrosion test: 30 min in 3.5 wt.% NaCl solution, vs SCE	Corrosion current density decreased from 1.6×10^{-6} to 2.6×10^{-8} mA/cm^2, corrosion potential increased from -1.5 to -1.4 V, polarization resistance increased from 1.6×10^4 to 1.9×10^5 Ω cm^2	[21]
AZ31 Mg, 10 g/L Al_2O_3, 500 nm	Wear test: 10 N, 3 min, stroke (10 mm), 10 Hz, counterpart (GCr15 steel ball) Corrosion test: 10 min in 3.5 wt.% NaCl solution, vs SCE	Increased hardness (from 130 to 358 HV), reduced friction coefficient (from 0.4 to 0.35), decreased corrosion current density (from 8.4×10^{-7} to 3.8×10^{-7} A/cm^2), corrosion potential increased from -1.2 to -1.1 V	[58]
AM60B Mg, 4 vol. % TiO_2	Corrosion test: 10 min in 3.5 wt.% NaCl solution, vs SCE	Corrosion current density decreased from 4.2×10^{-6} to 4.3×10^{-8} A/cm^2, corrosion potential increased from -1.6 to -1.5 V	[20]
AZ91D Mg, 5 and 10 vol.% titania sol	Corrosion test: 10 min for polarization test, up to 312 h for immersion in SBF solution at 37.4 °C , vs SCE	Corrosion current density increased from 3.2×10^{-8} to 7.8×10^{-8} A/cm^2 for 5 vol. % titania sol and 1.5×10^{-7} for 10 vol. % titania sol, much more pitting after 312 h immersion test	[60]

AZ91D Mg, 2, 4, 6 g/L TiO_2 nanoparticles	Corrosion test: 20 min in 3.5 wt.% NaCl solution, vs SCE Photocatalytic test: 100 mL methylthionine blue solution (30 mg/L), exposed 24 h to an incandescent light bulb	Corrosion current density decreased from 6.9×10^{-7} to 1.9×10^{-8} mA/cm^2 for 4 g/L particles and 3.8×10^{-8} for 6 g/L particles, corrosion potential increased from -1.51 to -1.49 V for 4 g/L particles and -1.43 V for 6 g/L particles; Enhanced photocatalytic properties	[38]
AZ91D Mg, 2 g/L SiC, 400 nm	Wear test: 5, 7.5 and 10 N, 5 min, sliding over 7 mm at 42 mm/s, counterpart (GCr15 steel ball)	Similar friction coefficient at 5 N and 7.5 N, reduced friction coefficient from 0.55-0.65 to 0.1 at 10 N	[62]
AZ31 Mg, 2 g/L SiC, 50 nm	Wear test: 10 and 20 N, stroke length of 7.8 mm, 30 min, 5 Hz, counterpart (SAE 521000 Cr steel ball)	Decreased wear rate from $(1.4\text{-}3.8) \times 10^{-3}$ to $(3.3\text{-}4.9) \times 10^{-4}$ mm^3/(N m)	[63]
SiCw/AZ91 (MMC), 20 vol.% SiC whisker, 0.1-1 μm in diameter and 30-100 μm in length	Corosion test: 10 min for polarization test and 4 days immersion test in 3.5 wt.% NaCl solution, vs SCE	Corrosion current density decreased from 1.0×10^{-5} to 1.1×10^{-8} A/cm^2, corrosion potential increased from -1.5 to -1.3 V, much less weight loss after 4 days immersion test	[64]
ZC71 Mg, 12 vol.% SiC, 2-20 μm	Corrosion test: 20 min in 3.5 wt.% NaCl solution, vs SCE	Corrosion rate of coating treated for 100 min was 55 times lower than the untreated material: 24.21 mm/y compared with 0.44 mm/y	[66]
AZ31 Mg, 10, 20, 30 g/L CeO_2, <5 μm	Corrosion test: 10 min in 3.5 wt.% NaCl solution, vs SCE	Corrosion current density decreased from 8.6×10^{-6} to 1.0×10^{-6} (10 g/L), 2.0×10^{-7} (20 g/L) and 4.0×10^{-8} A/cm^2 (30 g/L)	[37]
AM60B Mg, 3 vol. % PTFE, 170-270 nm	Wear test: 2 N, sliding amplitude (5 mm), 30 min, 5 Hz, counterpart (AISI52100 steel ball)	Decreased friction coefficient from 0.5-0.7 to 0.2, nearly no wear volume loss	[18]
AZ31 Mg, 10 g/L HA	Corrosion test: 1 h immersion in SBF solution at the body environment temperature, vs SCE	Corrosion resistance of outer layer increased from 6.1×10^4 to 2.6×10^5 Ω cm^2, enhanced apatite formation ability	[52]
Mg-2 Zn-0.24 Ca alloy, 2 g/L HA, 5 μm	Corrosion test: 10 min in SBF solution, vs SCE	Corrosion current density decreased from 1.2×10^{-5} to 1.1×10^{-5} A/cm^2, corrosion potential increased from -1.64 to -1.55 V, enhanced apatite formation ability	[70]

2.5.1 Mechanical and tribological properties

Due to the high porosity and limited range of phase compositions, PEO coatings on Mg and its alloys are unable to provide long-term wear protection [3, 75]. In order to overcome the drawbacks, either the porosity of the outer layer is suppressed or new stable phases are formed in the coating with the aid of particles. Incorporation of hard particles (inert incorporation [58, 74]) or formation of new phases with high hardness (reactive incorporation [39]) can increase wear resistance. For the PEO coated Mg alloy AZ31, the hardness increased from 130 HV to 358 HV due to the inertly incorporated Al_2O_3 nanoparticles. Consequently, the wear track (Figure 2-7) of coating with particle addition was much narrower and shallower in contrast to that of particle-free coating [58]. The hardness of PEO coatings on AZ91D Mg alloy was also increased by reactive incorporation of Al_2O_3 nanoparticles [39]. Figure 2-8 shows that the coating hardness increased from ~150 HV to ~375 HV with the increase of particle concentration in the electrolyte, which was related to the significant increase of $MgAl_2O_4$ phase in the layer. PEO coatings can also demonstrate higher hardness and better wear performance due to the denser and/or thicker coating after incorporation of particles (SiC and TiO_2) [59, 62, 63, 71]. Furthermore, solid lubricant particles (PTFE) were introduced to PEO coatings aiming to reduce the friction coefficient during wear test [18]. As a result, the friction coefficient of coatings with PTFE was stable and much lower (below 0.2) in comparison to that of coatings free of particles (0.5-0.7), preventing wear of the surface.

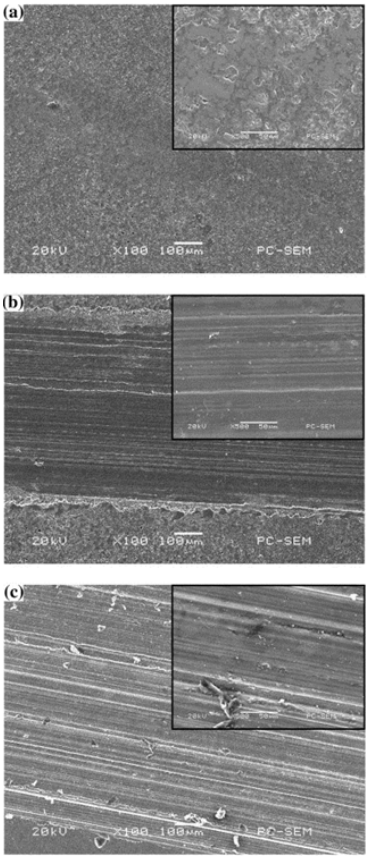

Figure 2-7 Wear tracks (a) coating with Al_2O_3 nanoparticles, (b) particle-free coating and (c) AZ31 substrate *(with permission from Elsevier* [58]).

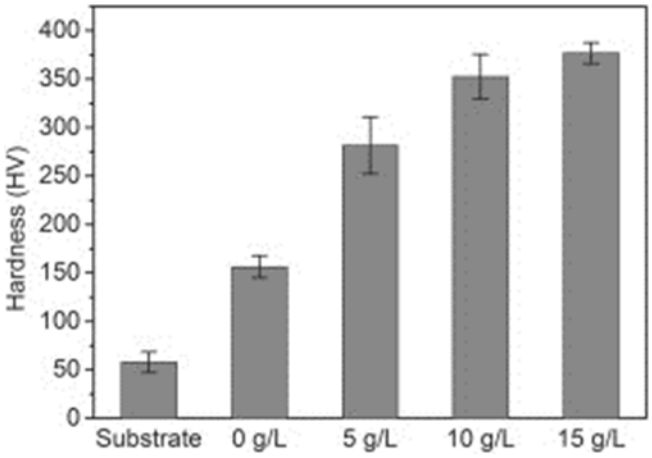

Figure 2-8 Vickers hardness of the substrate and PEO coatings with addition of different concentrations of Al_2O_3 nanoparticles *(with permission from Elsevier* [39]).

2.5.2 Corrosion performance

Regarding the corrosion behavior, different particles (ZrO_2, TiO_2, and CeO_2) have been utilized to improve the corrosion performance of PEO coatings on Mg and its alloys (Table 2-2), but controversial results have also been found. Enhanced corrosion properties are mainly caused by the newly formed stable phases (reactive incorporation of particles [38, 57]) or by the inertly incorporated particles [20, 37, 41, 67, 71] which have high chemical stability. For instance, the corrosion resistance of PEO coatings can be greatly improved by addition of ZrO_2 particles [41, 57]. After inert incorporation of ZrO_2 particles (200-400 nm), the corrosion current density (i_{corr}) of the coated Mg alloy was reduced from 7.27×10^{-7} A/cm^2 to 7.03×10^{-8} A/cm^2 with respective increase of polarization resistance and shift of the corrosion potential towards more positive values. Salt spray test demonstrated that the incorporation of ZrO_2 particles efficiently minimizes the incidence of pitting corrosion on PEO coated substrates [41]. Reactive incorporation of ZrO_2 obtained via sol route can also improve the corrosion performance of PEO coatings [57]. The corrosion current density was reduced by about two times and the corrosion potential significantly shifted to positive direction (from -1.50 V vs SCE to -1.22 V vs SCE). In some cases PEO coatings are less porous or thicker thus demonstrating better barrier properties after inert incorporation [18, 21, 46, 48, 58] or reactive incorporation [51] of particles. The improvement of the corrosion resistance is often attributed to the denser and thicker layer after particle addition. However coatings can also be more porous when the particle concentration in the electrolyte is beyond certain level, which is detrimental to the corrosion performance of PEO coated Mg [67]. Inertly incorporated particles can be considered as containers to load inhibitors to achieve self-healing functionality for PEO coatings. Sun et al. [43] used halloysite nanotubes as nanocontainers to load inhibitors (benzotriazole). The inhibitor containing PEO coatings confer active corrosion protection responding to the pH change triggered by the corrosion process.

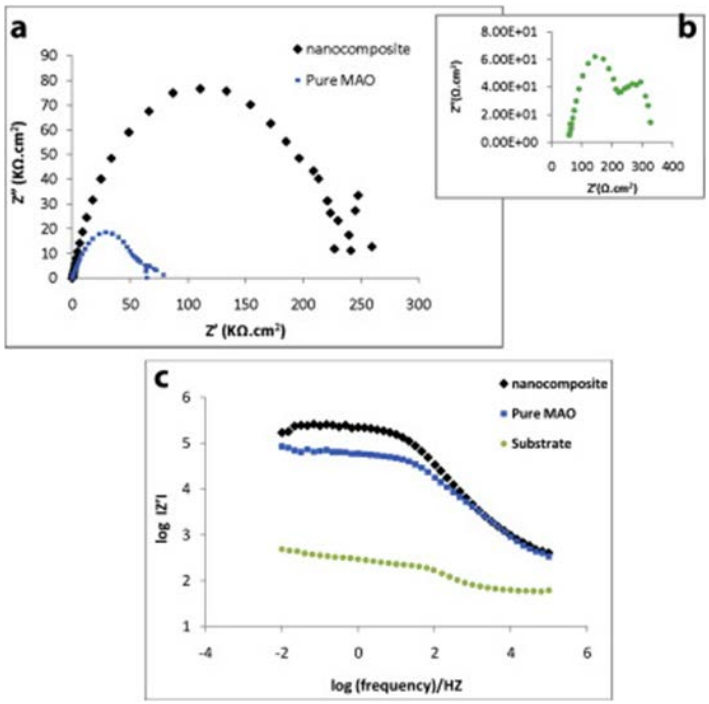

Figure 2-9(a, b) Nyquist and (c) Bode plots of particle-free coating, particle-containing coating and bare magnesium alloy *(with permission from Elsevier* [52]).

HA particles were used not only to improve the corrosion performance but also to provide apatite formation ability for PEO coatings on Mg alloys [52, 68-70]. Figure 2-9 shows the Nyquist and Bode plots of the coatings with and without particle addition. The resistance of the outer layer has increased by 3 times as a result of particle incorporation. Moreover introduction of HA particles endow the layer with superior apatite forming ability. The amount of apatite formed on the coating surface after 3 days of immersion was higher than that of blank PEO coating [52].

Although the abovementioned studies proved that particle addition can provide better corrosion resistance for PEO coatings, the improved properties show limitations depending on the amount of particles used in the electrolyte [60]. The long-term performance of the coatings remains an issue as well. In some cases additional particles are not effective but even deteriorating the corrosion protection performance of the coatings during long-term corrosion tests. Wang et al. [60] demonstrated that coatings produced from electrolytes containing 5 and 10 vol. % titania sol showed worse corrosion resistance than that of the unmodified coatings after relatively long-term immersion in SBF (Figure 2-10), which was attributed to the increasing amount of amorphous material by the incorporation of TiO_2.

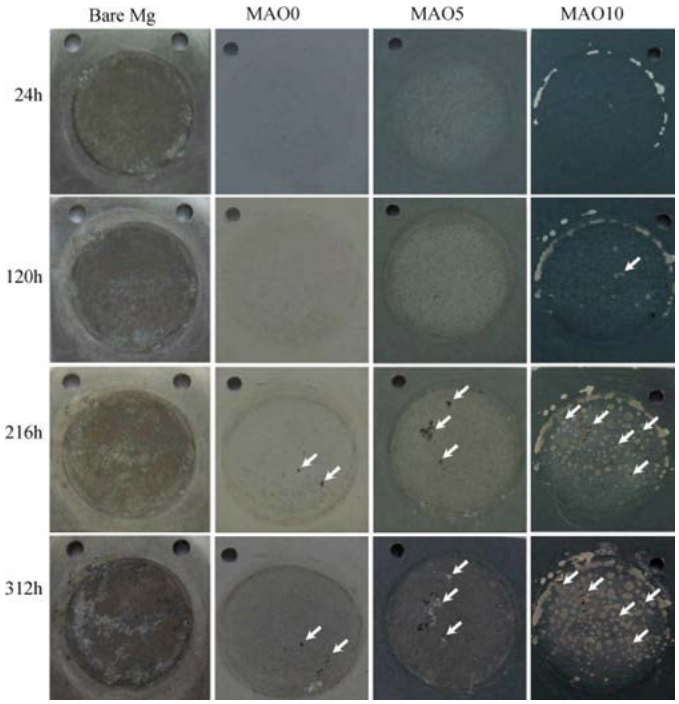

Figure 2-10 Surface morphology of bare Mg and coatings with and without addition of titania sol (5 and 10 vol.%) after immersion different times in SBF solution (arrows indicating the corrosion sites) *(with permission from Elsevier* [60]).

2.5.3 Other properties

The incorporation of particles allows to create surfaces with different functionalities such as hydrophobicity or enhanced photocatalytic properties. PEO coated AM60B Mg alloy was reported to show hydrophobicity after incorporation of polytetrafluoroethylene (PTFE) hydrophobic particles [18, 23]. Contact angle of the coatings has been increased from 50°-55° to 92°-101° after inert incorporation of PTFE particles [18]. Owing to the photocatalytic properties [76], TiO_2 particles were introduced to PEO coatings to provide this additional functionality for Mg alloy surfaces. It was found that PEO coatings with TiO_2 nanoparticle additions on AZ91D Mg alloy showed good photocatalytic performance (Figure 2-11), as the inertly incorporated TiO_2 particles greatly accelerated the decomposition rate of the methylthionine blue solution [38].

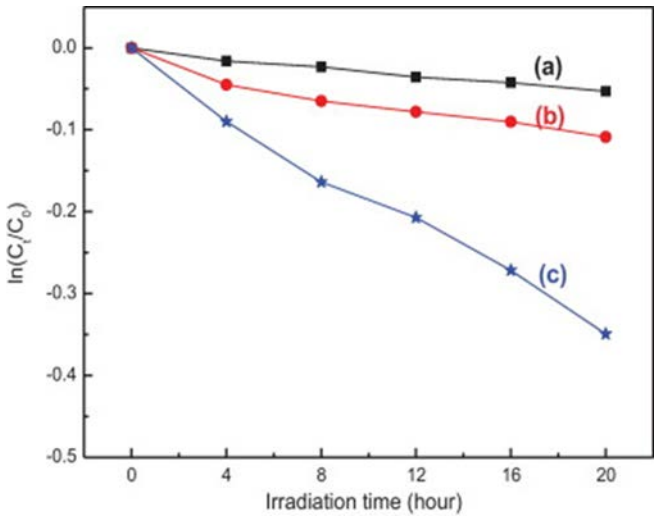

Figure 2-11 The decomposition rate of methylthionine blue (MB) (a) blank solution, (b) PEO coating formed in the base electrolyte and (c) PEO coating formed in electrolyte with 4 g/L TiO_2 nanoparticles *(with permission from Elsevier* [38]).

In summary, the addition of particles has significant effects on the properties of PEO coatings and provides multifunctionality for certain potential applications. In terms of wear and bio-application, addition of particles to PEO layers is of great potential. The layers in the presence of particles can demonstrate superior hardness and lubricating property providing desirable wear protection for the substrate. It is likely that particles loaded PEO coatings can exhibit biological properties, such as surface bioactivity, antibacterial effect and apatite forming ability. However, introduction of particles is not effective to achive long-term corrosion protection for the coating. It is also worthwhile to note that none of the coatings formed in electrolytes with particle additions is used commercially in an industrial application up to now, which might be related to the fact that keeping the particles uniformly dispersion is a challenge especially in large industrial treatment baths.

3 Motivation and objectives

Because of the inferior corrosion and wear performance of Mg and its alloys, PEO has been considered as one promising surface treatment for them to achieve a wider range of applications. Nevertheless, the coatings generally have high porosity and limited range of phase compositions, limiting the long-term protection for the Mg substrate. In-situ incorporation of particles into the coating has been explored in this work as a new strategy to alleviate the high porosity and to gain

enhanced/new properties for Mg surfaces. Thus it is indispensable to investigate the intrinsic mechanisms of particle addition during PEO treatment and to evaluate the influence of the introduced particles on the phase composition, microstructure, morphology and properties of PEO coatings. The addition of particles into the coating is a complex process, depending on numerous factors, for instance, the properties of the particle (size and melting point), compounds contained in the electrolyte, substrate, as well as the energy input provided by the power supply.

The objectives for this work are focused on understanding the:

- influence of particle properties (size and melting point) on the uptake and incorporation of particles into PEO coatings
- influence of electrolyte parameters, i.e., electrolyte composition and concentration, on the uptake and incorporation of particles into PEO coatings
- influence of electrical parameters, such as the frequency, duty ratio and voltage, on the uptake and incorporation of particles into PEO coatings
- understanding the mechanisms of the uptake and incorporation of particles into PEO coatings
- effect of particle addition on the composition, microstructure and morphology of PEO coatings
- understanding the coating growth mechanisms via addition of particles
- exploring the possibilities of enhancing the functionalities and improving the basic properties of PEO layers via particle addition is another important objective

4 Experimental

This chapter gives information regarding the experimental methods used in the present study.

4.1 Coating preparation

4.1.1 Substrate

Specimens of AM50 Mg alloy with size of 15mm × 15mm × 4mm were prepared from gravity cast ingot material. To get a stable current transfer through the sample and electrolyte, a threaded hole with a diameter of 2.5 mm was drilled on one of the lateral sides of the specimen and the samples were screwed to a holder. The chemical composition of AM50 Mg alloy was analyzed by using Arc Spark OES (Spark analyser M9, Spectro Ametek, Germany). The determined

composition is 4.74 wt.% Al, 0.383 wt.% Mn, 0.065 wt.% Zn, 0.063 wt.% Si, 0.002 wt.% Fe, 0.002 wt.% Cu and Mg balance. It should be noted that in the present thesis any phrases such as "substrate" or "bare alloy" refer to AM50 Mg alloy. The specimens were ground using emery sheets up to 1200 grit and then air-dried prior to PEO treatment.

4.1.2 Electrolyte

4.1.2.1 Particles

Table 4-1 Size and melting point of the selected particles

Particles	Melting point	Electrolyte composition	Processing parameters
Clay, ~10 µm (Rockwood Clay Additives GmbH)	1000-1200 °C	10, 15, 20 g/L Na_3PO_4 + 1, 5, 10 g/L KOH + 5 g/L particle	Paper 3: constant voltage (450 V), 10 min, 50 Hz, duty ratio: 10%
SiO_2, avg. 12 nm and 1-5 µm (Sigma-Aldrich)	1600 °C	20 g/L Na_3PO_4 + 1 g/L KOH + 5 g/L particle	Paper 1 and 2: constant voltage (450 V), 10 min, 250 Hz, duty ratio: 10%; Paper 4: constant voltage (450 V), 10 min, 50, 250 and 500 Hz, duty ratio: 10% and 30%; Paper 5: constant current density (27 mA/cm^2), 60 min, 250 Hz, duty ratio: 10%
TiO_2, ~200 nm (ChemPur GmbH)	1843 °C	20 g/L $Na_6P_6O_{18}$ + 8 g/L KOH + 5 g/L, 10 g/L and 20 g/L particle	Paper 8: constant voltage (400 and 500 V), 10 min, 250 Hz, duty ratio: 10%
Si_3N_4, 0.1-0.8 µm and 1-5 µm (Goodfellow Cambridge Ltd.)	1900 °C	10 g/L Na_3PO_4 + 1 g/L KOH + 5 g/L particle	Paper 7: constant voltage (450 V), 10 min, 50 Hz, duty ratio: 10%
SiC, 1-5 µm (Goodfellow Cambridge Ltd.)	2730 °C	20 g/L Na_3PO_4 + 1 g/L KOH + 5 g/L particle	Constant voltage (450 V), 10 min, 250 Hz, duty ratio: 10%

The detailed information of the used particles for this study is shown in Table 4-1. Figure 4-1 exhibits the morphology and XRD patterns of the particles. Relatively large-sized particles are crystalline while the peaks corresponding to SiO_2 nanoparticles are hardly to be detected.

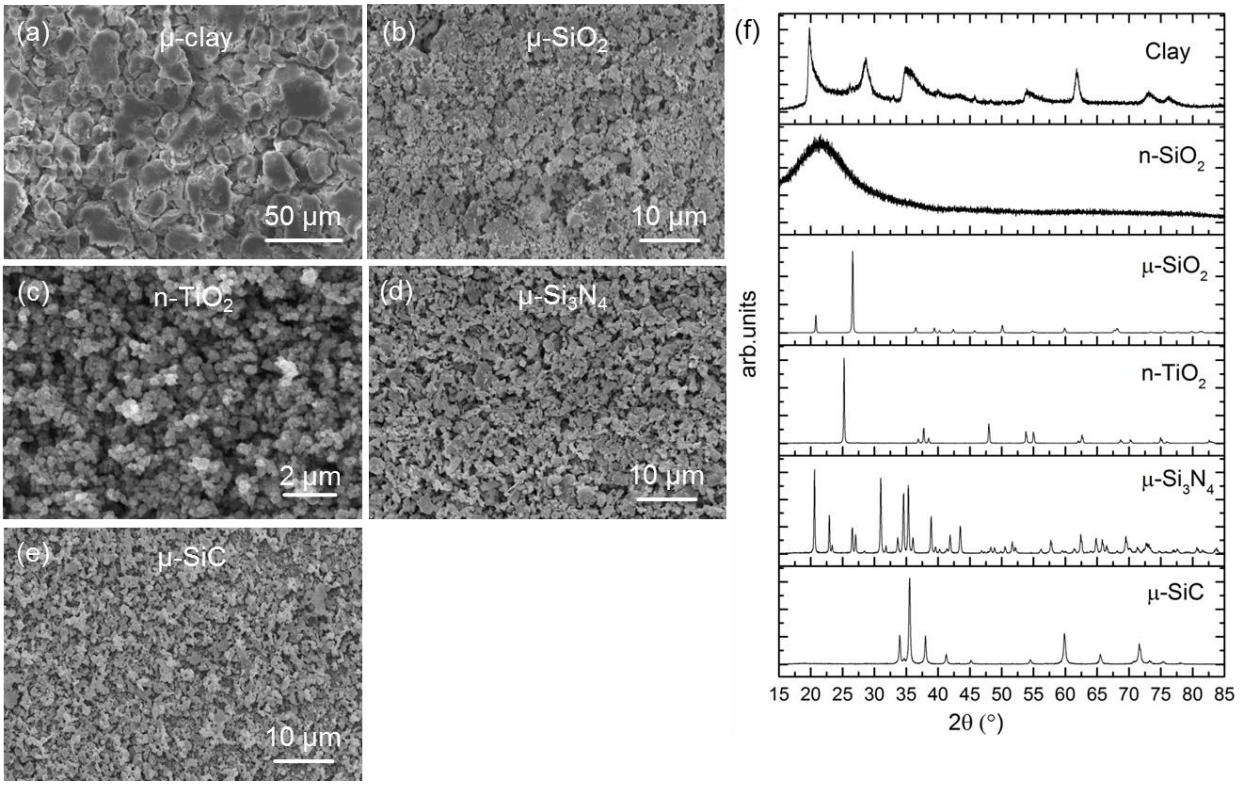

Figure 4-1 Morphology and XRD patterns of the particles.

4.1.2.2 Other chemical compounds

Phosphate based electrolytes were used to produce coatings with the purpose of eliminating the influence of Si source from the PEO electrolyte. The conductivity of the electrolytes was measured by using a Mettler Toledo Inlab 730 probe. The pH value was measured using a Metrohm 691 pH meter. It was found that the conductivity and pH value of the electrolyte was influenced only marginally by the addition of particles.

4.1.3 PEO processing

In the present study, the PEO process was performed using a DC power supply with a lab-produced pulse unit, as shown in Figure 4-2a. Figure 4-2b demonstrates the schematic of the utilized PEO set-up. The specimen was treated as the anode and a heat-exchange system based on a stainless steel tube was used as the cathode. The temperature of the electrolyte was maintained

at 20 ± 2 °C by a water cooling system. A stirrer and bubbling generator were used to facilitate the uniform distribution of the particles in the electrolyte during PEO processing. The frequency and duty ratio of the treatment can be achieved by changing the duration of the pulse. Constant voltage or constant current density regime was used for the present study. Consequently, the current decreases or voltage increases as a function of the treatment time due to the enhanced barrier properties and increased thickness of the coating. The evolution of the voltage/current during PEO processing was recorded by a data logging system produced by PeakTech. Additionally, the study of emission characteristics was performed by a Plasus EmiCon optical emission spectroscopy (OES) in order to identify the elements/species associated with plasma discharge as well as to understand the influence of particle addition on PEO processing. As the excited elements emit at some specific wavelengths, the atoms, molecules and ions involved in plasma could be determined. The emitted light during PEO treatment was analyzed by Plasus EmiCon system provided by PLASUS.

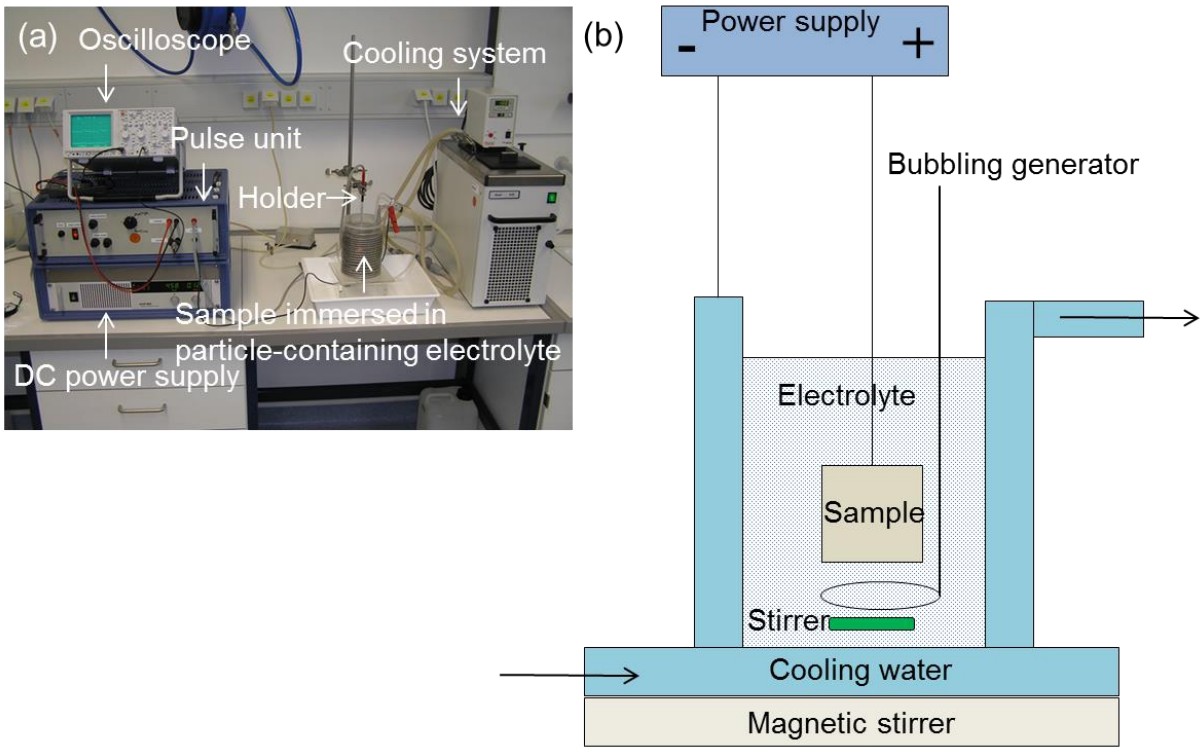

Figure 4-2 Set-up of PEO treatment

4.2 Coating characterization

4.2.1 Scanning electron microscopy

A scanning electron microscope (SEM), TESCAN Vega3 SB, combined with an energy dispersive spectrometer (EDS) system from eumeX (IXRFsystems) was used to examine the microstructure and composition of the coatings. An acceleration voltage of 15 kV was applied for SEM and EDS investigations. A sputter-coating with Au is required to prevent the charging effect for the non-conducting ceramic coatings. To avoid the influence of Au, sputtering is only used for SEM investigations instead of the EDS analysis. For observing the cross-sectional morphology, the coatings were embedded into resin and then prepared by polishing successively using 500, 800, 1200 and 2500 grit emery sheets, following by disc polishing using colloidal silica suspension.

4.2.2 Transmission electron microscopy

Transmission electron microscopy (TEM) is a microscopy technique in which a beam of electrons is transmitted through an ultra-thin specimen, interacting with the specimen as it passes through it. More information about the coating structure and phase composition was obtained by TEM. The TEM lamellae were milled from the bulk specimens with focused ion beam (FIB) in a Nova-200 dual-beam scanning electron microscope (SEM). TEM observations were performed on a Philips CM200 transmission electron microscope operating at a voltage of 200 kV.

4.2.3 X-ray diffraction analysis

In the present study, XRD was carried out by using a diffractometer (D8 Advance, Bruker AXS) equipped with Cu Kα radiation to determine the phase composition of the obtained coatings. The measurements were performed at 40 kV voltage and 40 mA current, with a step size of 0.02 degree and 3 s for each step.

4.2.4 Roughness and pore characteristics of the surface, and thickness measurement

Surface roughness measurements were carried out by a Hommel profilometer (HOMMEL TESTER T1000). Image analysis software Analysis Pro 5.0 was used to measure the pore characteristics. The average values were calculated from 3 SEM images per treatment condition. The coating thickness was measured by using an eddy-current gauge (MiniTest 2100,

Electrophysik, Germany). The resolution is about 0.1 µm with measurement ability in the range of 1-200 µm.

4.2.5 Synchrotron tomography

The synchrotron tomography experiments were performed at the P05 (IBL) beamline of PETRA III, DESY (Deutsches Elektronen-Synchrotron). During the acquisition of the tomograms, 1800 projections were taken with an acquisition time of 3s. The energy was set to 18 keV with a sample-to-detector-distance of 15 mm. The reconstructions resulted in volumes of (960×960×1528) voxel with a voxel size of $(1.1\ \mu m)^3$. The spatial resolution of the reconstructed volumes was 2.9 µm.

4.3 Coating properties

4.3.1 Corrosion resistance

In published Paper 2, 3 and 7, electrochemical experiments were performed in 0.5 wt% NaCl solution at room temperature using an ACM Gill AC computer controlled potentiostat to evaluate the corrosion behavior of PEO coated specimens. In addition, Hank's solution (8.00 g NaCl, 0.40 g KCl, 0.14 g $CaCl_2$, 0.35 g $NaHCO_3$, 0.20 g $MgSO_4 \cdot 7H_2O$, 0.12 g $Na_2HPO_4 \cdot 12H_2O$, 0.06 g KH_2PO_4) was prepared according to ASTM-G31-72 [77, 78] to preliminary study the biodegradability of the PEO coatings. A corrosion cell (333 ml) with a three electrode set-up consisted of a Ag/AgCl reference electrode, a platinum (mesh) counter electrode and the coated specimen as working electrode was used. Potentiodynamic polarization measurement is based on polarising the sample by applying an external voltage with the potentiostat. Depending on the polarization direction, this technique has two opposite reactions, namely reduction and oxidation. In the anodic reaction the metal is oxidized and dissolves, e.g. $Mg \rightarrow Mg^{2+} + 2e^-$. In the cathodic reaction the electrons provided by the potentiostat are used in the reduction reaction, e.g. $2H^+ + 2e^- \rightarrow H_2$. The corrosion current was determined using the current density at the intersection of the vertical through the corrosion potential with the cathodic Tafel slope (Figure 4-3). However, this approach is a result of criticisms due to the negative difference effect (NDE) [79-81]. Nevertheless it was used for semi-quantitative approximation in the current work. Polarization studies were carried out starting at -150 mV relative to the free corrosion potential (after immersion for 30 min) at a sweep rate of 0.2 mV s^{-1} until the anodic branch reached a final current density of 0.01 $mA.cm^{-2}$.

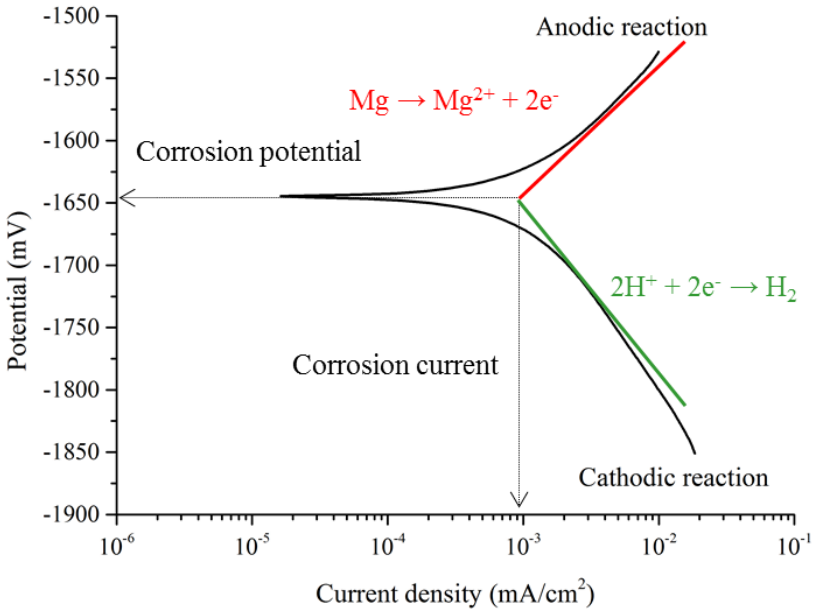

Figure 4-3 Schematic description of the determination of corrosion current from an experimental polarization curve (black solid curve) using Tafel slope (red and green lines)

Electrochemical impedance spectroscopy (EIS) studies were performed at open circuit potential with applied 10 mV RMS sinusoidal perturbation over the frequency range from 30 kHz to 0.01 Hz with 75 points in logarithm for full frequency range. The spectrum that correlates the real and imaginary parts of the impedance (Z) is called Nyquist plot, and the spectrum which correlates total impedance and the phase shift with the applied frequency is called Bode plot. Electrical equivalent circuits consisting of capacitors, resistors and other elements were used to describe appropriate components of the coating (see 6.5.1). Schematic representation of the equivalent circuit and its physical interpretation is shown in Figure 4-4. For instance, the impedance spectrum demonstrates three time constants, consisting of the resistance ($R_{outer\ layer}$) and capacitance ($C_{outer\ layer}$) of the outer layer, the resistance ($R_{inner\ layer}$) and capacitance ($C_{inner\ layer}$) of the inner layer and the polarization resistance (R_{polar}) and double-layer capacitance (C_{polar}) due to the initiation of the corrosion attack. The measurements were repeated at fixed intervals of 0 (after 5 min immersion), 1, 3, 6, 12, 24, 48 and 72 hours of immersion time. The impedance spectra were analyzed using ZView software. The chi-squared of the fitting was less than 0.01.

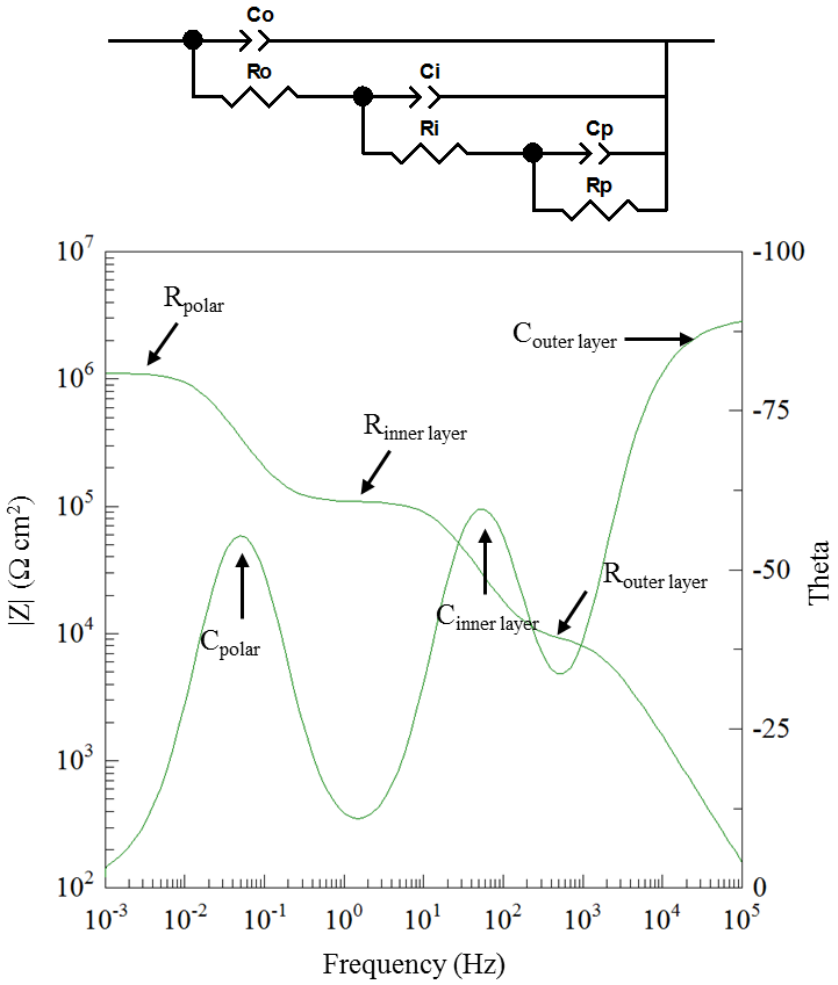

Figure 4-4 Schematic representation of the physical meaning and corresponding equivalent circuit used for fitting

4.3.2 Wear resistance

In Paper 2, the dry sliding wear behavior of the PEO coatings was assessed with a Tribotec ball-on-disc oscillating tribometer with an AISI 52100 steel ball of 6 mm diameter as static friction partner. The wear tests were performed at ambient conditions (25 ± 2 °C and 30 % r.H.) under 1, 3 and 5 N load with oscillating amplitude of 10 mm and at a sliding velocity of 5 mm s^{-1}, for a sliding distance of 12 m. Wear track depth measurements were performed with a Hommel profilometer.

4.3.3 Photocatalytic performance

In Paper 8, the photocatalytic activity of the PEO coatings was evaluated by measuring the degradation rate of aqueous methylene blue (MB) solution. The solution was exposed to light emitted from an incandescent light bulb (OSRAM ULTRA-VITALUX 300 W) for 8 h. The concentration of the MB solution was 5.6 mg/l and the solution volume was 20 ml. An UV-Vis spectrophotometer (Shimadzu UV-1240) was used to measure the concentration change of the MB solution, based on the Beer-Lambert equation stating $A = \varepsilon \times l \times C$ where A, ε, l, and C are absorption of the solution, molar absorptivity, path length, and solution concentration, respectively. Since l and ε are constant, the parameter C is linearly proportional to the absorption. The evolution of absorption of MB solution at λ = 663 nm was measured every 2 h.

5 Results on the basis of published/submitted work

5.1 Frame of the published/submitted paper

The experimental results obtained in frame of the PhD thesis are mainly presented and discussed in the papers published in scientific journals or submitted for publication. This section summarizes, assesses and dicusses 8 complementary published/submitted papers as main core of the thesis. The effect of particle properties (size and melting point), electrolyte composition and electrical parameters on uptake and incorporation of particles as well as the microstructure, composition and properties of PEO coatings has been investigated. The outlines of each paper are addressed below and the connections between the papers are shown in Figure 5-1.

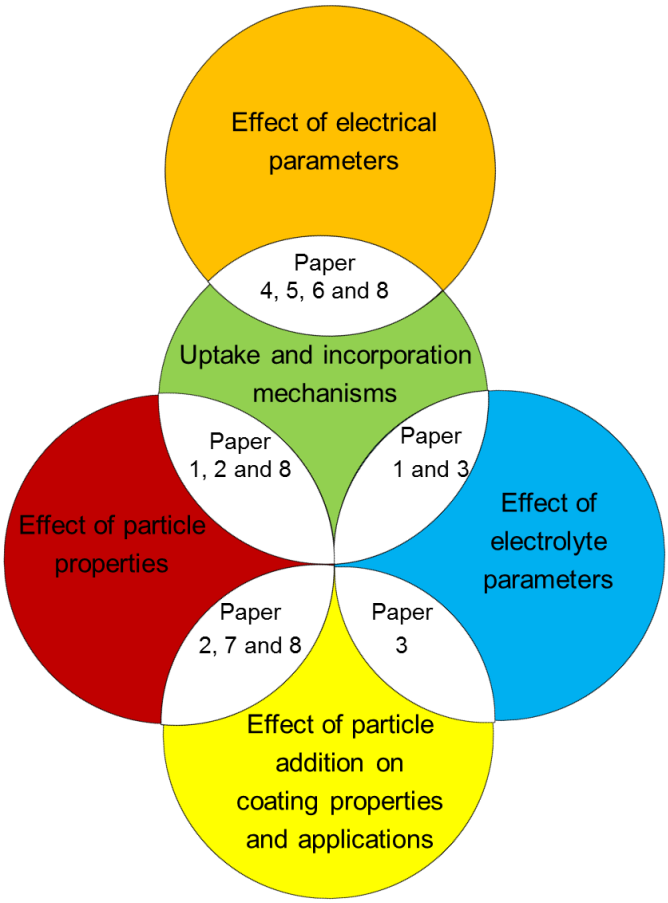

Figure 5-1 Schema of the connection between the papers.

Paper 1: Insights into plasma electrolytic oxidation treatment with particle addition.

In this paper, nano- and micro-sized SiO_2 particles were utilized to investigate the size effect of particles and to provide insights into the possible uptake and incorporation mechanisms of particles during PEO process. It was observed that the size and the melting point of the particles determine the uptake and incorporation mode. Change of the composition of the base electrolyte (concentrations of KOH) has slightly influence on the uptake and incorporation of the particles.

Paper 2: Plasma electrolytic oxidation coatings on Mg alloy with addition of SiO_2 particles.

Based on the findings in Paper 1, the uptake and incorporation mechanisms of particles during PEO process were investigated systematically. The effect of the different-sized SiO_2 particles on the PEO process, and the microstructure, composition and properties of PEO coatings was studied in detail. It was found that the uptake of the nanoparticles occurred mainly via discharge channels and open pores, while micro-sized particles were mainly absorbed via the coating

surface. The nanoparticles achieved reactive incorporation and micro-sized particles achieved inert incorporation, respectively. The results also showed that particle additions enhanced the wear resistance of PEO coating, while the corrosion resistance was reduced to some extent.

Paper 3: Degradation behavior of PEO coating on AM50 magnesium alloy produced from electrolytes with clay particle addition.

Low melting point particles (clay) were added to PEO electrolyte to further confirm the role of the melting point of particles. It was found that the clay particles achieved reactive incorporation into the coating, suggesting that the melting point of the particles has an effect on the incorporation mode. Meanwhile, the influence of the composion of the base electrolyte (concentration of phosphate and hydroxide ions) on the uptake and incorporation of the particles was studied. Single amorphous phase was detected in coatings produced from electrolytes containing higher concentration of phosphate, which degraded rapidly within a short-term in 0.5 wt% NaCl solution. Electrolytes containing higher concentration of KOH produced coatings composed of crystalline and amorphous phases. These layers demonstrated higher corrosion resistance and degradation stability. Thus, the degradation process of PEO coatings was governed mostly by the stability of their phase composition, which might be controlled by varying electrolyte composition.

Paper 4: Influence of electrical parameters on particle uptake during plasma electrolytic oxidation processing of AM50 Mg alloy.

The effect of electrical parameters (frequency and duty ratio) on the uptake and incorporation of SiO_2 particles during PEO treatment was investigated. It was found that frequency and duty ratio applied during PEO treatment have huge effects on the uptake of particles. Higher duty ratio and lower frequency can incorporate more particles into the layer. The size and number of the open pores on the coating surface can be considered as one important factor to determine the particle uptake during PEO process.

Paper 5: Investigation of the formation mechanisms of plasma electrolytic oxidation coatings on Mg alloy AM50 using particles.

In this work, the effect of voltage on the uptake and incorporation of the particles during PEO treatment was investigated. It was found that the incorporation mode of the particles can be

transformed from inert incorporation to reactive incorporation under higher voltage during PEO process. The uptake of the particles is primarily related to the pore feature on the coating surface. Additionally, inert particles were used as tracers to investigate the formation mechanisms of PEO coatings. The growth direction and kinetics of the coating formation were primarily controlled by the intensity and the number of discharges. High-intensity discharges enabled the inward growth of the PEO coating rapidly. Low-intensity discharges allowed the outward growth of the coating at a slow speed. At the initial stage of a treatment, conversion products formed locally around the intermetallics and disseminated gradually. Discharges appeared after reaching the breakdown potential, leading to rapid growth of the coating. The outward growth of the layer was non-uniform and the inward growth of the layer occurs preferentially around intermetallic phases and the formation of the inner layer was related to the inward growth.

Paper 6: 3D reconstruction of plasma electrolytic oxidation coatings on Mg alloy via synchrotron tomography.

In this paper, synchrotron-based microtomography was used to generate 3D visualization of PEO coatings on Mg alloy. The 3D reconstruction provided intuitional structure of the layer without the risk of embedding artificial materials from the conventional metallographic preparation. Inert La_2O_3 particles have been introduced as markers during the PEO process to understand the coating growth. The microtomography analysis showed that porosity of the coating reaches up to 26.25 % at the initial stage and decreases with the layer growth under a potentiostatic regime. The particles are individually distributed in the layer at the beginning of the treatment. Due to the coating growth, the uptake of the particles is continually increased leading to agglomeration in the layer.

Paper 7: Influence of incorporating Si_3N_4 particles into the oxide layer produced by plasma electrolytic oxidation on AM50 Mg alloy on coating morphology and corrosion properties.

The influence of addition of different sizes of Si_3N_4 particles on the microstructure and corrosion properties of PEO coatings was investigated. It was found that Si_3N_4 particles were inertly incorporated into the coating due to their relatively high melting point. Microstructure observations by SEM showed that the surface of the coating was sealed to some extent, while the coating became much thinner with the addition of particles. The corrosion performance of the layer was deteriorated after introduction of particles.

Paper 8: Formation of photocatalytic plasma electrolytic oxidation coatings on magnesium alloy by incorporation of TiO_2 particles.

Photocatalytically active plasma electrolytic oxidation coatings on AM50 Mg alloy were produced in this paper. The photocatalytic activity was achieved via introduction of anatase (TiO_2 particles) to the treatment bath. The photocatalytic performance of the coating was evaluated by measuring the degradation rate of aqueous methylene blue solution and was primarily related to the anatase content on the coating surface. It was found that higher amount of particles in the electrolyte and lower voltage applied during treatment can incorporate more anatase into the layer and generate superior photocatalytic coatings, suggesting that higher concentration of particles in the electrolyte contributed to particle uptake and higher voltage induced phase transformation of the particles.

5.2 Insights into plasma electrolytic oxidation treatment with particle addition *(with permission from Elsevier)*

Corrosion Science 101 (2015) 201–207

Contents lists available at ScienceDirect

Corrosion Science

journal homepage: www.elsevier.com/locate/corsci

Short communication

Insights into plasma electrolytic oxidation treatment with particle addition

Xiaopeng Lu*, Carsten Blawert, Mikhail L. Zheludkevich, Karl Ulrich Kainer

Institute of Materials Research, Helmholtz-Zentrum Geesthacht, Max-Plank-Str. 1, 21502 Geesthacht, Germany

ARTICLE INFO

Article history:
Received 13 April 2015
Received in revised form
18 September 2015
Accepted 19 September 2015
Available online 25 September 2015

Keywords:
A. Alloy
A. Magnesium
B. SEM
B. XRD
C. Oxide coatings

ABSTRACT

Plasma electrolytic oxidation (PEO) processing has received considerable attention for improving the corrosion or wear resistance of magnesium and its alloys. However, it cannot provide high-barrier long-term protection due to its high porosity. A novel approach is to introduce reactive particles to PEO coatings, aiming to seal the porosity and to provide wider range of coating compositions. Experiments with nano- and micro-sized SiO_2 particles and different concentrations of KOH in the electrolyte provide new insights into possible up-take and incorporation mechanisms of particles during PEO processing.

© 2015 Elsevier Ltd. All rights reserved.

1. Introduction

Plasma electrolytic oxidation (PEO) is a promising surface treatment process to produce ceramic-like coatings on light metals (Mg, Al and Ti) and their alloys, with incorporation of species originating from the substrate and the electrolyte, for corrosion protection and wear resistance for biomedical applications [1–6]. The process accompanies a large number of short-lived microdischarges, caused by dielectric breakdown of oxide film at relatively high voltages, leading to coatings with high porosity. Some defects are generated by entrapped gas or rapid cooling after the sparks are extinguished. Thus, sealing or avoidance of the high porosity is essential to improve the coating properties. Particle addition into PEO coatings is a novel approach to obtain a type of in situ sealing. Arrabal et al. [7,8] fabricated coatings with ZrO_2 nanoparticle additions and assumed that the particles were transferred to the interface between the inner/outer layer through short-circuit paths in the outer layer. Lee et al. demonstrated that the electrophoretic mobility and mechanical mixing in molten magnesium oxide were main factors leading to particle incorporation [9]. Necula et al. [10] introduced Ag nanoparticles to PEO coating. They assumed that particles can be preserved in the coating after they are delivered and entrapped in the sites of coating growth. Up to now, the proposed particle incorporation theories are limited, as they only focus on nanoparticles and do not explain the principles for various incorporation regimes.

If particles are incorporated without a reaction or no new phase formation, it is considered to be an inert incorporation. The other possibility is reactive or partly reactive incorporation, when the particles melt through the high energy discharges and then react with other components from the electrolyte and the matrix. The melting point of the particles is one crucial factor to determine the incorporation mode. Generally, the plasma electron temperature during PEO process is above 3000 K [11,12], which is much higher than the melting point of the most frequently used particles [8,10,13–15]. Nevertheless, partly reactive or inert incorporation of the particles into the coating is normally observed. Thus, it may be deduced that the particle size is an important factor as the short-lived discharges may not be able to completely melt large particles. It is also generally known that nanoparticles have a lower melting temperature compared with the large particles of the same material [16,17]. However, various nanoparticles can still be incorporated inertly [13,18]. Hence, the nature of the particle itself, i.e., chemical stability and type of bonds, may determine the way particles participate in the PEO processing. For example, it is hard to achieve reactive incorporation for metallic particles (Ag), while it is more easily to realize for inorganic particles.

The present work investigates the influence of the amount and the size of SiO_2 particles, and MgO/SiO_2 ratio on the coating formation, aiming to understand the different mechanisms of particle

* Corresponding author. Fax: +49 4152871960.
E-mail address: xiaopeng.lu@hzg.de (X. Lu).

http://dx.doi.org/10.1016/j.corsci.2015.09.016
0010-938X/© 2015 Elsevier Ltd. All rights reserved.

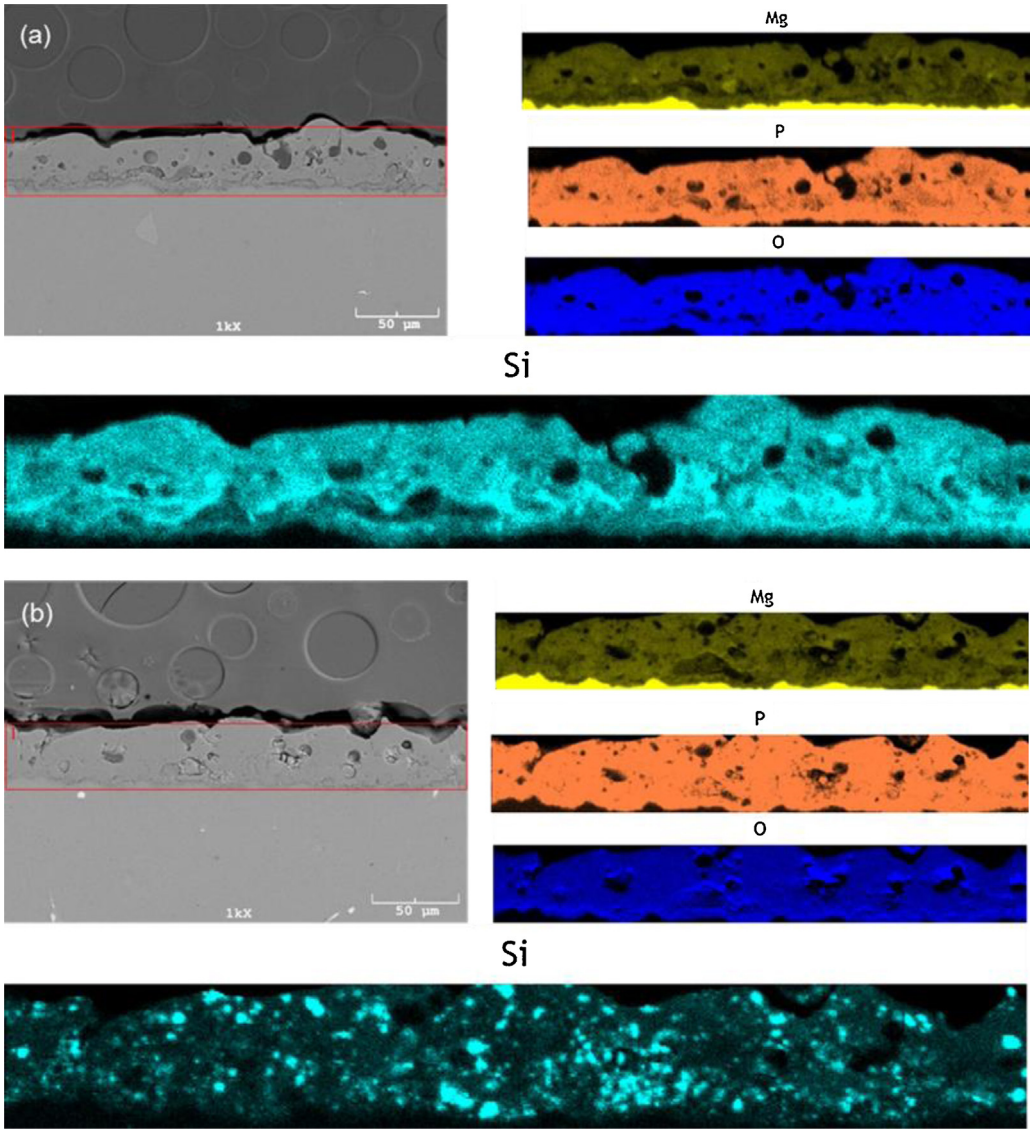

Fig. 1. SEM images of the cross section and Si mapping of the PEO coatings with particle addition (a) PEO (n), (b) PEO (μ).

up-take and incorporation based on analyses of the different coating microstructures and compositions.

2. Experimental

AM50 magnesium alloy samples with dimensions of 15 mm × 15 mm × 4 mm were treated by a pulsed DC power supply (t_{on}:t_{off} = 0.4 ms:3.6 ms) under constant voltage regime (450 V) for 10 min. The chemical composition of AM50 alloy, as measured with an Arc/Spark Optical Emission Spectroscopy system (Spark analyser M9, Spectro Ametek, Germany), is 4.74 wt.% Al, 0.383 wt.% Mn, 0.065 wt.% Zn, 0.063 wt.% Si, 0.002 wt.% Fe, 0.002 wt.% Cu and Mg balance. The electrolyte consisted of KOH (1 g/l), Na_3PO_4 (20 g/l) and 5 g/l SiO_2 particles with size of 12 nm avg. and 1–5 μm, respectively. Electrolytes with high concentration of KOH (8 g/l) were prepared to investigate the influence of the MgO/SiO_2 ratio on SiO_2 particles up-take (Table 1). PEO coatings without particle addition were produced for comparison. A stirrer and bubbling with compressed air were used to disperse particles uniformly. The temperature of the electrolytes was kept at 10 ± 2 °C using water cooling system. A scanning electron microscope (TESCAN Vega3 SB) equipped with EDS was used to examine the microstructure and composition of the PEO coatings. X-ray diffraction (XRD) investigations were conducted using a Siemens diffractometer operating at 40 kV and 40 mA with Cu Kα radiation.

Table 1
Electrolyte composition for PEO treatment.

Coating	KOH (g/l)	Na_3PO_4 (g/l)	SiO_2 (g/l, 12 nm)	SiO_2 (g/l, 1–5 μm)
PEO	1	20	–	–
PEO (n)	1	20	5	–
PEO (μ)	1	20	–	5
HPEO	8	20	–	–
HPEO ($n-2$)	8	20	2	–
HPEO ($n-5$)	8	20	5	–
HPEO ($\mu-2$)	8	20	–	2
HPEO ($\mu-5$)	8	20	–	5

3. Results and discussion

The cross-sections and EDS maps of the coatings with 5 g/l nano- and micro-sized SiO_2 particle addition are shown in Fig. 1. Mg, P, O and Si elements were detected as the main elements in both PEO

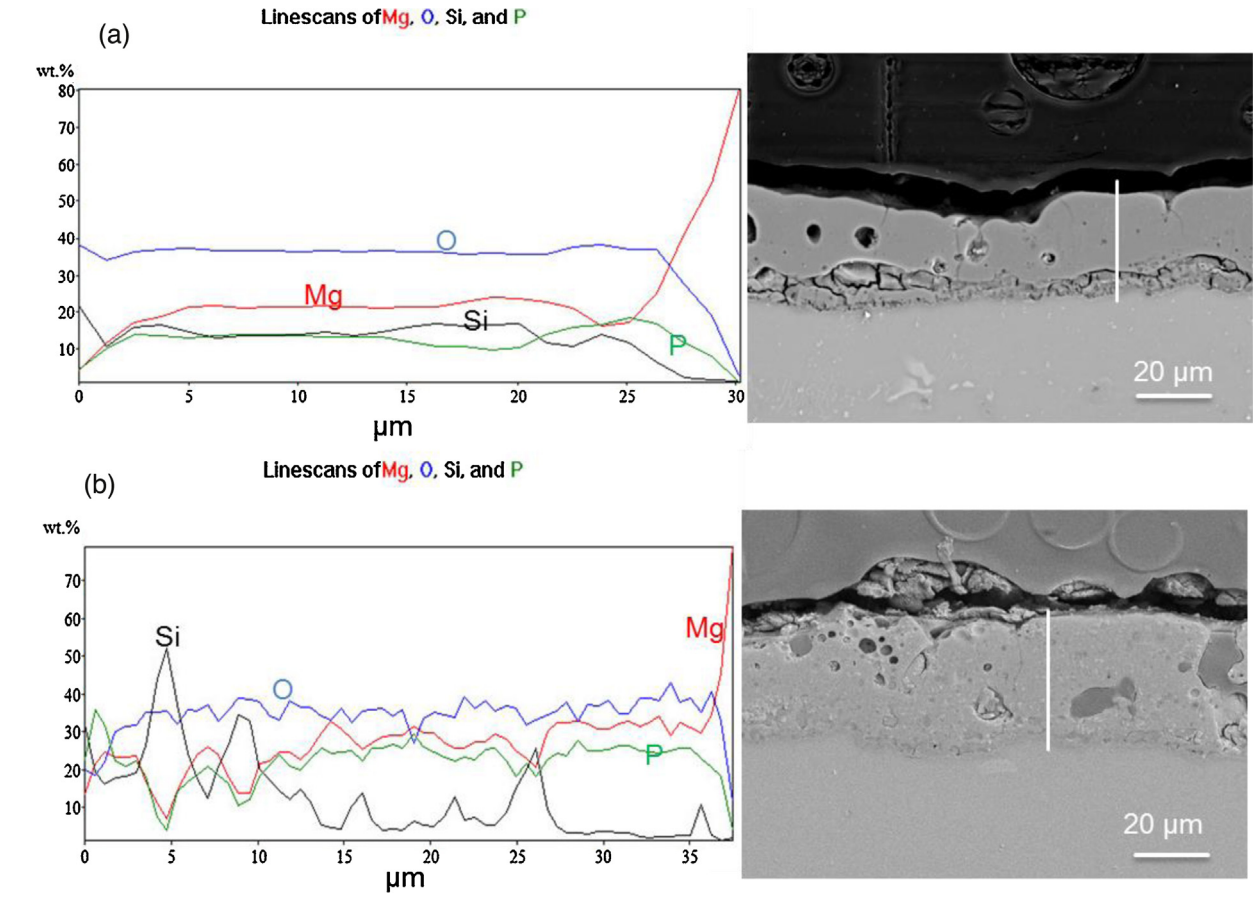

Fig. 2. EDS line scan across (a) PEO (n), (b) PEO (μ).

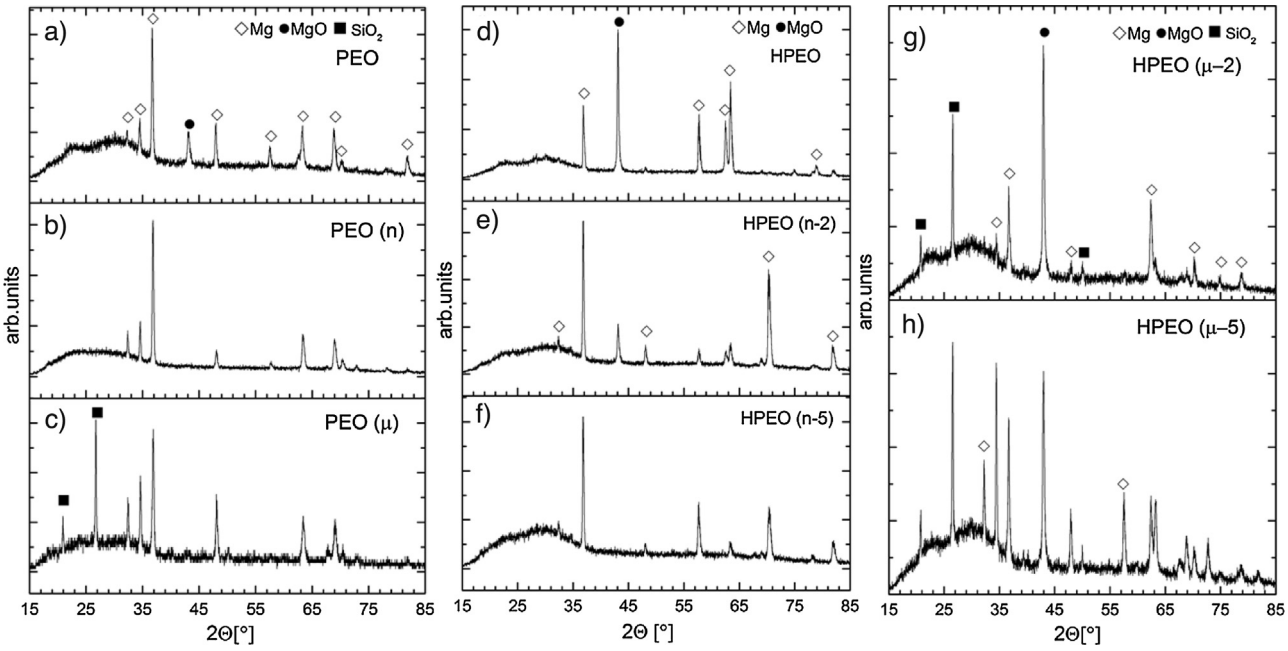

Fig. 3. XRD patterns of the PEO coatings (a) PEO, (b) PEO (n), (c) PEO (μ), (d) HPEO, (e) HPEO ($n-2$), (f) HPEO ($n-5$), (g) HPEO ($\mu-2$), (h) HPEO ($\mu-5$).

coatings. Significant amounts of potassium and sodium were not detected and, these maps are not shown. Phosphorus and oxygen are relatively uniformly distributed in the two coatings. As expected the magnesium signal is diluted in all the coatings. For Si, one could observe an important difference between the two coatings. If nano-sized particles were used, Si distributes more homogeneously and the Si signal is more intense throughout the entire layer. In addition, strong Si signals are detected from the walls of the pore band between the outer and inner layer in the presence of nanoparticles. If micro-sized particles are used, only localized signals of high

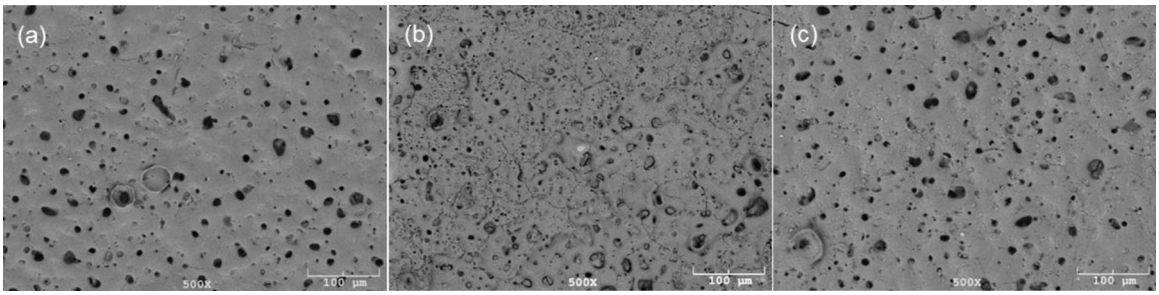

Fig. 4. Surface morphology of the PEO coatings (a) PEO, (b) PEO (n), (c) PEO (μ).

Table 2
Surface composition (at.%) of PEO coatings determined by EDS analysis.

Coating	O	Na	Mg	Al	Si	P	K
PEO	58	7	22	1.5	–	11	–
PEO (n)	56	8	17	1	9	9	–
PEO (μ)	60	6.5	18	1	5	9	–
HPEO	55	5	27.5	1.5	–	10	1
HPEO ($n-2$)	58	5	23	1.5	3	9	1
HPEO ($n-5$)	52	6	21	1	9.5	8	2
HPEO ($\mu-2$)	53	5	26	1	3.9	10	1
HPEO ($\mu-5$)	54	5	24	1	5	9	1.5

intensity are detected relatively uniformly throughout the coating. They are typically size of single macro-particles or small agglomerations of particles. There is only very weak Si signal in areas surrounding the particle of the coating, indicating that the particles are likely to be incorporated inertly into the coating. These observations are supported by the elemental distribution (Fig. 2) of EDS line scan across the cross section of both PEO coatings. All elements are quite uniformly distributed throughout the cross section for PEO (n). Si has a slightly higher concentration close to the surface and in the region of the pore band indicating that these two regions might be enriched with more SiO_2 nanoparticles. The surface and the open porosity of the coating are obviously places of a preferred up-take of nanoparticles. In the case of the coating loaded with large-sized particles, the concentrations of Mg, O, and P reveal much stronger variations in intensity. This is a hint that the coating is composed of several phases, which are not uniformly distributed. The same is true for the distribution of Si which shows intensity peaks when a particle is located within the region of the line-scan. The localized signals observed in the mapping and the appearance of peaks in the line-scan are indicative of some unreacted particles. Furthermore, different phases and growth mechanisms might be responsible for the different coating thicknesses, although the same treatment parameter except the particle size was used.

The XRD profiles show a large broad bump distributed over 2θ angles between 20–35° for all the coatings (Fig. 3). This shows that the coatings may contain amorphous or nanocrystalline phases, most likely $Mg_3(PO_4)_2$ [5,19]. Additionally, there are some magnesium peaks, suggesting that the X-rays reflection from substrate can also be observed. For the coating obtained from electrolyte without particles, the second main coating phase is magnesium oxide. After introduction of nanoparticles, the crystalline MgO phase is not visible (Fig. 3b). It can be inferred that the SiO_2 nanoparticles incorporate reactively through the formation of a new glassy phase together with MgO and $Mg_3(PO_4)_2$. For PEO (μ), SiO_2 peaks and a small MgO peak are observed (Fig. 3c). The influence of particles on coating composition is shown in Table 2. The detection of silicon suggests that all type of particles have been successfully incorporated into the coating, as there is no other silicon source except for SiO_2 particles in the phosphate electrolyte. A higher amount of Si was detected for coatings with nanoparticle addition, which might indicate that it is easier to incorporate nano-sized particles rather than micro-sized particles, mainly because of the size effect allowing nano-sized particles to enter the coating more easily and frequently via the open pores and old discharge channels.

As shown above, the differences in microstructure and coating composition suggest that the particle size has a significant effect on the up-take and incorporation mode of the particles. To further confirm the correlation between the particle size/incorporation mode and the reaction with MgO and $Mg_3(PO_4)_2$ phase, coatings were produced from electrolytes containing a higher concentration of KOH and different particle concentrations. A higher hydroxide concentration generally endows PEO coating with higher amount of MgO [20]. This is clearly observed in the XRD results in Fig. 3d. The intensity of MgO peak decreases to some extent with the addition of 2 g/l SiO_2 nanoparticle and then disappears when the particle concentration further increases to 5 g/l, suggesting that the MgO phase is consumed and react with the nanoparticles during coating formation. Thus, the presence of MgO is one of the preconditions for the reactive incorporation of SiO_2 particles. It is most likely that phosphate is also involved in the formation of the new phase, since Si and P are known to promote glass formation [21,22]. In contrast, the large-sized SiO_2 particles do not react and the amount of MgO is not significantly affected (Fig. 3g and h). Hence, it can be inferred that the nature of particles and the electrolyte have synergistic effect on the incorporation mode. According to the MgO–SiO_2 phase diagram [23], oxide mixtures can be melted easier than the pure oxides with the lowest melting temperatures obtained for the compositions close to the stoichiometric $MgSiO_3$ phase. Assuming that glass compositions are reached during PEO processing it can be deduced that the SiO_4-network is weakened by MgO addition resulting in a lower glass transition temperature or melting interval. Furthermore, Na_2O, K_2O and phosphate from the electrolyte are incorporated into the coating reducing the melting interval to even lower temperature. Considering the lower melting temperature of SiO_2 nanoparticles compared with the micro-sized particles, liquid phase sintering is likely to occur during PEO processing if the oxide mixture is in the appropriate composition range. The nanoparticle addition influences the pore distribution and appearance on the coating surface (Fig. 4). The number of large pores observed in the systems with micro-particles or particle free coating is significantly reduced and majority of the pores appear to be at least partially sealed with material in the center. Due to the molten nanoparticles, a larger volume of liquid phase is produced under the same energy input by the discharges, which was not observed for large-sized particles.

For particles to participate in the PEO processing, they need to be delivered to the electrolyte/coating interface with the aid of an external force. The interaction with particles during PEO processing can be divided into two steps consisting of firstly an uptake step and a final incorporation step. For the uptake step, one of the most prominent factors, which can bring the particles to the vicinity of the anode, is electrophoretic force. After dispersion in the alkaline electrolyte and combination with hydroxide ions, the particles will

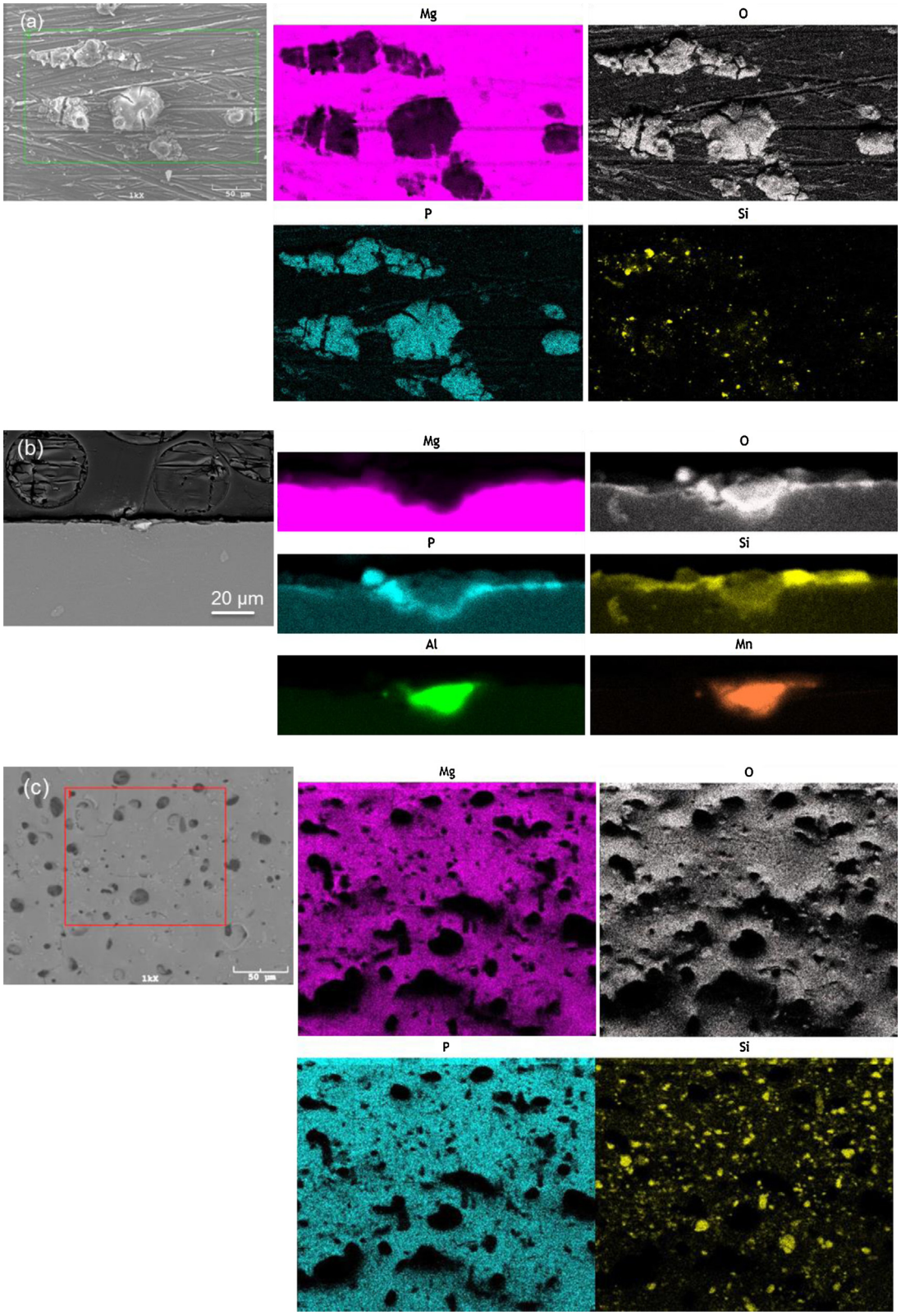

Fig. 5. Distribution of particles on coatings produced at different treatment time (a) and (b) before breakdown potential, (c) at the end of treatment.

become negatively charged [24]. Therefore the particles migrate towards the anode under the applied high electric field, but also the stirred and compressed air bubbled electrolyte may contribute to the movement of the particles towards the anode. In the beginning of a treatment the up-take of particles is dominated by adhering to the corrosion products. It is well-known that localized corrosion initiates around the interface between the intermetallics (Al–Mn particles) and Mg matrix due to galvanic coupling [25,26]. As a consequence, up-take of the negatively charged particles before the breakdown potential can be considered as an adsorption process in

regions with enhanced anodic dissolution and strong re-deposition of reaction products e.g. around cathodically acting intermetallics (Fig. 5a and b). After the breakdown potential, the existence of melt pools on the surface generated by the discharges would contribute to an easier up-take regime for particles which can stick easier on the melted coating surface (Fig. 5c).

Once a PEO coating covers the surface, the microstructure and pore distribution of PEO coating have an influence on the uptake and incorporation of particles. All defects in the coating can be considered as fast pathways for particles to propagate into the internal part of the coating. Somehow, the PEO coating can be considered as a ceramic sponge and the up-take of particles rely on the open porosity which normally changes with the processing time. The size and lifetime of the open pores on the coating surface, which can be linked to the intensity and lifetime of the discharges, determines the amount and size of particles which can penetrate into the coating. The discharges are the driving force for the growing coating with its open porosity and they close and generate new up-take option via the open pores throughout the whole process. The reservoir for these penetrated particles relies on the discharge type. Based on Hussein et al. [12], strong discharges may result in concentrated nanoparticles in the pore band, and weak discharges enrich the particles in the defects of the outer layer.

Thus the nano-sized particles find a second path way for up-take via open pores very early in the PEO process. In contrast, the only option for up-take of large particles during the early stages of a treatment is via pasting mode in molten material erupted by discharges forming melt pools on the surface. However, the chance for bigger particles to enter via open porosity increases with treatment time as the discharges change during the PEO processing. There is a direct link between the coating thickness, the strength or the size of the discharges and size of open porosity. Simply speaking, the thicker the coating grows, the stronger the driving discharges have to be and the larger the pores as a result of the remaining discharge channels are. The final result can be seen in a higher Si content in the coating if nano-sized particles are used instead of micro-sized particles.

After up-take the particles have to be fully integrated into the coating. This incorporation step is mainly controlled by the interaction of the particles with the discharges. The majority of the nano-sized particles will pile up in the open pores and the majority of the micro-sized particles adhere to the surface awaiting mixture with already existing coating material, conversion products (reaction products of dissolved substrate and electrolyte compounds deposited from the electrolyte when solubility is exceeded), and soluble compounds from the electrolyte and substrate by the discharges. Reactive incorporation occurs if the particles are melted and react with other phases in the coating. If the right amount and type of oxides form on the surface and if the additional elements and compounds provided by the electrolyte together give phase mixtures with lower fusion point, liquid phase sintering can occur to a larger extent when the energy of the discharges is sufficiently high. The liquid phases can react faster with the remaining solid compounds forming higher melt volumes and form new compounds if quenching is fast enough when the discharge finishes. Preferentially, this is the case when the mixed phases form a new phase with lower melting point (e.g., MgO and SiO_2 combining to $MgSiO_3$).

However, the nature of particle itself, the size and the melting point, determines its reactivity and incorporation mode. Size is an important factor because larger particles need longer heating-up time to reach the melting temperature and lifetime of a discharge might not be sufficiently long. The smaller particles can be heated up faster than larger particles thus the reactive incorporation is more likely for nanoparticles than for the micro-sized particles. Furthermore, the nanoparticles from the same material have lower melting point compared with the bulk or larger particles, so they can be used as a kind of sinter additive to ease coating formation. The results from the present study show that the concept works. The XRD results show the consumption of MgO in the presence of the nanoparticles and only a broad bump without the formation of crystalline $MgSiO_3$ was observed. Based on this, it may be speculated that the first formation of liquid phase by reactive $MgSiO_3$ formation stimulates further reaction with other oxides/phosphate phases forming a type of glass with even lower melting temperature (e.g., a combination of Na_2O, K_2O, MgO, SiO_2 and P_2O_5). Only with the addition of nano-sized particles, a reactive or partly reactive incorporation and the formation of new glassy phase can be reached. For micro-sized particles the coating formation works in the same mode as without particle addition. There is no significant reaction between the micro-sized particles and the other compounds, and the growing coating is simply embedding the particles.

4. Conclusions

The work described here demonstrates that particle addition into PEO coating can be divided into two steps consisting of a first uptake and a final incorporation step. Before reaching breakdown potential, up-take of particles occurs mainly via an adsorption process caused by electrophoretic force, resulting in adhering to the corrosion products around the intermetallics. The situation changes after reaching the breakdown potential. Up-take of the nanoparticles is by means of the open pores as well as the discharge channels of the sponge-like coating. Up-take of the micro-sized particles occurs mainly via the surface by sticking on the melted materials and then being encapsulated by the growing layer. The nanoparticles are more easily to be delivered to participate in the subsequent coating formation process in comparison to the micro-sized particles.

The nature of the particle itself, i.e., size and melting point, determines its reactivity and incorporation mode. Smaller particles with low melting point, i.e., SiO_2 nanoparticles, are reactively or partly reactively incorporated into the coating, while micro-sized SiO_2 particles are mainly inertly incorporated. Triggered by the additional SiO_2 nanoparticles, liquid phase sintering can occur to a larger extent if the energy of the discharges is high enough and if the MgO–SiO_2 ratio allows lowering of the fusion temperatures as the possible starting step of liquid phase sintering.

Acknowledgements

The authors thank Dr. Chamini Mendis for helpful discussions and English corrections. The technical support of Mr. Volker Heitmann and Mr. Ulrich Burmester during the course of this work is gratefully acknowledged. X. Lu thanks China Scholarship Council for the award of fellowship and funding.

References

[1] A.L. Yerokhin, X. Nie, A. Leyland, A. Matthews, S.J. Dowey, Plasma electrolysis for surface engineering, Surf. Coat. Technol. 122 (1999) 73–93.
[2] T.H. Teh, A. Berkani, S. Mato, P. Skeldon, G.E. Thompson, H. Habazaki, K. Shimizu, Initial stages of plasma electrolytic oxidation of titanium, Corros. Sci. 45 (2003) 2757–2768.
[3] F. Liu, D. Shan, Y. Song, E.-H. Han, W. Ke, Corrosion behavior of the composite ceramic coating containing zirconium oxides on AM30 magnesium alloy by plasma electrolytic oxidation, Corros. Sci. 53 (2011) 3845–3852.
[4] S.P. Sah, E. Tsuji, Y. Aoki, H. Habazaki, Cathodic pulse breakdown of anodic films on aluminium in alkaline silicate electrolyte—understanding the role of cathodic half-cycle in AC plasma electrolytic oxidation, Corros. Sci. 55 (2012) 90–96.
[5] Y. Mori, A. Koshi, J. Liao, H. Asoh, S. Ono, Characteristics and corrosion resistance of plasma electrolytic oxidation coatings on AZ31B Mg alloy formed in phosphate—silicate mixture electrolytes, Corros. Sci. 88 (2014) 254–262.

[6] L. Zhang, J. Zhang, C.-F. Chen, Y. Gu, Advances in microarc oxidation coated AZ31 Mg alloys for biomedical applications, Corros. Sci. 91 (2015) 7–28.
[7] R. Arrabal, E. Matykina, P. Skeldon, G.E. Thompson, Incorporation of zirconia particles into coatings formed on magnesium by plasma electrolytic oxidation, J. Mater. Sci. 43 (2008) 1532–1538.
[8] R. Arrabal, E. Matykina, F. Viejo, P. Skeldon, G.E. Thompson, M.C. Merino, AC plasma electrolytic oxidation of magnesium with zirconia nanoparticles, Appl. Surf. Sci. 254 (2008) 6937–6942.
[9] K.M. Lee, K.R. Shin, S. Namgung, B. Yoo, D.H. Shin, Electrochemical response of ZrO_2-incorporated oxide layer on AZ91 Mg alloy processed by plasma electrolytic oxidation, Surf. Coat. Technol. 205 (2011) 3779–3784.
[10] B.S. Necula, I. Apachitei, F.D. Tichelaar, L.E. Fratila-Apachitei, J. Duszczyk, An electron microscopical study on the growth of TiO_2–Ag antibacterial coatings on Ti_6Al_7Nb biomedical alloy, Acta Biomater. 7 (2011) 2751–2757.
[11] R.O. Hussein, X. Nie, D.O. Northwood, A. Yerokhin, A. Matthews, Spectroscopic study of electrolytic plasma and discharging behaviour during the plasma electrolytic oxidation (PEO) process, J. Phys. D: Appl. Phys. 43 (2010) 105203.
[12] R.O. Hussein, X. Nie, D.O. Northwood, An investigation of ceramic coating growth mechanisms in plasma electrolytic oxidation (PEO) processing, Electrochim. Acta 112 (2013) 111–119.
[13] L.J. Guo, S.C. Wang, J. Wang, Q. Liang, F.X. Yan, Preparation and performance of a novel multifunctional plasma electrolytic oxidation composite coating formed on magnesium alloy, J. Mater. Sci. 44 (2009) 1998–2006.
[14] T.S. Lim, H.S. Ryu, S.-H. Hong, Electrochemical corrosion properties of CeO_2-containing coatings on AZ31 magnesium alloys prepared by plasma electrolytic oxidation, Corros. Sci. 62 (2012) 104–111.
[15] R. Arrabal, A. Pardo, M.C. Merino, M. Mohedano, P. Casajús, E. Matykina, P. Skeldon, G.E. Thompson, Corrosion behaviour of a magnesium matrix composite with a silicate plasma electrolytic oxidation coating, Corros. Sci. 52 (2010) 3738–3749.
[16] W.H. Qi, M.P. Wang, Size and shape dependent melting temperature of metallic nanoparticles, Mater. Chem. Phys. 88 (2004) 280–284.
[17] A.F. Lopeandía, J. Rodríguez-Viejo, Size-dependent melting and supercooling of Ge nanoparticles embedded in a SiO_2 thin film, Thermochim. Acta 461 (2007) 82–87.
[18] B.S. Necula, L.E. Fratila-Apachitei, A. Berkani, I. Apachitei, J. Duszczyk, Enrichment of anodic MgO layers with Ag nanoparticles for biomedical applications, J. Mater. Sci.: Mater. Med. 20 (2009) 339–345.
[19] J. Liang, P.B. Srinivasan, C. Blawert, W. Dietzel, Comparison of electrochemical corrosion behaviour of MgO and ZrO_2 coatings on AM50 magnesium alloy formed by plasma electrolytic oxidation, Corros. Sci. 51 (2009) 2483–2492.
[20] Y.G. Ko, S. Namgung, D.H. Shin, Correlation between KOH concentration and surface properties of AZ91 magnesium alloy coated by plasma electrolytic oxidation, Surf. Coat. Technol. 205 (2010) 2525–2531.
[21] K. Ikarashi, T. Mizushima, A. Makino, A. Inoue, Preparation of the bulk Fe–Al–Ga–P–C–B–Si glassy alloys in a ringed form by copper mold casting, Mater. Sci. Eng. A 304–306 (2001) 763–766.
[22] B. Shen, M. Akiba, A. Inoue, Enhancement of glass-forming ability of FeGaPCB bulk glassy alloy with high saturation magnetization, Intermetallics 15 (2007) 655–658.
[23] P. Wu, G. Eriksson, A.D. Pelton, M. Blander, Prediction of the thermodynamic properties and phase-diagrams of silicate systems—evaluation of the FeO–MgO–SiO_2 System, ISIJ Int. 33 (1993) 26–35.
[24] L.Q. Zhu, Y.H. Li, W.P. Li, Influence of silica sol particle behavior on the magnesium anodizing process with different anions addition, Surf. Coat. Technol. 202 (2008) 5853–5857.
[25] A. Pardo, M.C. Merino, A.E. Coy, R. Arrabal, F. Viejo, E. Matykina, Corrosion behaviour of magnesium/aluminium alloys in 3.5 wt.% NaCl, Corros. Sci. 50 (2008) 823–834.
[26] A. Němcová, P. Skeldon, G.E. Thompson, B. Pacal, Effect of fluoride on plasma electrolytic oxidation of AZ61 magnesium alloy, Surf. Coat. Technol. 232 (2013) 827–838.

5.3 Plasma electrolytic oxidation coatings on Mg alloy with addition of SiO_2 particles *(with permission from Elsevier)*

Electrochimica Acta 187 (2016) 20–33

Contents lists available at ScienceDirect

Electrochimica Acta

journal homepage: www.elsevier.com/locate/electacta

Plasma electrolytic oxidation coatings on Mg alloy with addition of SiO_2 particles

Xiaopeng Lu*, Carsten Blawert, Yuanding Huang, Henry Ovri, Mikhail L. Zheludkevich, Karl Ulrich Kainer

Institute of Materials Research, Helmholtz Zentrum Geesthacht, Max-Plank-Str. 1, 21502 Geesthacht, Germany

ARTICLE INFO

Article history:
Received 21 July 2015
Received in revised form 5 November 2015
Accepted 6 November 2015
Available online 10 November 2015

Keywords:
Plasma electrolytic oxidation
Magnesium alloy
Particle addition

ABSTRACT

The addition of particles into plasma electrolytic oxidation (PEO) electrolyte provides a possibility to produce functionalized coatings with a wider range of compositions and new phases. In this study, nano- and micro-sized SiO_2 particles were in-situ incorporated into phosphate-based coatings and the effect of these particles on the microstructure, composition and properties of the coatings was investigated. It was observed that the size and the melting point of the particles have a synergistic effect on the uptake and incorporation mode. The uptake of the nanoparticles occurred mainly via discharge channels and open pores, while micro-sized particles were mainly absorbed via the coating surface. Different particle properties result in reactive and inert incorporation for the nano- and micro-sized SiO_2 particles, respectively. The results show that particle additions improve the wear resistance of PEO coating, although corrosion resistance is slightly reduced. Due to superior wear performance and degradability, PEO coatings with reactively incorporated nanoparticles on Mg alloy might be suitable for bio-medical application.

© 2015 Elsevier Ltd. All rights reserved.

1. Introduction

Various surface treatments have been applied to magnesium and its alloys, such as conversion coatings, electroplating and electroless plating, anodizing, plasma electrolytic oxidation, organic coatings and vapor-phase processes [1–6], aiming to improve their corrosion and wear resistance. In particular, plasma electrolytic oxidation (PEO) has been regarded as an effective and environmental-friendly method for enhancing the properties of Mg and its alloys [7,8]. The formation mechanisms of the PEO coating are complex, as it involves electro-, thermo-, and plasma-chemical reactions in the electrolyte and metal-electrolyte interface [9]. The process is accompanied by a large number of short-lived microdischarges, caused by dielectric breakdown of the oxide film at relatively high voltage, leading to the coatings with high porosity. PEO coatings on Mg alloys typically reveal a two-layered structure, comprising a thin inner barrier layer adjacent to the substrate and an outer porous layer [10–12]. It is generally accepted that the barrier layer is responsible for the anticorrosion properties, whereas the outer layer is of high porosity but provides wear resistance. It has also been shown that long treatment time or high voltages promote the formation of large discharge channels, resulting in more porous coatings [13,14]. Even though the porous coating can avoid direct contact between the substrate and the corrosive environment, the corrosive medium (NaCl) can penetrate through the layer rapidly, especially when the coating possesses large volume of discharge channels and defects. Thus sealing the porous layer is crucial to improving the corrosion and wear performance of PEO coatings.

There are several possibilities to seal or prevent the high porosity of PEO coatings. Sealing with additional coatings, such as sol-gel [15,16] and polymer coating [17], are commonly used to improve protective ability of the PEO coating. For instance, better anti-corrosion properties were achieved after deposition of a titanium sol-gel layer on a PEO film [15]. Similarly, the introduction of corrosion inhibitors into the pores before sealing has shown considerable improvement in corrosion resistance of PEO coatings [16]. Duan et al. [17] showed that better corrosion performance can be achieved by fabricating an additional layer on top of the PEO coating with sealing agent. Another way is adding additives directly to the electrolyte to improve the microstructure and properties of the coatings. For example, the addition of glycerol to the electrolyte led to the formation of a smooth coating with reduced pore size and cracks [18]. In another work [19], it was

* Corresponding author. Tel.: +494152871943; fax: +494152871960.
E-mail address: xiaopeng.lu@hzg.de (X. Lu).

http://dx.doi.org/10.1016/j.electacta.2015.11.033
0013-4686/© 2015 Elsevier Ltd. All rights reserved.

Table 1
Composition, conductivity and pH value of the electrolytes for PEO treatment.

Electrolytes	KOH (g/l)	Na_3PO_4 (g/l)	SiO_2 (g/l)	Conductivity (mS cm^{-1})	pH
Without particle	1	20	0	22.5	12.5
With nano-sized particle (amorphous)	1	20	5	22.2	12.7
With micro-sized particle (crystalline)	1	20	5	22.7	12.6

reported that addition of $CeCl_3$ increased the conductivity of the base electrolyte, decreased the breakdown voltage and enabled the formation of a uniform coating.

In-situ incorporation of particles into the coating, such as Ag, ZrO_2, CeO_2, TiO_2, Si_3N_4, Al_2O_3, SiC, SiO_2, hydroxyapatite (HA) and clay, have been explored as new strategies to provide the coatings with a wider range of compositions and functionalities [11,20–27]. Normally, nano-sized particles are preferred choice of additives for PEO electrolytes. All the aforementioned reports clearly indicate that incorporation of particles can occur either by reactive, partly reactive or inert incorporation during PEO processing. Futhermore, the melting point of the particles seems to play an important role in the incorporation mode. Particles with high melting point, for example, SiC (2730 °C), CeO_2 (2400 °C), Si_3N_4 (1900 °C), were mainly incorporated inertly regardless of their size. Particles with relatively lower melting points (between 1000 and 1200 °C), e.g. clay particles [28,29], were incorporated reactively. Latter resulted in uniform coating compositions which were close to commercial bio-glasses. The size of the particles also influences the particle incorporation mode and by extension, the PEO process and coating

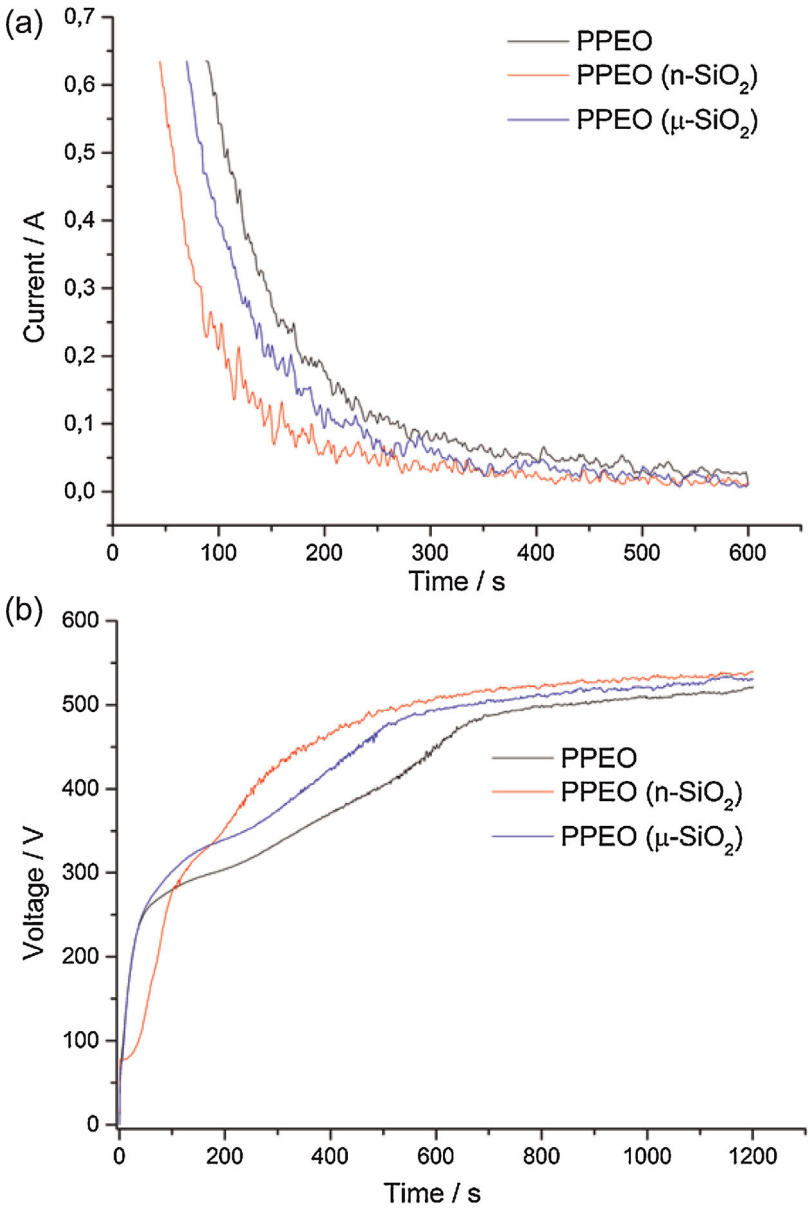

Fig. 1. Current (a) and Voltage (b) vs. Time plots during PEO processing in electrolytes with and without particle addition.

properties. For instance, nano-sized ZrO_2 particles (150-300 nm) have shown a reaction with Mg species to form $Mg_2Zr_5O_{12}$ in the outer coating layer even though they have a high melting point (2715 °C) [30]. Li et al. [25] also demonstrated that Al_2O_3 particles participated in chemical reactions during the coating formation process. It has also been observed that TiO_2, either in particle or sol form, partly undergoes reactive incorporation into the coating [31–33].

Although the size effect of particle addition on PEO coatings has been investigated, there are still open questions. Specifically, the uptake and incorporation mode of particles with different sizes and melting points is yet to be established. Moreover, the intrinsic mechanism of particle addition into the PEO coating is still unclear. For instance, Arrabal et al. [30,34] argued that ZrO_2 nanoparticles added into the PEO coating were transferred to the interface between the inner/outer layer through short-circuit paths in the outer layer. In contrast, Lee et al. [20] demonstrated that the electrophoretic mobility and mechanical mixing in molten magnesium oxide were main factors leading to particle incorporation. Necula et al. [35] introduced Ag nanoparticles to PEO coating and assumed that particles can be preserved in the coating after they are delivered and entrapped to the sites of coating growth. However, it still needs more investigations to find out the uptake and incorporation mode of particles with different sizes and melting points.

In the present work, a detailed study of the effects of nano-sized (12 nm avg.) and micro-sized (1-5 μm) SiO_2 particles addition on the PEO process, coating morphology, phase composition and properties of PEO coatings is presented. The uptake and incorporation mechanism of the different sized SiO_2 particles is also proposed herein.

2. Experimental

Specimens of AM50 magnesium alloy with a size of 15 mm × 15 mm × 4 mm were prepared from gravity cast ingot material. The chemical composition of AM50 alloy, as measured with an Arc Spark OES (Spark analyser M9, Spectro Ametek, Germany), is 4.74 wt. % Al, 0.383 wt. % Mn, 0.065 wt. % Zn, 0.063 wt. % Si, 0.002 wt. % Fe, 0.002 wt. % Cu and Mg balance. The specimens were ground using emery papers up to 1200 grit and then air-dried prior to PEO treatment.

The PEO process was carried out by using a pulsed DC power source with a pulse ratio of t_{on}: t_{off} = 0.4 ms: 3.6 ms. The specimens and a stainless steel tube were used as the anode and cathode, respectively. The composition, conductivity and pH values of the electrolytes used for the PEO treatments are given in Table 1. A stirrer and bubbling generator were used to facilitate the uniform distribution of the particles in the electrolyte. In order to easily identify the particle incorporation, only phosphate containing base electrolyte was used (1 g/l KOH and 20 g/l Na_3PO_4). The corresponding coatings are named as PPEO, PPEO (n-SiO_2) and PPEO (μ-SiO_2). All the PEO treatments were performed at a constant voltage of 450 V for 10 min and the maximum average current density provided by the DC power supply was limited to 300 mA/cm^2. Treatments were also done at a constant average current

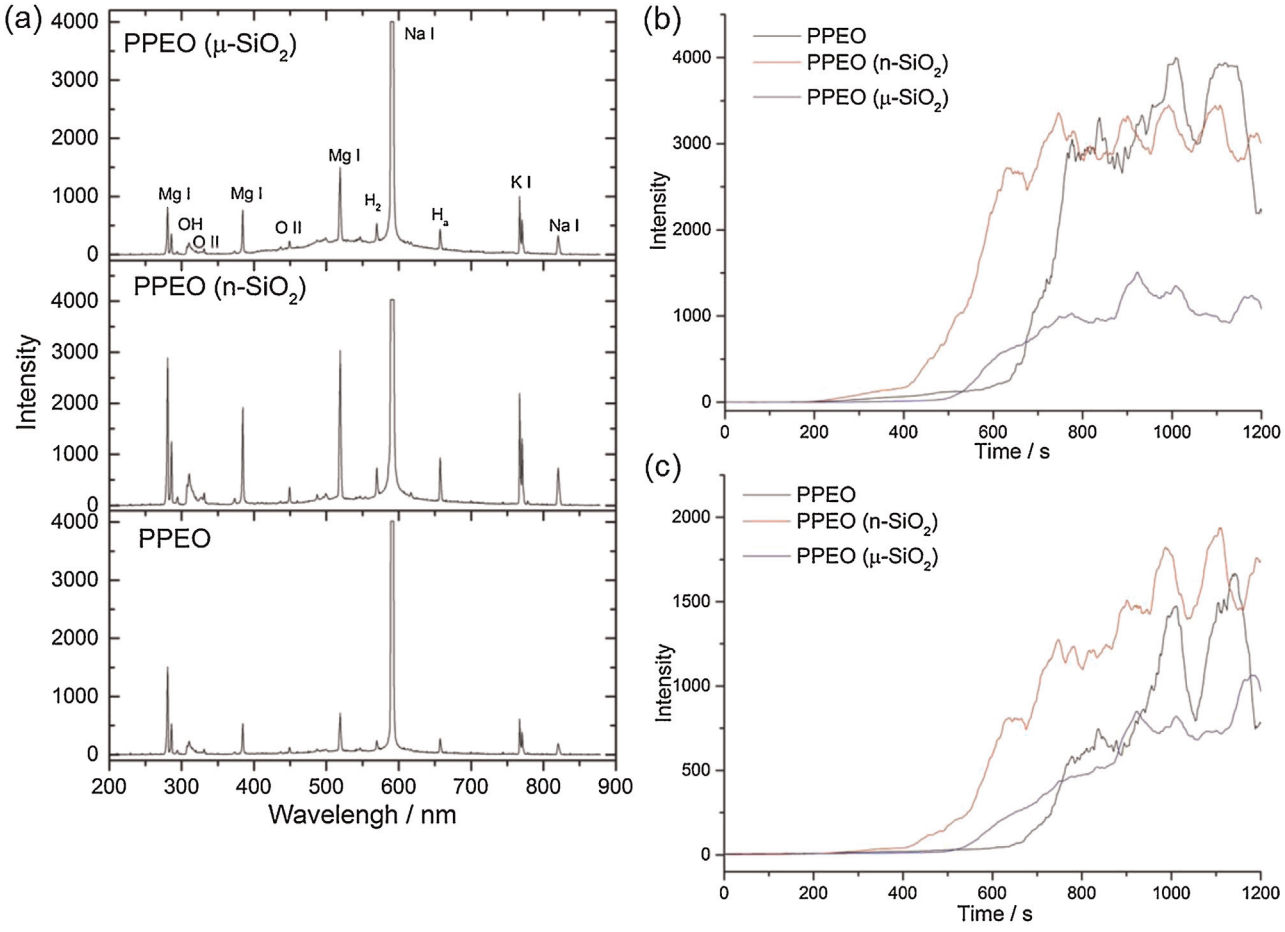

Fig. 2. Optical emission spectra (a) and OES intensity plots: (b) Mg (I) at 280.98 nm and (c) Mg (I) at 383.8 nm obtained during PEO processing in three electrolytes.

density (27 mA/cm^2) for optical emission spectroscopy study. The study of emission characteristics was performed with a Plasus Emicon optical emission spectroscopy (OES) system in order to identify the elements/species associated with plasma discharge as well as to understand the influence of particle addition on the PEO process. The temperature of the electrolytes was kept at 10 ± 2 °C by a water cooling system.

Surface roughness measurements were carried out with a Hommel profilometer (HOMMEL TESTER T1000). A scanning electron microscope (TESCAN Vega3 SB) combined with an energy dispersive spectrometer (EDS) system from eumeX (ixrfsystems) was used to examine the surface morphology, composition and microstructure of the PEO coatings. An acceleration voltage of 15 kV was applied for SEM and EDS investigations. The phase crystal structure analysis was done with a Bruker X-ray diffractometer using Cu Kα radiation. Further information about the coating structure and phase composition was obtained by transmission electron microscopy (TEM). The TEM lamellae were milled from the bulk specimens with focused ion beam (FIB) in a Nova-200 dual-beam scanning electron microscope (SEM). TEM observations were performed on a Philips CM200 transmission electron microscope operating at a voltage of 200 kV.

The corrosion behavior of the PEO coatings was assessed by potentiodynamic polarization and electrochemical impedance spectroscopy (EIS) tests, which were carried out using an ACM Gill AC computer controlled potentiostat. A typical three-electrode cell with the coated specimen as the working electrode (0.5 cm^2 exposed area), a saturated Ag/AgCl electrode as the reference electrode, and a platinum mesh as counter electrode was used. Polarization investigations were carried out starting at −150 mV relative to OCP (after 30 min of exposure at OCP) at a sweep rate of 0.2 mV s^{-1} until the anodic branch reached a final current density of 0.01 mA cm^{-2}. Electrochemical impedance spectroscopy (EIS) studies were performed at open circuit potential with AC amplitude of 10 mV RMS sinusoidal perturbations over the frequency range from 30 kHz to 0.01 Hz. The measurements were repeated at fixed intervals of 0 (after 5 min immersion), 1, 3, 6, 12, 24, 48 and 72 hours of immersion time.

The dry sliding wear behavior of the PEO coatings was assessed with a Tribotec ball-on-disc oscillating tribometer with an AISI 52100 steel ball of 6 mm diameter as static friction partner. The wear tests were performed at ambient conditions (25 ± 2 °C and 30 % r.H.) under 5 N load with oscillating amplitude of 10 mm and at a sliding velocity of 5 mm s^{-1}, for a sliding distance of 12nm. Wear depth measurements were performed with a Hommel

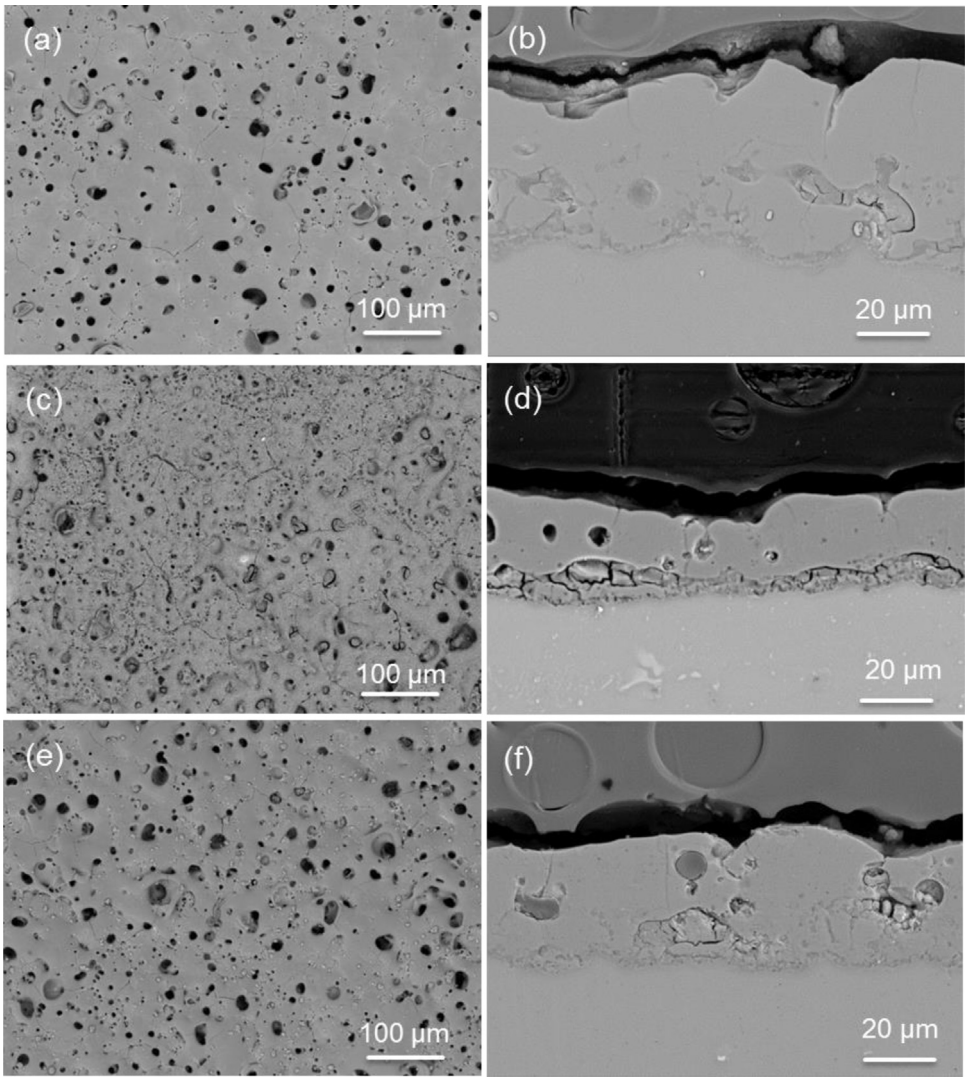

Fig. 3. Surface morphology and cross section of the PEO coatings (a) and (b) PPEO, (c) and (d) PPEO (n-SiO2), (e) and (f) PPEO (μ-SiO2).

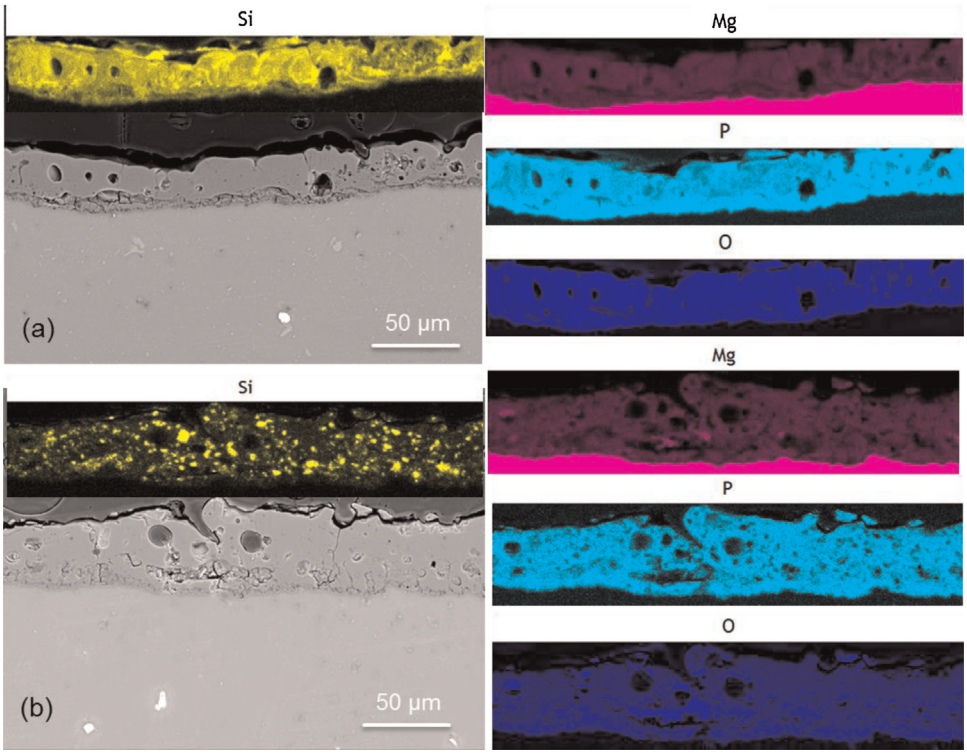

Fig. 4. EDS maps of the PEO coatings (a) PPEO (n-SiO2) and (b) PPEO (μ-SiO2).

profilometer. Coating hardness was evaluated using an AKASHI MVK-E3 Vickers micro-hardness tester on polished cross sections under a load of 0.025 kg for 20 s.

3. Results

3.1. Coating evolution

The change of current as a function of treatment time under constant voltage regime with and without particle addition is shown in Fig. 1a. The particle addition affects the evolution of the current during the whole process. Due to a limitation of our recording technique, the applied maximum current (2 A) cannot be displayed, thus the record started from a relatively low current value. For the coatings with incorporated particles, especially for PPEO (n-SiO_2), the current decreases faster than the one without particles, indicating that particle addition may result in thicker or denser PEO coatings. To further confirm this, PEO coatings were produced under a constant current mode (27 mA/cm^2). Fig. 1b shows the change of voltage as a function of treatment time. PEO coatings with particle addition register higher final voltage. The final voltage of PPEO (n-SiO_2) is 540 V and that of PPEO (μ-SiO_2) is 531 V. In contrast, the final voltage of PPEO is 521 V, indicating a lower resistance of the coating free of particles. It was also observed that the coating with nanoparticle addition needed more time to reach the breakdown potential.

Table 2
Surface compositions (at. %) of the coatings determined by EDS analysis.

Coating	O	Na	Mg	Al	Si	P
PPEO	58	7	22	1.5	-	11
PPEO (n-SiO_2)	56	8	17	1	9	9
PPEO (μ-SiO_2)	60	6.5	18	1	5	9

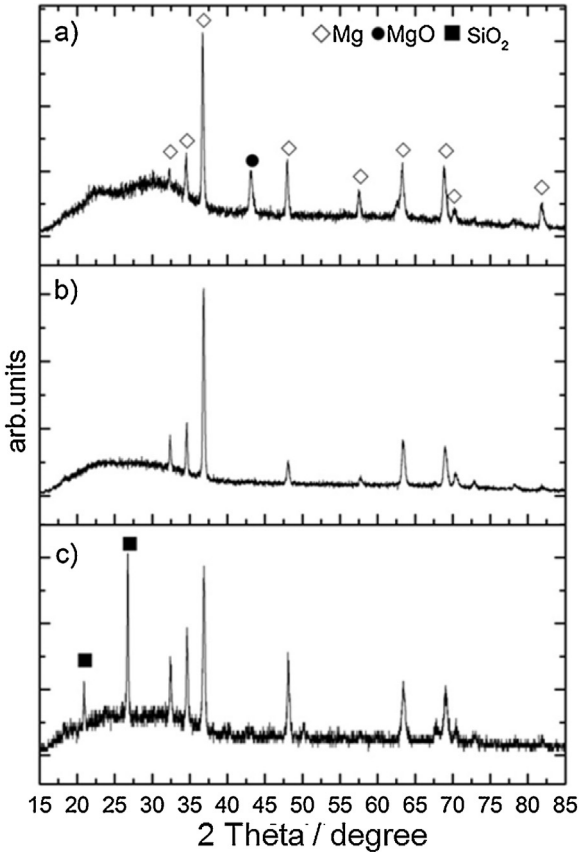

Fig. 5. XRD patterns of the PEO coatings (a) PPEO, (b) PPEO (n-SiO2) and (c) PPEO (μ-SiO2).

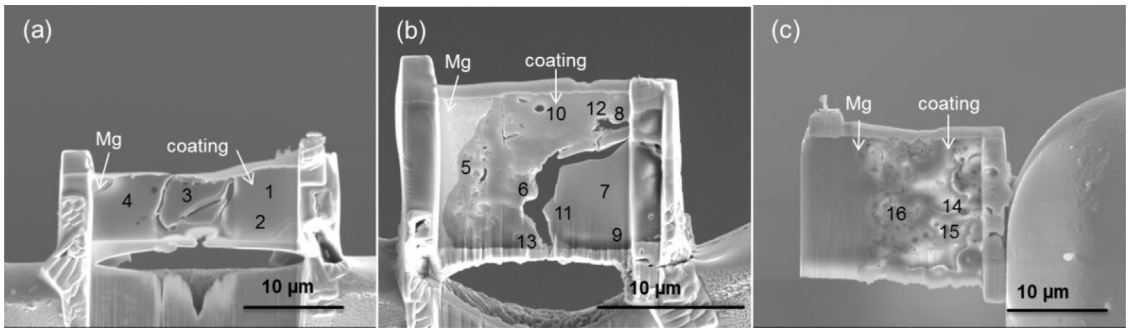

Fig. 6. TEM specimens prepared by focused ion beam (FIB) and EDS point analyses.

In addition, the progress of the PEO process was monitored by OES measurements. For the constant voltage mode, the intensity of the discharges was relatively weak throughout the whole treatment. A possible explanation might be that in the beginning the thin coating does not require high energy to be punctured, and only few large and long-living sparks exist at the final stage, giving an overall discharge with low intensity. In order to study the elements and ions participating in the PEO process, a constant current regime was applied for 20 min to achieve strong and sufficient discharges. The OE spectra (Fig. 2a) were recorded at the end of the treatment, indicating that the emission of the discharges is essentially from the components of the electrolyte and substrate, i.e., excited species of Na, OH, K and Mg. Similar observations have been reported by other researchers [36–38]. Furthermore, it was observed that the discharge intensity of PPEO (n-SiO_2) is the maximum among all three treatments. More so, the intensity level of the discharges for treatment with micro-sized particle addition is still higher than that of particle free electrolyte, except for the Mg (I) line at 280.98 nm. It can be argued that SiO_2 particles are not directly involved in the plasma discharges, since no excited states of Si are observed by OES although Si is incorporated into the coating. It is likely that the discharges generated during PEO processing do only provide the required energy for melting/sintering the surface with its conversion products deposited on it, and the pulse-off period may contribute to the coating growth via deposition and conversion processes as well.

Representative time vs. intensity plots for Mg (I) at 280.98 nm and 383.8 nm are presented in Fig. 2b and c. The intensity of Mg (I) increases earlier in the presence of particles, i.e. PPEO (n-SiO_2) (400 s) and PPEO (µ-SiO_2) (500 s) in comparison to that of PPEO (650 s), which is consistent with the potential vs. time data obtained in the same electrolytes (Fig. 1b). It is interesting to note that the strong intensity increase is not related to the start of arcing at breakdown potential but to the intense arcing when the flat plateau region close to the final voltage is reached. After the breakdown potential, fluctuations of the intensity are visible for all three coatings and the intensity of PPEO and PPEO (n-SiO_2) is higher in contrast with PPEO (µ-SiO_2). It is possible that the high turbidity of the micro-sized particle containing electrolyte might affect the emission of the OES signal, leading to the detected lower intensity of the discharges.

3.2. Microstructure, phases and elemental compositions

Fig. 3a,c and e reveal differences in the surface morphology of the PEO coatings with and without particle addition. PPEO (n-SiO_2) has a higher number of pores but their size is smaller compared to those of the other two coatings and a large amount of pores are partially filled. There is no distinct difference between PPEO and PPEO (µ-SiO_2), apart from many tiny particles adhering on the surface of the latter coating. The addition of micro-sized particles to the electrolyte does not change significantly the coating roughness; R_a is 3.1 ± 0.2 µm for PPEO (µ-SiO_2) and 3.0 ± 0.3 µm for PPEO. The surface of the coating with nano-particles is somehow a little bit smoother ($R_a = 2.6 \pm 0.3$ µm). Based on the cross section of the PEO coatings (Fig. 3b,d and f), it is obvious that the growth rate of the coatings is reduced by the addition of particles. Specifically, PPEO had the thickest layer (45 ± 5 µm) while the thickness of PPEO (n-SiO_2) and PPEO (µ-SiO_2) were 25 ± 4 µm and 33 ± 3 µm respectively. Two main coating regions are visible for all the coatings, namely, an outer layer and an inner layer, separated by a pore band. This is typical for coatings produced from phosphate based electrolytes [30,36].

In order to investigate the distribution of SiO_2 particles in the cross section of PEO coatings, EDS elemental mapping was carried out (Fig. 4). The main coating forming elements, Mg, P, O and Si, were detected in both coatings. P and O are uniformly distributed in the two coatings. As expected, the magnesium signal is diluted in all the coatings. However, Si is inhomogenously distributed in PPEO (µ-SiO_2), as can be seen in Fig. 4b, indicating that the particles are still existing. The Si signal from the nanoparticles is less uniformly distributed with strong signals along the pore band and discharge channels, suggesting that there might be different incorporation modes for the two kinds of particles.

The chemical composition of the different PEO coatings as determined by EDS is given in Table 2. The content of O and Al is nearly equal for all the coatings. The Mg and P concentrations of PPEO are a little bit higher than those of the coatings with particles. The identification of silicon is an indication that particles have been successfully incorporated into the coating, because there is no other silicon source except from SiO_2 particles in the phosphate

Table 3
Main elements (at. %) of different areas determined by EDS analysis in TEM.

Point	O	Mg	P	Si
1	48	30	22	-
2	50	27	23	-
3	53	23	24	-
4	58	22	20	-
5	7	59	32	2
6	43	19	29	9
7	53	15	31	1
8	55	9	20	16
9	48	17	35	0.5
10	42	31	18	9
11	54	16	29	1
12	47	21	25	7
13	45	17	23	15
14	66	-	-	34
15	59	29	12	-
16	60	24	16	-

based electrolyte. The concentration of the incorporated nanoparticles (9 at. %) is nearly twice as high as that of the micro-sized particles (5 at. %). The PPEO coating is found to be mainly composed of MgO phase, as evidenced from the XRD pattern in Fig. 5. Mg peaks and a large broad bump with 2θ angle distributed over 20°–35° are visible in the spectrum. Similar peaks are found in the spectrum of the other coatings, indicating that X-rays have penetrated the whole layer reaching the substrate and that the coating may contain amorphous or nanocrystalline phases. SiO_2 peaks are detected in the coating with large-sized particles. Together with the elemental mapping analysis, it can be inferred that micro-sized SiO_2 particles may not be melted to form new phases, while the nanoparticles are melted and react with MgO.

Fig. 6 shows the TEM lamellae produced from the cross section of coatings with FIB milling. Results of EDS point analyses performed by SEM at the marked positions in Fig. 6 are displayed in Table 3. Fig. 7 shows the TEM micrographs taken from the outer layer of three coatings as well as the corresponding diffraction patterns. A large number of nanocrystals are visible in the particle-free coating especially in the outer layer (Fig. 7a); the associated diffraction pattern suggests that these are likely crystalline MgO. In addition, a few isolated and spherical pores appear, suggesting that they might have been formed by gas inclusions during rapid solidification of the coating. In regions free of MgO particles, the coating is composed of an amorphous phase and nanocrystalline MgO grains. The compositions at these two areas are similar (point 1-4), with only slightly higher content of Mg and lower content of O (point 1) for the MgO-particle enriched region. The coating structures and compositions however changed completely after introducing nanoparticles. Two typical areas are shown in Fig. 7b. On the one hand, with the participation of nanoparticles (point 6, 8, 10, 12 and 13), a network-like and dense microstructure is visible, which is composed of completely amorphous material. On the other hand, nanoporous material can be observed in the absence or lack of nanoparticles (point 7, 9 and 11). Corresponding diffraction rings were identified as nanocrystalline MgO. Moreover, nanoparticles have not been detected when magnification was up to 20000 times. In the case of coating loaded with big-sized particles, isolated SiO_2 particles were identified by EDS (point 14). Apart from that, the coating is mainly composed of amorphous phase (Fig. 7c)

3.3. Corrosion performance

3.3.1. Potentiodynamic polarization

The corrosion resistance of PEO coatings was evaluated by potentiodynamic polarization technique. The results after OCP exposure for 0.5 h in 0.5 wt. % NaCl solution are presented in Fig. 8. The corrosion potential (E_{corr}), corrosion current density (i_{corr}) and breakdown potential (E_{bd}) derived from potentiodynamic polarization plots are summarized in Table 4. It is worth mentioning that coatings with particle addition (Fig. 8b and c) are less stable than PPEO. The smaller the particle size is, the more variation in corrosion properties was observed. PPEO (n-SiO_2) ($(2.4 \pm 1.6) \times 10^{-4}$ mA.cm^{-2}) and PPEO (μ-SiO_2) ($(1.9 \pm 0.7) \times 10^{-4}$ mA.cm^{-2}) have higher corrosion current than coatings without particle addition ($(1.2 \pm 0.2) \times 10^{-4}$ mA.cm^{-2}). The calculated values from polarization curves mainly indicate the barrier property of the coating at early stage. Hence further EIS measurements for determining the long-term corrosion performance of the coatings were conducted.

3.3.2. EIS results

The degradation of PEO coated specimens in 0.5 wt. % NaCl with prolonged immersion of up to 72 h was examined by EIS measurements. The EIS spectra (Bode plots) of PEO coatings obtained in different electrolytes are presented in Fig. 9. In the first

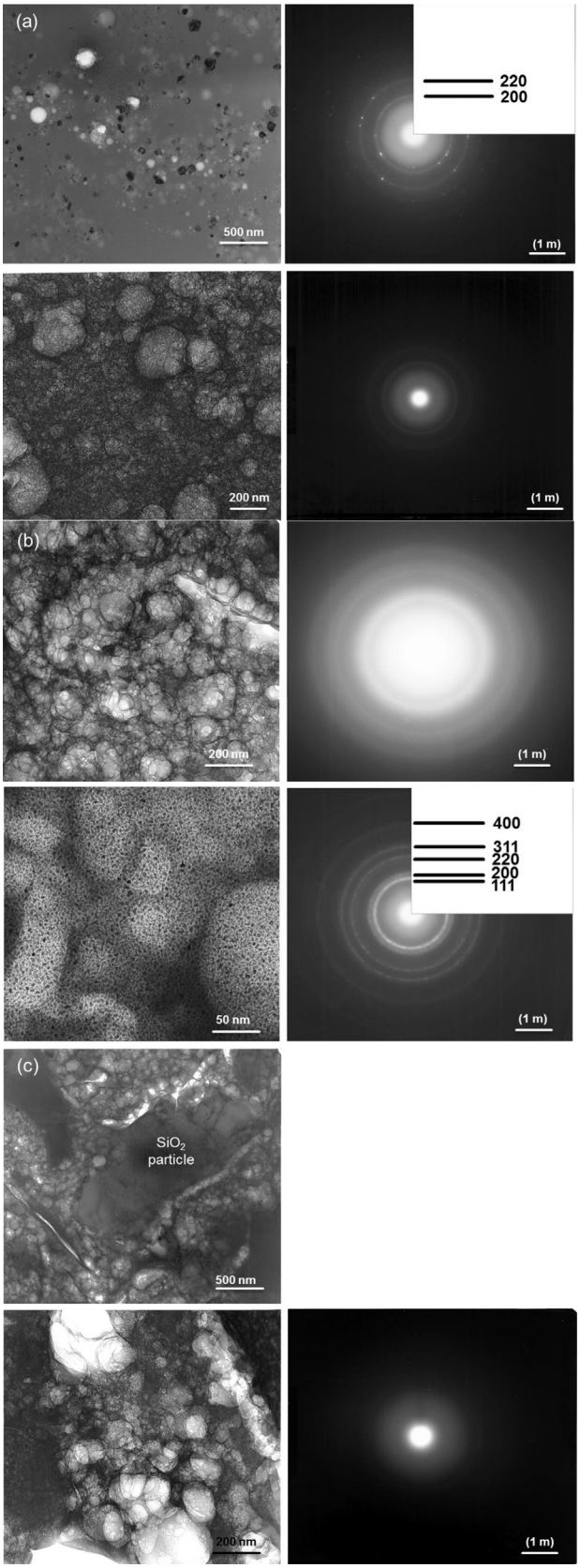

Fig. 7. TEM micrographs and corresponding diffraction patterns of the PEO coatings (a) PPEO, (b) PPEO (n-SiO_2) and (c) PPEO (μ-SiO_2).

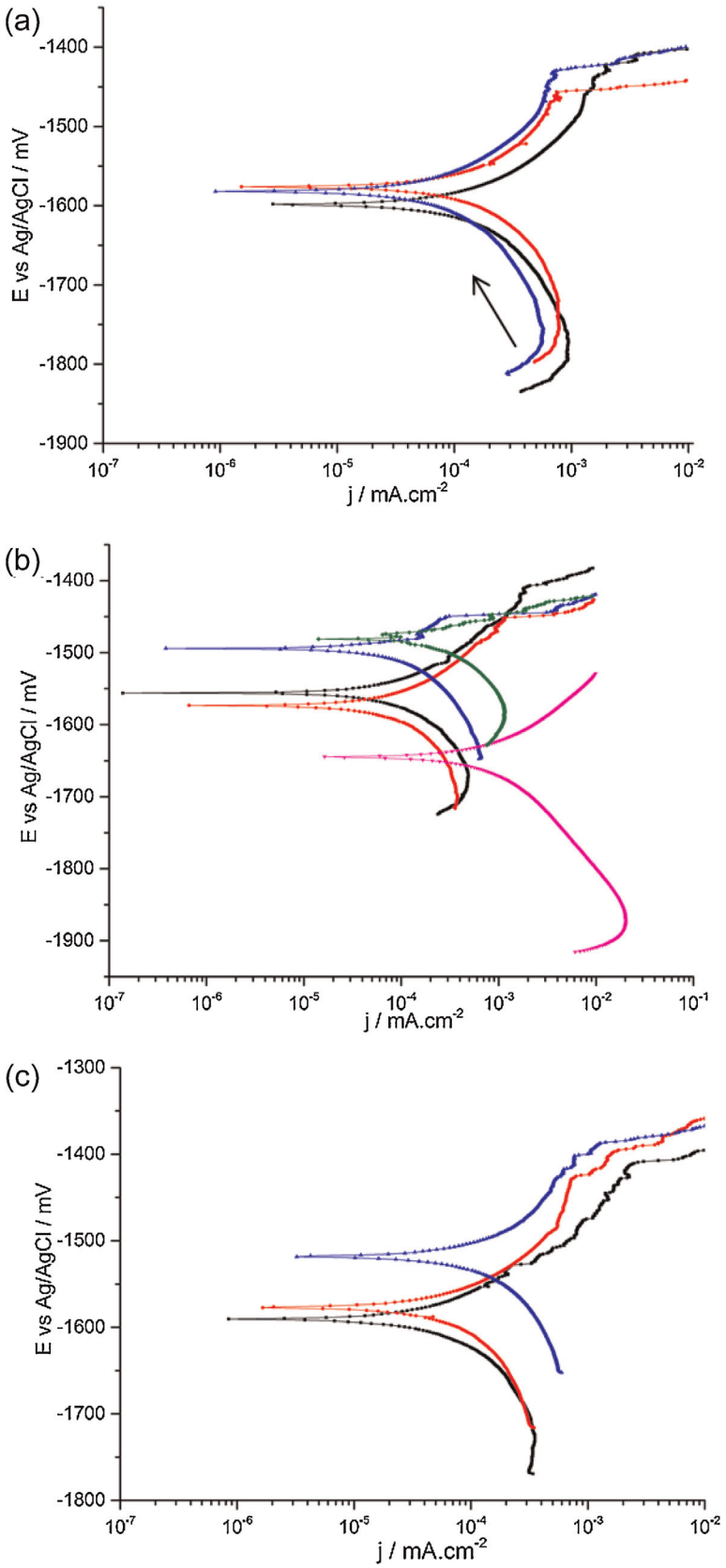

Fig. 8. Potentiodynamic polarization behavior of the PEO coatings (a) PPEO, (b) PPEO (n-SiO_2) and (c) PPEO (μ-SiO_2).

Table 4
Electrochemical data of PEO coated specimens from potentiodynamic polarization studies.

Coating	E_{corr} vs Ag/AgCl (mV)	j_{corr} ($\times 10^{-4}$/mA.cm^{-2})	E_{bd} (mV)
PPEO	-1588 ± 10	1.2 ± 0.2	-1449 ± 8
PPEO (n-SiO_2)	-1550 ± 95	2.4 ± 1.6	-1440 ± 28
PPEO (μ -SiO_2)	-1566 ± 36	1.9 ± 0.7	-1433 ± 6

measurement directly after immersion, two well-defined time constants are detected in all Bode plots at low and high frequencies. It should be mentioned that this measurement was done after immersion for 5 min. The corrosive solution had not fully filled the pores of the outer layer yet. Therefore, the time constant at high frequency (10^4 Hz) relates to the outer layer, while the time constant at lower frequencies (1 Hz) can be assigned to the response of the intact inner layer. After one hour, the outer layer is fully penetrated by water and the corrosive Cl^- ions filling the defects, such as cracks, open pores, discharge channels, and the volume freed by dissolved unstable amorphous material. From that very moment, the outer layer contributes nearly nothing to the high frequency impedance, and hence it is difficult to distinguish the respective time constant because it has been merged with the time constant of the inner layer. Meanwhile the corrosion process takes place at the metal/barrier layer/electrolyte interface for all the coatings. First signs of an additional time constant in the low frequencies range (0.1 Hz) appear. Subsequently, the time constant related to the outer layer will disappear as the inner barrier layer or the substrate will be exposed to the corrosion medium. Only two time constants are visible between 3 and 72 hrs. From this point of view, particle addition does not result in better corrosion performance. The same equivalent circuit can be applied for the coating with and without SiO_2 particle addition [29]. The impedance at the lowest frequency (0.01 Hz) in Fig. 10, which is one of the parameters that can be easily used to assess the corrosion performance of different systems [16,39], could represent the total corrosion resistance of the PEO coating. Obviously, the starting corrosion resistance for coatings with particle addition is higher than that for the particle-free one, especially for the coating loaded with nanoparticles, which can be considered as temporary sealing effect. However, the coatings in the presence of particles demonstrate a faster degradation rate in the next 72 h, reaching similar value as the coating free of particles.

3.4. Tribological performance

The variation of the friction coefficient determined for the respective coating against AISI 52100 steel ball is shown in Fig. 11. In the first 2 m of sliding, the friction coefficient is observed to rise to 0.87 for PPEO, followed by large fluctuations in the range of 0.46-0.78 for the remaining distance, indicating failure of the coating. In the case of coatings with particle addition, the friction coefficient value increased to around 0.6 in the first 2 m of sliding, reaching a steady-state value of 0.72 ± 0.02 and 0.66 ± 0.02 for PPEO (n-SiO_2) and PPEO (μ-SiO_2) after 12 m of sliding, respectively. This is a clear indication that there was no coating failure.

The wear tracks of the PEO coatings slid against the steel ball are shown in Fig. 12. The coating in the wear track of PPEO seems to be removed completely during the wear test, which is consistent with the deep wear depth profile (Fig. 13) and the recorded friction coefficient. However, the coatings with particles appear to be intact in the wear track. This observation is also supported by the low wear track depth. The width and depth of the wear track of PPEO were 987 ± 181 μm and 55 ± 6 μm, respectively. This corresponds to a specific wear rate of $(3.7 \pm 0.9) \times 10^{-3}$ mm^3 N^{-1} m^{-1}. It was difficult to precisely measure the depth in the wear track of coatings with particle addition. However, the specific wear rate of PPEO (n-SiO_2) and PPEO (μ-SiO_2) was calculated to be $(4 \pm 0.9) \times 10^{-4}$ mm^3 N^{-1} m^{-1} and $(7.3 \pm 0.6) \times 10^{-4}$ mm^3 N^{-1} m^{-1}, assuming a depth of 14 ± 2 μm from the highest valley in the wear profile. This value may even be an overestimation, but it is still lower by one order of magnitude compared to the particle free coating. Please not that the wear resistance corresponds to the hardness of the coatings. The hardness of the PEO coating increased with the addition of particles. Specifically, the PPEO (n-SiO_2) coating showed the highest hardness of 396 ± 72HV, while the hardness of the PPEO (μ-SiO_2) and the particle free coating were 338 ± 74HV and 327 ± 72HV respectively.

The surface morphology of the corresponding counterparts (steel ball) is presented in Fig. 14. Flattened worn surfaces are observed for all the balls, which means the steel balls have suffered abrasive wear damage against the PEO coatings. However, the wear rate of the steel balls varies for the different coatings. The steel ball slid against PPEO shows the highest wear rate (3.1 ±1.2) × 10−4 mm^3 N^{-1} m^{-1} due to the largest volume loss. This is ascribed to the three-body-abrasive wear which is induced by the entrapment of wear debris in the sliding couples involving from the failed PEO coating [40]. The steel ball slid against coating with nanoparticle addition exhibits lower wear rate $(5.8 \pm 3.6) \times 10^{-6}$ mm^3 N^{-1} m^{-1} in contrast to the one slid against the coating containing micro-sized particles ($(5.5 \pm 3.2) \times 10^{-5}$ mm^3 N^{-1} m^{-1}).

4. Discussion

It is obvious that the addition of SiO_2 particles into the electrolyte influences the PEO processing. Under constant voltage mode, the current decreases earlier and faster in the presence of particles. In the case of constant current regime, the voltage increases more quickly after the breakdown potential is exceeded and reaches higher values with particle addition. To drive the current higher energy discharges are required, and detectable discharges with higher intensity occur firstly for coatings with nanoparticles, followed by micro-sized particles and the particle free coatings, according to the OES measurements. Both trends indicate that particles addition produces coatings with higher electrical resistivity against current flow. Since the coatings become thinner after particles incorporation, the coatings must be denser (less open porosity) or the barrier layer must be strengthened. This improvement is also visible in the higher starting impedance values during corrosion testing.

The microstructure, phase composition and properties of PEO coating were also significantly changed with particle addition. The surface porosity of the coating with nanoparticle was sealed to a certain extent, although the porosity in the cross section was not substantially reduced by the particles. The incorporated micro-sized particles resulted in the PEO coating with slightly higher roughness and reduced coating thickness. In terms of phase composition, the participation of particles could open up new range of compositions for the PEO coating. Mg_2SiO_4 phase is normally observed for PEO coatings produced from silicate-based electrolyte [36,41], while amorphous phase and unreacted SiO_2 particles have been detected for the coating loaded with nano- and micro-sized particles, respectively. In general, the composition of

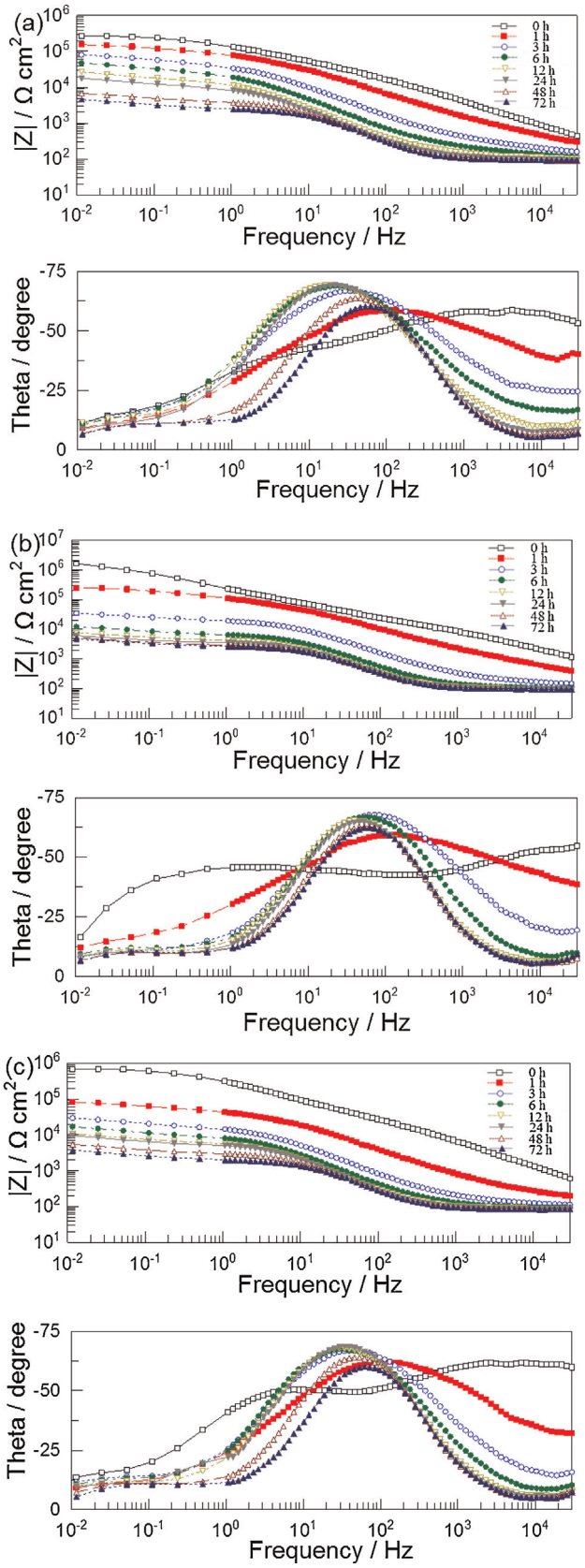

Fig. 9. Electrochemical impedance behavior of the PEO coatings (a) PPEO, (b) PPEO (n-SiO_2) and (c) PPEO (μ-SiO_2).

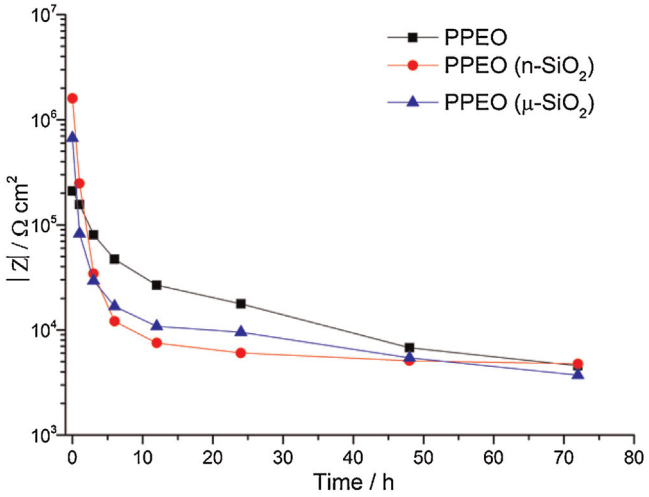

Fig. 10. Fitted impedance of the PEO coatings at low frequency (0.01 Hz).

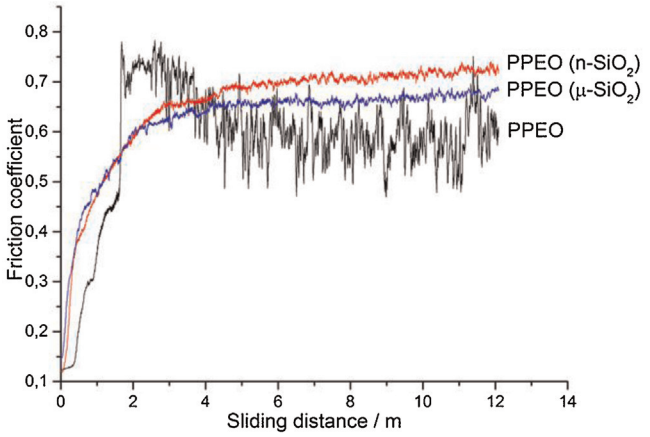

Fig. 11. Variation of the friction coefficient during the 12 m sliding in the oscillating wear tests under a load of 5 N.

PEO coating depends on the electrolyte composition and the matrix. However, the coating composition can also be controlled by the electrical parameters during PEO processing. According to our previous studies [11,29], sintering is an important step in the coating formation by PEO. Compounds with high melting point will only be formed if the energy of the discharges reaches a certain level, which is related to the melting temperature of the phases. Although MgO has a relatively high melting point, it still dominates in the coating if the energy of the discharges is not sufficient, which

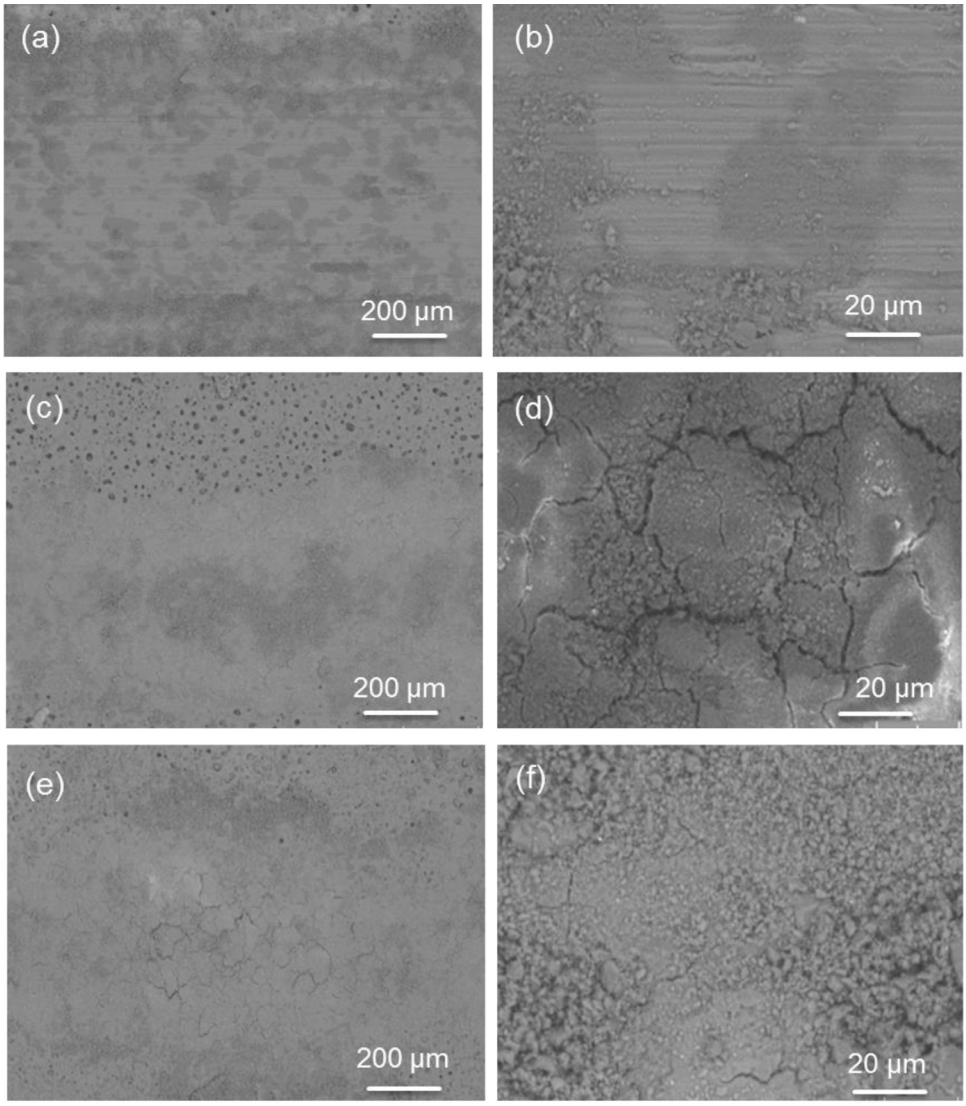

Fig. 12. Surface morphology of the wear tracks of the PEO coatings (a) and (b) PPEO, (c) and (d) PPEO (n-SiO_2), (e) and (f) PPEO (μ-SiO_2).

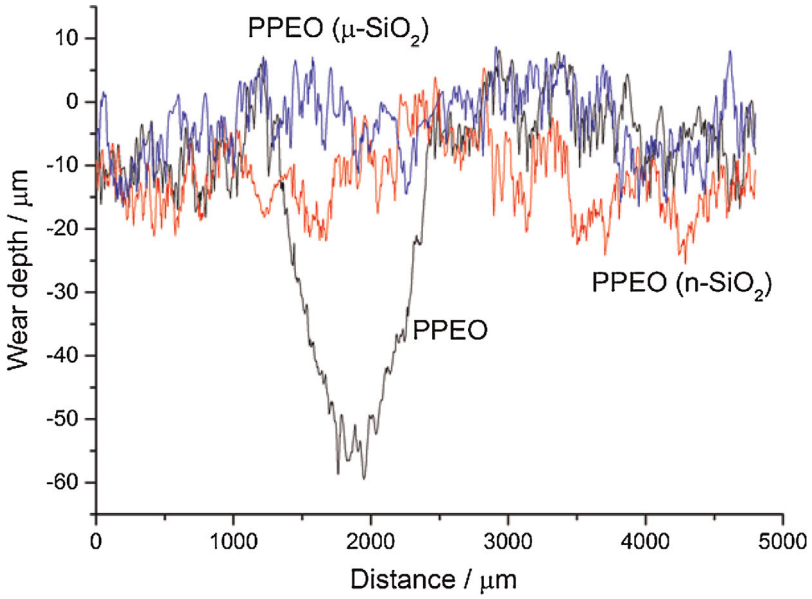

Fig. 13. Wear depth profile of the PEO coatings.

is caused by the decomposition of $Mg(OH)_2$ at 350 °C [11]. This is a temperature that is easily reached by the discharges even at low current density or low discharge voltage. Particles which have a low melting point or small size can be considered as sintering additive to ease coating formation, since the melted particles can either lower sintering temperature or improve the speed of sintering. Due to the increase in the fraction of liquid phase provided by the melted particles, liquid phase sintering process can be easily achieved together with the unmelted solid phase. For example, according to the MgO-SiO_2 phase diagram [42], oxide mixtures can be melted more easily than their constituents with the lowest melting temperatures obtained for the compositions close to the stoichiometric $MgSiO_3$ phase. Meanwhile, nano-crystalline MgO with fine nanoporous structure has been observed in the coating with nanoparticle addition. It can be inferred that the porous structure is likely capable to hold and interact with the entrapped nanoparticles and subsequently form the glass-like amorphous material. As for the coating with micro-sized particles, an inert incorporation is exhibited probably because there might be a limit of the size that can be melted by the short-lived discharges. Therefore, the particles survive and the surrounding material is phosphorous-rich amorphous phase free of Si. In general, amorphous material has superior mechanical properties but poor corrosion resistance [29,43]. Such a behavior was

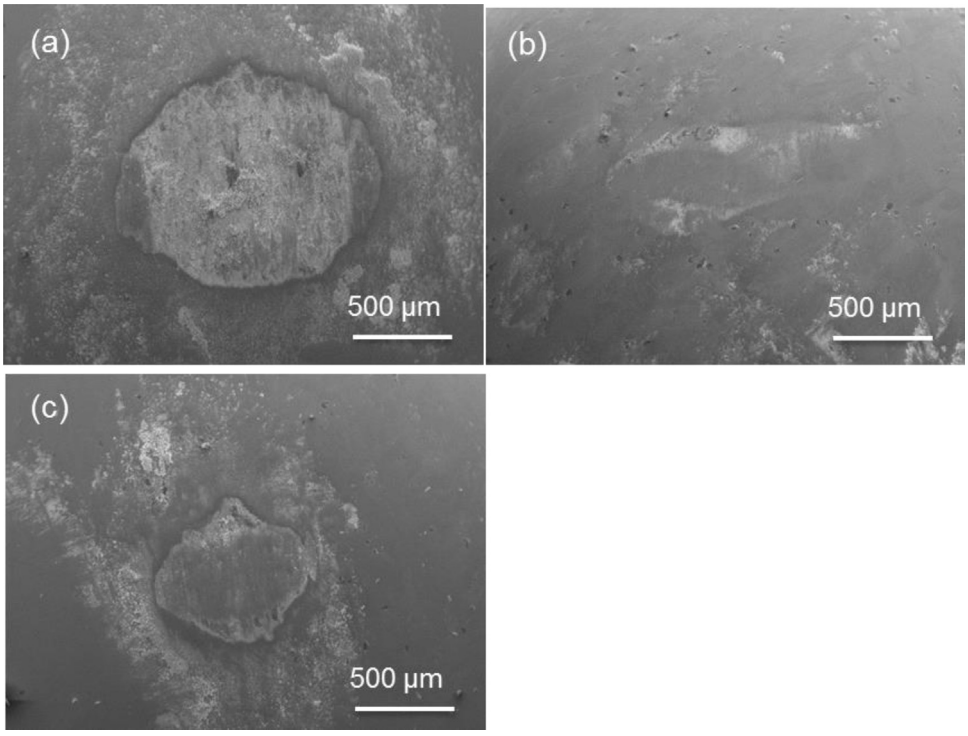

Fig. 14. Surface morphology of the corresponding counterparts (steel ball) (a) PPEO, (b) PPEO (n-SiO_2) and (c) PPEO (μ-SiO_2).

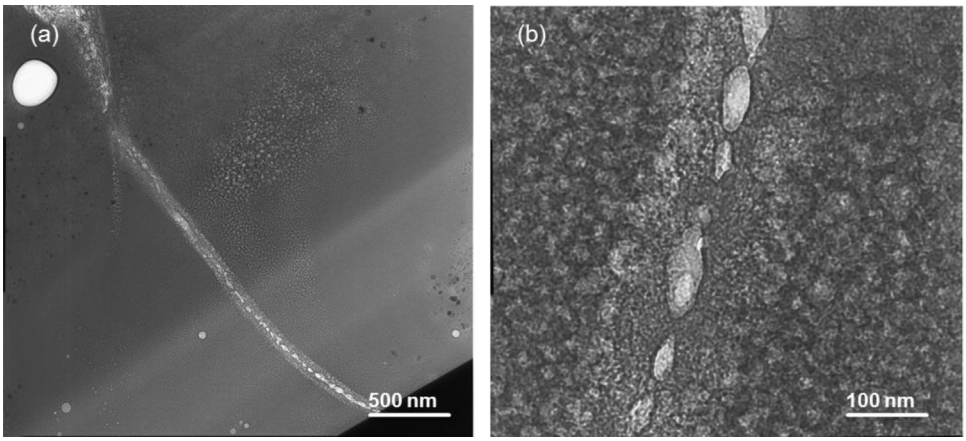

Fig. 15. Typical discharge channel for PEO coating.

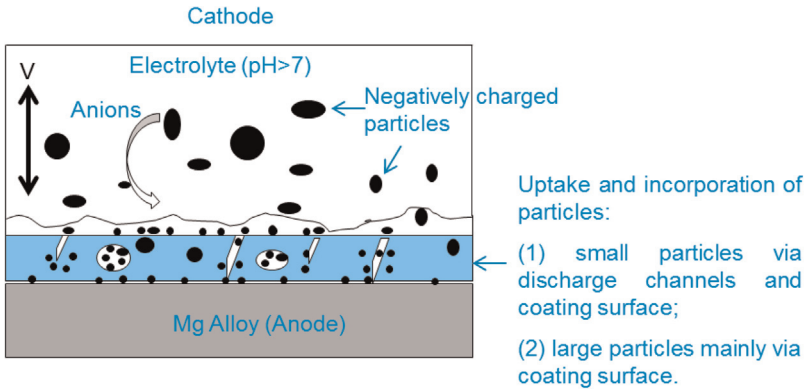

Fig. 16. Schematic diagram of the uptake and incorporation mechanism of particles into PEO coating.

observed for the amorphous PEO coatings in the presence of nanoparticles. Although the PEO coating with nanoparticles shows relatively poor corrosion performance (continuous degradation), it exhibits a good tribological performance (relatively low wear rate for the coating and its counterpart), making it suitable for use as biodegradable material.

In terms of mechanisms of particle addition into PEO coating, the size and the melting point of the particles have a synergistic effect on the uptake and incorporation modes. In principle, uptake of particles into the coating is mainly accompanied with the discharges, which produces discharge channels perpendicular to the coating surface. These channels allow water, anion species and particles to approach the pore band and the inner layer. One typical discharge channel connected to the inner layer can be observed in Fig. 15. The diameter is estimated to be less than 100 nm. Therefore, the uptake path for particles into PEO coating after breakdown potential mainly relies on the particle size, as shown by the schematic diagram (Fig. 16). Nanoparticles which are smaller than the discharge channels are capable of entering the coating down to the pore band while relatively large-sized particles will only enter from the surface or very large discharge channels formed at the end of a PEO process. Incorporation occurs under the extremly high temperature and pressure environment of the discharges, and the nature of the particle itself determines the incorporation mode. The possibility for micro-sized particles to transform to new phase via discharge channels is much less than that for the nanoparticles unless the particles have relatively low melting point. For example, clay particles have realized fully reactive incorporation [11,29]. In contrast, large-sized SiO_2 particles are normally inertly incorporated, since the short-lived discharges cannot melt such particles completely. Nano-sized particles of the same material have lower melting point and less chemical stability, leading to reactive incorporation into the coating. In short, the size of particle plays a crucial role in its uptake and incorporation mode besides its melting point and chemical stability. The discussed effects indicate a possibility to design and fine tune the composition and degradation properties of the PEO coatings with particle addition.

Conclusions

1) The addition of SiO_2 particles into the electrolyte does have influence on the PEO processing, coating microstructure and properties.
2) Uptake of the nanoparticles occurs mainly via discharge channels and open pores, while large-sized particles mainly enter via the surface. Incorporation mode is mainly related to a size effect.
3) SiO_2 nanoparticles can be used as sintering additive for PEO coating to ease coating formation. Reactive incorporation of SiO_2 nanoparticles into PEO coating results in the formation of nanocrystalline MgO and amorphous material. Inert particle incorporation into PEO coating has been observed for micro-sized particles.
4) Addition of SiO_2 particles could improve the wear resistance of PEO coating, but reduce the corrosion resistance slightly.
5) Due to superior wear performance and degradability, PEO coatings produced from SiO_2 nanoparticles containing electrolyte can be considered for biomedical application.

Acknowledgements

The technical support of Mr. Volker Heitmann and Mr. Ulrich Burmester during this work is gratefully acknowledged. X. Lu thanks China Scholarship Council for the award of fellowship and funding.

References

[1] J.E. Gray, B. Luan, Protective coatings on magnesium and its alloys—a critical review, Journal of Alloys and Compounds 336 (2002) 88–113.
[2] F. Fracassi, R. d'Agostino, F. Palumbo, E. Angelini, S. Grassini, F. Rosalbino, Application of plasma deposited organosilicon thin films for the corrosion protection of metals, Surface and Coatings Technology 174-175 (2003) 107–111.
[3] C. Blawert, W. Dietzel, E. Ghali, G.L. Song, Anodizing treatments for magnesium alloys and their effecton corrosion resistance in various environments, Advanced Engineering Materials 8 (2006) 511–533.
[4] H.H. Elsentriecy, K. Azumi, H. Konno, Improvement in stannate chemical conversion coatings on AZ91 D magnesium alloy using the potentiostatic technique, Electrochimica Acta 53 (2007) 1006–1012.
[5] Y.W. Song, D.Y. Shan, E.H. Han, Corrosion behaviors of electroless plating Ni–P coatings deposited on magnesium alloys in artificial sweat solution, Electrochimica Acta 53 (2007) 2009–2015.
[6] X.B. Chen, M.A. Easton, N. Birbilis, H.Y. Yang, T.B. Abbott, 11 - Corrosion-resistant electrochemical plating of magnesium (Mg) alloys, in: G.-L. Song (Ed.), Corrosion Prevention of Magnesium Alloys, Woodhead Publishing, 2013, pp. 315–346.
[7] A.L. Yerokhin, X. Nie, A. Leyland, A. Matthews, S.J. Dowey, Plasma electrolysis for surface engineering, Surface and Coatings Technology 122 (1999) 73–93.
[8] R. Arrabal, E. Matykina, T. Hashimoto, P. Skeldon, G.E. Thompson, Characterization of AC PEO coatings on magnesium alloys, Surface and Coatings Technology 203 (2009) 2207–2220.
[9] R.O. Hussein, D.O. Northwood, X. Nie, The effect of processing parameters and substrate composition on the corrosion resistance of plasma electrolytic oxidation (PEO) coated magnesium alloys, Surface and Coatings Technology 237 (2013) 357–368.
[10] Y. Song, K. Dong, D. Shan, E.H. Han, Study of the formation process of titanium oxides containing micro arc oxidation film on Mg alloys, Applied Surface Science 314 (2014) 888–895.
[11] C. Blawert, S.P. Sah, J. Liang, Y. Huang, D. Höche, Role of sintering and clay particle additions on coating formation during PEO processing of AM50 magnesium alloy, Surface and Coatings Technology 213 (2012) 48–58.
[12] R.O. Hussein, X. Nie, D.O. Northwood, An investigation of ceramic coating growth mechanisms in plasma electrolytic oxidation (PEO) processing, Electrochimica Acta 112 (2013) 111–119.
[13] E. Matykina, A. Berkani, P. Skeldon, G.E. Thompson, Real-time imaging of coating growth during plasma electrolytic oxidation of titanium, Electrochimica Acta 53 (2007) 1987–1994.
[14] P. Bala Srinivasan, J. Liang, C. Blawert, M. Störmer, W. Dietzel, Effect of current density on the microstructure and corrosion behaviour of plasma electrolytic oxidation treated AM50 magnesium alloy, Applied Surface Science 255 (2009) 4212–4218.
[15] Z. Li, X. Jing, Y. Yuan, M. Zhang, Composite coatings on a Mg-Li alloy prepared by combined plasma electrolytic oxidation and sol-gel techniques, Corrosion Science 63 (2012) 358–366.
[16] S.V. Lamaka, G. Knörnschild, D.V. Snihirova, M.G. Taryba, M.L. Zheludkevich, M. G.S. Ferreira, Complex anticorrosion coating for ZK30 magnesium alloy, Electrochimica Acta 55 (2009) 131–141.
[17] H. Duan, K. Du, C. Yan, F. Wang, Electrochemical corrosion behavior of composite coatings of sealed MAO film on magnesium alloy AZ91D, Electrochimica Acta 51 (2006) 2898–2908.
[18] D. Wu, X. Liu, K. Lu, Y. Zhang, H. Wang, Influence of C3H8O3 in the electrolyte on characteristics and corrosion resistance of the microarc oxidation coatings formed on AZ91D magnesium alloy surface, Applied Surface Science 255 (2009) 7115–7120.
[19] M. Laleh, F. Kargar, A. Sabour Rouhaghdam, Formation of a compact oxide layer on AZ91D magnesium alloy by microarc oxidation via addition of cerium chloride into the MAO electrolyte, Journal of Coatings Technology Research 8 (2011) 765–771.
[20] K.M. Lee, K.R. Shin, S. Namgung, B. Yoo, D.H. Shin, Electrochemical response of ZrO_2-incorporated oxide layer on AZ91 Mg alloy processed by plasma electrolytic oxidation, Surface and Coatings Technology 205 (2011) 3779–3784.
[21] Y.L. Song, X.Y. Sun, Y.H. Liu, Effect of TiO_2 nanoparticles on the microstructure and corrosion behavior of MAO coatings on magnesium alloy, Materials and Corrosion 63 (2012) 813–818.
[22] Y. Yang, H. Wu, Effects of Current Frequency on the Microstructure and Wear Resistance of Ceramic Coatings Embedded with SiC Nano-particles Produced by Micro-arc Oxidation on AZ91D Magnesium Alloy, Journal of Materials Science & Technology 26 (2010) 865–871.
[23] T.S. Lim, H.S. Ryu, S.-H. Hong, Electrochemical corrosion properties of CeO_2-containing coatings on AZ31 magnesium alloys prepared by plasma electrolytic oxidation, Corrosion Science 62 (2012) 104–111.
[24] X. Lu, C. Blawert, N. Scharnagl, K.U. Kainer, Influence of incorporating Si3N4 particles into the oxide layer produced by plasma electrolytic oxidation on AM50 Mg alloy on coating morphology and corrosion properties, Journal of Magnesium and Alloys 1 (2013) 267–274.
[25] X. Li, B.L. Luan, Discovery of Al_2O_3 particles incorporation mechanism in plasma electrolytic oxidation of $AM_{60}B$ magnesium alloy, Materials Letters 86 (2012) 88–91.
[26] D. Sreekanth, N. Rameshbabu, Development and characterization of MgO/hydroxyapatite composite coating on AZ31 magnesium alloy by plasma electrolytic oxidation coupled with electrophoretic deposition, Materials Letters 68 (2012) 439–442.
[27] S.V. Gnedenkov, S.L. Sinebryukhov, D.V. Mashtalyar, I.M. Imshinetskiy, A.V. Samokhin, Y.V. Tsvetkov, Fabrication of Coatings on the Surface of Magnesium Alloy by Plasma Electrolytic Oxidation Using ZrO_2 and SiO_2 Nanoparticles, Journal of Nanomaterials 2015 (2015) 12.
[28] C. Blawert, D. Höche, Y., Huang, J. Liang, process for producing a coating on the surface of a substrate based on lightweight metals by plasma-electrolytic oxidation, United States Patent, No.:US 2012/0261266 A1 (2012).
[29] X. Lu, S.P. Sah, N. Scharnagl, M. Störmer, M. Starykevich, M. Mohedano, C. Blawert, M.L. Zheludkevich, K.U. Kainer, Degradation behavior of PEO coating on AM50 magnesium alloy produced from electrolytes with clay particle addition, Surface and Coatings Technology 269 (2015) 155–169.
[30] R. Arrabal, E. Matykina, F. Viejo, P. Skeldon, G.E. Thompson, M.C. Merino, AC plasma electrolytic oxidation of magnesium with zirconia nanoparticles, Applied Surface Science 254 (2008) 6937–6942.
[31] J. Liang, L. Hu, J. Hao, Preparation and characterization of oxide films containing crystalline TiO_2 on magnesium alloy by plasma electrolytic oxidation, Electrochimica Acta 52 (2007) 4836–4840.
[32] P.B. Srinivasan, J. Liang, C. Blawert, M. Stormer, W. Dietzel, Development of decorative and corrosion resistant plasma electrolytic oxidation coatings on AM50 magnesium alloy, Surface Engineering 26 (2010) 367–370.
[33] K.M. Lee, B.U. Lee, S.I. Yoon, E.S. Lee, B. Yoo, D.H. Shin, Evaluation of plasma temperature during plasma oxidation processing of AZ91 Mg alloy through analysis of the melting behavior of incorporated particles, Electrochimica Acta 67 (2012) 6–11.
[34] R. Arrabal, E. Matykina, P. Skeldon, G.E. Thompson, Incorporation of zirconia particles into coatings formed on magnesium by plasma electrolytic oxidation, Journal of Materials Science 43 (2008) 1532–1538.
[35] B.S. Necula, I. Apachitei, F.D. Tichelaar, L.E. Fratila-Apachitei, J. Duszczyk, An electron microscopical study on the growth of TiO_2–Ag antibacterial coatings on $Ti_6A_{17}Nb$ biomedical alloy, Acta Biomaterialia 7 (2011) 2751–2757.
[36] J. Liang, P.B. Srinivasan, C. Blawert, M. Stormer, W. Dietzel, Electrochemical corrosion behaviour of plasma electrolytic oxidation coatings on AM50 magnesium alloy formed in silicate and phosphate based electrolytes, Electrochimica Acta 54 (2009) 3842–3850.
[37] R.O. Hussein, P. Zhang, X. Nie, Y. Xia, D.O. Northwood, The effect of current mode and discharge type on the corrosion resistance of plasma electrolytic oxidation (PEO) coated magnesium alloy AJ62, Surface and Coatings Technology 206 (2011) 1990–1997.
[38] S. Stojadinović, R. Vasilić, J. Radić-Perić, M. Perić, Characterization of plasma electrolytic oxidation of magnesium alloy AZ31 in alkaline solution containing fluoride, Surface and Coatings Technology 273 (2015) 1–11.
[39] S.V. Lamaka, M.F. Montemor, A.F. Galio, M.L. Zheludkevich, C. Trindade, L.F. Dick, M.G.S. Ferreira, Novel hybrid sol-gel coatings for corrosion protection of AZ31B magnesium alloy, Electrochimica Acta 53 (2008) 4773–4783.
[40] P.B. Srinivasan, J. Liang, C. Blawert, W. Dietzel, Dry sliding wear behaviour of magnesium oxide and zirconium oxide plasma electrolytic oxidation coated magnesium alloy, Applied Surface Science 256 (2010) 3265–3273.
[41] H. Duan, C. Yan, F. Wang, Effect of electrolyte additives on performance of plasma electrolytic oxidation films formed on magnesium alloy AZ91D, Electrochimica Acta 52 (2007) 3785–3793.
[42] P. Wu, G. Eriksson, A.D. Pelton, M. Blander, Prediction of the Thermodynamic Properties and Phase-Diagrams of Silicate Systems - Evaluation of the Feo-Mgo-Sio_2 System, Isij Int 33 (1993) 26–35.
[43] Z.H. Stachurski, On Structure and Properties of Amorphous Materials, Materials 4 (2011) 1564–1598.

5.4 Degradation behavior of PEO coating on AM50 magnesium alloy produced from electrolytes with clay particle addition *(with permission from Elsevier)*

Surface & Coatings Technology 269 (2015) 155–169

Contents lists available at ScienceDirect

Surface & Coatings Technology

journal homepage: www.elsevier.com/locate/surfcoat

Degradation behavior of PEO coating on AM50 magnesium alloy produced from electrolytes with clay particle addition

Xiaopeng Lu [a,*], Santosh Prasad Sah [b], Nico Scharnagl [a], Michael Störmer [a], Maksim Starykevich [c], Marta Mohedano [a], Carsten Blawert [a], Mikhail.L. Zheludkevich [a,c], Karl Ulrich Kainer [a]

[a] Helmholtz-Zentrum Geesthacht Zentrum für Material- und Küstenforschung GmbH, Institute of Materials Research, Max-Plank-Str. 1, Geesthacht 21502, Germany
[b] Department of Chemistry and Materials Science, Tokyo Institute of Technology, 2-12-1 Ookayama, Meguro-ku, Tokyo 152-8550, Japan
[c] Department of Materials and Ceramic Engineering, CICECO, University of Aveiro, Aveiro 3810-193, Portugal

ARTICLE INFO

Available online 15 Novenber 2014

Keywords:
Magnesium
Plasma electrolytic oxidation
Clay particle
Amorphous phase
Degradation control

ABSTRACT

Amorphous plasma electrolytic oxidation (PEO) coating with sealed discharge channels can be formed in alkaline phosphate electrolyte containing montmorillonite clay particles. The effect of various concentrations of phosphate and hydroxide ions in the clay-containing electrolyte on the microstructure of the coatings was studied in the present work and correlated with the corrosion behavior. The clay particles were reactively incorporated into the coating. Single amorphous phase appears in PEO coatings produced from electrolytes containing higher concentration of phosphate. These amorphous coatings are degrading within a relatively short period in 0.5 wt% NaCl solution. Electrolytes containing higher concentration of KOH tend to produce mixed PEO coatings composed of crystalline and amorphous phases. These layers demonstrate higher corrosion resistance and degradation stability. Thus, the degradation rate of PEO coatings is governed mostly by the stability of their phase composition, which might be controlled by varying electrolyte composition.

© 2014 Elsevier B.V. All rights reserved.

1. Introduction

Over the last years, some efforts have been done to enhance the corrosion resistance of magnesium alloys using surface treatments, such as chemical conversion coatings, anodizing, electroplating, PVD, and organic coatings [1–3]. Among all of them, ceramic-like hard plasma electrolytic oxidation (PEO) coatings have shown to be good candidates to improve both wear and corrosion properties. These coatings are developed in an aqueous solution at high voltage leading to the local formation of plasma discharges at the metal surface converting part of it into a ceramic-like coating as a result of interaction with components of electrolyte [3,4]. Many studies have utilized wide range of chemical compositions and concentrations of electrolytes, different electrical parameters, and processing time for PEO coating on magnesium alloys [5–9]. Among these parameters, the composition and concentration of electrolyte have an important impact on the final coating morphology, composition, and performance. There are also numerous reports on controlling microstructure and properties of coatings by introducing inorganic particles into the electrolyte, for example, silica, titania, zirconia, alumina, etc., aiming to improve the microstructure and corrosion resistance of the PEO coatings [10–17].

Most of the particles used so far have a relatively high melting point (>1700 °C) [14,18], resulting in partly reactive or inert incorporation into the coatings depending on their intrinsic chemical stability and whether they can be melted by the energy generated in discharges during the PEO processing in the respective electrolytes or not. To clarify the plasma temperature during plasma oxidation processing, Lee et al. [18] incorporated different kinds of particles to evaluate the temperature of the plasma in discharge which is in the range of 1843–2370 °C. In recent work [19], our research group has applied a new approach by employing low melting point clay particles (<1200 °C) and demonstrated that they contribute to ease the coating formation process and to seal discharge channels/micropores on the surface of the PEO coating. Moreover, amorphous coating has been produced when clay particles are incorporated into the phosphate based electrolyte. This coating composition is close to bio-glasses, and first corrosion tests suggest that those coatings might slowly dissolve in aqueous electrolytes [20].

Furthermore, it is known that the increase in concentration of KOH increased the volume fraction of MgO in the PEO coating, which exhibited better corrosion performance [21]. The addition of Na_3PO_4 would favor uniform spark distribution and thereby guarantee the formation of more uniform layer [22]. The thickness of the coatings also increases with phosphate concentration [23]. This indicates clearly that there is potential to further optimize coating composition, structure, and properties. The influence of variation of KOH and Na_3PO_4 in the electrolyte containing a constant clay particle concentration on the microstructure, phase composition, and corrosion behavior of PEO coating has been investigated in the present work. Conversely, different electrolytes might also affect the incorporation of clay particles.

* Corresponding author. Tel.: +49 4152871943; fax: +49 4152871960.
E-mail address: xiaopeng.lu@hzg.de (X. Lu).

http://dx.doi.org/10.1016/j.surfcoat.2014.11.027
0257-8972/© 2014 Elsevier B.V. All rights reserved.

2. Experimental

Specimens of AM50 magnesium alloy with size of 15 mm × 15 mm × 4 mm were prepared from gravity cast ingot material. The chemical composition of AM50 was analyzed by using Arc Spark OES (Spark analyser M9, Spectro Ametek, Germany). The determined composition of the AM50 alloy was 4.74% Al, 0.383% Mn, 0.065% Zn, 0.063% Si, 0.002% Fe, 0.002% Cu, and Mg balance. The specimens were ground using emery sheets up to 2500 grit and then air-dried prior to PEO treatment.

The PEO process was carried out using a pulsed DC power source with a pulse ratio of t_{on}:t_{off} = 2 ms:18 ms. During the PEO process, the specimen and stainless steel tube were used as the anode and cathode, respectively. The electrolytes for the PEO process were composed of different concentrations of potassium hydroxide and sodium phosphate (Table 1). Clay particles, 5 g/l (Rockwood Nanofil® 116, natural montmorillonite (about 100% bentonite) of average size of 12 μm [24]), were dispersed into each of five different electrolytes. The corresponding coatings are named hh-coating (high hydroxide concentration), mh-coating (medium hydroxide concentration), s-coating (standard concentration), mp-coating (medium phosphate concentration), and hp-coating (high phosphate concentration), respectively. All of the PEO treatments were performed at a constant voltage of 450 V for 10 min, and the current was limited to 0.3 A/cm^2. All treatment reached 450 V within the first 2 min and then continuously decreasing current was observed. The temperature of the PEO electrolytes was kept at 10 ± 2 °C by a water cooling system. The conductivity of the electrolytes was measured using a Mettler Toledo Inlab 730 probe. The pH value was measured using a Metrohm 691 pH meter.

Surface roughness measurements were carried out with a Hommel profilometer (HOMMEL TESTER T1000), and the coating thickness was measured with a MiniTest 2100 before and after corrosion tests. The given values are the average of three measurements. For measurements of insulating coating thickness on non-ferrous metals, the eddy current principle is used. A scanning electron microscope (Cambridge Stereoscan, cathode: W) was used to examine the surface morphology and cross section of the PEO coatings. An acceleration voltage of 15 kV was applied for SEM investigation. Image analysis software analySIS pro 5.0 was used to measure the number and size of the pores. Average values were calculated from 3 SEM images per treatment condition randomly taken from the specimen surface at 500× magnification. For observing the cross-sectional morphology, it was necessary to embed the PEO coatings into resin. Specimens were prepared by polishing successively using 500, 800, 1200, and 2500 grit emery sheets, following by disc polishing using colloidal silica suspension. Severe charging effect of the non-conducting coatings required a sputter-coating with Au to prevent the charging. A Zeiss Ultra55 SEM equipped with an energy dispersive spectrometer (EDS) was used to determine the elemental composition of the surface of the PEO coatings. The acceleration voltage is also 15 kV, and tungsten is the cathode. X-ray diffraction (XRD) was carried out by using a diffractometer (D8 Advance, Bruker AXS) equipped with Cu Kα radiation to determine the structure of the obtained coatings. GDOES depth profile analysis of the coatings was completed using a HORIBA GD-Profiler 2. Analyses were performed with a 4 mm diameter anode and operating at a pressure of 650 Pa and power of 20 W.

Additionally, electrochemical experiments were performed in 0.5 wt% NaCl solution at room temperature using an ACM Gill AC computer controlled potentiostat to evaluate the corrosion behavior of PEO-coated specimens. A corrosion cell (333 ml) with a three electrode set-up consisted of a saturated Ag/AgCl reference electrode, a platinum (mesh) counter electrode, and the coated specimen as working electrode was used. Polarization studies were carried out starting at −150 mV relative to OCP (measured after 30 min of immersion) at a sweep rate of 0.2 mV s^{-1} until the anodic branch reached a final current density of 0.01 mA cm^{-2}. Electrochemical impedance spectroscopy (EIS) studies were performed at open circuit potential with applied 10 mV RMS sinusoidal perturbation over the frequency range from 30 kHz to 0.01 Hz with 75 points for full frequency range. The measurements were taken at 0 (after 5 min immersion), 1, 3, 6, 12, 24, 48 and 72 h immersion time. The impedance spectra were analyzed using ZView software. The chi-squared of the fitting was less than 0.01.

Table 1
Composition, conductivity and pH value of the five electrolytes for PEO treatment.

Electrolytes	KOH (g/l)	Na_3PO_4 (g/l)	Clay particle (g/l)	Conductivity (mS cm^{-1})	pH
High hydroxide	10	10	5	41.7	12.8
Medium hydroxide	5	10	5	25.4	12.7
Standard	1	10	5	15.1	12.1
Medium phosphate	1	15	5	19.1	12.2
High phosphate	1	20	5	22.8	12.3

3. Results

3.1. Microstructure

The surface morphology of PEO coatings obtained from the five electrolytes is shown in Fig. 1. SEM images reveal that the surface of all PEO coatings is dominated by numerous pores which are characteristic of PEO coatings. In particular, almost all the pores of s-coating (Fig. 1c) are sealed and such a high degree of sealing is not obvious in the other four PEO coatings. The lowest surface roughness (3.9 ± 0.2 μm) of s-coating further proves that open pores might be filled. For the rest of the coatings, there are several open pores, protrusions, and cracks that might be due to powerful dielectric breakdown and extreme thermal conditions. Therefore, they exhibit higher surface roughness than s-coating, for instance, hh-coating (9.2 ± 1 μm), mh-coating (5.8 ± 1 μm), mp-coating (6.1 ± 0.4 μm), and hp-coating (8.5 ± 1 μm). One can also find numerous small particles sticking firmly on the coating indicating clay particles might take part in PEO process via an up-take over the surface. The effect of concentration and composition of electrolyte is well reflected by the surface morphology of the coatings. Plenty of small pores (4210 ± 552/mm^2) in the range of 1–10 μm are visible for hh-coating, which are much more than for the other coatings. The pores of mh-coating (1026 ± 184/mm^2) and s-coating (1315 ± 316/mm^2) are less but bigger in size (larger than 10 μm). Coatings obtained from higher concentration of phosphate have the least number of pores, mp-coating (474 ± 131/mm^2), and hp-coating (421 ± 131/mm^2) and rarely exhibit small-sized pores (1–10 μm). The majority of the pores are larger than 20 μm, several pores even reach up to 50 μm. For hh-coating, one can hardly find such big pores. The area covered by the pores is analyzed by analySIS pro 5.0 software. For coatings obtained from higher concentration of hydroxide, hh-coating (15.8%), and mh-coating (13.2%), the pores cover a larger surface area than for the others (s-coating (12.7%), mp-coating (10.8%), and hp-coating (11.5%)). In addition, all coatings except s-coating are dominated by many hairline shaped micro-cracks, which might be a result of thermal stress due to rapid solidification of molten material in the relatively cool electrolyte [4].

Fig. 2 presents the backscattered electron (BSE) micrographs showing the cross section of the PEO-coated specimens formed in the different electrolytes. The coating thickness and further details are given in Table 2. The thickest is hp-coating (67 ± 6 μm, Fig. 2e) compared to hh-coating (40 ± 5 μm, Fig. 2a), mh-coating (50 ± 8 μm, Fig. 2b), s-coating (15 ± 5 μm, Fig. 2c), and mp-coating (43 ± 7 μm, Fig. 2d). Particles are not visible in all cross sections, which have already been proved in former studies [19], suggesting that the clay particle have been converted forming new coating material fully with components

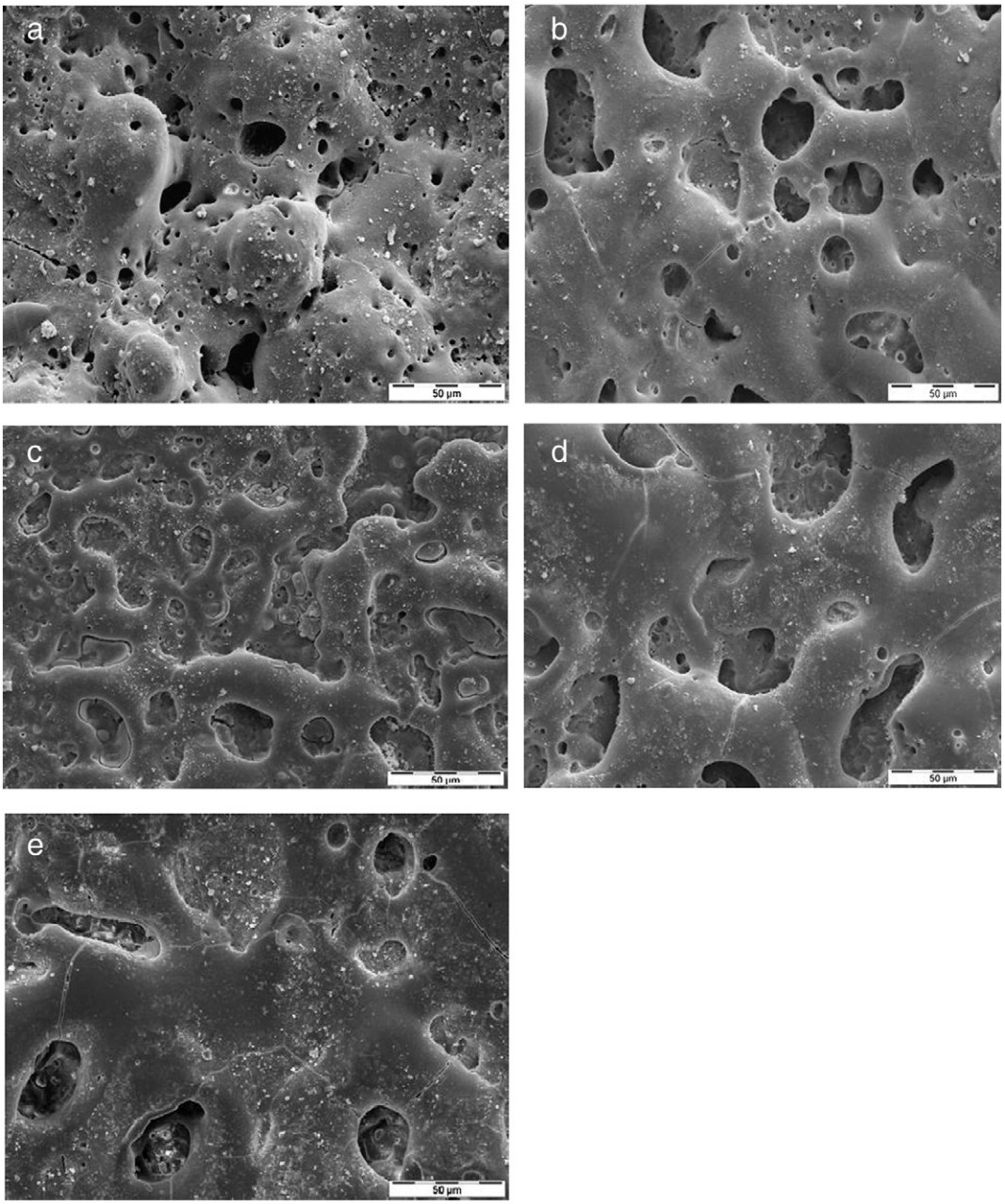

Fig. 1. SEM images of the surface morphology of the five PEO coatings (a) hh-coating, (b) mh-coating, (c) s-coating, (d) mp-coating, and (e) hp-coating.

from the electrolyte and/or substrate. All PEO coatings consist of an outer layer, a pore band, and an inner layer; thus, a simplified model structure of the cross section can be proposed (Fig. 2f) helping the further analysis. However, the volume ratios of these three regions vary among the different systems. The thickest coating (hp-coating) has the thickest outer layer. The small-sized pores seem to be gas inclusions entrapped during solidification after micro-sparks disappeared. Several discharge channels are visible for all the coatings and the open pores, which exist at the surface are not fully penetrating. To see more clearly about the pore band, higher magnification SEM images are given in Fig. 3. The area which looks deeper and darker in contrast with adjacent coating (outer layer and inner layer) is the pore band. During specimens preparation, resin could reach the defective pore band through discharge channels; thus, the pore band is filled by resin and debris of the grinding and is unfortunately not clearly visible. It is evident that the volume of the pore band of hp-coating is larger than that of the other coatings. Nevertheless, the volume of pore band of s-coating is not that large as expected in the low magnification image. It is thinner (1.1 ± 0.3 μm) in comparison to the other four PEO coatings (Table 2). The order regarding volume of the pore band of the five coatings is as follows: hp-coating > mp-coating > mh-coating > hh-coating > s-coating. With regard to the inner layer, a very thin continuous layer (~1 μm or less) close to the substrate can be observed. This layer is generally composed of nanocrystalline MgO [19,25].

3.2. Phase and chemical composition

The XRD patterns for the five PEO-coated specimens before carrying out the corrosion test are shown in Fig. 4. All of them contain amorphous phase indicated by a large broad bump distributed over 20°–35° of 2θ. Besides the amorphous phase, the hh-coating and mh-coating consist of MgO, $Mg_3(PO_4)_2$, and Mg_2SiO_4. Additionally, Mg peaks from the substrate are visible. In mh-coating, the intensity of MgO and Mg_2SiO_4 peaks seems to be much weaker compared to hh-

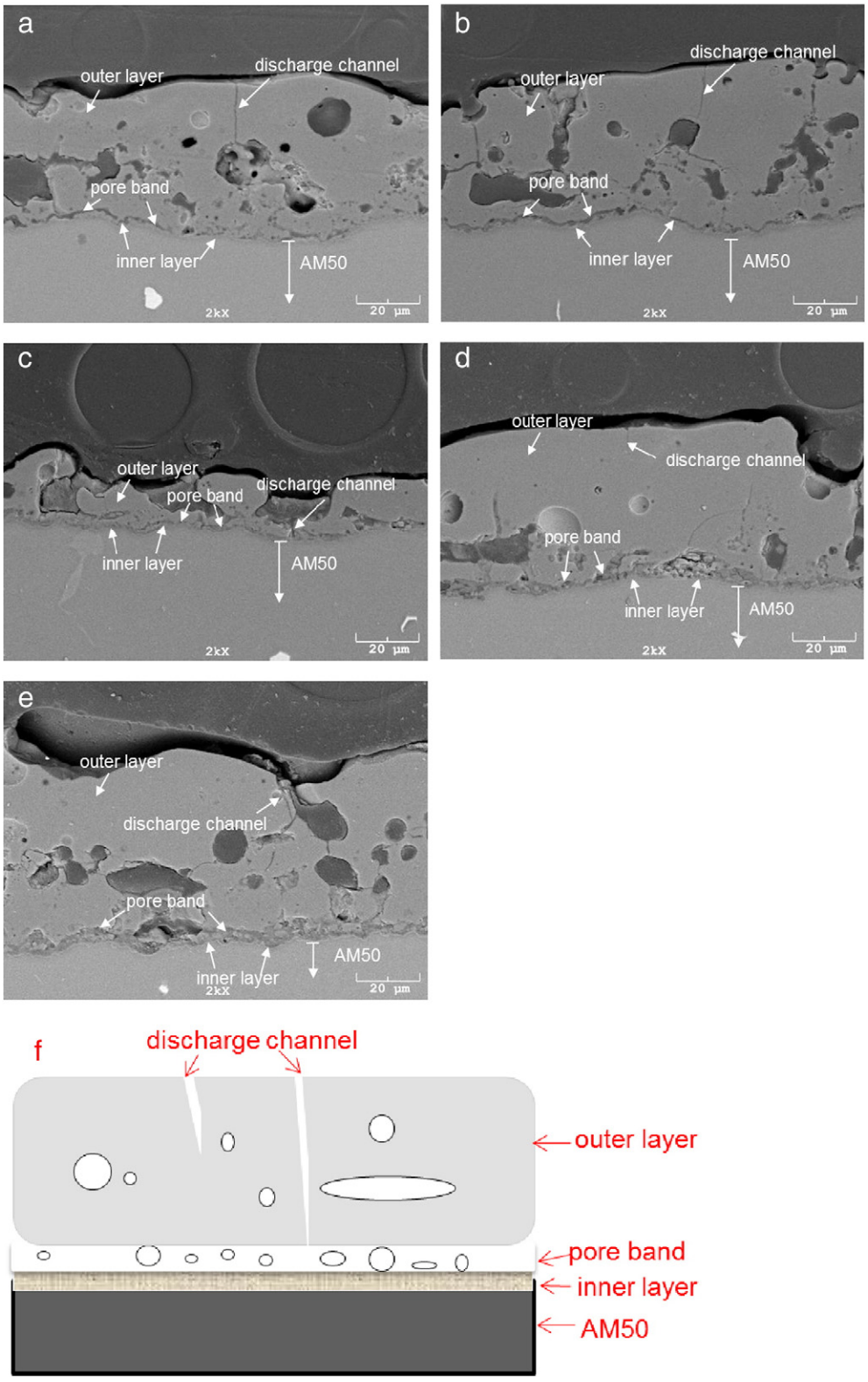

Fig. 2. BSE images of the cross section of the five PEO coatings (a) hh-coating, (b) mh-coating, (c) s-coating, (d) mp-coating, (e) hp-coating, and (f) schematic representation of the cross section.

coating. S-coating shows strong magnesium peaks and a small MgO peak, confirming this coating is as thin as that X-rays have penetrated the whole layer reaching the substrate. Interestingly, mp-coating and hp-coating only demonstrate amorphous phase and there is no other phase detectable. The absence of Mg peaks from hp-coating shows the coating is the thickest. Even though Si and P have been detected from EDS analysis, crystalline phases associated with silicate and phosphate are not found in mp-coating and hp-coating. Thus, only amorphous phases are formed in these coatings and the higher concentration of phosphate should be responsible for it.

The chemical composition determined by EDS of the near surface for different PEO coatings is given in Table 3. The oxygen content for all

Table 2
Thickness of the whole layer and its different regions determined from cross-sectional micrographs.

Coating	Thickness of total layer (μm)	Thickness of outer layer (μm)	Thickness of pore band (μm)	Thickness of inner layer (μm)
hh-coating	40 ± 5	38 ± 3	1.2 ± 0.3	0.8 ± 0.2
mh-coating	50 ± 8	47 ± 4	1.7 ± 0.5	1.2 ± 0.3
s-coating	15 ± 5	13 ± 4	1.1 ± 0.3	0.7 ± 0.2
mp-coating	43 ± 7	40 ± 5	2.2 ± 0.2	0.8 ± 0.2
hp-coating	60 ± 6	56 ± 8	4.9 ± 1.4	0.6 ± 0.3

coatings is nearly equal. As expected, the phosphorus and sodium concentration for the five PEO coatings increase with high concentration of phosphate in the electrolyte. Fe also could be identified, which originates from the Nanofil powder. The appearance of silicon testifies clay particles have been successfully incorporated into the coating, because there is no other silicon source except from clay in the silicon-free phosphate electrolyte. Moreover, the content of Si is nearly the same, demonstrating that variation of phosphate electrolyte does not affect the incorporation of clay particle.

3.3. Corrosion behavior

3.3.1. Potentiodynamic polarization

The corrosion behavior of the five PEO coatings evaluated by potentiodynamic polarization measurements after 0.5 h immersion in 0.5 wt% NaCl solution is presented in Figs. 5 and 6. Due to a great variation in the corrosion behavior of s-coating, their polarization curves are presented separately (Fig. 5). For all other coatings, the difference of three or more measurements was marginal and thus only one representative measurement for each type of coating is shown in Fig. 6. The corrosion potential (E_{corr}), corrosion current density (i_{corr}), and breakdown potential (E_{bd}) derived from potentiodynamic polarization plots are summarized in Table 4. Generally, the cathodic polarization curves indicate the hydrogen evolution through water reduction, while the anodic polarization curves represent the dissolution of magnesium matrix. The

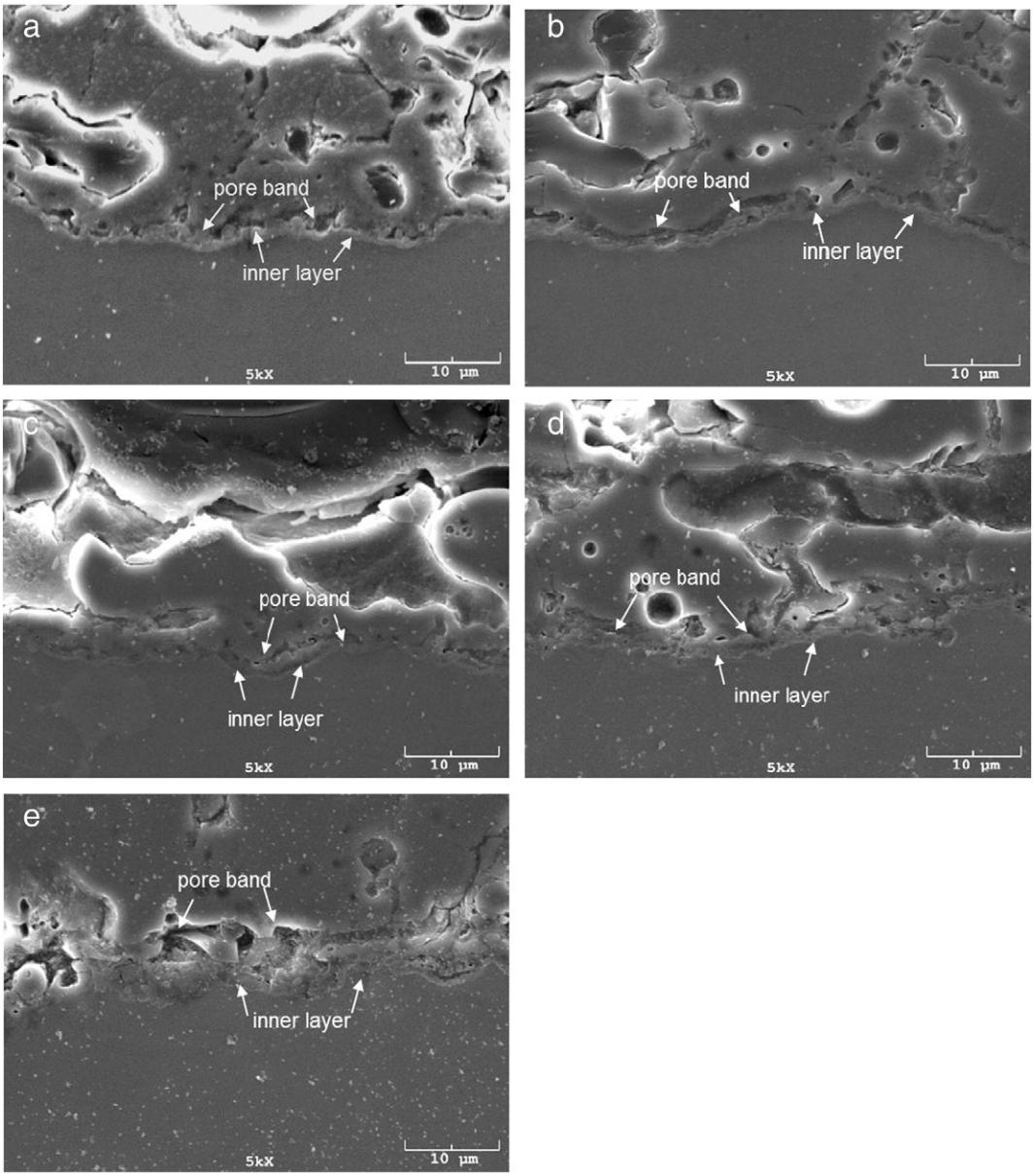

Fig. 3. Higher magnification (5000) of SEM images of the interface region towards the substrate (a) hh-coating, (b) mh-coating, (c) s-coating, (d) mp-coating, and (e) hp-coating.

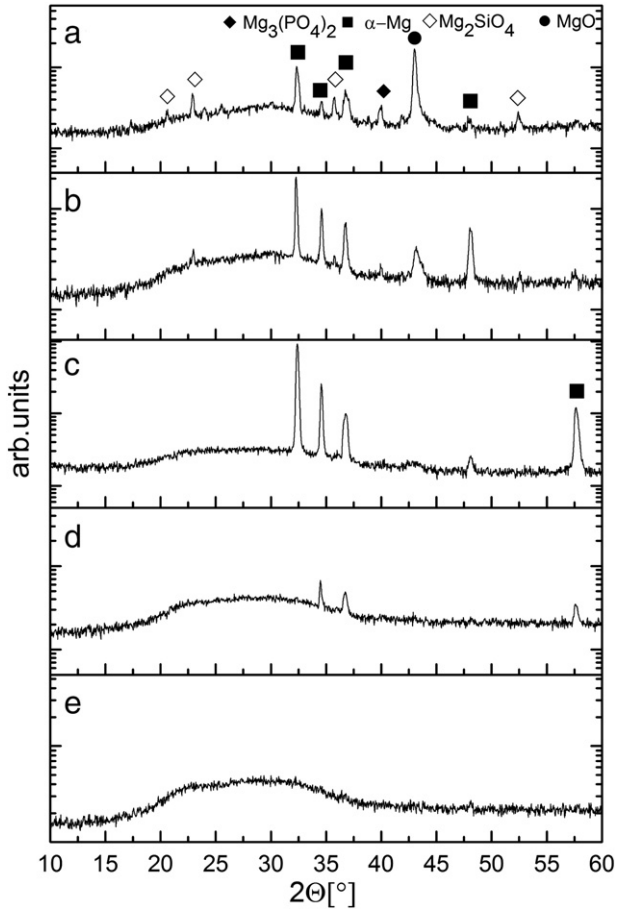

Fig. 4. XRD patterns of the PEO coatings (a) hh-coating, (b) mh-coating, (c) s-coating, (d) mp-coating, and (e) hp-coating.

existence of coating could significantly influence the anodic and cathodic reaction. It should be noted that polarization curves do not necessarily give a real picture of corrosion resistance due to the negative difference effect (NDE) [26,27]. Therefore, the i_{corr} above was determined using the current density at the intersection of the vertical through the corrosion potential with the cathodic Tafel slope (−50 mV). The calculated values are quite qualitative and mainly indicate the barrier properties of the coating and are not giving any information on the kinetics of electrochemical charge transfer as one normally expects in the case of Tafel approach. The cathodic polarization current of all coatings is apparently lower than that of magnesium substrate, indicating that the cathodic hydrogen evolution is restricted by the coating. However, the difference in corrosion current density of all the three s-coated specimens is up to two orders of magnitude. As a consequence, s-coating is highly unstable in the test solution. The selected area of the thin s-coating for polarization test can have a compact and less defective layer and sometimes not. It also depends on whether the selected area has though-going pores or not.

From the aforementioned, it is reasonable and significant to vary the concentration of the used electrolyte to get more stable and uniform

Table 3
Surface composition (at.%) of the five coatings determined by EDS analysis of a larger surface area (1 mm^2).

Coating	C	O	Mg	P	Na	K	Si	Al	Fe
hh-coating	8	50	21	5	4	2.5	6	3	0.9
mh-coating	7	50	19	7	5	2	6	3	0.7
s-coating	6.5	51	17	8.5	4.5	0.7	7	3.5	1
mp-coating	7	50	16	9	6	0.8	6.5	3	0.9
hp-coating	8	51	16	9.5	7	0.5	5.5	3	0.5

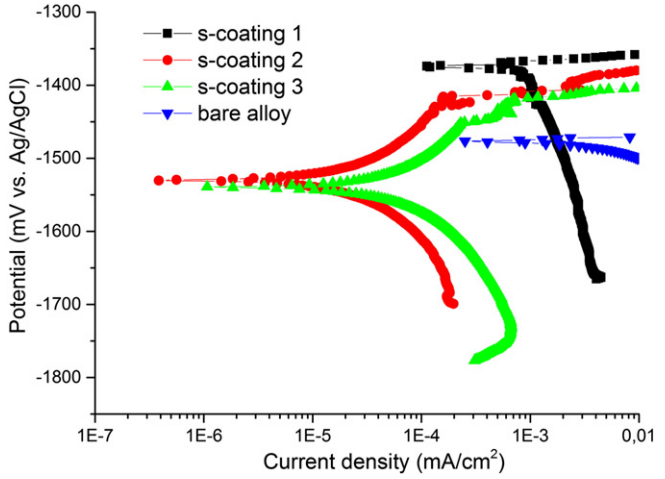

Fig. 5. Potentiodynamic polarization behavior of different specimens for s-coating (test electrolyte: 0.5 wt% NaCl).

PEO coatings. The free corrosion potentials (Table 4) of all coatings except s-coating are more active than that of the bare alloy at least by 64 mV. It can be seen that the i_{corr} values of hh-coating ($(5.8 \pm 0.8) \times 10^{-5}$ mA/cm^2), mh-coating ($(2.3 \pm 1.4) \times 10^{-5}$ mA/cm^2), and mp-coating ($(6.3 \pm 1.7) \times 10^{-5}$ mA/cm^2) are in the same order of magnitude, whilst the i_{corr} value of hp-coating ($(1.9 \pm 1.6) \times 10^{-4}$ mA/cm^2) is higher by nearly one order of magnitude. Therefore, hp-coating should be the least corrosion resistant. However, the breakdown potential of all the coatings differs marginally indicating almost same corrosion resistance of all coatings against localized corrosion [28]. The resistance of AM50 magnesium alloy against localized corrosion attack in the short term is improved by the coating, but independent from the electrolyte composition. Due to NDE, the corrosion current densities form polarization tests differ from the real values and are only qualitative. Hence, further electrochemical impedance spectroscopy measurements for long-term corrosion test are indispensable.

3.3.2. EIS results

To get additional information on the properties of the formed layers as well as on the corrosion process at metal/electrolyte interface, EIS spectra were recorded during immersion in 0.5 wt% NaCl solution at room temperature for prolonged duration up to 72 h. Fig. 7 shows the

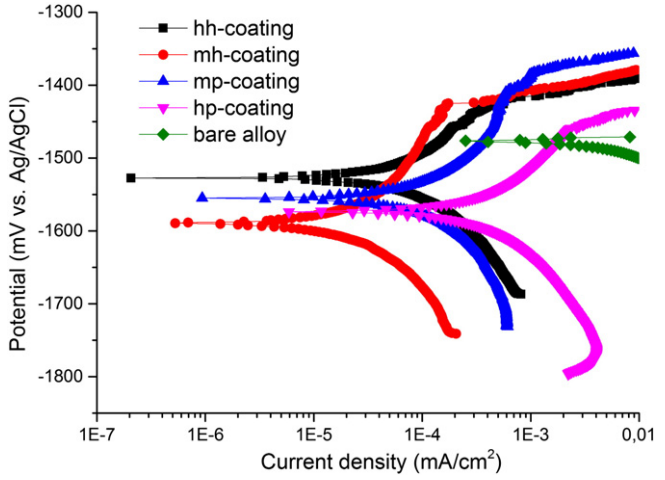

Fig. 6. Potentiodynamic polarization behavior of the other PEO coatings (test electrolyte: 0.5 wt% NaCl).

Table 4
Electrochemical data for PEO-coated specimens from potentiodynamic polarization test.

Coating	E_{corr} (mV)	i_{corr} (mA/cm^2)	E_{bd} (mV)
hh-coating	−1542 ± 40	(5.8 ± 0.8) × 10^{-5}	−1430 ± 20
mh-coating	−1563 ± 35	(2.3 ± 1.4) × 10^{-5}	−1436 ± 21
s-coating	−1477 ± 95	(6.3 ± 10.7) × 10^{-4}	−1401 ± 29
mp-coating	−1557 ± 18	(6.3 ± 1.7) × 10^{-5}	−1420 ± 20
hp-coating	−1567 ± 7	(1.9 ± 1.6) × 10^{-4}	−1450 ± 25
Bare alloy	−1478 ± 19	(3.5 ± 1.1) × 10^{-3}	

impedance spectra of the five PEO coatings. Two well-defined time constants are detected on all bode plots at low and high frequencies after the first measurement. The time constant at high frequency (10^4 Hz) relates to the outer layer, while the time constant at lower frequencies (1 Hz) can be assigned to the response of the intact inner layer. Further immersion in NaCl solution results in migration of corrosive species through the outer layer towards the inner layer. Consequently, first signs of an additional time constant in the low frequencies range appear after 1 h. This is ascribed to the initiation of the corrosion process and is attributed to the existence of the double-layer capacitance at the metal/electrolyte interface, CPE_{dl}, and the corresponding polarization resistance, R_{polar}. With increasing immersion time, the time constant at high frequencies disappears, which indicates the strong reduction of the barrier properties of the outer layer. For coatings obtained from electrolytes containing higher concentration of KOH, the high frequency time constant is maintained for a relatively long period (12 h) in contrast with mp- and hp-coating (1 h) because the outer layer in this case has smaller pores (pathways for electrolyte) and is not dissolving fast. While s-coating is the most unstable one, only the time constants associated to inner layer and corrosion process are visible after the first measurement. In order to evaluate the evolution of the coatings during immersion, all the impedance spectra were fitted to appropriate equivalent circuits. Different RC elements are used to describe appropriate components of the PEO coatings. Constant phase elements (CPE) are

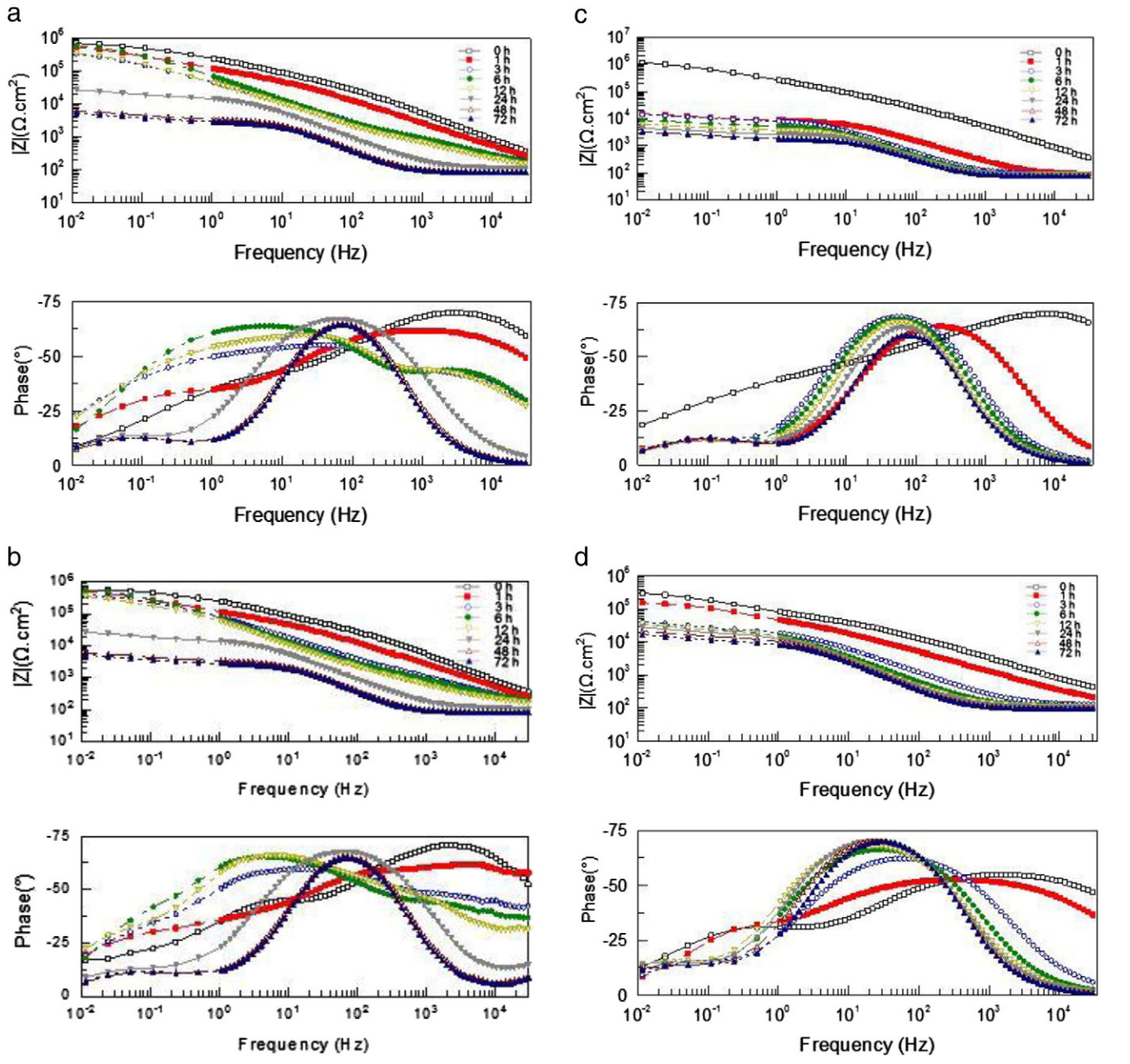

Fig. 7. Electrochemical impedance behavior (Bode plots) of the PEO coatings (a) hh-coating, (b) mh-coating, (c) s-coating, (d) mp-coating, and (e) hp-coating (after different durations of exposure).

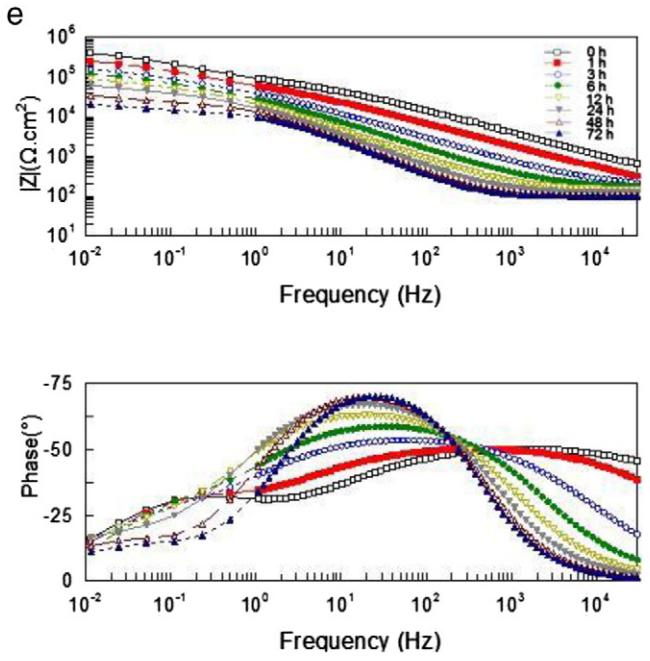

Fig. 7 (*continued*).

used rather than capacitances due to the non-ideal character of the PEO coating surface and corresponding response with phase shifts differing from −90° [29,30]. Fig. 8 aims to elucidate the degradation kinetics of the five PEO coatings. For ease of describing the entire degradation process, separated periods of 0–1, 1–12, and 12–72 h are considered to elucidate the coating degradation mechanism. The elements in the equivalent circuit include R_s (the solution resistance), R_o (resistance of the outer layer) paralleled with CPE_o (a constant phase element representing the outer layer/coating capacitance), R_i (resistance of the inner layer) paralleled with a constant phase element CPE_i (representing the inner layer), CPE_{dl} is the capacitance of electrochemical double layer at the metal/electrolyte interface, and R_{polar} is the polarization resistance of the corrosion process. In the case of spectra with a reduced number of relaxation processes, the corresponding RC elements were removed from the equivalent circuit. For example, if a spectrum (Fig. 8a) does not display a third time constant at low frequencies that is related to the corrosion processes (first measurement), the polarization resistance (R_{polar}) and the constant phase element related to the double layer capacitance (CPE_{dl}) are removed. After certain immersion time, the barrier properties of the outer layer have strongly decreased; hence, the R_o and CPE_o are removed (Fig. 8c). The impedance spectra and fitting of the five coatings after 3 h immersion are presented in Fig. 9. Table 5 records the results of the fitting, confirming the appropriateness of the selected circuit. Considering similar starting low-frequency impedance values (around 10^6 Ω cm^2), it demonstrates as well how different is the degradation progresses for the different coatings.

To evaluate the corrosion degradation behavior, the changes of R_o, R_i, R_{polar} and the corrosion resistance of the whole coating (R_{sum}) corresponding to the different PEO coatings with immersion time are presented in Fig. 10. At the beginning, the outer layer of mh-, mp-, and hp-coating has much higher resistance than that of hh-coating, which is probably due to the porosity which covers a larger area of the coating surface assuming that also the internal pore volume might be higher. A huge decrease is observed after 1 h, indicating that this outer layer has almost lost its resistance caused by the penetration of water regardless of the amorphous or crystalline phase. As for mp- and hp-coating, the time constant representing the outer layer is not visible anymore after 1 h immersion, however, this time constant lasts until 12 h for hh- and mh-coating.

For hh- and mh-coating, R_i decreases after first hour followed by a sudden increase which is maintained at the same level (10^5 Ω cm^2) for 12 h. The decrease of R_i is related to the initiation of corrosion

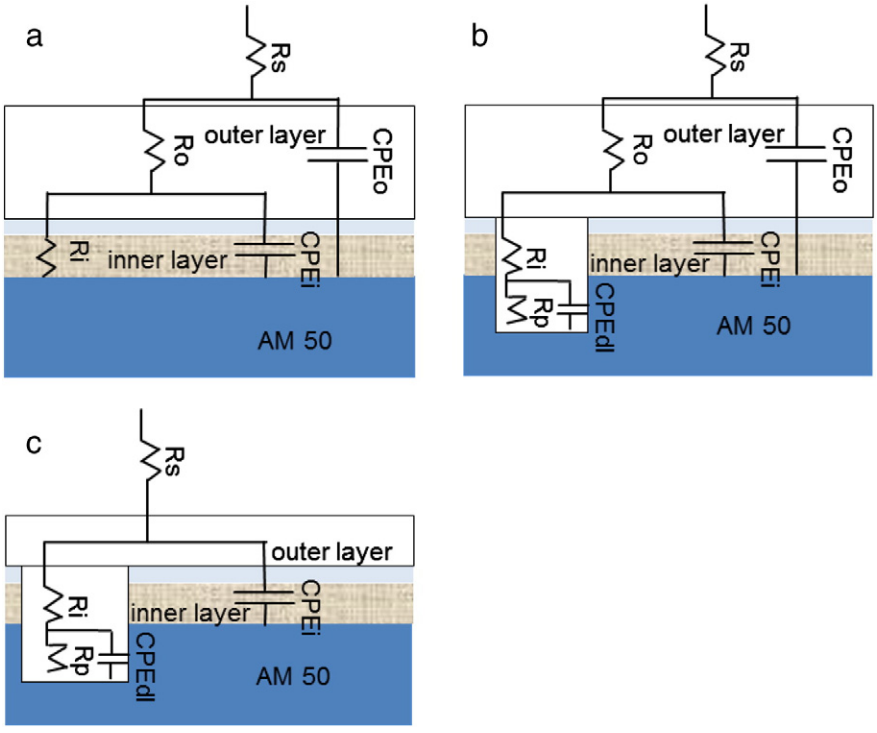

Fig. 8. Schematic representation of the coating degradation during different periods (a) initial time for all the coatings; (b) 1–12 h for hh and mh-coating, 0–1 h for mp- and hp-coating; (c) 12–72 h for hh- and mh- coating, 1-72 h for s-, mp-, and hp-coating.

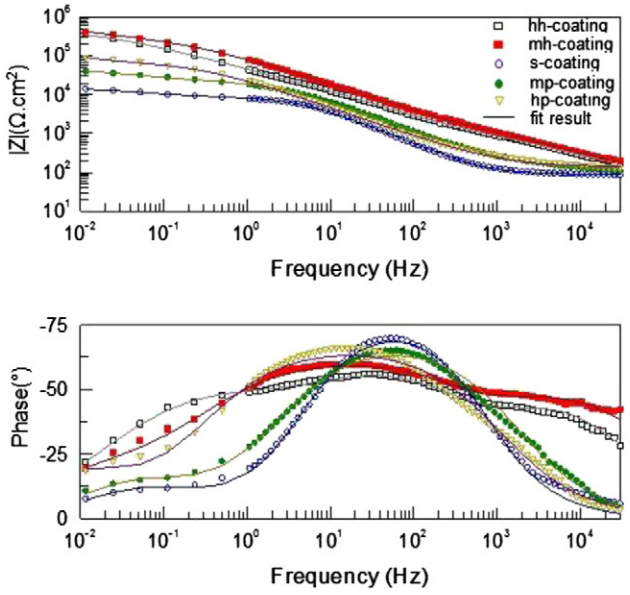

Fig. 9. Impedance spectra and fitting of the five coatings after 3 h immersion.

process, while the increase can be ascribed to the formation of corrosion product which acts as a temporary protective layer together with the original inner layer. There is no increase for the other three coatings during the whole corrosion test. The rate of the corrosion process can be compared using the polarization resistance. R_{polar} of hh- and mh-coating remains at the level of 10^5 Ω cm^2 during first 12 h which is 1 or 2 orders of magnitude higher than for the other three coatings and then decreases down to 10^4 Ω cm^2 as well. While the polarization resistance of mp- and hp-coating stays in the same magnitude (10^4 Ω cm^2) after 1 h immersion. The lowest R_{polar} (10^3 Ω cm^2) is found for s-coating. As for R_{sum}, hh- and mh-coating have been kept around 10^5 Ω cm^2 for the first 12 h due to the high value of R_i, which is much higher compared to the other three coatings. However, mh-coating shows better corrosion performance than hh-coating due to its relatively thicker inner layer. After 3 days, the R_{sum} of hh-coating (21236 Ω cm^2), mp-coating (21935 Ω cm^2), and hp-coating (26000 Ω cm^2) is much higher than mh-coating (5877 Ω cm^2) and s-coating (3500 Ω cm^2).

3.3.3. Morphology, phase, and composition of corroded coatings

The macroscopic appearances and SEM images of the corroded surface of different PEO coatings after 72 h of EIS test in 0.5 wt% NaCl solutions are depicted in Fig. 11. These surfaces reflect well how the coatings degraded in the electrolyte. The surface of all the coatings changed significantly, which is evident from the morphology of coatings before (inset image) and after corrosion. The degraded surface morphology of hh-coating (Fig. 11b) exhibits less defects than the other four coatings. The magnesium substrate is already visible for s-coating (shown by arrows in Fig. 11f), which means the surface has changed completely. The surface of mp- and hp-coating also changed a lot and is dominated by cracks, possibly formed due to corrosion or due to stress by drying after corrosion. To evaluate the uniformity of degradation, the cross section of all PEO coatings after corrosion test were prepared and shown in Fig. 12. Horizontal cracking can be seen for all the coatings after preparation work, indicating the adhesion of the layer is reduced after corrosion. There are many island-like remains of coating material for s-coating while the other coatings are still covering the whole surface. Thickness measurements are not easy because the coating loss was not always uniform; thus, we used the information from cross section (giving the lowest and highest coating thickness observed) and the average values of gauge measurements. The cross-sectional thickness decreases to some extent for all the coatings, for example, hh-coating (from 40 ± 5 μm to 30/40 μm), mh-coating (from 50 ± 8 μm to 20/40 μm), s-coating (from 15 ± 5 μm to 0/20 μm), mp-coating (from 43 ± 7 μm to 20/40 μm), and hp-coating (from 67 ± 6 μm to 40/70 μm). Coating thickness measured by MiniTest 2100 before and after corrosion measurements is depicted in Table 6. The measurement is averaging to a larger extent compared to the cross-sectional minimum-maximum thickness values determined by the eye. Thus, the thickness of corroded areas for the hydroxide specimens reduces from 45 ± 7 μm to 30 ± 6 μm (hh-coating) and from 48 ± 7 μm to 25 ± 5 μm (mh-coating) and for the phosphate specimens from 35 ± 5 to 20 ± 8 μm (mp-coating) and from 65 ± 10 to 36 ± 8 μm (hp-coating) decreases. Therefore, the measurements of the coating thickness by MiniTest 2100 are consistent with the micrographs, except for the s-coating where it was not possible to measure the areas without coating. However, from the values of the other four coatings, it is nearly impossible to evaluate the degradation rate, even if one would assume a constant degradation rate over time. The coating thicknesses do vary too much and also due to the stirring of the electrolyte we see an additional influence on coating thickness depending if the side was in the shadow of the container or not. Thus, only a qualitative ranking is given based on uniformity of attack and from the micrographs shown in Fig. 12 one can find in increasing uniformity in degradation in the following order: s-coating < mp-coating < hp-coating < mh-coating < hh-coating. However, the uniformity of degradation is probably more important for any bio-application than the degradation rate as one can adjust the life time of a component via coating thickness or composition.

In order to know how coating composition changed after 72 h corrosion test, a representative coating (s-coating) was selected to do GDOES measurement. The GDOES profiles of the s-coating before and after corrosion test are shown in Fig. 13. For the coating without corrosion (Fig. 13a), a two layer structure can be seen. There is a top layer rich in Si, P, and O followed by a uniform distribution of those elements representing the majority of the coating. Finally, the intensity of O, Si, and P spectra simultaneously and sharply decreases at around 700 s of sputtering time, and the intensity of Mg spectrum increases at the same sputtering time. Thus, this point indicates the interface between the coating and matrix. In the case of coating after corrosion test (Fig. 13b), the thickness of the layer has reduced to a large extent, as indicated by the interface at about 150 s, which can be also confirmed by the SEM result. In addition, the intensity of Si and P decreases and O increases greatly, demonstrating the loss of the majority of the coating which might be replaced by an oxygen rich conversion product. Unlike Si and O, which decrease continuously from the surface towards the interface, P is depleted in the near surface (Fig. 13b). Therefore, it can be inferred that the dissolution of coating material starts with the removal

Table 5
Fitting results of the impedance spectrum depicted in Fig. 9.

Coating	R_o (Ω cm^2)	CPE_o:Q_o, 1/Ohm s^n cm^{-2}	R_i (Ω cm^2)	CPE_i:Q_i, 1/Ohm s^n cm^{-2}	R_{polar} (Ω cm^2)	CPE_{polar}:Q_{polar}, 1/Ohm s^n cm^{-2}	Goodness of fit
hh-coating	4594	6.2×10^{-6}, where $n = 0.58$	276860	2.4×10^{-7}, where $n = 0.91$	262670	2.6×10^{-6}, where $n = 0.66$	2.6×10^{-4}
mh-coating	5230	6.1×10^{-6}, where $n = 0.59$	263480	2×10^{-7}, where $n = 0.93$	288320	2.8×10^{-6}, where $n = 0.68$	4.1×10^{-4}
s-coating			8600	6.3×10^{-6}, where $n = 0.88$	6600	4.3×10^{-4}, where $n = 0.75$	7.2×10^{-5}
mp-coating			25290	5.9×10^{-6}, where $n = 0.77$	19229	1.9×10^{-4}, where $n = 0.82$	4.8×10^{-4}
hp-coating			79000	5.3×10^{-6}, where $n = 0.64$	118000	1.4×10^{-5}, where $n = 0.71$	6.6×10^{-4}

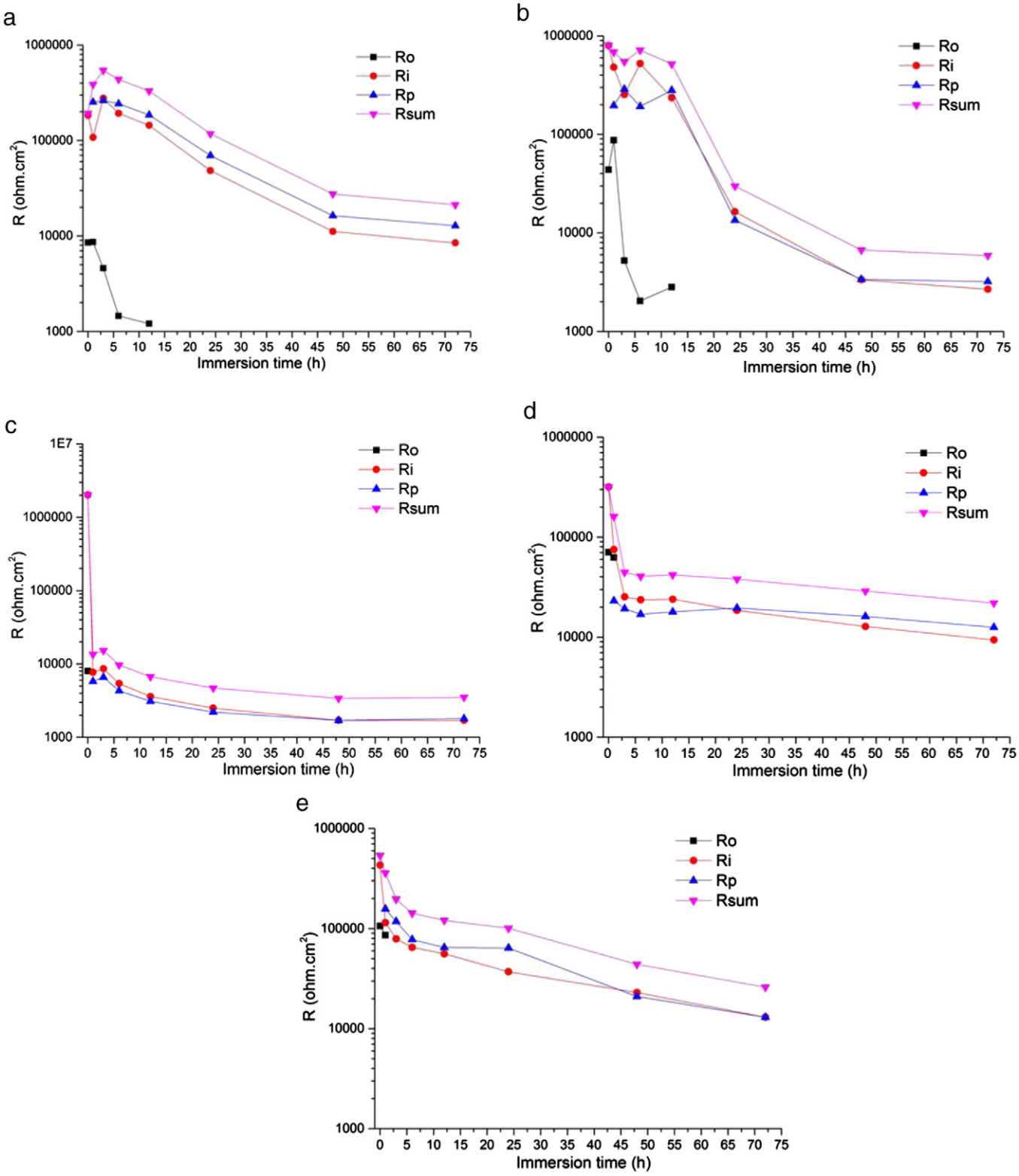

Fig. 10. The change of R_o, R_i, R_{polar}, and R_{sum} of the PEO coatings as a function of immersion time (a) hh-coating, (b) mh-coating, (c) s-coating, (d) mp-coating, and (e) hp-coating.

of P from the amorphous phase because the main phase of s-coating is amorphous phase which is unstable and may dissolve fast [31,32]. However, locally parts of the coating might be lost additionally by flaking off.

Fig. 14 shows the phases present in PEO coatings after dissolution. The relative increase in intensity and/or appearance of new peaks of Mg in all coatings shows coatings underwent remarkable loss of thickness in 0.5 wt% NaCl solution. It is also obvious that the bump at 20°–35° of amorphous phase is significantly reduced after dissolution, which is a strong evidence for dissolution of mainly amorphous phases. However, hh-coatings still shows several peaks corresponding to crystalline Mg_2SiO_4. Few peaks corresponding to $Mg_3(PO_4)_2$ are also present in the coating even after dissolution. These data show that crystalline

phases did not degrade greatly during immersion. For the mh-coating, a lower intensity of MgO and several small Mg_2SiO_4 peaks still appear. However, a new bump appears in the 2θ range of 10°–12.5° for all the coatings except for hp-coating. In the range of 20°–35° of 2θ, a second small bump can be seen for s- and mp-coating. These new bumps might be attributed to new amorphous or nanocrystalline phases manifesting that the coating composition has been changed after 3 days corrosion test.

EDS was also used to determine the elemental composition of the PEO coatings after 3 days EIS test. Table 7 reveals that the content of phosphorus and silicon decrease. The vanishing of other elements or compounds leads to the increase of Fe and Al. In the case of s-coating, oxygen and phosphorus decrease to a large extent, while the content of magnesium increases from 17% to 35%, demonstrating substrate has been exposed to NaCl solution (Fig. 11f).

4. Discussion

In previous studies [19], amorphous PEO coatings with compositions close to commercial bio-glasses were produced in phosphate and silicate based electrolytes containing clay particles. The formation of amorphous phase is caused by clay particle additions, which can lower the sintering temperature and change the coating composition to ease amorphous film formation. As clay particles have the ability to lower the melting point, more volume substrate-electrolyte conversion products are melted by the discharges during PEO processing and cooling is slower offering more time for them to flow back filling pores before solidifying. It is known that Si and P have good glass forming ability [33, 34]. In other words, phosphorus and silicon could endow the ability of PEO coatings to have a glassy composition under certain processing parameters. Indeed, a single amorphous phase appears with the increasing concentration of Na_3PO_4, indicating phosphorus could promote a glassy PEO coating. Higher concentration of hydroxide may facilitate the formation of crystalline phases. The increasing number of big-sized pores on the surface of mp- and hp-coating manifests that more volume of the coating can be melted and mixed together, which may also promote the formation of an amorphous phase. In addition, variation of phosphate electrolyte does not affect the incorporation of clay particle because the Si content of all coatings is nearly the same. Apart from the phase composition, the structure of the coating is important for the corrosion performance.

According to the investigation of Hussein et al. [35], in PEO process, the ceramic coating grows inwards to the alloy substrate (inner layer) and outwards to the coating surface (outer layer) simultaneously. After the passive film was punctured, Mg and Mg^{2+} from the substrate were ejected and reached the coating/electrolyte interface and then reacted with O_2 generated by electrolysis and finally deposited the outer layer. The growth of the inner layer depends on the diffusion process of oxygen and probably other elements (phosphorous from the electrolyte). Therefore, it can be deduced that the pore band is induced by the different growth directions. Sah et al. [23] showed that discharge intensity is accelerated by higher concentration of phosphate and thicker PEO coatings with large discharge pores, often reaching to coating/substrate interface, are formed. After the discharges quench, melted material will flow back towards inner part of the coating. The end of large discharge channels might not be filled in time; thus, the pore band appears.

Potentiodynamic polarization shows that PEO coatings formed in electrolytes with higher phosphate concentration have higher corrosion rates. It can be assumed that not much volume of coating dissolves within short time (0.5 h); thus, the inner layer and defects of the coating are the most dominant influence for short-term polarization test. In this case, small volume of the pore band and thicker inner layer could provide coating with lower corrosion current. It is understandable the more defective cross section (hp-coating) has higher corrosion rate and relatively thicker inner layer provides the lower corrosion current for mh-coating compared to the other coatings. The order of corrosion resistance is correlated well with the combination of lower pore band thickness and increasing inner layer thickness.

Nevertheless, the long-term deterioration process of the five PEO coatings is controlled by different factors. On the one hand, the thickness and composition of the outer layer and the compactness of the inner layer endow original protection capability for the AM50 magnesium alloy against the corrosive solution. On the other hand, the porosity of the whole layer and the volume of the pore band in combination with the coating composition control the coating degradation process. Based on the changing content of P and Si, corroded surface and XRD patterns after corrosion test, it can be inferred that silicate compound, and the other crystalline phases such as MgO and $Mg_3(PO_4)_2$, is more stable and contributes to better protective ability than amorphous material. The amorphous material is unstable under the attack of Cl^- containing aqueous solution, converting into new material or dissolving during immersion.

Due to the compact inner layer, s-coating shows higher corrosion resistance than all other coatings at the beginning. After a short period (1 h), through-going paths across the whole layer are produced in selected areas by discharge channels, large-sized pores and dissolving amorphous material (especially for s-, mp-, and hp-coating), making the permeation of corrosive electrolyte into the inner coating easier and faster. In this case, the formation rate and volume of the through-going paths of s-, mp- and hp-coating is larger than hh- and mh-coating because of more large-sized pores and single amorphous phase. During this period, corrosion processes occur in the pore band and a new passive film formed by corrosion products, mainly $Mg(OH)_2$, might be deposited on the inner layer. While $Mg(OH)_2$ is not stable in aqueous solutions with a pH lower than 10.5 [36]. The pH value can increase in the small volume of the pore band. Hence, whether newly formed $Mg(OH)_2$ stays in the pore band and replenishes the protective ability of the inner layer rely on the pH value of the electrolyte in the pore band. Considering the volume of the pore band (hp-coating > mp-coating > mh-coating > hh-coating > s-coating) and size and amount of the through-going paths (s-coating > hp-coating ≈ mp-coating > mh-coating > hh-coating), one can assume that the higher alkaline pH values can be established in the following order: hh-coating > mh-coating > mp-coating ≈ hp-coating > s-coating. Thus, the higher pH value of the electrolyte in the pore band can inhibit the dissolution of corrosion products and stimulate redeposition of Mg $(OH)_2$. From this point of view, R_i can be kept at a high range ($10^5\ \Omega\ cm^2$) for PEO coatings produced from electrolytes containing higher concentration of KOH, while s-, mp-, and hp-coating degrade continuously with time considering the EIS results. For hh- and mh-coating, the increasing number and size of the through-going paths is much lower due to the stable crystalline silicate phase in the coating compared to the other coatings. Thus, the resistance of the outer layer (hh- and mh-coating) is kept for 12 h, while the other three coatings only maintain it at the first or second measurement. In the last period (12–72 h), more amounts of fresh corrosive solution will penetrate into the inner layer via increasing through-going paths. It is inevitable that the $Mg(OH)_2$ film at the pore band of hh- and mh-coating is also dissolved with the decreasing pH value, leading to a continuous decrease of the corrosion resistance. Although the EIS suggests a uniform degradation of the phosphate coatings the reality looks different. The evaluation of the cross sections has demonstrated that the hydroxide versions of the coatings are degrading more uniform in the sense of losing parts of the coating. S-coating is not suitable at all to guarantee uniform degradation because in the thin regions substrate is already reached while the thicker parts are still present. The mp-coating has lost also large parts from the top coating while an inner continuous layer is still visible. However, this may not be critical for industrial coating applications, but for bio-applications, larger particle flakes detaching from the coating need to be prevented. In that sense, also hp- and mh-coating appears to be critical as larger areas are missing. The most uniform coating is the hh-coating.

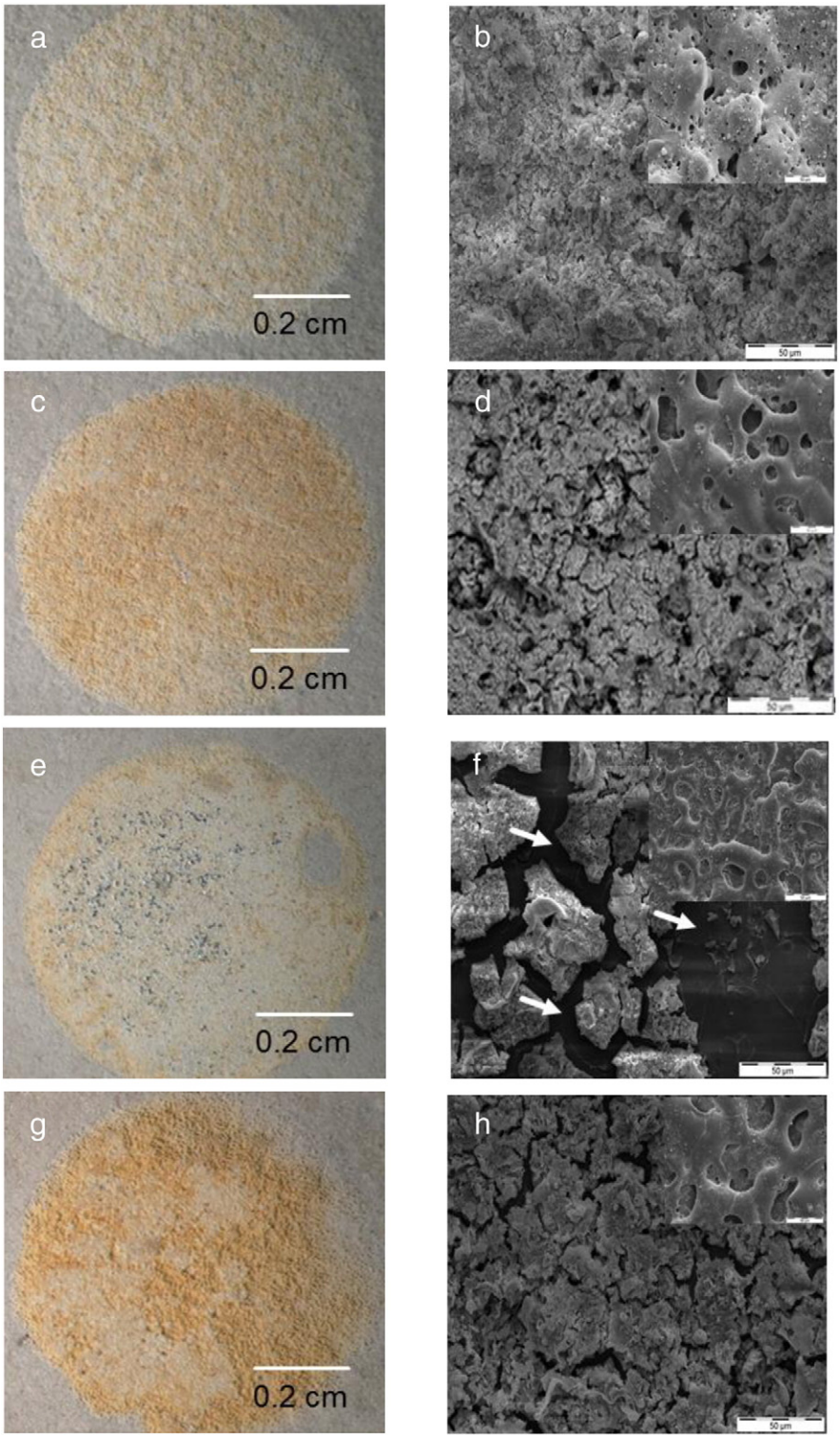

Fig. 11. The macroscopic appearance and SEM pictures of corroded surfaces of the five PEO coatings after 72 h immersion in 0.5 wt% NaCl solution: (a and b) hh-coating, (c and d) mh-coating, (e and f) s-coating, (g and h) mp-coating, and (i and j) hp-coating.

Nevertheless, one has to keep in mind that this loss of material might be also a result of localized dissolution of certain phases and the whole performance might be changing by altering the electrolyte composition. Therefore, more studies are required, but it is obvious that the degradation behavior can be influenced via the treatment electrolyte composition which is influencing the phase composition of the final coating.

Summarizing, it can be stated that PEO coatings formed in electrolytes with higher concentration of phosphate will degrade less uniform and more rapidly, while coatings produced from electrolytes containing higher concentration of hydroxide appears to degrade slower and more uniform. This statement is based on the SEM cross sections taken after corrosion testing. However, EIS shows more or less the opposite

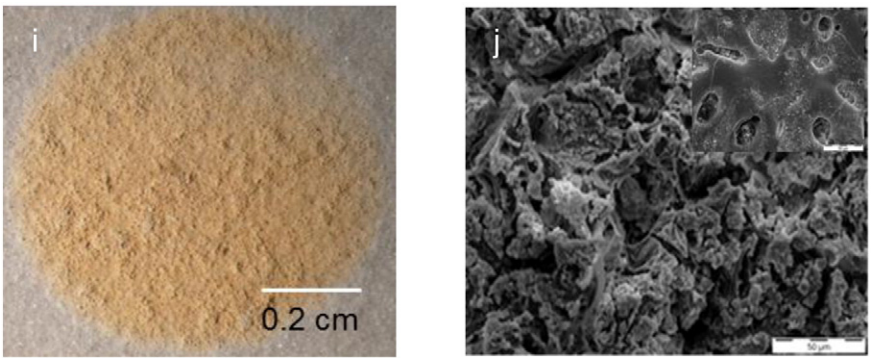

Fig. 11 (*continued*).

behavior with the phosphate coatings degrading more uniform if the change of impedance values with time is considered. A possible explanation might be that the actual appearance of the cross section is caused by drying of the layer and induced stresses causing flaking-off of coating parts. Nevertheless, the degradation process of the PEO coating is obviously a synergetic effect of phase composition and micro-morphology of the coating. In other words, it might be feasible to control the degradation rate of PEO coating in a certain range by varying the PEO electrolyte composition and thus the phase composition. The amorphous phase dissolves or degrades differently compared to the mixture of crystalline and amorphous phase and it should be possible to adjust certain degradation rates by a change of the electrolyte composition. Degradable coatings are essential for biomedical applications of magnesium alloys. It will be interesting to see if this different behavior can be

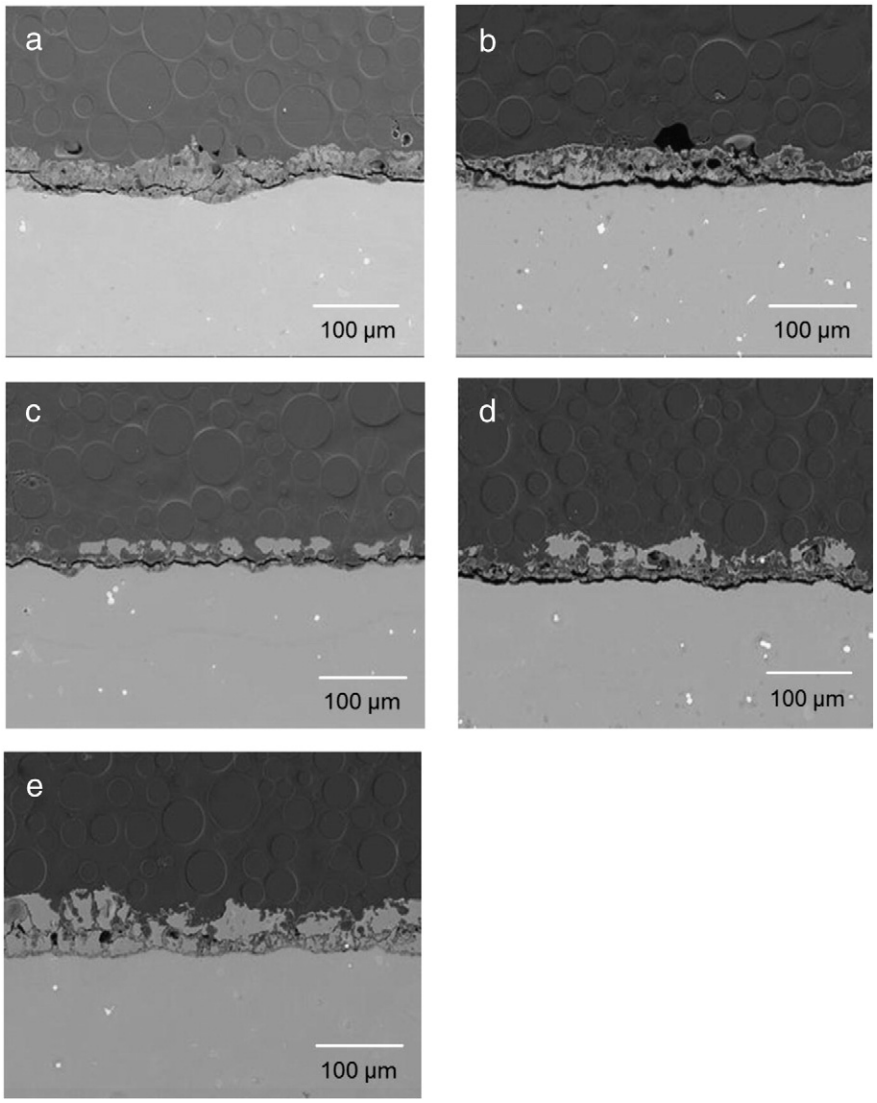

Fig. 12. Cross section of the five PEO coatings after 72 h corrosion test (a) hh-coating, (b) mh-coating, (c) s-coating, (d) mp-coating, and (e) hp-coating.

Table 6
Coating thickness before and after 72 h corrosion test.

Coating	Thickness before corrosion test by MiniTest 2100 (μm)	Thickness after corrosion test by MiniTest 2100 (μm)	Thickness before corrosion test by SEM (μm)	Thickness after corrosion test by SEM (μm)
hh-coating	45 ± 7	30 ± 6	40 ± 5	30/40
mh-coating	48 ± 7	25 ± 5	50 ± 8	20/40
s-coating	17 ± 4	8 ± 4	15 ± 5	0/20
mp-coating	35 ± 5	20 ± 8	43 ± 7	20/40
hp-coating	65 ± 10	36 ± 8	67 ± 6	40/70

used to tune the degradation of degradable Mg implants in the future. Future studies are required, e.g., influence of physiological solutions and flow rate of the solutions.

5. Conclusions

The composition of electrolyte containing clay particles is highly effective to control the morphology and phase composition of PEO coating. Single amorphous phase can be produced from electrolytes with higher concentration of Na_3PO_4. Electrolytes containing higher concentration of KOH tend to produce PEO coatings with mixture of crystalline and amorphous phases.

The first factor determining degradation is the phase composition of the coating. The stability of coating phases under the attack of Cl^- containing aqueous solutions is as follows: amorphous material < MgO < $Mg_3(PO_4)_2$ < Mg_2SiO_4.

The micro-morphology of the coating is the second important factor influencing the coating degradation. There is only a thin barrier layer in all the coatings which is in direct contact to a pore band and which has direct contact to the electrolyte via defects in the outer coating. Thus, electrolyte can easily penetrate and reach the pore band. The stability of the barrier layer depends thus on the pH value of the electrolyte in the pore band. At higher pH values, the barrier layer is not only more stable it can be also strengthen by the formation of new passive film, mainly $Mg(OH)_2$. Such a high pH value can be more easily obtained in small pore band volumes due to dissolution of the magnesium substrate and coating phase. Thus, there is a direct link between pore band volume and path way size towards the outer electrolyte with the corrosion resistance and life time of the coating.

Amorphous PEO coatings degrade differently compared to PEO coatings with mixed crystalline and amorphous phases. The corrosion rate of PEO coating is obviously controlled by the phase composition and layer morphology by influencing the extension of through-going

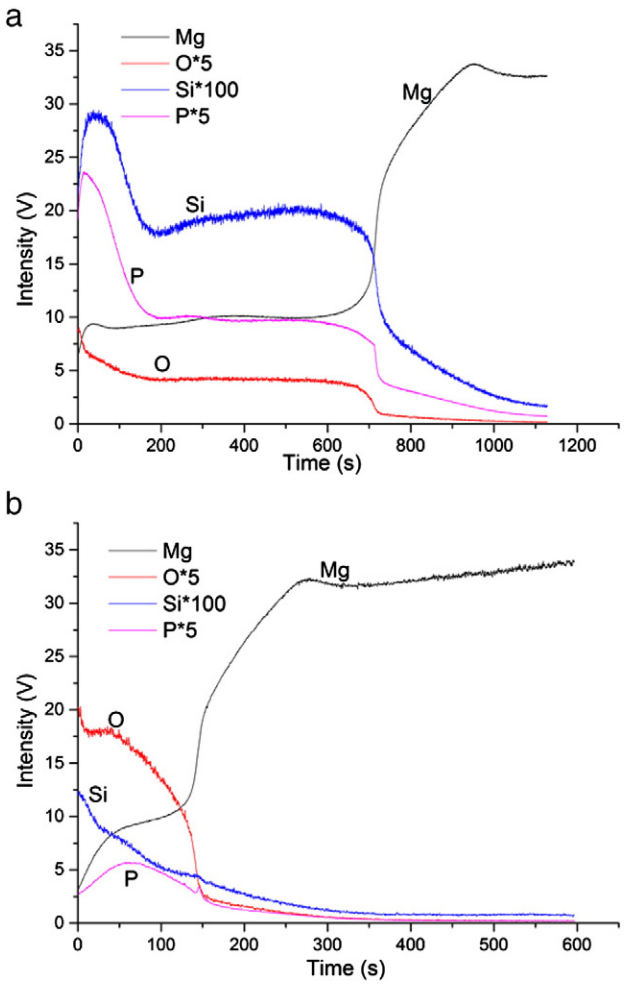

Fig. 13. GDOES profiles of the s-coating (a) before and (b) after 72 h corrosion test.

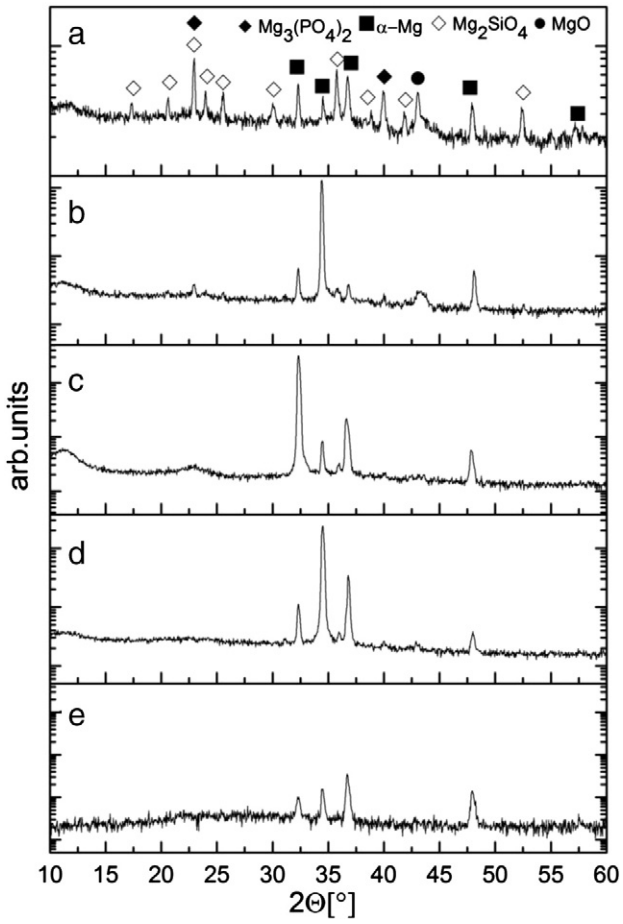

Fig. 14. XRD patterns of the PEO coatings after 72 h corrosion test (a) hh-coating, (b) mh-coating, (c) s-coating, (d) mp-coating, and (e) hp-coating.

Table 7
Surface composition of the five PEO coatings determined by EDS analysis after EIS tests.

Concentration (at.%)	C	O	Mg	P	Na	K	Si	Al	Fe
hh-coating	8	49	24	5	2	1	4	4.5	2
mh-coating	8	55	20	4	2	1	3	5	3
s-coating	11	40	35	3	1	0.4	2	6.5	0.4
mp-coating	10	49	19	6	3	0.9	3	5	4
hp-coating	6	50	25	6	3	0.4	4	4	2.5

paths, controlling the pH value of electrolyte in the coating (coating can be compared with a sponge soaking in electrolyte) and conversion into new phases replacing the original coating. In that sense, it might be possible to use this different performance to control and adjust certain degradation rates which might be necessary for bio-medical applications.

Acknowledgments

The technical support of Mr. Volker Heitmann and Mr. Ulrich Burmester during the course of this work is gratefully acknowledged. X. Lu thanks China Scholarship Council for the award of fellowship and funding. M. Mohedano is grateful to the Alexander von Humboldt Foundation, Germany, for the award of AvH research fellowship and financial assistance.

References

[1] A.L. Yerokhin, X. Nie, A. Leyland, A. Matthews, S.J. Dowey, Surf. Coat. Technol. 122 (1999) 73–93.
[2] T.S.N. Sankara Narayanan, I.S. Park, M.H. Lee, Prog. Mater. Sci. 60 (2014) 1–71.
[3] C. Blawert, W. Dietzel, E. Ghali, G.L. Song, Adv. Eng. Mater. 8 (2006) 511–533.
[4] H. Duan, C. Yan, F. Wang, Electrochim. Acta 52 (2007) 3785–3793.
[5] A.A. Zuleta, E. Correa, C. Villada, M. Sepúlveda, J.G. Castaño, F. Echeverría, Surf. Coat. Technol. 205 (2011) 5254–5259.
[6] J.E. Gray, B. Luan, J. Alloys Compd. 336 (2002) 88–113.
[7] H. Duan, C. Yan, F. Wang, Electrochim. Acta 52 (2007) 5002–5009.
[8] R. Arrabal, E. Matykina, F. Viejo, P. Skeldon, G.E. Thompson, Corros. Sci. 50 (2008) 1744–1752.
[9] A. Němcová, P. Skeldon, G.E. Thompson, B. Pacal, Surf. Coat. Technol. 232 (2013) 827–838.
[10] J. Liang, L. Hu, J. Hao, Electrochim. Acta 52 (2007) 4836–4840.
[11] J. Liang, P.B. Srinivasan, C. Blawert, W. Dietzel, Corros. Sci. 51 (2009) 2483–2492.
[12] R. Arrabal, E. Matykina, P. Skeldon, G.E. Thompson, J. Mater. Sci. 43 (2008) 1532–1538.
[13] M. Laleh, A.S. Rouhaghdam, T. Shahrabi, A. Shanghi, J. Alloys Compd. 496 (2010) 548–552.
[14] J. Guo, L.P. Wang, S.C. Wang, J. Liang, Q.J. Xue, F.Y. Yan, J. Mater. Sci. 44 (2009) 1998–2006.
[15] W. Li, L. Zhu, H. Liu, Surf. Coat. Technol. 201 (2006) 2505–2511.
[16] K.M. Lee, K.R. Shin, S. Namgung, B. Yoo, D.H. Shin, Surf. Coat. Technol. 205 (2011) 3779–3784.
[17] X. Lu, C. Blawert, N. Scharnagl, K.U. Kainer, J. Magnes. Alloys 1 (2013) 267–274.
[18] K.M. Lee, B.U. Lee, S.I. Yoon, E.S. Lee, B. Yoo, D.H. Shin, Electrochim. Acta 67 (2012) 6–11.
[19] C. Blawert, S.P. Sah, J. Liang, Y. Huang, D. Höche, Surf. Coat. Technol. 213 (2012) 48–58.
[20] C. Blawert, D. Höche, Y. Huang, J. Liang, United States Patent, No.:US 2012/0261266 A1 (2012).
[21] Y.G. Ko, S. Namgung, D.H. Shin, Surf. Coat. Technol. 205 (2010) 2525–2531.
[22] A. Da Forno, M. Bestetti, Surf. Coat. Technol. 205 (2010) 1783–1788.
[23] S.P. Sah, Y. Aoki, H. Habazaki, Mater. Trans. 51 (2010) 94–102.
[24] Nanofil®116, product bulletin and safety data sheeth, www.scprod.com.
[25] R. Arrabal, E. Matykina, T. Hashimoto, P. Skeldon, G.E. Thompson, Surf. Coat. Technol. 203 (2009) 2207–2220.
[26] G. Song, A. Atrens, D.S. John, X. Wu, J. Nairn, Corros. Sci. 39 (1997) 1981–2004.
[27] S. Yagi, K. Kuwabara, Y. Fukuta, K. Kubota, E. Matsubara, Corros. Sci. 73 (2013) 188–195.
[28] G.-L. Song, Surf. Coat. Technol. 203 (2009) 3618–3625.
[29] M.L. Zheludkevich, R. Serra, M.F. Montemor, K.A. Yasakau, I.M.M. Salvado, M.G.S. Ferreira, Electrochim. Acta 51 (2005) 208–217.
[30] M. Schem, T. Schmidt, J. Gerwann, M. Wittmar, M. Veith, G.E. Thompson, I.S. Molchan, T. Hashimoto, P. Skeldon, A.R. Phani, S. Santucci, M.L. Zheludkevich, Corros. Sci. 51 (2009) 2304–2315.
[31] H. Fleisch, R. Russell, S. Bisaz, J. Termine, A. Posner, Calcif. Tissue Res. 2 (1968) 49–59.
[32] Y. Mori, A. Koshi, J. Liao, H. Asoh, S. Ono, Corros. Sci. 88 (2014) 254–262.
[33] B. Shen, M. Akiba, A. Inoue, Intermetallics 15 (2007) 655–658.
[34] K. Ikarashi, T. Mizushima, A. Makino, A. Inoue, Mater. Sci. Eng. A 304–306 (2001) 763–766.
[35] R.O. Hussein, X. Nie, D.O. Northwood, Electrochim. Acta 112 (2013) 111–119.
[36] J. Liang, P.B. Srinivasan, C. Blawert, W. Dietzel, Corros. Sci. 52 (2010) 540–547.

5.5 Influence of electrical parameters on particle uptake during plasma electrolytic oxidation processing of AM50 Mg alloy *(with permission from Elsevier)*

Surface & Coatings Technology 289 (2016) 179–185

Contents lists available at ScienceDirect

Surface & Coatings Technology

journal homepage: www.elsevier.com/locate/surfcoat

Influence of electrical parameters on particle uptake during plasma electrolytic oxidation processing of AM50 Mg alloy

Xiaopeng Lu *, Carsten Blawert, Marta Mohedano, Nico Scharnagl, Mikhail L. Zheludkevich, Karl Ulrich Kainer

Institute of Materials Research, Helmholtz-Zentrum Geesthacht, Max-Plank-Str. 1, 21502 Geesthacht, Germany

ARTICLE INFO

Article history:
Received 11 November 2015
Revised 31 January 2016
Accepted in revised form 2 February 2016
Available online 3 February 2016

Keywords:
Magnesium
Coatings
Plasma electrolytic oxidation
SiO_2 particle
Electrical parameter

ABSTRACT

The influence of electrical parameters on microstructure and composition of coatings by plasma electrolytic oxidation (PEO) with particle addition was investigated. PEO coatings were produced on AM50 magnesium alloy from an alkaline phosphate based electrolyte (1 g/l KOH + 20 g/l Na_3PO_4) with 5 g/l SiO_2 particle (1–5 μm) addition. Besides the most common electrical parameters (voltage and current density), frequency and duty ratio have effect on the uptake of particles during PEO processing. Higher duty ratio and lower frequency allow to incorporate more particles into the PEO coating. The area of the melting pools, as indicated by the size and area of the open pores on the coating surface, can be considered as one important factor to determine the particle uptake during PEO processing.

© 2016 Elsevier B.V. All rights reserved.

1. Introduction

Plasma electrolytic oxidation (PEO) is a promising surface treatment process derived from conventional anodizing to form ceramic-like coatings on light alloys (Al, Mg and Ti), which are used for corrosion, wear protection and biomedical applications [1–5]. PEO uses aqueous eco-friendly, usually alkaline, electrolytes and the coatings are formed by high voltage, when short-lived discharges occur locally on the coating surface leading to a high pressure and temperature environment [6,7]. Regarding Mg and its alloys, a two- or three-layer structure is typically observed with a characteristic thin barrier layer laying directly on the metal surface, of a few hundred nanometer thickness, and an outer porous layer which exhibits relatively low corrosion resistance [8,9]. The properties of the coating mainly depend on the substrate, treatment time, electrical regime (DC, AC and bipolar) and electrolyte, where the electrolyte plays a decisive role due to the incorporation of species from the bath into the oxide film [10,11].

Introducing particles to the PEO electrolyte, such as clay, ZrO_2, CeO_2, Si_3N_4, Al_2O_3, SiO_2, SiC and hydroxyapatite (HA), have been explored as new strategies to seal pores and provide a wider range of compositions for PEO coatings on Mg/Mg alloys [12–20]. Metal oxide particles (e.g. Fe_3O_4 and ZrO_2) can also be incorporated into the coatings by adding related metal salts to the electrolyte [21,22]. Besides the electrolyte parameters and treated matrix, the process parameters such as applied voltage/current density, frequency and duty cycle have a significant influence on the coating microstructure and properties [23–25], which will also determine the uptake and incorporation of particles during PEO processing. It is expected that the amount of incorporated particles will be in direct relation to the applied voltage and current density, since the dispersed particles in the alkaline electrolyte are negatively charged [26] and will move towards the anode continuously. Therefore, higher voltage and current density will result in a higher number of incorporated particles together with other components from the electrolyte. So far, there are only a limited number of reports about the effect of frequency and duty ratio on particle addition during PEO processing.

2. Experimental

Specimens of AM50 magnesium alloy with a size of 15 mm × 15 mm × 4 mm were prepared from gravity cast ingot material. The chemical composition of AM50 alloy, as measured with an Arc Spark OES (Spark analyser M9, Spectro Ametek, Germany), is 4.74 wt.% Al, 0.383 wt.% Mn, 0.065 wt.% Zn, 0.063 wt.% Si, 0.002 wt.% Fe, 0.002 wt.% Cu and Mg balance. The specimens were ground using emery papers up to 1200 grit and then air-dried prior to PEO treatment.

The PEO process was carried out by using a pulsed DC power source with different frequencies and pulse ratios, as shown in Table 1. Pulse-on and pulse-off time were varied to study the effect

* Corresponding author.
E-mail address: xiaopeng.lu@hzg.de (X. Lu).

http://dx.doi.org/10.1016/j.surfcoat.2016.02.006
0257-8972/© 2016 Elsevier B.V. All rights reserved.

Table 1
Electrical parameters used for PEO treatment.

Frequency and duty ratio	Pulse-on and pulse-off time (ms)
50 Hz and 10%	2 + 18
250 Hz and 10%	0.4 + 3.6
500 Hz and 10%	0.2 + 1.8
50 Hz and 30%	6 + 14
250 Hz and 30%	1.2 + 2.8
500 Hz and 30%	0.6 + 1.4

on the particle uptake. The specimens and a stainless steel tube were used as the anode and cathode, respectively. 5 g/l of SiO_2 particles in the range of 1–5 μm was added into a phosphate based electrolyte (1 g/l KOH and 20 g/l Na_3PO_4). A stirrer and bubbling generator were used to facilitate the uniform distribution of the particles in the electrolyte. All the PEO treatments were performed at a constant voltage of 450 V for 10 min and the average current density provided by the DC power supply was limited to 300 mA/cm^2. The temperature of the electrolytes was kept at 10 ± 2 °C by a water cooling system.

A scanning electron microscope (TESCAN Vega3 SB) combined with an energy dispersive spectrometer (EDS) system from eumeX (ixrfsystems) was used to examine the surface morphology, composition and microstructure of the PEO coatings. An acceleration voltage of 15 kV was applied for SEM and EDS investigations. According to the EDS analysis, the Si content of the same specimen between different positions was nearly the same (<5%). The phase crystal structure analysis was done with a Bruker X-ray diffractometer using Cu Kα radiation. Image analysis software analySIS pro 5.0 was used to measure the number and size of the pores on coating surface.

3. Results and discussion

3.1. Microstructure

The effect of frequency and duty ratio on the surface morphology of the resulting coatings is shown in Fig. 1. Regardless of the duty ratio, the surface of the coatings at 50 Hz condition contains relatively large pores in comparison to coatings produced by use of higher frequencies (250 and 500 Hz). In other words, the specimens coated at higher frequencies result in much higher pore density, constituted from smaller and uniformly distributed pores. As for the influence of duty ratio on coating surface, it is obvious that the size of the pores becomes larger with the increase of the duty ratio, resulting in a more porous PEO coating. It is also worth to note that the pores of the coating surface produced from 500 Hz and 10% duty ratio are smaller than those of the other coatings. After quantitative analysis of the open pores (0.22 mm^2 surface area), the number and the total area of the pores on coating surface are given in Fig. 2. With the increase of frequency, the number of the pores on coating surface is increasing. For low duty ratio (10%), the pore number increases from 90 ± 4 (50 Hz) to 242 ± 18 (250 Hz) and 378 ± 24 (500 Hz). A similar trend can also be observed when using high duty ratio. In the case of total area, it is decreasing with higher frequency and lower duty ratio. For instance, the total area of the pores of the coating obtained from the same duty ratio (10%)

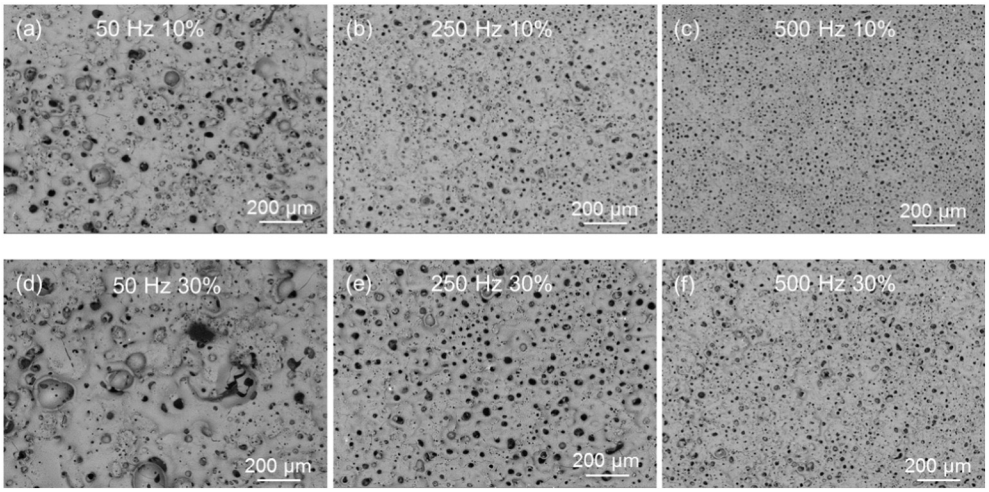

Fig. 1. Surface morphology of the coatings produced from different frequencies and duty ratios. (a) 50 Hz and 10%, (b) 250 Hz and 10%, (c) 500 Hz and 10%, (d) 50 Hz and 30%, (e) 250 Hz and 30%, and (f) 500 Hz and 30%.

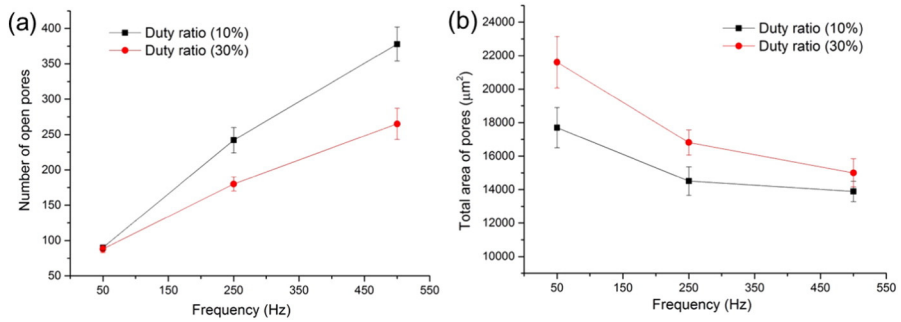

Fig. 2. Number (a) and total area (b) of the pores on coating surface at a magnification of 500× (0.22 mm^2 surface area).

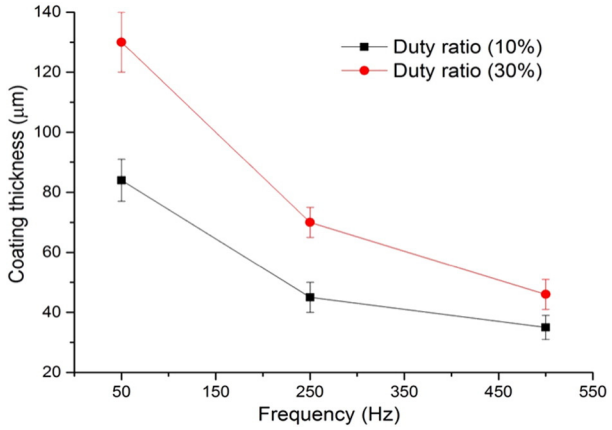

Fig. 3. Thickness of the PEO coatings.

decrease from 17,696 ± 1200 μm^2 (50 Hz) to 14,508 ± 850 μm^2 (250 Hz) and 13,889 ± 610 μm^2 (500 Hz). In other words, lower frequency and higher duty ratio enable PEO coating to have less number of pores but with larger area.

According to Fig. 3, the thickness of the PEO coating is influenced significantly by the applied frequency and duty ratio. Higher duty ratio and lower frequency produce thicker PEO coatings. For example, the coating thickness decreases from 84 ± 7 μm (50 Hz) to 45 ± 5 μm (250 Hz) and 35 ± 4 μm (500 Hz) at low duty ratio. Therefore, coating produced at 50 Hz with 30% duty ratio has the thickest layer, which means the growth rate is higher than for other conditions. Moreover, cross section of the coatings produced by different frequencies with 10% duty ratio was prepared by embedding the specimens into resin, as can be seen in Fig. 4. These observations corroborate the eddy current probe thickness measurements since there is not too much error between the different techniques. It was reported that lower frequency could provide higher growth rate for PEO coating [27], which is consistent with the observations of the current work. The coatings are composed of two layers, an outer porous layer and an inner barrier layer. A pore band between the outer layer and inner layer is clearly observed, which is normally stated for PEO coatings produced from phosphate based electrolyte [28,29].

Fig. 5 demonstrates the distribution of SiO_2 particles on the surface and cross section of the coating produced from treatment with 50 Hz and 10% duty ratio. Plenty of particles can be found on the coating surface (Fig. 5a), indicating that the uptake of the particles is via the coating/electrolyte interface. In addition, a small region lack of particles can be observed at the lower right corner of the

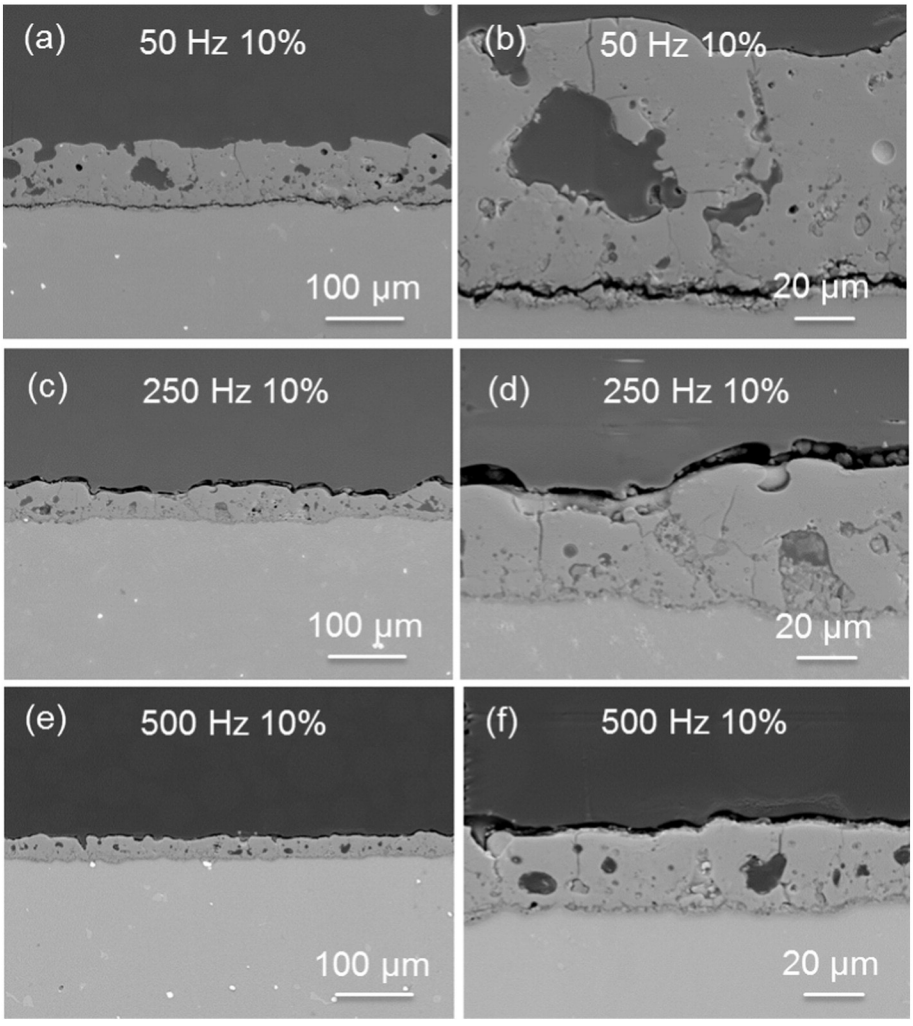

Fig. 4. Cross section of the PEO coatings produced from different frequencies and duty ratios. (a) 50 Hz and 10%, (b) 250 Hz and 10%, (c) 500 Hz and 10%, (d) 50 Hz and 30%, (e) 250 Hz and 30%, and (f) 500 Hz and 30%.

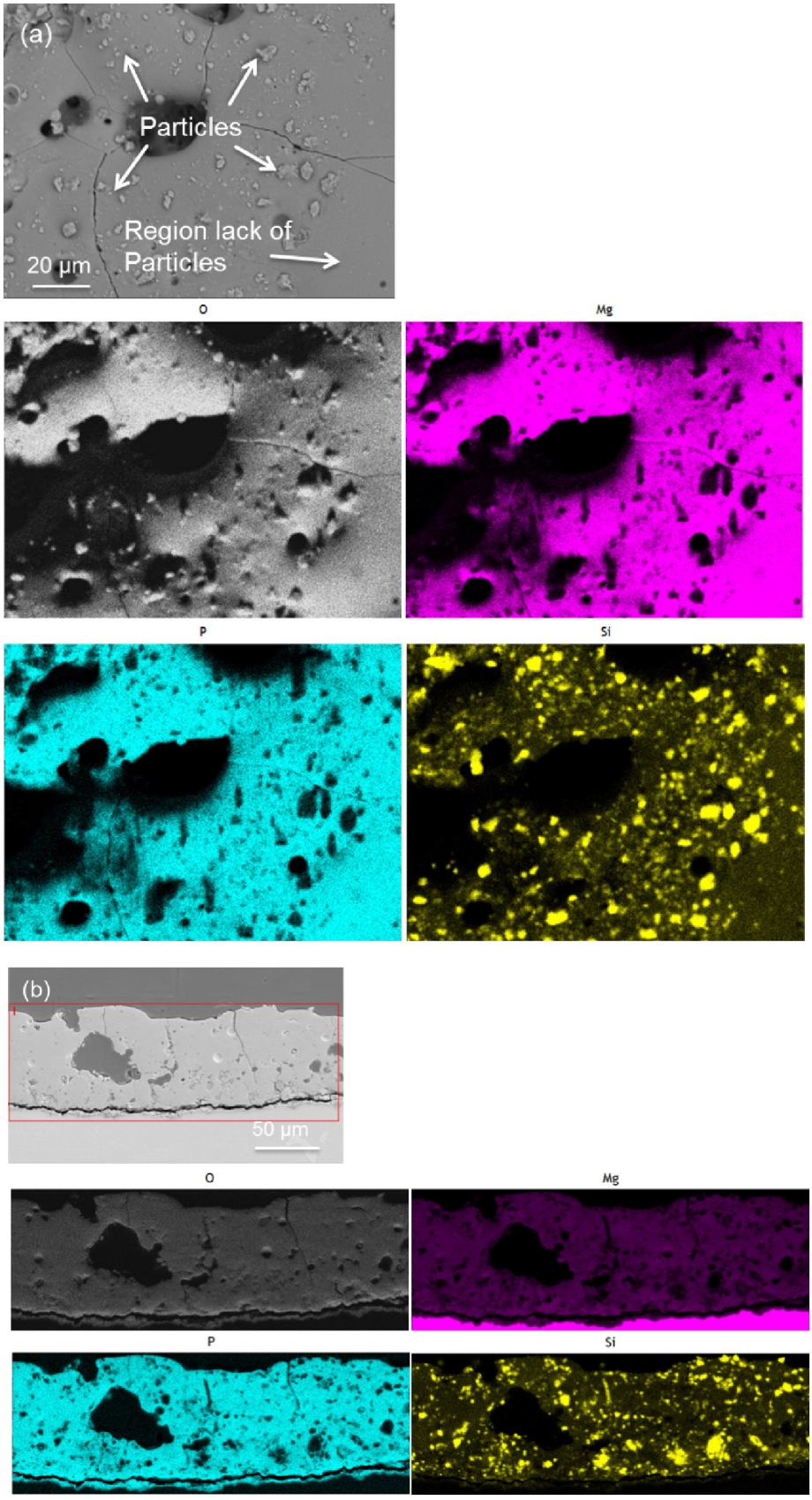

Fig. 5. EDS maps of the PEO coatings obtained from 50 Hz and 10% (a) surface and (b) cross section.

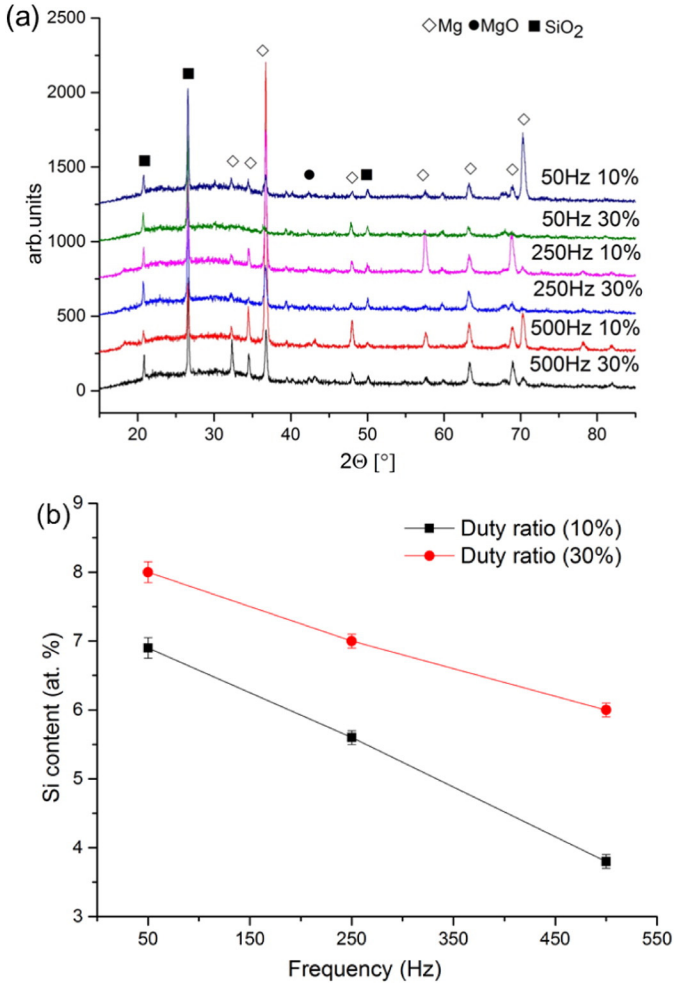

Fig. 6. XRD patterns (a) and Si content (b) of the PEO coatings.

selected image. It can be inferred that the last discharge has not melted this region since it is too far away from the discharge channel. As shown in Fig. 5b, the particles are distributed randomly across the whole layer. It is worth to note that the outer layer of the coating has been detached from the inner layer at the location of the pore band. Based on the mapping results, there is nearly no Si signal in the same region at the inner part of the coating in comparison to P and O, suggesting that the ending position for particles penetration through a coating is the pore band.

3.2. Phase and chemical composition

The X-ray diffraction patterns of the coatings are depicted in Fig. 6a. It can be seen that all the coatings are composed of amorphous phase in the 2θ range of 20–35°, possibly containing phosphorus, except the small amount of MgO. The appearance of magnesium peaks in all conditions is due to the penetration of the X-ray through the whole layer and reaching the substrate. SiO_2 peaks are also visible, indicating that the micro-sized particles are inertly incorporated into PEO coating. This is consistent with our previous investigations [29]. In order to study the influence of electrical parameters on particle uptake, EDS analysis was performed on the surface of all the coated specimens and the Si content is presented in Fig. 6b. It is found that the Si content is decreasing with the increasing frequency, and higher duty ratio enables PEO coating with more particles, which might be attributed to the relatively longer pulse-on time per pulse. For instance, less amount of Si (3.8 at.%) was detected for coating produced at higher frequency (500 Hz with 10% duty ratio) compared with the coating obtained from lower frequency, e.g., 5.6 at.% (250 Hz) and 6.9 at.% (50 Hz). It is worthwhile to note that the tendency of the incorporated particles is similar to the trend of the total area of the pores and coating thickness, which are most likely to be controlled by the applied frequency and duty ratio. Thus changing the pulse-on or pulse-off time is necessary to be further investigated to identify the role of electrical parameters in the uptake of particles during PEO processing.

3.3. Influence of pulse-on and pulse-off time on particle uptake

Coating produced at 250 Hz with 10% duty ratio was used as the standard coating for this study. To identify the effect of pulse-on and pulse-off time on particle uptake during PEO process, either the pulse-on or the pulse-off time of a single pulse will be changed. First, the pulse-off time was changed from 3.6 ms to 1.8 ms and 7.2 ms. The resultant coating microstructure is shown in Fig. 7. After reducing the pulse-off time, the coating thickness decreases and becomes nonuniform, as the thickness of the layer reduces from 41 ± 7 μm to 20 ± 11 μm. However, the coating thickness (40 ± 4 μm) is not influenced greatly when increasing the pulse-off time from 3.6 ms to 7.2 ms. As for the particle content, there is no significant effect of pulse-off time on uptake of particle into PEO coating. The Si content is nearly the same for all the three coatings, 6.3 at.% (0.4 ms + 1.8 ms), 6.0 at.% (0.4 ms + 3.6 ms) and 6.1 at.% (0.4 ms + 7.2 ms), respectively.

In case of pulse-on time, it seems to markedly affect the uptake of the external particles into PEO coatings. Fig. 8 shows the surface and cross section of the coatings obtained from different pulse-on time, namely, 0.2 ms + 3.6 ms and 0.8 ms + 3.6 ms in comparison to the standard coating (0.4 ms + 3.6 ms). It is apparent that longer pulse-on time could produce more porous coating, since the size of the open pores on the coating surface are becoming uneven and larger to some extent. Meanwhile, increase the pulse-on time of a single pulse leads to formation of a thicker layer, as the coating thickness increases from 28 ± 9 μm (0.2 ms) to 41 ± 7 μm (0.4 ms) and 49 ± 6 μm (0.8 ms). With regard to the Si content, the particle concentration increases linearly from 5 at.% to 6 at.% and 7.2 at.%, indicating that pulse-on time plays an important role in the particle uptake during PEO treatment.

3.4. Role of pores on coating surface in particle uptake

There is no doubt that the applied electrical parameters determine the formation of the PEO coating. Like other anions in the electrolyte, the negatively charged particles will move towards the anode with the aid of applied electric field. The main electrochemical reactions occurring at the coating/electrolyte interface during PEO processing is the dissolution of the Mg and subsequent combination with anions (OH^- and PO_4^{3-}) from the electrolyte. As the discharges are unavoidable for PEO process, the coating material will be melted by the high temperature and ejected outwards. As a consequence, melting pools appear on the coating surface accompanying with the discharges, leading to adhesion of some anions in the electrolyte/coating interface, including the particles. Large-sized pores on the coating surface are indications of strong discharges, which can absorb large number of anions and result in thicker layer. The mixture of the original material with the new absorbed anions will flow back after the discharge extinguishes. It is unlikely for particles which are larger than the discharge channel to flow back during solidification process, which means that large-sized particles will remain on the coating surface instead of entering into the inward coating, while some small-sized particles might pass through the open pores on the coating surface reaching the internal layer. Therefore, uptake of particles into PEO coating is mainly via sticking on the

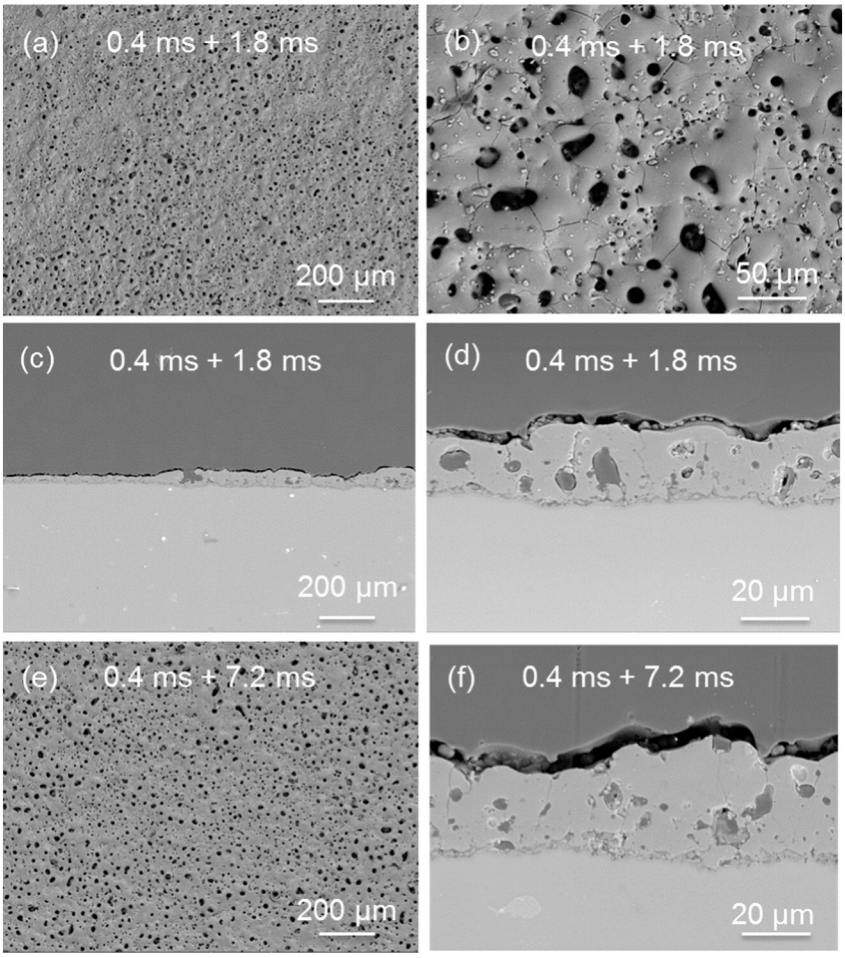

Fig. 7. Surface and cross section morphology of the coatings produced from different pulse-off time: (a–d) 0.4 ms + 1.8 ms and (e, f) 0.4 ms + 7.2 ms.

melting pools that are generated by the discharges during PEO processing. In short, the surface area of the melting pool, as indicated by the size and total area of the pores on the coating surface which are mainly dependent on the applied electrical parameters, can be considered as an important factor to determine the particle uptake during PEO processing.

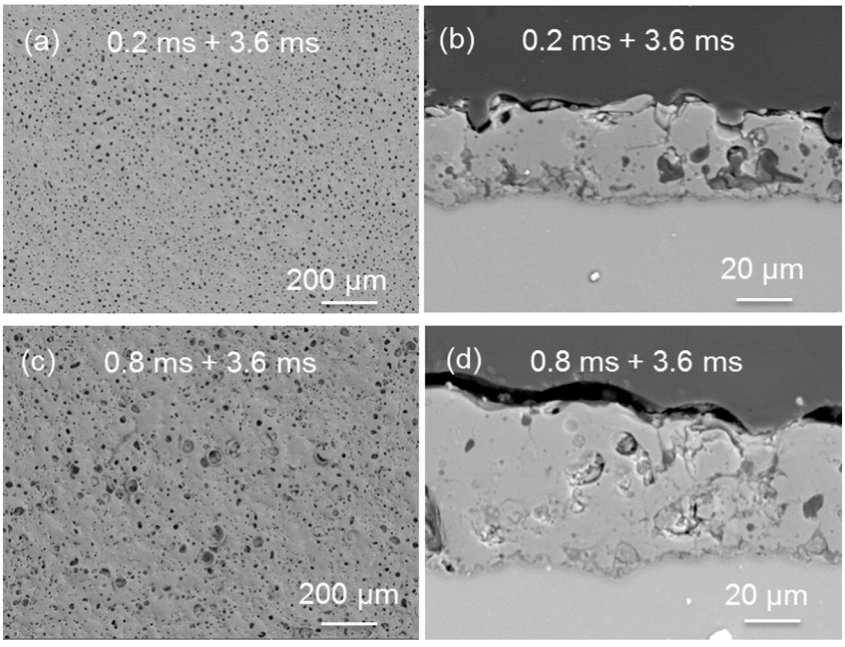

Fig. 8. Surface and cross section morphology of the coatings produced from different pulse-on time: (a, b) 0.2 ms + 3.6 ms and (c, d) 0.8 ms + 3.6 ms.

4. Conclusions

1) The area of the melting pool, as indicated by the pores, on the coating surface is responsible for the particle uptake. Particles can directly enter into the coating via open pores, but mainly by sticking on the coating surface.
2) Lower frequency and higher duty ratio produce PEO coatings with large-area and large-sized pores, leading to uptake of more particles.
3) Pulse-on time of per pulse is more important than pulse-off time for particle uptake during PEO processing.

Acknowledgements

The technical support of Mr. Volker Heitmann and Mr. Ulrich Burmester during the course of this work is gratefully acknowledged. X. Lu thanks the China Scholarship Council (201207090010) for the award of fellowship and funding. M. Mohedano is grateful to the Alexander von Humboldt Foundation (7000273793), Germany, for the award of AvH research fellowship and financial assistance.

References

[1] A.L. Yerokhin, A. Shatrov, V. Samsonov, P. Shashkov, A. Pilkington, A. Leyland, A. Matthews, Oxide ceramic coatings on aluminium alloys produced by a pulsed bipolar plasma electrolytic oxidation process, Surf. Coat. Technol. 199 (2005) 150–157.
[2] S. Yagi, K. Kuwabara, Y. Fukuta, K. Kubota, E. Matsubara, Formation of self-repairing anodized film on ACM522 magnesium alloy by plasma electrolytic oxidation, Corros. Sci. 73 (2013) 188–195.
[3] M. Mu, J. Liang, X. Zhou, Q. Xiao, One-step preparation of TiO_2/MoS_2 composite coating on Ti6Al4V alloy by plasma electrolytic oxidation and its tribological properties, Surf. Coat. Technol. 214 (2013) 124–130.
[4] G. Wu, J.M. Ibrahim, P.K. Chu, Surface design of biodegradable magnesium alloys — a review, Surf. Coat. Technol. 233 (2013) 2–12.
[5] Y. Song, K. Dong, D. Shan, E.H. Han, Study of the formation process of titanium oxides containing micro arc oxidation film on Mg alloys, Appl. Surf. Sci. 314 (2014) 888–895.
[6] R.O. Hussein, X. Nie, D.O. Northwood, An investigation of ceramic coating growth mechanisms in plasma electrolytic oxidation (PEO) processing, Electrochim. Acta 112 (2013) 111–119.
[7] R.O. Hussein, D.O. Northwood, X. Nie, Coating growth behavior during the plasma electrolytic oxidation process, J. Vac. Sci. Technol. A 28 (2010) 766–773.
[8] J.E. Gray, B. Luan, Protective coatings on magnesium and its alloys — a critical review, J. Alloys Compd. 336 (2002) 88–113.
[9] R. Arrabal, E. Matykina, P. Skeldon, G.E. Thompson, Coating formation by plasma electrolytic oxidation on ZC71/SiC/12p-T6 magnesium metal matrix composite, Appl. Surf. Sci. 255 (2009) 5071–5078.
[10] A.L. Yerokhin, X. Nie, A. Leyland, A. Matthews, Characterisation of oxide films produced by plasma electrolytic oxidation of a Ti–6Al–4V alloy, Surf. Coat. Technol. 130 (2000) 195–206.
[11] R. Arrabal, E. Matykina, T. Hashimoto, P. Skeldon, G.E. Thompson, Characterization of AC PEO coatings on magnesium alloys, Surf. Coat. Technol. 203 (2009) 2207–2220.
[12] R. Arrabal, E. Matykina, F. Viejo, P. Skeldon, G.E. Thompson, M.C. Merino, AC plasma electrolytic oxidation of magnesium with zirconia nanoparticles, Appl. Surf. Sci. 254 (2008) 6937–6942.
[13] K.M. Lee, K.R. Shin, S. Namgung, B. Yoo, D.H. Shin, Electrochemical response of ZrO_2-incorporated oxide layer on AZ91 Mg alloy processed by plasma electrolytic oxidation, Surf. Coat. Technol. 205 (2011) 3779–3784.
[14] T.S. Lim, H.S. Ryu, S.-H. Hong, Electrochemical corrosion properties of CeO_2-containing coatings on AZ31 magnesium alloys prepared by plasma electrolytic oxidation, Corros. Sci. 62 (2012) 104–111.
[15] X. Li, B.L. Luan, Discovery of Al_2O_3 particles incorporation mechanism in plasma electrolytic oxidation of AM60B magnesium alloy, Mater. Lett. 86 (2012) 88–91.
[16] D. Sreekanth, N. Rameshbabu, Development and characterization of MgO/hydroxyapatite composite coating on AZ31 magnesium alloy by plasma electrolytic oxidation coupled with electrophoretic deposition, Mater. Lett. 68 (2012) 439–442.
[17] X. Lu, C. Blawert, N. Scharnagl, K.U. Kainer, Influence of incorporating Si_3N_4 particles into the oxide layer produced by plasma electrolytic oxidation on AM50 Mg alloy on coating morphology and corrosion properties, J. Magnesium Alloy. 1 (2013) 267–274.
[18] M. Mohedano, C. Blawert, M.L. Zheludkevich, Silicate-based plasma electrolytic oxidation (PEO) coatings with incorporated CeO_2 particles on AM50 magnesium alloy, Mater. Des. 86 (2015) 735–744.
[19] X. Lu, C. Blawert, M.L. Zheludkevich, K.U. Kainer, Insights into plasma electrolytic oxidation treatment with particle addition, Corros. Sci. 101 (2015) 201–207.
[20] L. Yu, J. Cao, Y. Cheng, An improvement of the wear and corrosion resistances of AZ31 magnesium alloy by plasma electrolytic oxidation in a silicate–hexametaphosphate electrolyte with the suspension of SiC nanoparticles, Surf. Coat. Technol. 276 (2015) 266–278.
[21] S. Lu, W. Qin, X. Wu, X. Wang, G. Zhao, Effect of Fe^{3+} ions on the thermal and optical properties of the ceramic coating grown in-situ on AZ31 Mg alloy, Mater. Chem. Phys. 135 (2012) 58–62.
[22] H. Li, S. Lu, X. Wu, W. Qin, Influence of Zr^{4+} ions on solar absorbance and emissivity of coatings formed on AZ31 Mg alloy by plasma electrolytic oxidation, Surf. Coat. Technol. 269 (2015) 220–227.
[23] X.H. Wu, P.B. Su, Z.H. Jiang, S. Meng, Influences of current density on tribological characteristics of ceramic coatings on ZK60 Mg alloy by plasma electrolytic oxidation, ACS Appl. Mater. Interfaces 2 (2010) 808–812.
[24] R.O. Hussein, P. Zhang, X. Nie, Y. Xia, D.O. Northwood, The effect of current mode and discharge type on the corrosion resistance of plasma electrolytic oxidation (PEO) coated magnesium alloy AJ62, Surf. Coat. Technol. 206 (2011) 1990–1997.
[25] R.O. Hussein, D.O. Northwood, X. Nie, The effect of processing parameters and substrate composition on the corrosion resistance of plasma electrolytic oxidation (PEO) coated magnesium alloys, Surf. Coat. Technol. 237 (2013) 357–368.
[26] K.M. Lee, B.U. Lee, S.I. Yoon, E.S. Lee, B. Yoo, D.H. Shin, Evaluation of plasma temperature during plasma oxidation processing of AZ91 Mg alloy through analysis of the melting behavior of incorporated particles, Electrochim. Acta 67 (2012) 6–11.
[27] P. Bala Srinivasan, J. Liang, R.G. Balajeee, C. Blawert, M. Störmer, W. Dietzel, Effect of pulse frequency on the microstructure, phase composition and corrosion performance of a phosphate-based plasma electrolytic oxidation coated AM50 magnesium alloy, Appl. Surf. Sci. 256 (2010) 3928–3935.
[28] X. Lu, S.P. Sah, N. Scharnagl, M. Störmer, M. Starykevich, M. Mohedano, C. Blawert, M.L. Zheludkevich, K.U. Kainer, Degradation behavior of PEO coating on AM50 magnesium alloy produced from electrolytes with clay particle addition, Surf. Coat. Technol. 269 (2015) 155–169.
[29] X. Lu, C. Blawert, Y. Huang, H. Ovri, M.L. Zheludkevich, K.U. Kainer, Plasma electrolytic oxidation coatings on Mg alloy with addition of SiO_2 particles, Electrochim. Acta 187 (2016) 20–33.

5.6 Investigation of the formation mechanisms of plasma electrolytic oxidation coatings on Mg alloy AM50 using particles *(with permission from Elsevier)*

Electrochimica Acta 196 (2016) 680–691

Contents lists available at ScienceDirect

Electrochimica Acta

journal homepage: www.elsevier.com/locate/electacta

Investigation of the formation mechanisms of plasma electrolytic oxidation coatings on Mg alloy AM50 using particles

Xiaopeng Lu*, Carsten Blawert, Karl Ulrich Kainer, Mikhail L. Zheludkevich

Institute of Materials Research, Helmholtz Zentrum Geesthacht, Max-Plank-Str. 1, 21502 Geesthacht, Germany

ARTICLE INFO

Article history:
Received 22 December 2015
Received in revised form 1 March 2016
Accepted 7 March 2016
Available online 9 March 2016

Keywords:
Plasma electrolytic oxidation coating
Magnesium alloy
Formation mechanisms
Particles

ABSTRACT

The growth of plasma electrolytic oxidation (PEO) coatings can be considered a complex process that includes discharge breakdown, sintering, and deposition process. In this work, inert SiO_2 and La_2O_3 particles were used as tracers to investigate the formation mechanisms of PEO coatings on Mg alloy AM50. The growth direction and kinetics of the coating formation are primarily controlled by the intensity and the number of discharges. High-intensity discharges enable the inward growth of the PEO coating rapidly. Low-intensity discharges allow the outward growth of the coating at a slow speed. At the initial stage of a treatment, conversion products form locally around the intermetallics and disseminate gradually. Discharges appear after reaching the breakdown potential, leading to rapid growth of the coating. The outward growth of the layer is non-uniform because the protruding conversion products are the last locations converted by the discharges. Inward growth of the layer occurs preferentially around intermetallic phases and the formation of the inner layer is related to the inward growth.

© 2016 Elsevier Ltd. All rights reserved.

1. Introduction

Plasma electrolytic oxidation (PEO) is a promising surface engineering technology, which is considered one of the most versatile methods to provide enhanced properties and new functionalities for light metals and their alloys (Al, Mg and Ti) [1–6]. PEO usually uses eco-friendly alkaline electrolytes, and the coatings are formed under high voltage accompanied by a number of short-lived discharges. The formation mechanisms of the coating by PEO are complex due to the involvement of electro-, thermal-, and plasma-chemical reactions in the electrolyte [7,8]. Discharge/plasma is the primary driving force for the coating growth. It was found that the formation of plasma is influenced by the current density, the defects of local uneven electrical conductivity, the impurity level, the resistance of the coating, and the ionization coefficient of the metal oxide coating [9]. The type of the discharges during PEO processing was studied to understand the coating formation mechanisms. Based on spectroscopic and morphological studies, Hussein et al. [10] proposed a model for the growth of PEO coatings on aluminium in silicate electrolyte involving three types of discharges that occur at the metal-oxide interface (type B), at the oxide-electrolyte interface within the upper coating (type C) and at the coating top layer (type A). The type B discharges result in a coating that contains the substrate metal species as the main component, while types A and C correspond to material with relatively large amounts of components from the electrolyte. Later, a modified growth model was proposed by Cheng et al. [11] that includes discharges (type D), occurring in large pores near the interface between the inner and outer layers. These discharges lead to the growth of the inner layer and the incorporation of electrolyte species into the coating material. Thus, discharges may occur at the pore band, which is normally observed for coatings produced from phosphate electrolytes [12,13].

Apart from the discharge type, special PEO electrolytes have also been utilized to investigate the coating growth mechanisms. ^{18}O was used as a tracer to investigate the mechanism of plasma electrolytic oxidation of aluminium under AC conditions. The transport of the oxygen species to the inner part of the coating is via short-circuit paths, leading to the formation of fresh alumina within the coating material near the substrate [14]. Furthermore, sequential treatments in different electrolytes have been performed to investigate the coating formation process. According to Matykina et al. [2], titanium was treated first in silicate electrolyte and then in phosphate electrolyte. The coating material formed in the first electrolyte was lost to the electrolyte through its destruction at breakdown sites in the second electrolyte. Oxide particles were also used as tracers to investigate the growth process of the PEO coatings. Aluminium was treated by using a zirconia-containing electrolyte first and then an electrolyte free of

* Corresponding author. Tel.: +494152871943; fax: +494152871960.
E-mail address: xiaopeng.lu@hzg.de (X. Lu).

http://dx.doi.org/10.1016/j.electacta.2016.03.042
0013-4686/© 2016 Elsevier Ltd. All rights reserved.

Table 1
Electrolytes used for sequential treatments.

First electrolyte	Second electrolyte	Electrical parameter
1 g/l KOH + 20 g/l Na_3PO_4 + 5 g/l SiO_2	1 g/l KOH + 20 g/l Na_3PO_4 + 5 g/l La_2O_3	Constant current density (27 mA/cm^2) for 10 min and then for 1, 10 min
1 g/l KOH + 20 g/l Na_3PO_4	1 g/l KOH + 20 g/l Na_3PO_4 + 5 g/l SiO_2	Constant current density (27 mA/cm^2) for 10 min and then for 1, 5,10 min

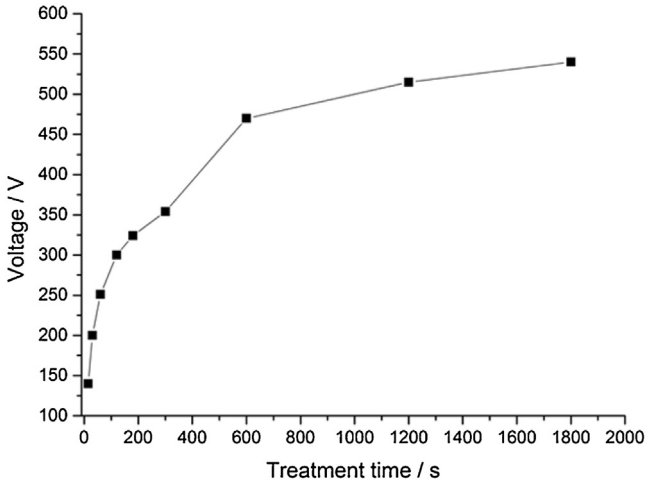

Fig. 1. Evolution of voltage as a function of treatment time.

zirconia. It was found that zirconia only reached to the middle of the intermediate layer, indicating its limited inward mass transfer during microdischarges [15].

In the case of Mg and its alloys, the knowledge of the coating growth mechanisms is scarce in compared with Al-based materials. Hussein et al. [16] used an aluminate electrolyte to produce PEO coatings on Mg alloy AJ62. The ceramic coating grows inwards to the alloy substrate (inner layer) and outwards to the coating surface (outer layer) simultaneously. During the early stages, the coating primarily grows outwards. After the coating reaches a certain thickness, the inner layer grows faster than the outer layer. However, it is not always possible to quantitatively measure the authentic thickness of the inner and outer layer by SEM micrographs. Particles were used to evaluate the plasma temperature during PEO processing on Mg alloy AZ91 [17]. According to Lee et al. [18], electrophoretic force and mechanical

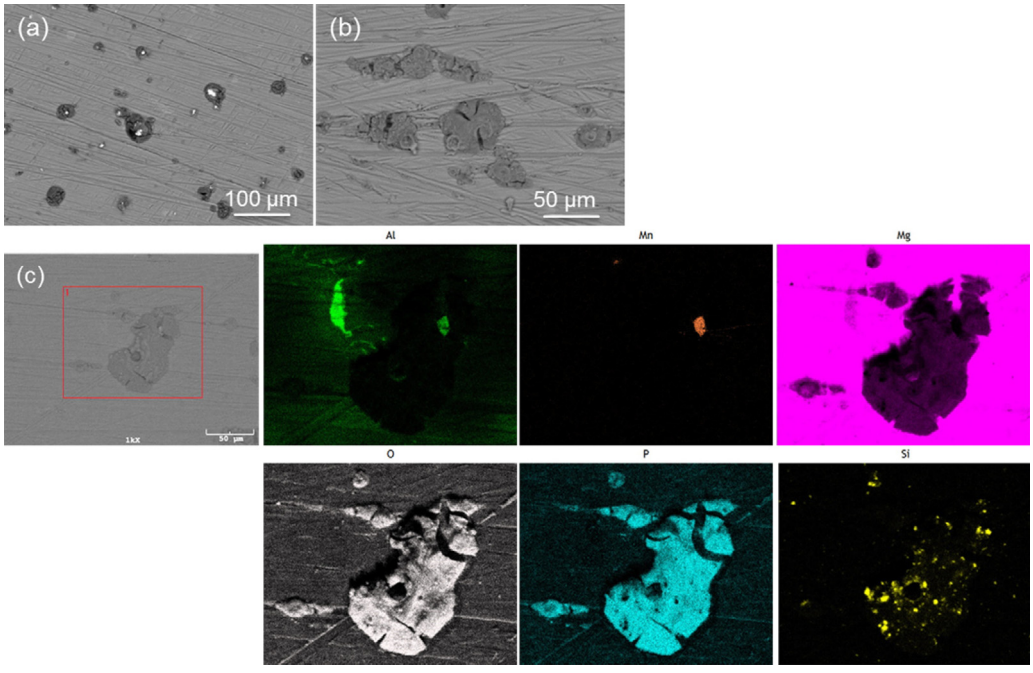

Fig. 2. Surface morphology and EDS mappings of the coating produced before the breakdown potential (15 s).

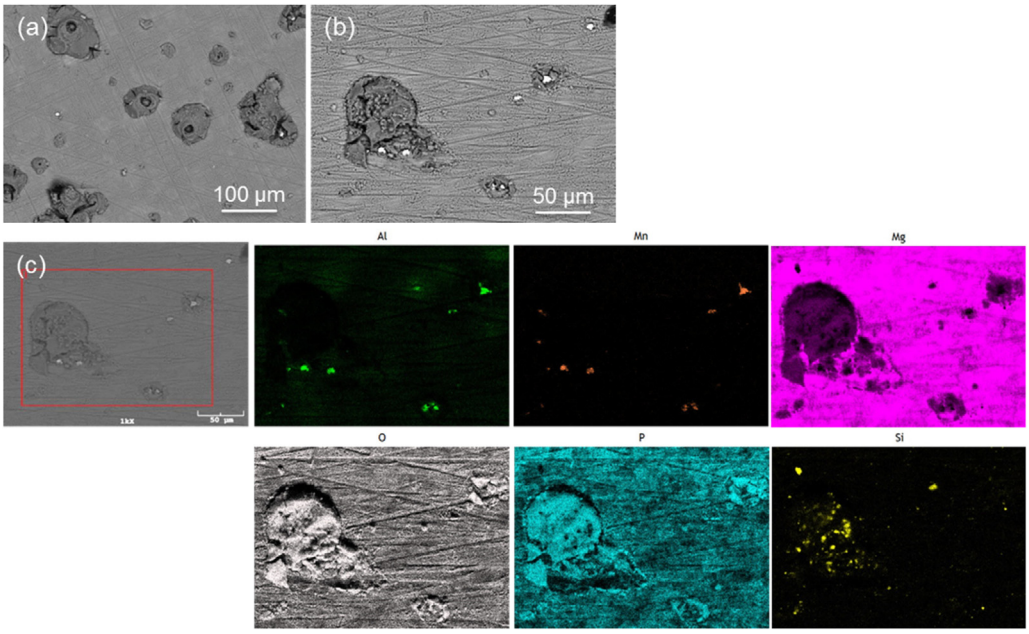

Fig. 3. Surface morphology and EDS mappings of the coating produced after the breakdown potential (30 s).

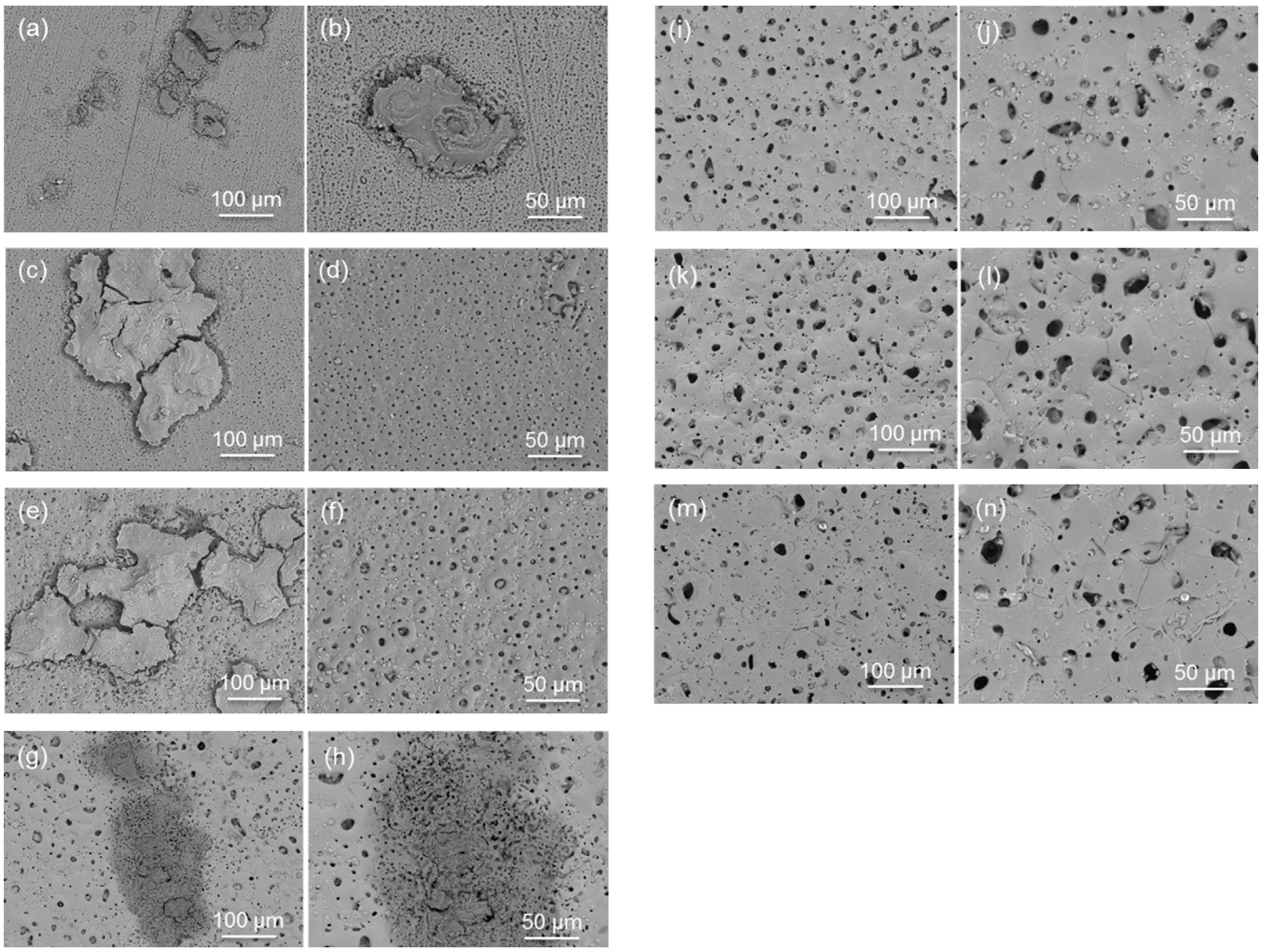

Fig. 4. Surface morphology of the coatings with a longer treatment time (a) and (b) 1 min, (c) and (d) 2 min, (e) and (f) 3 min, (g) and (h) 5 min, (i) and (j) 10 min, (k) and (l) 20 min, (m) and (n) 30 min.

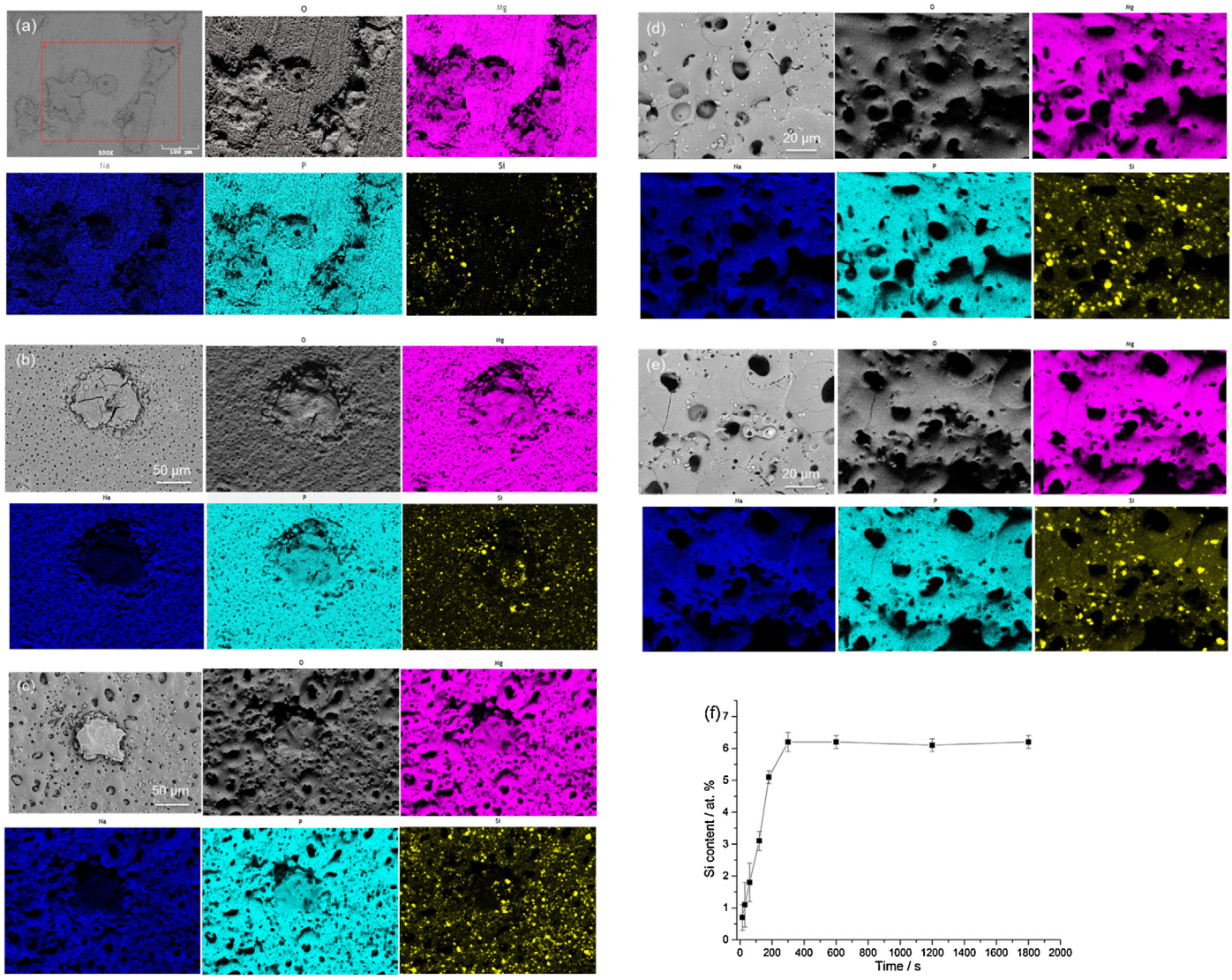

Fig. 5. EDS mappings of the coating surface (a) 1 min, (b) 2 min, (c) 5 min, (d) 10 min, (e) 30 min and (f) Si content of the coatings.

stirring are the main driving forces bringing the particles, as well as other anions, near the anode. Our previous studies proved that particles with a higher melting point and larger size more easily achieve inert incorporation into PEO coatings [19,20]. Accordingly, the inertly incorporated particles can assist in tracing the coating growth route and in investigating the coating formation mechanisms, which are explored in the present study.

2. Experimental

Specimens of the Mg alloy AM50 with dimensions of 15 mm × 15 mm × 4 mm were cut from gravity cast ingot material. The chemical composition of the AM50 alloy, as measured with an Arc Spark OES (Spark analyser M9, Spectro Ametek, Germany), is 4.74 wt.% Al, 0.383 wt.% Mn, 0.065 wt.% Zn, 0.063 wt.% Si, 0.002 wt.% Fe, 0.002 wt.% Cu and Mg balance. The specimens were ground using emery papers up to 1200 grit and then air-dried prior to PEO treatment.

The PEO process was performed by using a lab-produced pulse unit with a DC power supply (PS 8000 2U, ELEKTRO AUTOMATIK, Germany). The frequency is 250 Hz, and the duty ratio is 10%. A hole with a diameter of 2.5 mm was drilled in one side of the specimen and was screwed to a holder to act as the anode. A heat-exchange system based on a stainless steel tube was used as the cathode. The temperature of the electrolyte was maintained at 20 ± 2 °C by a water cooling system. SiO_2 or La_2O_3 particles (5 g/l) in the range of 1–5 μm were added to a phosphate-based electrolyte (1 g/l KOH and 20 g/l Na_3PO_4). A stirrer and bubbling generator were used to facilitate the uniform distribution of the particles in the electrolyte. PEO coatings were produced under a constant current density (27 mA/cm^2) regime for different treatment times (15 s, 30 s, 1 min, 2 min, 3 min, 5 min, 10 min, 20 min, 30 min and 1 h). To trace the transport path of the newly formed material, sequential treatments were performed using different electrolytes under a constant current density (27 mA/cm^2) regime, as shown in Table 1. A scanning electron microscope (TESCAN Vega3 SB) combined with an energy dispersive spectrometer (EDS) system from eumeX (IXRFsystems) was used to examine the microstructure and composition of the PEO coatings. An acceleration voltage of 15 kV was applied for SEM and EDS investigations. Image analysis software Analysis Pro 5.0 was used to measure the pore characteristics. The average values were calculated from 3 SEM images at 1000× magnification per treatment condition. X-ray diffraction (XRD) was performed using a diffractometer (D8 Advance, Bruker AXS) equipped with Cu Kα radiation to determine the coating phase composition.

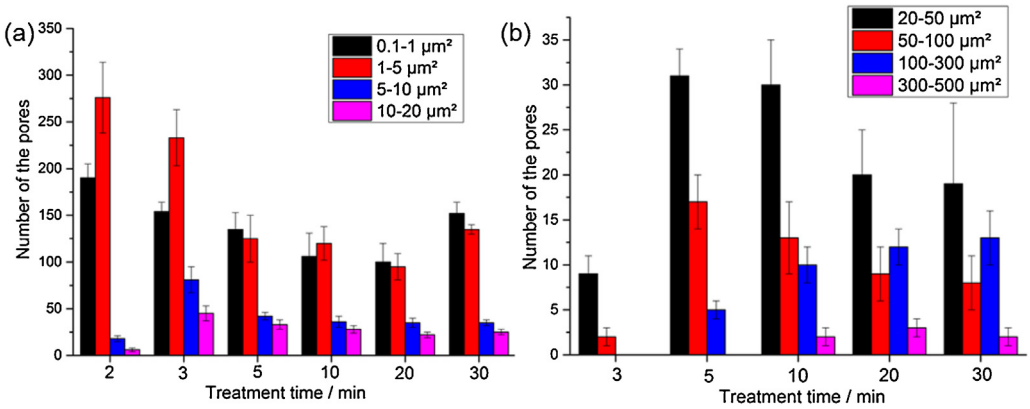

Fig. 6. Pore characteristics of the coating surface at a magnification of 1000× (55350 μm^2 surface area) (a) small-sized pores and (b) large-sized pores.

3. Results

3.1. Growth of the coating in a single treatment

3.1.1. Coating evolution

Fig. 1 shows the voltage as a function of treatment time during the PEO treatment. The first stage is normally observed by a rapid increase in voltage with the dissolution of the substrate and the formation of a passive film on the surface. Then, fine discharges start to appear at the breakdown potential (at approximately 200 V, depending on the electrolyte and substrate). The discharges will grow in size with the increase of voltage, in addition to exhibiting a change in colour and intensity. However, the discharges are not visible in this study due to the turbid electrolyte. The evolution of the voltage can be divided into two stages (0–300 s and 300–1800 s), which show the same tendency, i.e., a higher increase rate at the beginning and a lower increase rate at the end. Moreover, the increase rate at the later stage is much slower than the earlier stage.

3.1.2. Microstructure, phase and elemental composition

The surface morphology of the treated Mg specimens before the breakdown potential is shown in Fig. 2. At the very beginning (15 s), thick conversion products are observed around some bright particles, which are proved to be Al-Mn intermetallics by the EDS analysis, indicating that these regions will be involved in the initial coating formation process. After 30 s (Fig. 3), the surface of the substrate is covered by the conversion products with some scratches from the grinding process. Many tiny pores appear adjacent to the initial conversion products, and the elements (O and P) from the electrolyte start to dominate the entire surface. However, the surface is still not fully covered with a dense film, as many intermetallics are still visible. When the treatment time increases to 1 min (Fig. 4a and b), the entire surface is covered with

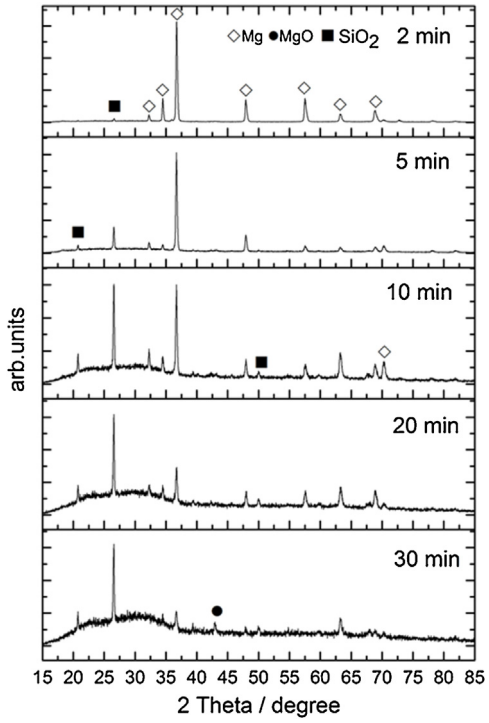

Fig. 7. XRD patterns of the coatings produced from different treatment times.

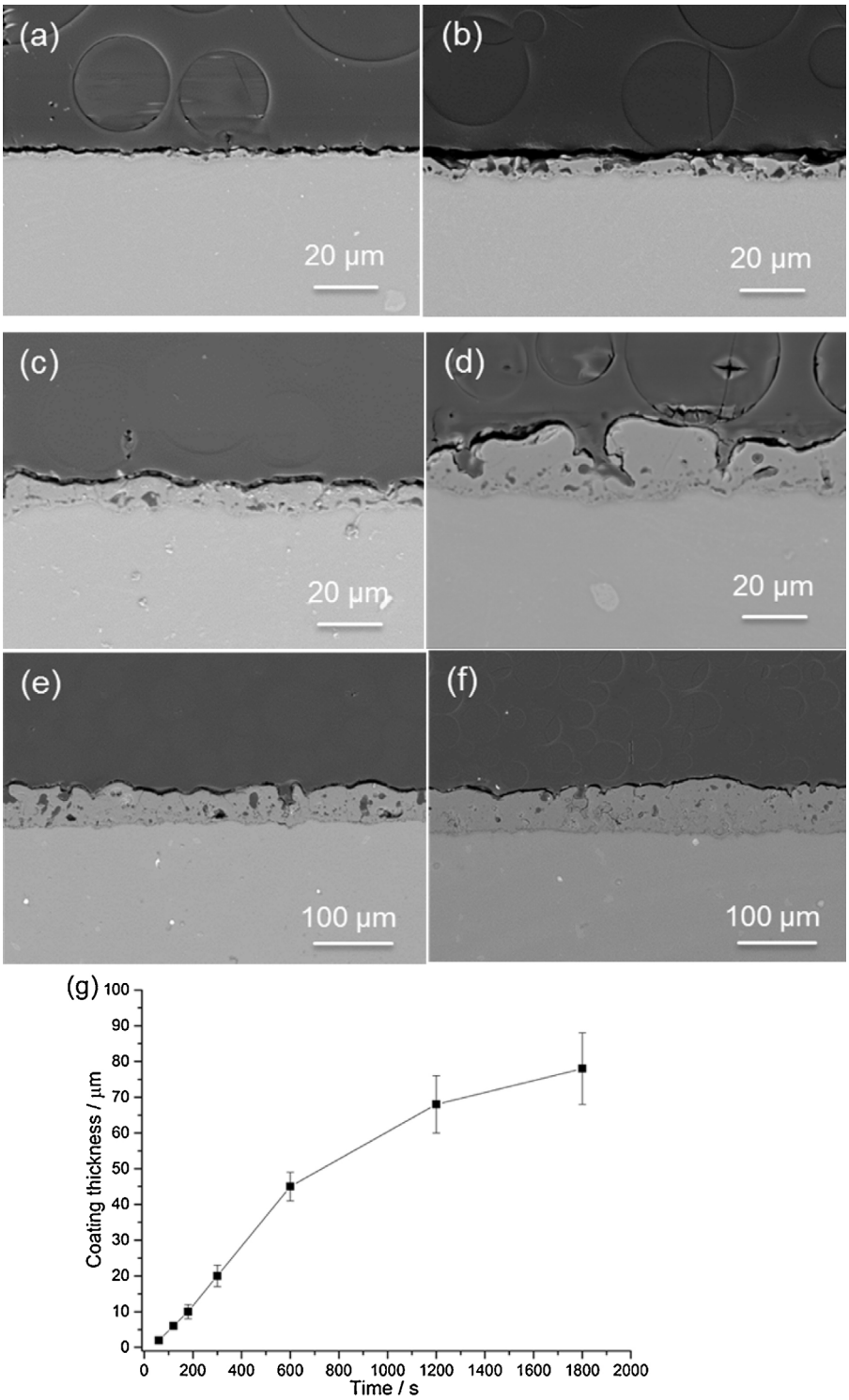

Fig. 8. Cross section and coating thickness of the coatings produced from different treatment times (a) 1 min, (b) 2 min, (c) 3 min, (d) 5 min, (e) 10 min, (f) 20 min and (g) coating thickness as a function of treatment time.

a layer, although previously formed conversion products are still protruding compared with the adjacent area. Many fine and tiny pores appear on the coating surface, which are most likely caused by the discharges after reaching the breakdown potential. At this time, the pores are dominating the surface, and the hill-like conversion products initially formed on the intermetallic phases start to disappear after 5 min of treatment time. These islands are barely observable when the treatment time further increases to 10 min. It can be inferred that the discharges are gradually converting the old layer, including the conversion products (Fig. 4g and h), into new coating material. Hence, the coating is growing outwards at the beginning of a treatment. For the pores on the coating surface (Fig. 4b, d, f, h and j), it is apparent that the pore size is increasing with the treatment time, while the pore growth stops after 10 min and remains at the same level (Fig. 4i, k and m).

Fig. 5 demonstrates the distribution of the main elements (O, P and Si from the electrolyte, Mg from the matrix) on the coating surface after reaching the breakdown potential. For the coating

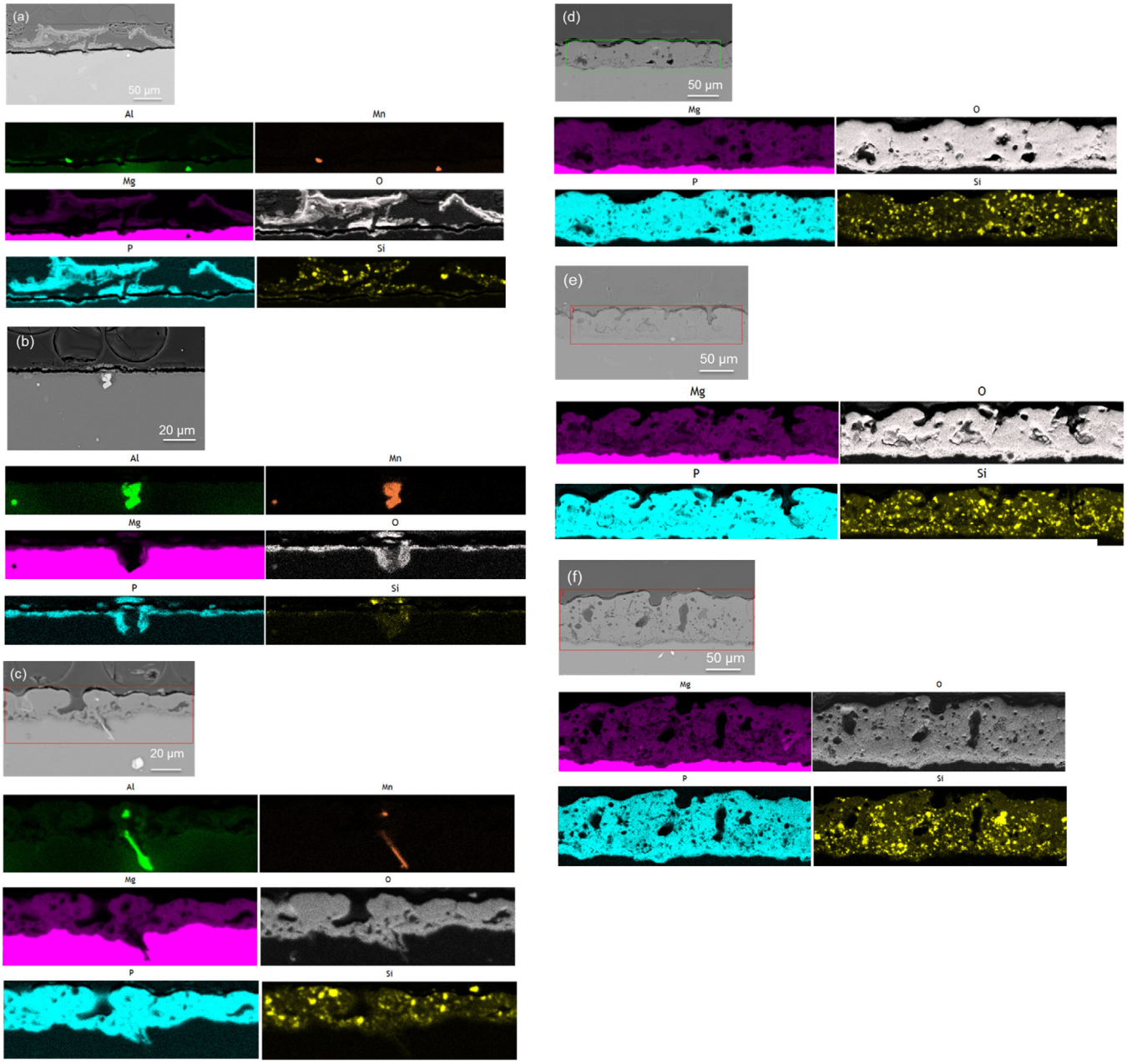

Fig. 9. EDS mappings of the coatings obtained from different treatment times (a) 15 s, (b) 60 s, (c) 5 min, (d) 10 min, (e) 20 min and (f) 30 min.

treated for 1 min (Fig. 5a), SiO_2 particles are only concentrated on the hill-like conversion products because the pores on the coating surface are too small for particles to enter. The probability that the coating will entrap the particles increases with the growing pore size, as shown in Fig. 5b, c and d. Apart from the unreacted particles, Na can also be regarded as a tracer for coating growth because $NaPO_4^{2-}$ is among the most stable species in an alkaline electrolyte [21]. Note that the signal of Na (Fig. 5b and c) is much weaker in the original conversion products compared with the area with the discharge pores, suggesting that new coating materials are formed in the latter area. After 10 min, the conversion products disappear, and all of the elements are distributed uniformly on the coating surface. According to Fig. 5f, the particle content increases rapidly within the first 5 min and then is maintained at a constant level (approximately 6.2 at.%) without further increase. Note that the Si content will not be affected by the coating thickness after being treated for 2 min (~6 μm) because the penetration depth of the X-rays is approximately 3 μm under the present conditions.

Because the pores are too small to be detected at the beginning of the treatment, Fig. 6 only shows the pore characteristics on the surface (55350 μm^2 surface area) of the coatings at later stage (from 2 min to 30 min). The small-sized pores (0.1–5 μm^2) are dominant for all of the coatings. At the early stage of treatment (2 min), only few pores (24 ± 5) in the range of 5–20 μm^2 are observed, and no pores larger than 20 μm^2 are found. As the treatment time increases, the probability that large-sized pores will appear increases. Pores in the range of 20 to 100 μm^2 (11 ± 2) are detected on the surface of the coatings treated for 3 min, and pores with area of 100–300 μm^2 (5 ± 1) can be found for coating treated for 5 min. Large-sized pores in the range of 300–500 μm^2 are visible when the treatment time further increases to 10 min. Although the number of pores in the range of 0.1–20 μm^2 decreases with the treatment time, i.e., from ~500 (2–3 min) to

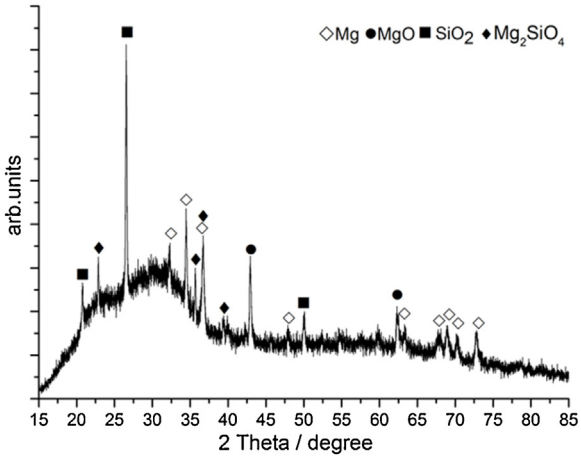

Fig. 10. XRD pattern of the coating treated for 1 h.

~300 (5–30 min), the total number of large-sized pores (20–500 μm^2) increases greatly from ~11 (3 min) to ~50 (5–30 min), which might account for the large amount of incorporated particles.

The coatings are mainly composed of amorphous material, as evidence from the XRD patterns (Fig. 7). The intensity of the Mg peaks decreases as the treatment time increases, indicating that the coating is becoming thicker. The detection of SiO_2 peaks begins in the coating treated for 2 min, and the intensity of the incorporated particles increases with the treatment time. In terms of coating thickness (Fig. 8), the coating grows non-uniformly as a function of treatment time. The growth rate of the coating is 3.3 μm/min in the first 3 min, and then increases to 5 μm/min from 3 min to 10 min. Then, the coating growth rate decreases substantially with increasing treatment time, with a rate of 2.3 μm/min from 10 min to 20 min and a rate of 1 μm/min from 20 min to 30 min.

EDS mappings (Fig. 9) were performed to study the element distribution in the cross sections of the coatings treated for different times. Before reaching the breakdown potential (Fig. 9a), Si is only detected in the conversion products. The particles are randomly distributed across the entire conversion product, indicating that the conversion products are progressively formed around the intermetallics by the anions from the electrolyte and the dissolved Mg ions. After reaching the breakdown potential (Fig. 9b), the matrix is covered by a thin layer. However, this layer is still incapable of preserving the large-sized particles because the coating is thin and the pores (Fig. 4b) are too small to absorb and retain the particles. As the treatment time increases, particles can be detected in the internal coating (Fig. 9c). A small protuberance of coating material can be observed by the Mg, O and P signal. This is exactly the location of an Al-Mn intermetallic phase. It can be inferred that new coating material forms preferentially around the intermetallics when growing inwards. After the conversion products disappeared, the coating starts to grow relatively uniformly, resulting in a homogeneous distribution of the particles (Fig. 9d and e). Note that the Si signal (Fig. 9f) of the outermost region of the coating treated for 30 min is greatly diluted compared with the inner layer. It is well known that the intensity of the discharges increases with the treatment time under a galvanostatic regime. Thus, some inertly incorporated particles might be melted by the high-intensity discharges and be transformed into new coating materials; this was confirmed by extending the treatment time to one hour. Based on Fig. 10, additional Mg_2SiO_4 peaks and MgO peaks were detected, suggesting that the amorphous coating was converted into crystalline coating to a certain extent. This provides evidence that "soft sparking", which can always be observed for Al and its alloys [22,23], is unlikely to occur on Mg alloy under the applied galvanostatic regime.

3.2. Growth of the coating in sequential treatments

Mg samples were treated sequentially in different electrolytes with and without particles, with the goal of investigating the transport path of the newly formed coating material and the growth of the inner barrier layer. Hence, the coating was first treated for 10 min in the SiO_2-containing electrolyte and then in a La_2O_3-containing electrolyte under constant current mode. Fig. 11a shows the surface of the coating treated for 1 min in the La_2O_3-containing electrolyte. It is apparent that the La_2O_3 particles are present locally on the coating surface. In this zone, the Si signal is much lower than in the remainder of the surface, suggesting that this region is the preferential location for the formation of new coating material. Regarding the cross section, La_2O_3 particles are only found in one defect of the outer layer (Fig. 11b). Hence, the low-intensity discharges are not able to puncture the entire layer, leading to outward growth of the coating. With the increase of treatment time (10 min), the original coating material is gradually replaced by the newly formed material (Fig. 11c). It can be inferred that a number of high-intensity discharges occurred and enabled the coating to grow inwards rapidly. The sequential treatments do not significantly affect the coating formation process because the final voltage of the two treatments is similar (~515 V). In addition, the two-step coating is less uniform (65 ± 15 μm) compared with the coating obtained from the single treatment (67 ± 8 μm). Thus, the embedded SiO_2 particles in the original coating might be transferred to an adjacent region or reacted with other coating material rather than experiencing material loss, leading to a diluted Si signal in the final coating.

Sequential treatments were also performed using particle-free electrolyte first for 10 min and then using the SiO_2 particles-containing electrolyte under a constant current regime. Fig. 12a shows the distribution of the SiO_2 particles on the coating surface after the subsequent treatment for 1 min. Similar to the coating formed in La_2O_3-containing electrolyte, the SiO_2 particles are non-uniformly distributed and can only be found in regions where new discharges occurred, suggesting that the incorporation of particles into the PEO coating is determined by the discharges. The amount of the incorporated particles into the coating increases with the treatment time (Fig. 12b–d) because a larger fraction of the coating

was converted/mixed by the discharges. Some parts of the original coating (Fig. 12d) are still visible after the 10 min treatment, indicating that the compact regions are difficult to be punctured and converted into new material. The discharges occur preferentially at the relatively thin or defective locations. Meanwhile, the original inner layer is gradually replaced by a new inner layer. Thus, the formation of the inner barrier layer is strongly related to the inward growth.

4. Discussion

Due to the relatively low corrosion potential of the matrix [24], the coating initially grows from the area adjacent to the Al-Mn intermetallic phases (Fig. 2c), as shown by the schematic diagram (Fig. 13a). Electrochemical-enhanced dissolution of Mg occurs, and conversion products (Mg-based compounds) with low solubility are deposited around the intermetallic phases. After local growth, the conversion products spread over the entire surface with a longer treatment time and higher potential, resulting in an insulating conversion layer (Fig. 13b). This thin film will be punctured after the breakdown potential is reached, accompanied by many discharges. From this moment, the growth rate of the coating will be enhanced and controlled by the discharges because the high temperature and pressure generated by the discharges can promote chemical- and plasma-chemical reactions. It is evident that new materials are mainly derived from the chemical reaction between the anions from the electrolyte and cations from the substrate. The coating grows inwards to the substrate and outwards simultaneously, which has been proved by Hussein et al. [16]. However, it is likely that there are preferential locations for

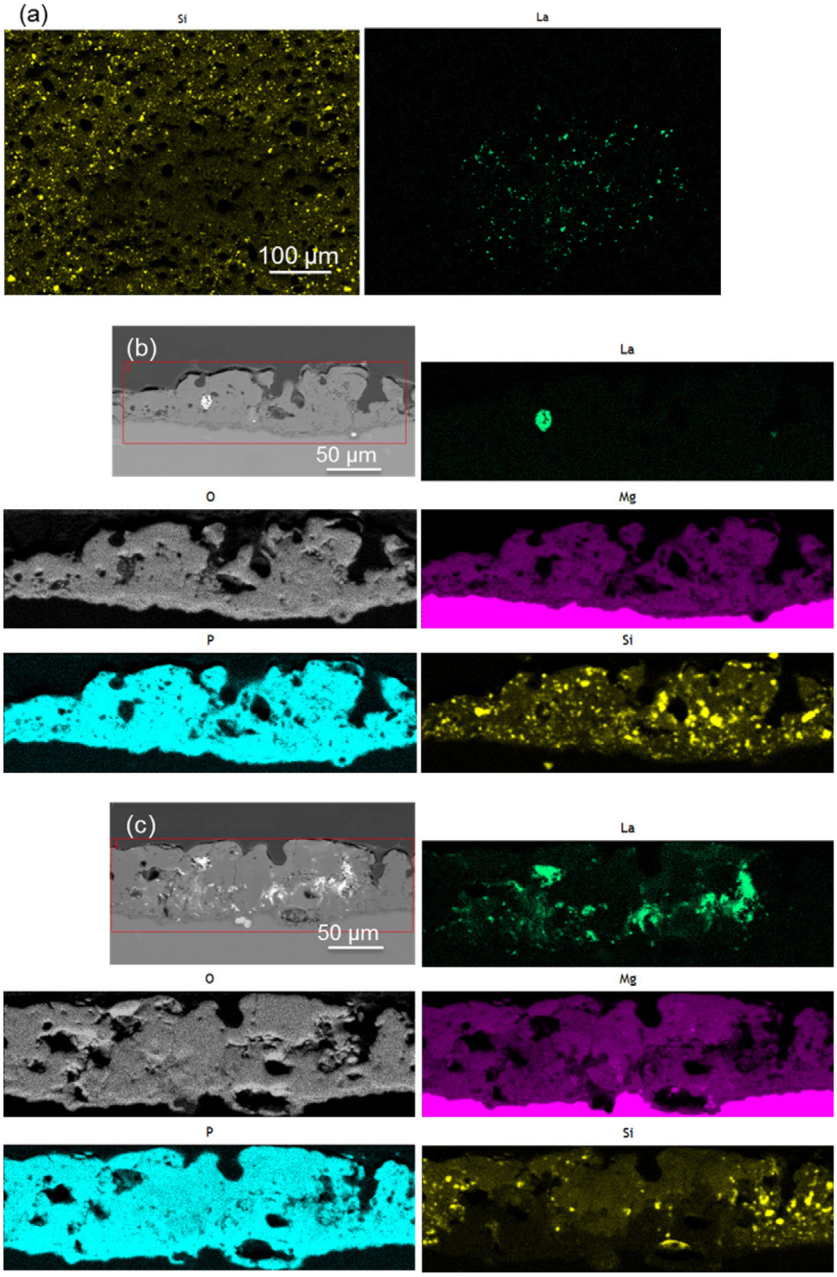

Fig. 11. First treatment in SiO_2 containing electrolyte and then in La_2O_3-containing electrolyte (a) surface morphology of the coating treated for 1 min, (b) cross section of the coating treated for 1 min and (c) cross section of the coating treated for 10 min.

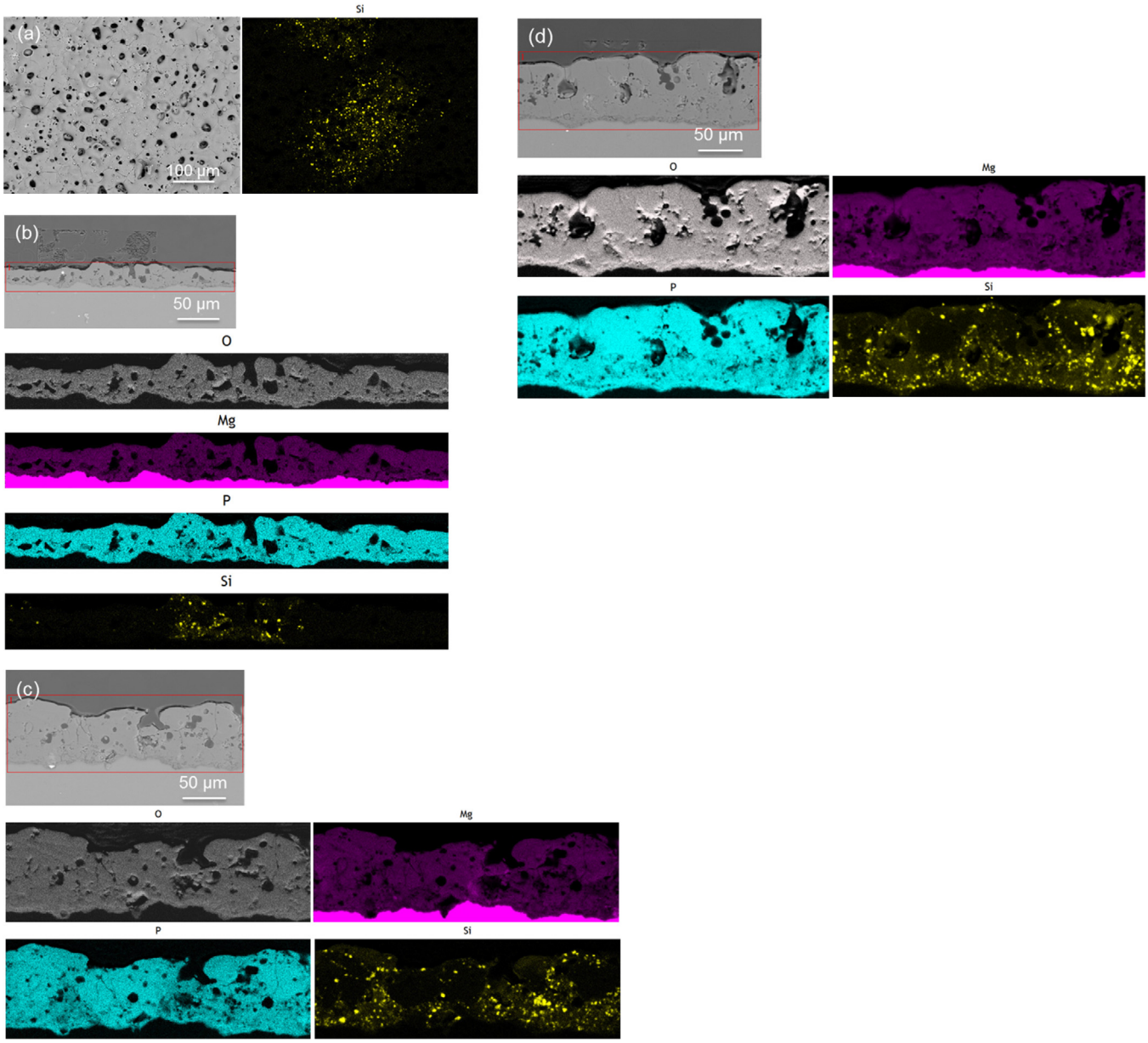

Fig. 12. First treatment in particle-free electrolyte and then in SiO_2-containing electrolyte (a) surface morphology of the coating treated for 1 min, (b) cross section of the coating treated for 1 min, (c) cross section of the coating treated for 5 min and (d) cross section of the coating treated for 10 min.

the coating growth. For the outward growth, the growth rate of the protruding conversion products is much lower than that of their adjacent regions until both coating regions reach a comparable thickness (Fig. 13c). Then, the island-like conversion products are punctured by the discharges and are converted into new coating material (Figs. 4 g and h, 13 d). After the disappearance of the conversion products, the coating grows uniformly at the relatively thin or defective locations due to the generation of the discharges (Fig. 13e). In terms of inward growth, the coating grows preferentially around the intermetallic phases (Figs. 9 c, 13 e), which can be considered as defect promoting discharge formation.

The growth rate of the PEO coating is mainly controlled by the intensity and number of discharges, which can be related to the pore characteristics on the coating surface. Although the intensity of the discharges is relatively low after reaching the breakdown potential (1–3 min), the number of discharges is much higher (Fig. 6) in comparison to that of the later stage, resulting in a relatively high growth rate (3.3 μm/min) for the PEO coating. In the middle of a treatment (3–10 min), the coating demonstrates the highest growth rate (5 μm/min), which is due to the appearance of high-intensity discharges. Although high-intensity discharges are still visible, the coating growth rate is reduced substantially at the late stage of a treatment. This could be ascribed to the reduced number of discharges and probably material loss caused by the extremely strong discharges.

The coating formation process can be considered as a cyclic and/or synchronous process that includes dielectric breakdown, sintering and deposition process. Due to the breakdown of the original film, some coating material will be melted and ejected outwards, causing discharge channels to remain inside the coating and causing protrusions of melted material on the coating surface. The melted material can absorb ions and particles at the electrolyte/coating interface to form new compounds. Sintering occurs at the high-temperature area generated by the discharges and determines the phase composition of the PEO coating, which is mainly dependent on the temperature of the discharges. High-

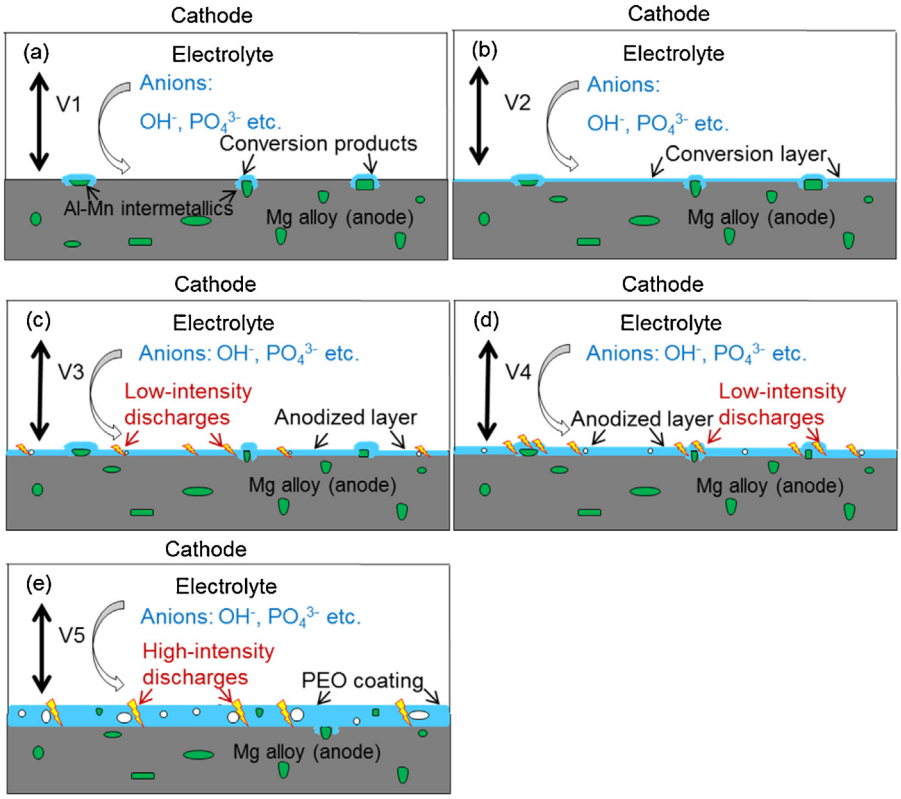

Fig. 13. Schematic diagram of the coating formation mechanisms (a) conversion products formed around the Al-Mn intermetallics, V1 << breakdown potential, (b) conversion layer formed over the entire surface, V2 < breakdown potential, (c) anodized layer formed by low-intensity discharges, V3 > breakdown potential, (d) protruding conversion products: last locations punctured by discharges, V4 > V3 and (e) PEO coating formed by high-intensity discharges, V5 > V4.

intensity discharges enable coatings with more crystalline and high-temperature phases (Fig. 10). Particularly, interfacial chemical reactions are likely to occur during the sintering process when the particles are interacting and are mixed with the melt, resulting in reactive or partially reactive incorporation if the energy of the discharge is sufficient. Later, the sintered products will flow back along the discharge channel, which can be called a deposition process. The sintering and deposition processes determine the phase composition and growth direction of the PEO coating. Low-intensity discharges promote outward growth of the layer at a low speed. High-intensity discharges, such as penetrating discharges (type B), facilitate the generation of a large volume of discharge channels and melt, allowing a larger fraction of melted material to flow back along the discharge channels, thus rebuilding the coating by the formation of fresh coating material between the original coating and the substrate and leading to inward growth. Therefore, the regrowth of the layer after breakdown is determined by sintering and deposition of the mixture of the original material and the newly formed material.

5. Conclusions

1) The formation of a PEO coating can be considered a cyclic and/or synchronous process that includes dielectric breakdown, sintering and deposition process.
2) The growth rate and direction of the PEO coating are primarily controlled by the intensity and number of discharges. Discharges with high intensity enable the inward growth of the PEO coating rapidly. Low-intensity discharges promote the outward growth of the coating at a low speed.
3) There are five stages for the coating formation process. At the first stage, the conversion products grow locally around the Al-Mn intermetallics and disseminate gradually. Before the breakdown potential (second stage), the surface of the substrate is converted into a conversion layer. During the third stage, this layer is punctured by the discharges, and the coating grows rapidly but non-uniformly. Protruding conversion products are the last locations to be punctured by the discharges, which is considered as the fourth stage. At the final stage, the coating grows slowly but uniformly due to the increasing coating thickness and the appearance of high-intensity discharges. New coating material forms preferentially around the intermetallic phases when growing inwards. The formation of the inner layer is related to the inward growth.

Acknowledgements

The technical support of Mr. Volker Heitmann and Mr. Ulrich Burmester during this work is gratefully acknowledged. X. Lu thanks China Scholarship Council for the award of fellowship and funding.

References

[1] A.L. Yerokhin, X. Nie, A. Leyland, A. Matthews, S.J. Dowey, Plasma electrolysis for surface engineering, Surface and Coatings Technology 122 (1999) 73–93.
[2] E. Matykina, G. Doucet, F. Monfort, A. Berkani, P. Skeldon, G.E. Thompson, Destruction of coating material during spark anodizing of titanium, Electrochimica Acta 51 (2006) 4709–4715.
[3] R. Arrabal, E. Matykina, T. Hashimoto, P. Skeldon, G.E. Thompson, Characterization of AC PEO coatings on magnesium alloys, Surface and Coatings Technology 203 (2009) 2207–2220.
[4] J. Liang, P.B. Srinivasan, C. Blawert, W. Dietzel, Influence of chloride ion concentration on the electrochemical corrosion behaviour of plasma electrolytic oxidation coated AM50 magnesium alloy, Electrochimica Acta 55 (2010) 6802–6811.

[5] K. Venkateswarlu, N. Rameshbabu, D. Sreekanth, M. Sandhyarani, A.C. Bose, V. Muthupandi, S. Subramanian, Role of electrolyte chemistry on electronic and in vitro electrochemical properties of micro-arc oxidized titania films on Cp Ti, Electrochimica Acta 105 (2013) 468–480.
[6] A. Zomorodian, C. Santos, M.J. Carmezim, T.M.e. Silva, J.C.S. Fernandes, M.F. Montemor, In-vitro corrosion behaviour of the magnesium alloy with Al and Zn (AZ31) protected with a biodegradable polycaprolactone coating loaded with hydroxyapatite and cephalexin, Electrochimica Acta 179 (2015) 431–440.
[7] M.D. Klapkiv, Simulation of synthesis of oxide-ceramic coatings in discharge channels of a metal-electrolyte system, Materials Science 35 (1999) 279–283.
[8] A.L. Yerokhin, A. Shatrov, V. Samsonov, P. Shashkov, A. Pilkington, A. Leyland, A. Matthews, Oxide ceramic coatings on aluminium alloys produced by a pulsed bipolar plasma electrolytic oxidation process, Surface and Coatings Technology 199 (2005) 150–157.
[9] T. Mi, B. Jiang, Z. Liu, L. Fan, Plasma formation mechanism of microarc oxidation, Electrochimica Acta 123 (2014) 369–377.
[10] R.O. Hussein, X. Nie, D.O. Northwood, A. Yerokhin, A. Matthews, Spectroscopic study of electrolytic plasma and discharging behaviour during the plasma electrolytic oxidation (PEO) process, Journal of Physics D: Applied Physics 43 (2010) 105203.
[11] Y.-l. Cheng, Z.-g. Xue, Q. Wang, X.-Q. Wu, E. Matykina, P. Skeldon, G.E. Thompson, New findings on properties of plasma electrolytic oxidation coatings from study of an Al–Cu–Li alloy, Electrochimica Acta 107 (2013) 358–378.
[12] C. Blawert, S.P. Sah, J. Liang, Y. Huang, D. Höche, Role of sintering and clay particle additions on coating formation during PEO processing of AM50 magnesium alloy, Surface and Coatings Technology 213 (2012) 48–58.
[13] X. Lu, S.P. Sah, N. Scharnagl, M. Störmer, M. Starykevich, M. Mohedano, C. Blawert, M.L. Zheludkevich, K.U. Kainer, Degradation behavior of PEO coating on AM50 magnesium alloy produced from electrolytes with clay particle addition, Surface and Coatings Technology 269 (2015) 155–169.
[14] E. Matykina, R. Arrabal, D.J. Scurr, A. Baron, P. Skeldon, G.E. Thompson, Investigation of the mechanism of plasma electrolytic oxidation of aluminium using 18O tracer, Corrosion Science 52 (2010) 1070–1076.
[15] E. Matykina, R. Arrabal, P. Skeldon, G.E. Thompson, Investigation of the growth processes of coatings formed by AC plasma electrolytic oxidation of aluminium, Electrochimica Acta 54 (2009) 6767–6778.
[16] R.O. Hussein, X. Nie, D.O. Northwood, An investigation of ceramic coating growth mechanisms in plasma electrolytic oxidation (PEO) processing, Electrochimica Acta 112 (2013) 111–119.
[17] K.M. Lee, B.U. Lee, S.I. Yoon, E.S. Lee, B. Yoo, D.H. Shin, Evaluation of plasma temperature during plasma oxidation processing of AZ91 Mg alloy through analysis of the melting behavior of incorporated particles, Electrochimica Acta 67 (2012) 6–11.
[18] K.M. Lee, K.R. Shin, S. Namgung, B. Yoo, D.H. Shin, Electrochemical response of ZrO2-incorporated oxide layer on AZ91 Mg alloy processed by plasma electrolytic oxidation, Surface and Coatings Technology 205 (2011) 3779–3784.
[19] X. Lu, C. Blawert, M.L. Zheludkevich, K.U. Kainer, Insights into plasma electrolytic oxidation treatment with particle addition, Corrosion Science 101 (2015) 201–207.
[20] X. Lu, C. Blawert, Y. Huang, H. Ovri, M.L. Zheludkevich, K.U. Kainer, Plasma electrolytic oxidation coatings on Mg alloy with addition of SiO2 particles, Electrochimica Acta 187 (2016) 20–33.
[21] S. Yagi, A. Sengoku, K. Kubota, E. Matsubara, Surface modification of ACM522 magnesium alloy by plasma electrolytic oxidation in phosphate electrolyte, Corrosion Science 57 (2012) 74–80.
[22] F. Mécuson, T. Czerwiec, T. Belmonte, L. Dujardin, A. Viola, G. Henrion, Diagnostics of an electrolytic microarc process for aluminium alloy oxidation, Surface and Coatings Technology 200 (2005) 804–808.
[23] F. Jaspard-Mécuson, T. Czerwiec, G. Henrion, T. Belmonte, L. Dujardin, A. Viola, J. Beauvir, Tailored aluminium oxide layers by bipolar current adjustment in the Plasma Electrolytic Oxidation (PEO) process, Surface and Coatings Technology 201 (2007) 8677–8682.
[24] M. Jönsson, D. Thierry, N. LeBozec, The influence of microstructure on the corrosion behaviour of AZ91D studied by scanning Kelvin probe force microscopy and scanning Kelvin probe, Corrosion Science 48 (2006) 1193–1208.

5.7 3D reconstruction of plasma electrolytic oxidation coatings on Mg alloy via synchrotron tomography

3D Reconstruction of Plasma Electrolytic Oxidation Coatings on Mg Alloy via Synchrotron Tomography

Xiaopeng Lu[1,*], Carsten Blawert[1], Domonkos Tolnai[1], Tungky Subroto[1], Karl Ulrich Kainer[1], Mikhail L. Zheludkevich[1, 2]

[1]Institute of Materials Research, Helmholtz-Zentrum Geesthacht, Max-Plank-Str. 1, 21502 Geesthacht, Germany

[2]Institute for Materials Science, Christian Albrechts University of Kiel, 24143 Kiel, Germany

E-mail: xiaopeng.lu@hzg.de

Keywords: synchrotron tomography, plasma electrolytic oxidation coating, Mg alloy

Abstract

Synchrotron-based microtomography is demonstrated here for the first time to generate 3D visualization of plasma electrolytic oxidation (PEO) coatings on Mg alloy. Additionally inert La_2O_3 particles have been introduced as markers during the PEO process to understand the coating growth process. The obtained distribution and evolution of the pores and the particles confer more quantitative and precise assessment of the layer compared to conventional characterization methods. The microtomography analysis shows that porosity of the coating reaches up to 26.25 % at the initial stage and decreases with the layer growth under a potentiostatic regime.

1. Introduction

Magnesium and its alloys are attractive for various applications because of their excellent light-weight properties. [1-3] However, the poor corrosion resistance limits their applications in aggressive environments. [4, 5] Plasma electrolytic oxidation (PEO) is a promising surface treatment process derived from conventional anodizing to form ceramic-like coatings to obtain enhanced corrosion and wear properties. [6, 7] However PEO coatings on Mg alloys are generally of high porosity which can be an important issue for achieving high-barrier long-term protection or can be beneficial when layers with enhanced biocompatibility and controllable bio-degradability are targeted. [8] Thus information on the structure and morphology of the layer as well as the size, volume and distribution of the pores is crucial for the design of functional PEO

coatings. Normally the porosity of the coatings is analyzed using conventional microscopic observations of cross-sections. However extrapolating 2D information to 3D structure is limited and can be misleading. Moon et al. [9] applied an epoxy replica method to infiltrate PEO coatings on AZ31 Mg alloy and revealed three-dimensional network of the open pores. It was found that large pores were irregularly shaped and distributed in the middle part of the coating, and small pores were near the coating/alloy interface. This method provides only information on open porosity and even some small open pores are not easily accessible during the infiltration. Synchrotron tomography is a unique non-destructive tool allowing the volume and shape of the pores to be quantified. [10-12] Although X-ray tomography has been utilized to generate three-dimensional images of the porosity in PEO coatings on aluminum and titanium, [13, 14] the feature of the pores (size, volume and sphericity) has not been analyzed. Moreover the PEO coatings on Mg alloys have never been studied by X-ray tomography and there is no reliable information about porosity parameters of such layers. In this study, the distribution and characteristic of the pores in PEO coatings on Mg alloy have been investigated with the aid of synchrotron tomography. Inert La_2O_3 particles have also been introduced to PEO coating to better understand the coating mechanism.

2. Experimental

The synchrotron tomography experiments were performed at the P05 (IBL) beamline of PETRA III, DESY (Deutsches Elektronen-Synchrotron). During the acquisition of the tomograms, 1800 projections were taken with an acquisition time of 3s. The energy was set to 18 keV with a sample-to-detector-distance of 15 mm. The reconstructions resulted in volumes of (960×960×1528) voxel with a voxel size of $(1.1\ \mu m)^3$. The spatial resolution of the reconstructed volumes was 2.9 µm. Mg alloy AM50 specimens with average diameter of 1.2 mm are prepared from gravity cast ingot material. The nominal composition is 4.74 wt. % Al, 0.383 wt. % Mn, 0.065 wt. % Zn, 0.063 wt. % Si, 0.002 wt. % Fe, 0.002 wt. % Cu and Mg balance. The specimens were anodized by a pulsed DC power supply (ton: toff = 0.4 ms: 3.6 ms) for 0.5, 1 and 10 min under a constant voltage regime (400 V) with maximum 2 A. The corresponding coatings are named as PEO_30 s, PEO_1 min and PEO_10 min, respectively. The electrolyte consisted of KOH (1 g/l), Na_3PO_4 (30 g/l) and 5 g/l La_2O_3 particles sized in the range of 1-5 µm. Continuous mechanical stirring together with bubbling of the compressed air were used to ensure the uniform distribution of the particles in the electrolyte. A scanning electron microscope (TESCAN Vega3

SB) equipped with EDS was used to examine the microstructure and composition of the PEO coatings.

3. Results and discussion

The evolution of the PEO coating morphology with treatment time is visualized in Figure 1. The distribution of the pores and particles in the coatings can be seen in 3D micrographs. The quantitative analysis of volume of the pores, particles and the coating is summarized in Table 1. The pore volume decreases slightly from 2.10×10^7 μm^3 to 1.75×10^7 μm^3 and 1.48×10^7 μm^3 with the increase of treatment time, 30s, 1 min and 10 min respectively. As the number of the pores increases from 16025 to 21652 and 27868, it can be inferred that the average size of the pores decreases and the coating becomes denser with treatment time. The total volume of the particles in the layer drastically increases by about 16 times when the sample is anodized for 10 minutes in comparison to 30 s treatment. In contrast, the coating volume has merely increased only by about two times from 5.85×10^7 μm^3 to 1.15×10^8 μm^3 during the same treatment time. It is obvious that the increment of the coating volume is much less than that of the particle volume. As a consequence, the porosity of the layer has reduced from 26.25 % to 15.99 % and 10.88 % after 30 s, 1 min and 10 min, respectively. This is still much higher than the porosity (5.7 %) of PEO coating on Ti measured with X-ray tomography. [14]

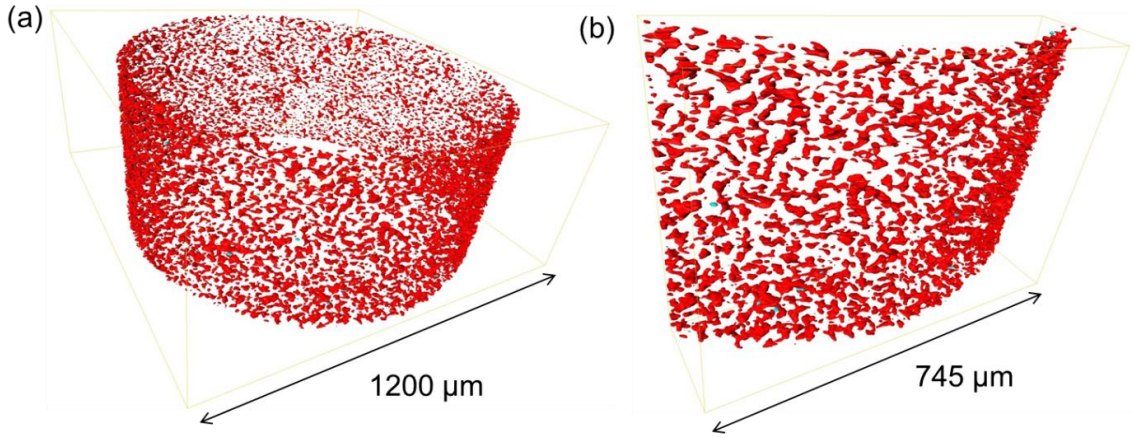

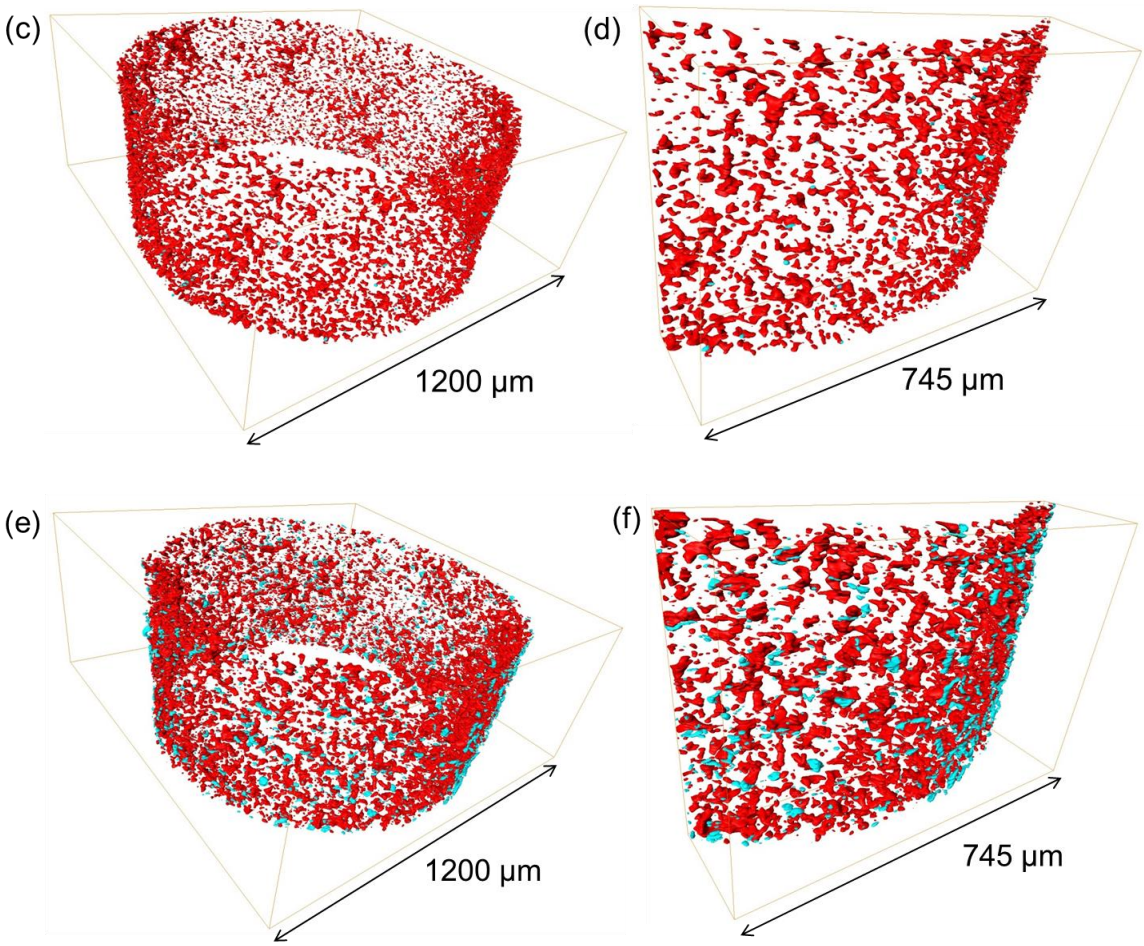

Figure 1. Distribution of the pores (in red) and particles (in light blue) in the coatings. a,b) PEO_30 s. c,d) PEO_1 min. e,f) PEO_10 min.

Table 1. Volume of the pores, particles and the coating in Figure 1.

Coating	Volume and number of the pores	Volume and number of the particles	Volume of the coating	Porosity
PEO_30 s	2.10×10^7 µm^3, 16025	4.90×10^5 µm^3, 3760	5.85×10^7 µm^3	26.25 %
PEO_1 min	1.75×10^7 µm^3, 21652	1.43×10^6 µm^3, 10350	9.05×10^7 µm^3	15.99 %
PEO_10 min	1.48×10^7 µm^3, 27868	6.25×10^6 µm^3, 17603	1.15×10^8 µm^3	10.88 %

The PEO coatings were additionally analyzed using a conventional metallographic cross-sectional method to compare with the tomographic slicing (Figure 2). The thickness of the

coating increases significantly with the treatment time. The critical through-going defects (Figure 2d and g) well visible in the nondestructive slicing from the synchrotron tomography are no longer observable when a polished cross-section is analyzed with SEM. The coatings appear also to be denser after metallographic preparation (Figure 2e and h). This sealing effect might be ascribed to the embedded resin and the coating debris generated during metallographic preparation process. The tomographic slicing shows that through-going defects are still visible after 10 min treatment, indicating that dielectric breakdown of the layer is not dependent on the coating thickness but primarily occurs at relatively defective place. In terms of particle distribution (Figure 2c, f and i), the majority of the particles are located along the large-sized pores in the outer layer. Isolated particles can be observed at the beginning of a treatment, while the particles tend to agglomerate with the coating growth. Figure 3 shows the coatings surface morphology observed by SEM. The layer appears to be coarser and has a higher number of large-sized pores on the surface as a function of treatment time. Additionally, Figure 3d exhibits the reconstruction of one of the largest pores in PEO_10 min, which is one of the through-going defects in the layer (Figure 2g). This implies that several small open pores on the coating surface can derive from one large-sized pore, which is unlikely to be detected by traditional characterization methods. It is also a fact that pore band exists between the outer porous layer and the inner barrier layer.

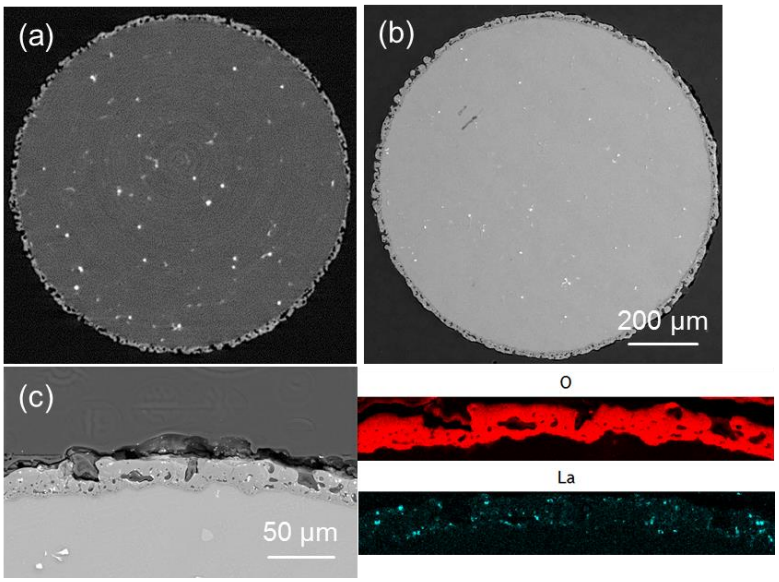

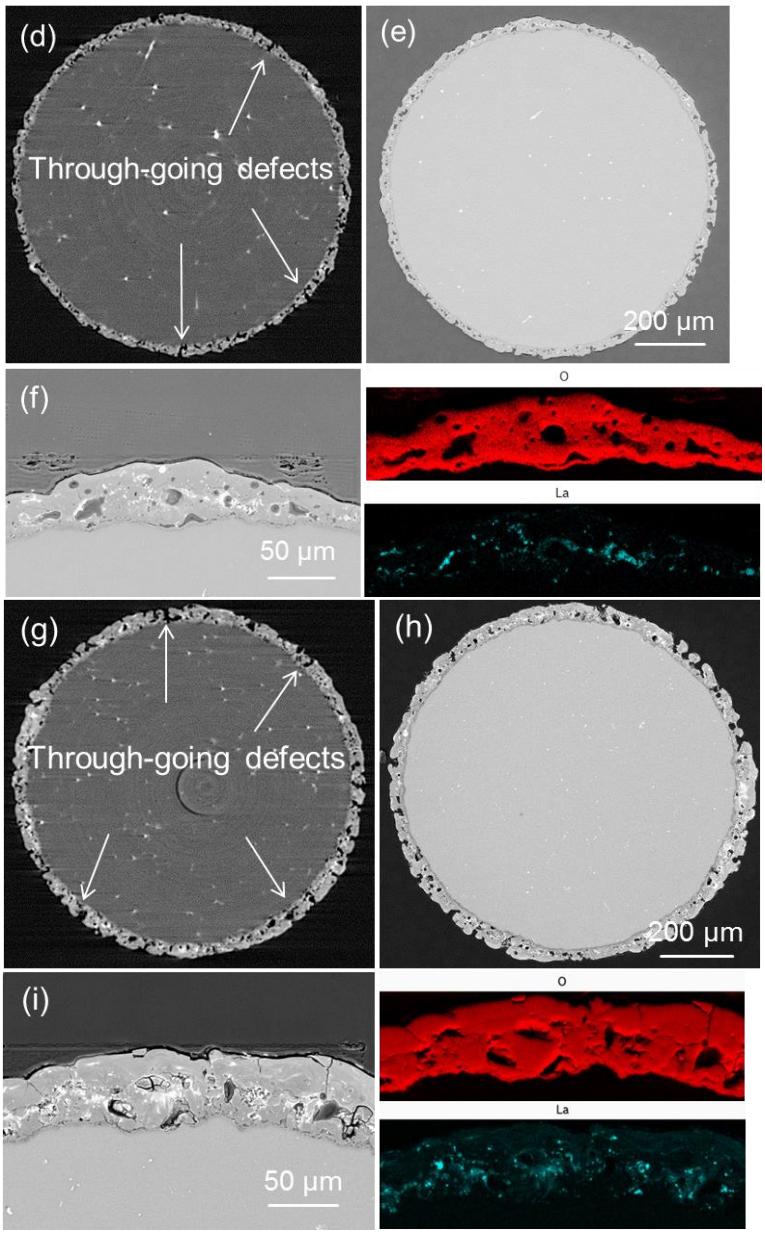

Figure 2. Coating morphology from tomographic slicing a) PEO_30s. d) PEO_1 min. g) PEO_10 min. Surface and cross-sectional morphology from conventional metallographic method b,c) PEO_30s. e,f) PEO_1 min. h,i) PEO_10 min.

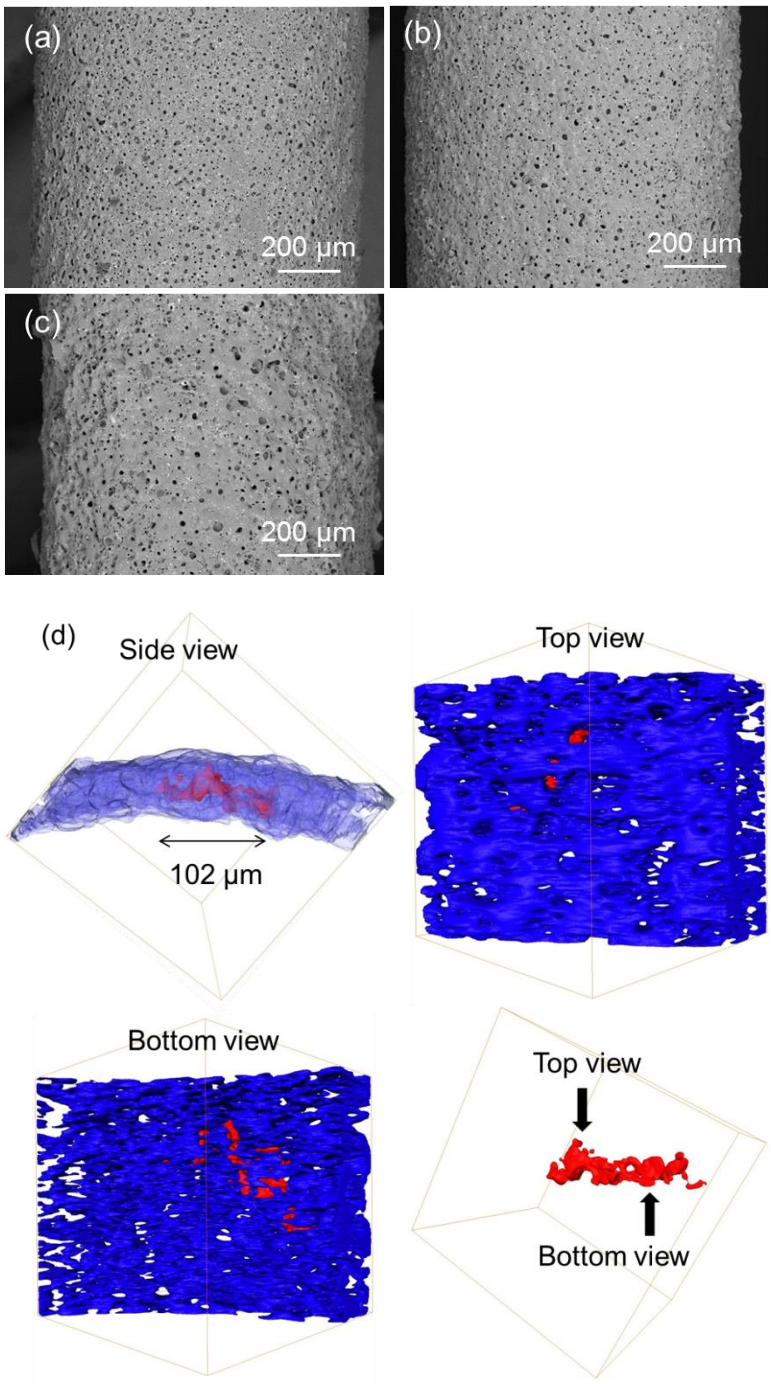

Figure 3. Surface morphology of the coatings obtained by SEM a) PEO_30 s. b) PEO_1 min. c) PEO_10 min. d) reconstruction of the largest pore in PEO_10 min.

Furthermore, the pores and particles in PEO layers were quantified in terms of geometry and size distribution in order to understand how these critical parameters evolve with treatment time. The sphericity of pores/particles, Ψ, is calculated by equation (1), where V and A are the volume and

the surface area of the pores/particles, respectively. [15] $\Psi = 1$ corresponds to a sphere, while $\Psi = 0$ corresponds to an infinite plate. The Ψ distribution of the pores and particles is presented in Figure 4.

$$\Psi = \frac{\pi^{1/3}(6V)^{2/3}}{A} \quad (1)$$

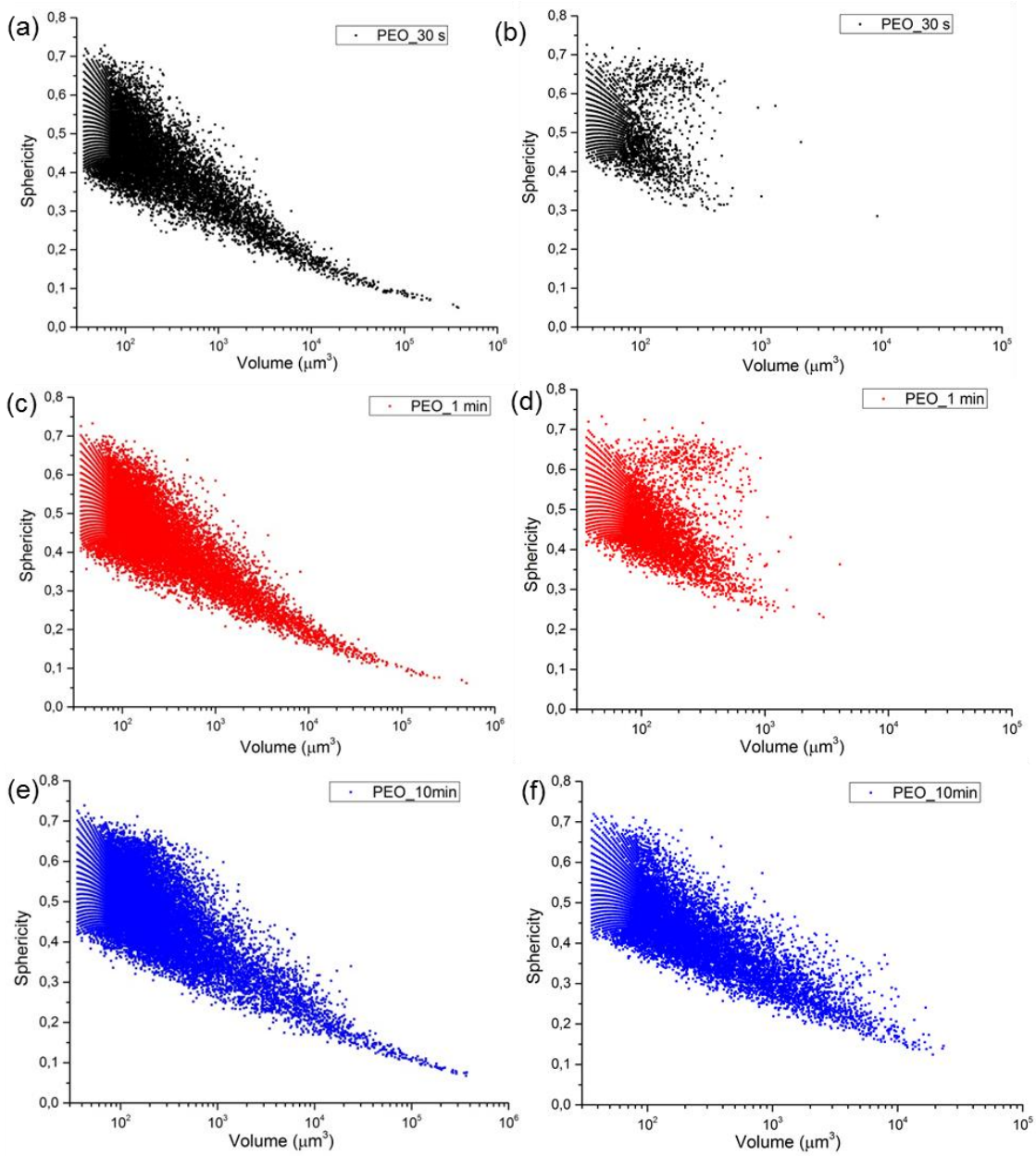

Figure 4. Sphericity distribution of the pores a, c, e). Sphericity distribution of the particles b, d, f).

The correlation between the volume and sphericity of the pores remains unchanged with the growth of the layer. The majority of the pores are below 10^4 µm^3 which are of higher sphericity in comparison to the large-sized pores. In particular, there are few extremely large-sized pores in the coating with sphericity close to 0. More fractions of pores have transformed into spheroid-like shape with relatively high sphericity in the range of 10^2 µm^3 to 10^4 µm^3 along with the treatment time (Figure 4a, c and e). In terms of particles, the number and volume increase with the coating growth, as indicated by Figure 4b, d and f. The particles are individually distributed in the layer at the beginning of the treatment. Due to the coating growth, the uptake and incorporation of the particles is continually increased leading to agglomeration in the layer. The agglomeration of large number of particles results in complex shapes and low sphericity. Thus a large fraction of large-sized and convex-shaped particles are detected (Figure 4f) in the later stage of the treatment.

4. Conclusion

The evolution and distribution of the pores and particles obtained from synchrotron-based microtomography contribute to understanding the coating growth along with the PEO treatment. The porosity of the layer decreases and more fractions of pores with high sphericity appear owing to formation of new coating materials. It was found that several open pores on the coating surface can stem from one large-sized pore, which is beyond the capability of traditional characterization methods. The uptake of the particles into the coating is probably via molten material and deposition in the open pores. Agglomeration of the particles is related to the coating growth and can be only observed at the later stage of the treatment. In summary, synchrotron-based microtomography is an effective technique to confer 3D visualization of PEO coating and to generate more quantitative and precise assessment of the layer, e.g., size, volume and sphericity of the pores, in comparison to the conventional metallographic methods.

5. References

[1] T.M. Pollock, Weight Loss with Magnesium Alloys, Science, 328 (2010) 986-987.
[2] B.L. Mordike, T. Ebert, Magnesium: Properties — applications — potential, Materials Science and Engineering: A, 302 (2001) 37-45.
[3] W. Xu, N. Birbilis, G. Sha, Y. Wang, J.E. Daniels, Y. Xiao, M. Ferry, A high-specific-strength and corrosion-resistant magnesium alloy, Nat Mater, advance online publication (2015).
[4] G. Song, A. Atrens, D.S. John, X. Wu, J. Nairn, The anodic dissolution of magnesium in chloride and sulphate solutions, Corrosion Science, 39 (1997) 1981-2004.

[5] N. Birbilis, M.A. Easton, A.D. Sudholz, S.M. Zhu, M.A. Gibson, On the corrosion of binary magnesium-rare earth alloys, Corrosion Science, 51 (2009) 683-689.
[6] R. Arrabal, E. Matykina, T. Hashimoto, P. Skeldon, G.E. Thompson, Characterization of AC PEO coatings on magnesium alloys, Surface and Coatings Technology, 203 (2009) 2207-2220.
[7] R.O. Hussein, D.O. Northwood, X. Nie, The effect of processing parameters and substrate composition on the corrosion resistance of plasma electrolytic oxidation (PEO) coated magnesium alloys, Surface and Coatings Technology, 237 (2013) 357-368.
[8] X. Lu, C. Blawert, M.L. Zheludkevich, K.U. Kainer, Insights into plasma electrolytic oxidation treatment with particle addition, Corrosion Science, 101 (2015) 201-207.
[9] S. Moon, R. Arrabal, E. Matykina, 3-Dimensional structures of open-pores in PEO films on AZ31 Mg alloy, Materials Letters, 161 (2015) 439-441.
[10] D. Tolnai, G. Requena, P. Cloetens, J. Lendvai, H.P. Degischer, Sub-micrometre holotomographic characterisation of the effects of solution heat treatment on an AlMg7.3Si3.5 alloy, Materials Science and Engineering: A, 550 (2012) 214-221.
[11] D. Tolnai, G. Requena, P. Cloetens, J. Lendvai, H.P. Degischer, Effect of solution heat treatment on the internal architecture and compressive strength of an AlMg4.7Si8 alloy, Materials Science and Engineering: A, 585 (2013) 480-487.
[12] E. Maire, P.J. Withers, Quantitative X-ray tomography, International Materials Reviews, 59 (2014) 1-43.
[13] E.K. Tillous, T. Toll-Duchanoy, E. Bauer-Grosse, Microstructure and 3D microtomographic characterization of porosity of MAO surface layers formed on aluminium and 2214-T6 alloy, Surface and Coatings Technology, 203 (2009) 1850-1855.
[14] X. Zhang, S. Aliasghari, A. Němcová, T.L. Burnett, I. Kuběna, M. Šmíd, G.E. Thompson, P. Skeldon, P.J. Withers, X-ray Computed Tomographic Investigation of the Porosity and Morphology of Plasma Electrolytic Oxidation Coatings, ACS Applied Materials & Interfaces, 8 (2016) 8801-8810.
[15] H. Wadell, Volume, Shape, and Roundness of Quartz Particles, The Journal of Geology, 43 (1935) 250-280.

5.8 Influence of incorporating Si_3N_4 particles into the oxide layer produced by plasma electrolytic oxidation on AM50 Mg alloy on coating morphology and corrosion properties *(with permission from Elsevier)*

Available online at www.sciencedirect.com

ScienceDirect

Journal of Magnesium and Alloys 1 (2013) 267–274
www.elsevier.com/journals/journal-of-magnesium-and-alloys/2213-9567

Full length article

Influence of incorporating Si_3N_4 particles into the oxide layer produced by plasma electrolytic oxidation on AM50 Mg alloy on coating morphology and corrosion properties

Xiaopeng Lu*, Carsten Blawert, Nico Scharnagl, Karl Ulrich Kainer

Helmholtz-Zentrum Geesthacht Zentrum für Material-und Küstenforschung GmbH, Institute of Materials Research, Max-Plank-Str. 1, 21502 Geesthacht, Germany

Abstract

The influence of incorporating different sizes of Si_3N_4 particles on the microstructure and corrosion properties of a phosphate-based plasma electrolytic oxidation (PEO) coating on AM50 magnesium alloy was investigated. The experiments for this study were performed in alkaline electrolytes containing 1 g/L KOH, 10 g/L Na_3PO_4 with and without three different sized of Si_3N_4 particles. The corrosion properties of PEO coatings were investigated by potentiodynamic polarization and electrochemical impedance spectroscopy (EIS) in 0.5 wt.% NaCl solution. Microstructure observations by SEM showed that the surface morphology and composition of the PEO coating were affected greatly by particle addition. Si_3N_4 particles can still be found without decomposition in the final coating due to their high melting point.
Copyright 2013, National Engineering Research Center for Magnesium Alloys of China, Chongqing University. Production and hosting by Elsevier B.V. Open access under CC BY-NC-ND license.

Keywords: Magnesium; Plasma electrolytic oxidation; Microstructure; Corrosion resistance

1. Introduction

Plasma electrolytic oxidation (PEO) is a promising process which produces relatively thick, ceramic-like coatings containing amorphous and crystalline phases, with incorporation of species originating from substrate and electrolyte [1–3]. This method is based on the anodic polarization of a metal in an aqueous electrolyte at high voltage that causes the occurrence of plasma micro discharges at the metal surface which converts the surface into a ceramic top coating. Unfortunately, the discharges create not only the coating, but also some defects, for example discharge channels, pores from gas inclusions and cracks. This has negative effects on the corrosion resistance. In order to improve the corrosion properties of PEO coated magnesium and its alloys, different particles suspended in the electrolyte have been incorporated into the coating to improve the microstructure. Examples of such particles include silica, titanium dioxide, alumina and zirconia [4–9].

Silicon nitride (Si_3N_4) has been frequently used and studied for its unique properties such as high hardness, high wear resistance, good inert chemical behavior and high temperature properties [10]. However, only little work has been done on the influence of corrosion resistance by incorporating Si_3N_4 particles into PEO coating for magnesium alloys. In this paper, three different sizes of Si_3N_4 particles have been incorporated into a plasma electrolytic oxidation coating from an alkaline electrolyte. The effect of different sizes of Si_3N_4 particles on the alteration of microstructural morphology and corrosion resistance are evaluated by different characterization methods.

* Corresponding author. Tel.: +49 4152871943; fax: +49 4152871960.
E-mail addresses: xiaopeng.lu@hzg.de (X. Lu), carsten.blawert@hzg.de (C. Blawert), nico.scharnagl@hzg.de (N. Scharnagl), karl.kainer@hzg.de (K.U. Kainer).
Peer review under responsibility of National Engineering Research Center for Magnesium Alloys of China, Chongqing University

Production and hosting by Elsevier

2213-9567 Copyright 2013, National Engineering Research Center for Magnesium Alloys of China, Chongqing University. Production and hosting by Elsevier B.V. Open access under CC BY-NC-ND license.
http://dx.doi.org/10.1016/j.jma.2013.11.001.

2. Experimental

An AM50 magnesium alloy with a nominal composition of (mass fraction) 4.7% Al, 0.38% Mn, max. 0.1% Zn, max. 0.1% Si, max. 0.002% Fe, max. 0.002% Cu, max. 0.001% Ni and Mg balance was used in this investigation. Specimens of size 15 mm × 15 mm × 4 mm were polished using 320, 500 and 1200 grit emery sheets successively and cleaned with ethanol before the PEO treatment. The PEO treatment was carried out using an unipolar pulsed power source with a pulse ratio of t_{on}:t_{off} = 2 ms:18 ms in electrolyte composed by 1 g of KOH and 10 g of Na_3PO_4 in 1 l of deionized water with additional 5 g of three different sizes of Si_3N_4 particles. The sizes of the three different Si_3N_4 particles varied from nano-particle to micro-sized particle, i.e. about 0.02 μm, 0.1–0.8 μm and 1–5 μm, which can be seen in Fig. 1. The smallest particles are agglomerated and the real shape is hardly to be seen but most likely globular. Medium-sized particles contain many fibers and globular particles. In the case of the largest particles, irregular and flaky particles can be observed. The same composition and concentration of alkaline electrolyte without particle was used for comparison and evaluation of the particle influence. During the PEO process, the magnesium alloy sample and stainless steel tube were used as the anode and cathode, respectively. All of the PEO treatments were performed at a constant voltage of 450 V for 10 min. The temperature of the PEO electrolytes was kept at 10 ± 2 °C by a water cooling system.

Scanning electron microscope (Cambridge Stereoscan) was used to examine the surface morphology and cross section of the PEO coatings. A Zeiss Ultra55 SEM equipped with an energy dispersive spectrometer (EDS) was used to determine the elemental composition and distribution of the PEO coatings. The phase composition analysis was done in a Bruker X-ray diffractometer equipped with Cu Kα radiation.

The corrosion behavior of the PEO coated magnesium alloy specimen was assessed by potentiodynamic polarization and electrochemical impedance spectroscopy (EIS) tests, which were carried out using an ACM Gill AC computer, controlled potentiostat. A typical three-electrode cell with the coated specimen as the working electrode (0.5 cm^2 exposed area), a saturated Ag/AgCl electrode as the reference electrode, and a platinum mesh as counter electrode was used. Polarization studies were carried out starting at −150 mV with reference to OCP (after 30 min of exposure at OCP) at a sweep rate of 0.2 mV s^{-1} until reaching a final current density of 0.01 mA cm^{-2}. Electrochemical impedance spectroscopy (EIS) studies were performed at open circuit potential with AC amplitude of 10 mV over the frequency range from 30 kHz to 0.01 Hz. The measurements were repeated at certain fixed times (0, 1, 3, 6, 12, and 24 h) up to 3 days of immersion time.

3. Results

3.1. Evolution of PEO coating

As a constant voltage of 450 V was used for performing the coating process in all the cases, the current decreased rapidly with the passage of time. For the PEO coating obtained from the electrolyte without particle addition, very fine sized discharges began to appear at a voltage termed as

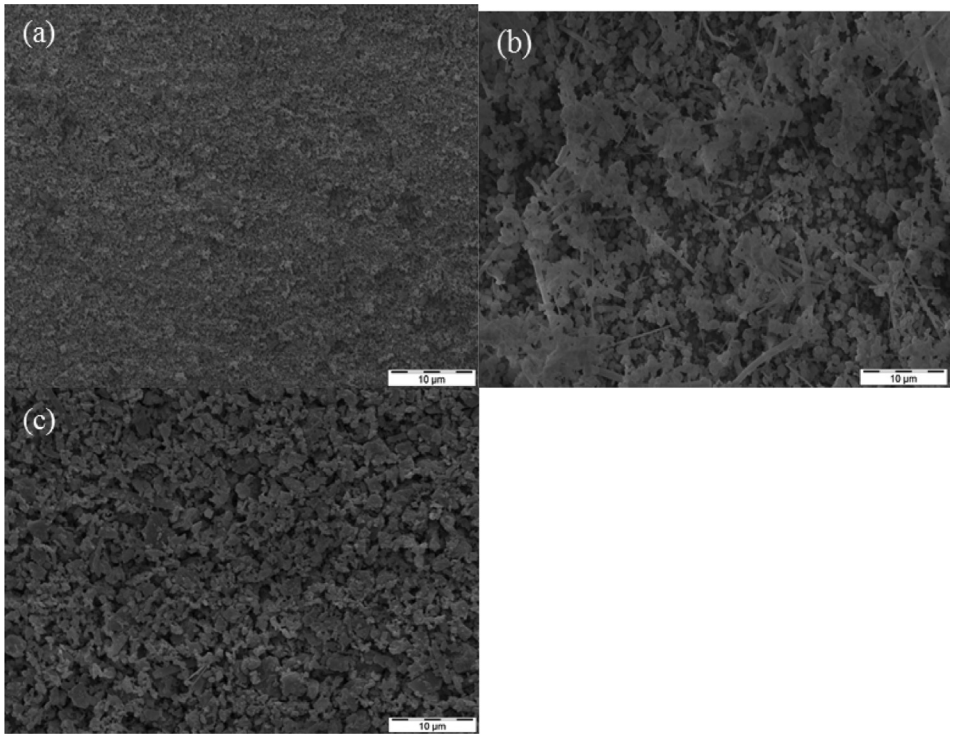

Fig. 1. SEM image of Si_3N_4 particles (a) 0.02 μm, (b) 0.1–0.8 μm, (c) 1–5 μm.

breakdown potential (250 V in this electrolyte). By increasing processing time, the size of the sparks grew and changed their color, in addition to the decrease of discharge density on the surface. The size, density and color variation of the sparks may be ascribed to the changes of the number and type of the active plasma species, the growth of the films and the applied energy [11]. The physical changes that might occur on the surface of PEO coating in electrolytes with particle addition cannot be observed due to the milky character of the solution. The only change one can see was the continuous decrease to 0.01 A of current accompanying with the constant voltage which is similar to PPEO. However, treatment was not successful in the case of using the 0.02 μm sized nanoparticles. The voltage could only reach 380 V and current remain at a high value (1.6 A). Therefore, PEO coating obtained from the electrolyte containing the 0.02 μm sized nanoparticles is excluded from further characterization of microstructure and properties. For ease of referencing, the coatings obtained in phosphate based electrolyte with smallest size (0.02 μm), medium size (0.1–0.8 μm), large-sized particle (1–5 μm) and without particle are named PPEO(S), PPEO(M), PPEO(L) and PPEO, respectively.

3.2. Microstructure

The surface morphologies of PPEO coated specimens are shown in Fig. 2. The typical morphology of PPEO coating presented in Fig. 2a reveals many micropores and some cracks on the surface. The size of those pores is in the range of 1–20 μm. These open pores are formed by the discharges and gas inclusions during PEO processing. Melted material has been expelled by the discharges and has solidified quickly before it could flow back to close the discharge channels. Significant change (Fig. 2c and e) can be observed on the surface of PEO coatings obtained in electrolytes with particle addition. On the one hand, many particles are sticking on the surface, indicating they might take part in PEO processing; on

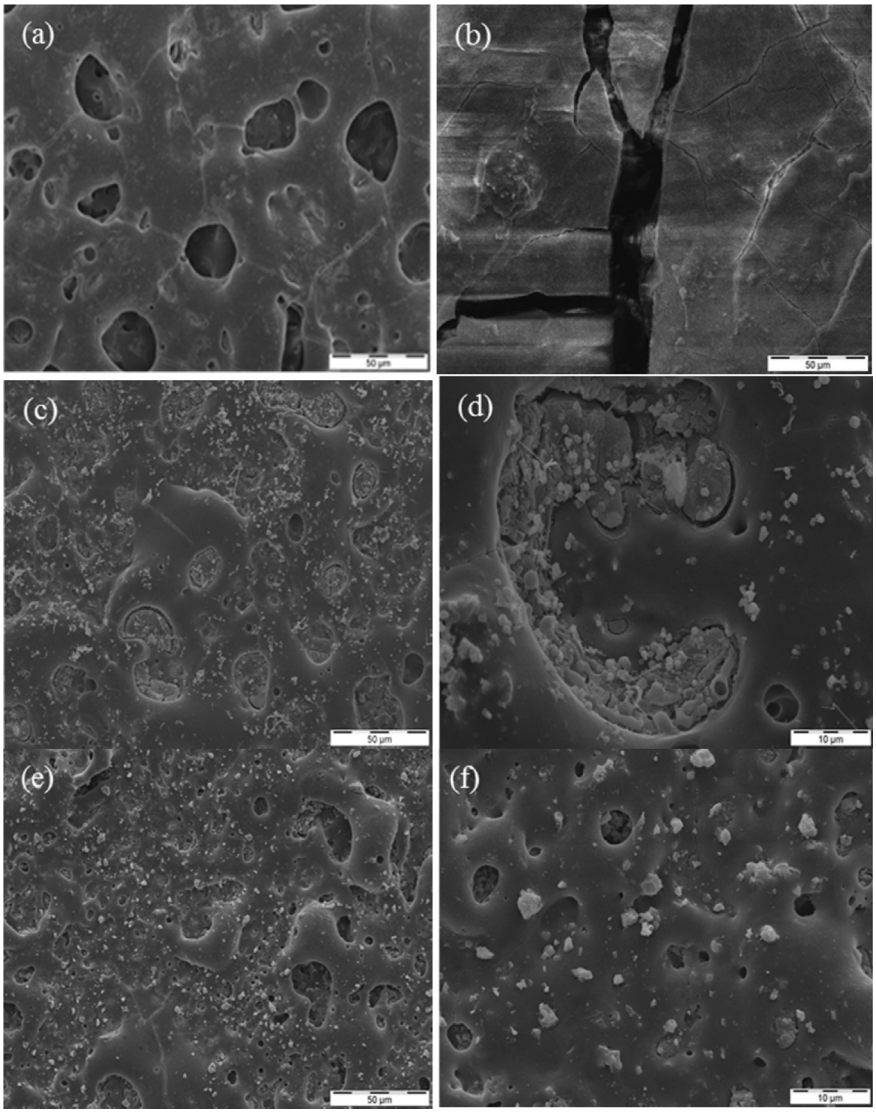

Fig. 2. Surface morphology of PPEO coatings (a) PPEO, (b) PPEO(S), (c) and (d) PPEO(M), (e) and (f) PPEO(L).

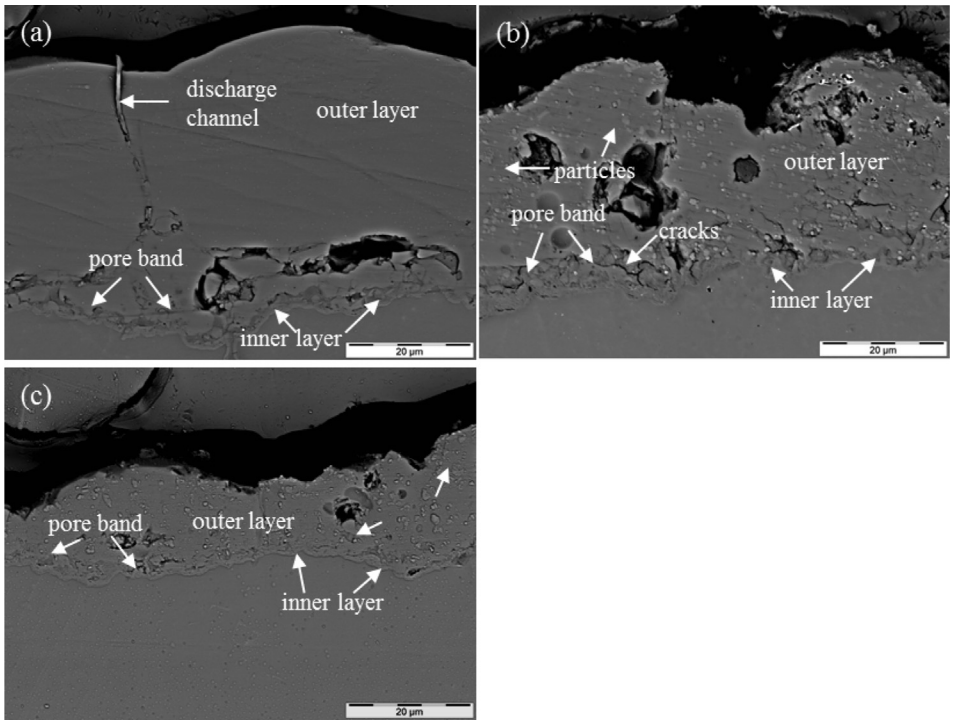

Fig. 3. Backscattered scanning electron micrographs of cross-section of PEO coatings (a) PPEO (b) PPEO(M) (c) PPEO(L).

the other hand, large-sized pores are sealed by solidified material, especially in the case of PPEO(M). As for PPEO(L), the surface is dominated by many tiny pores, which are in the range of 1−5 μm. Interestingly, many particles and fibers together with solidified material are piled up in some large-sized pores of PPEO(M) (Fig. 2d), which is in agreement with the original particles morphology. In addition, all coatings are also dominated by many hairline micro-cracks, which may result from thermal stress due to rapid solidification of molten material in the relatively cool electrolyte [12]. As for the PPEO(S), the coating surface is brittle and full of cracks, as can be seen in Fig. 2b.

The backscattered scanning electron micrographs showing the cross-sectional feature of the PEO coated specimens obtained from the different electrolytes are presented in Fig. 3. The PPEO consists of three parts: outer layer, pore band and inner layer. The build-up of the PEO coatings has not been varied by particle addition. Some large-sized pores (3−12 μm) can be observed in the outer layer of PPEO and PPEO(M). In contrast, the size of the defects of PPEO(L) is a little bit smaller (1−4 μm). Many cracks reaching from the pore band towards the outer layer can be observed for the PPEO(M). Interestingly, pore band can hardly be observed between outer layer and inner layer for PPEO(L), but larger magnification reveal that it is still present. The growth rate of coating produced from electrolyte without particle addition is much faster than in the case of Si_3N_4 addition, resulting in PPEO with an average layer thickness of 40 μm compared to PPEO(M) (25 μm) and PPEO(L) (10 μm). Some large-sized pores can be observed at the outer layer for all coatings. Moreover, some particles are found incorporated in the outer layer even reaching inner layer in Fig 3b and c, indicating that they might not react with other material during PEO processing.

3.3. Chemical and phase composition

The composition of near surface of PEO coatings is given in Table 1. The content of O, Mg, P and Na of PEO coatings with particle addition is less but nearly the same compared to PPEO, which is consistent with the additional presence of Si. More particles seem to be incorporated in PPEO(L) (9%) than PPEO(M)(7%). However, it might be caused by the particle size and not by the number of particles incorporated.

To study the distribution of Si_3N_4 particles in the cross section of PEO coatings with particle addition, elemental mapping by EDS was carried out and is shown in Figs. 4 and 5. The elements Si, Mg, O and P were detected in both PEO coatings. Because light elements below oxygen cannot be routinely analyzed by EDS in our system, the distribution of nitrogen is not given. However, the uniform distribution of particles indicated by intensity dots of Si, which can be observed across the whole cross section of the PEO coatings obtained with particle addition. Some dots seem to be larger than the original particle size. Due to some defects (pores), small Si_3N_4 particles might be piled up to a

Table 1
Surface composition of the PEO coatings determined by EDS analysis.

Concentration (at. %)	O	Mg	P	Na	Si
PPEO	65	20	10	5	0
PPEO(M)	63	19	7	4	7
PPEO(L)	60	18	8	5	9

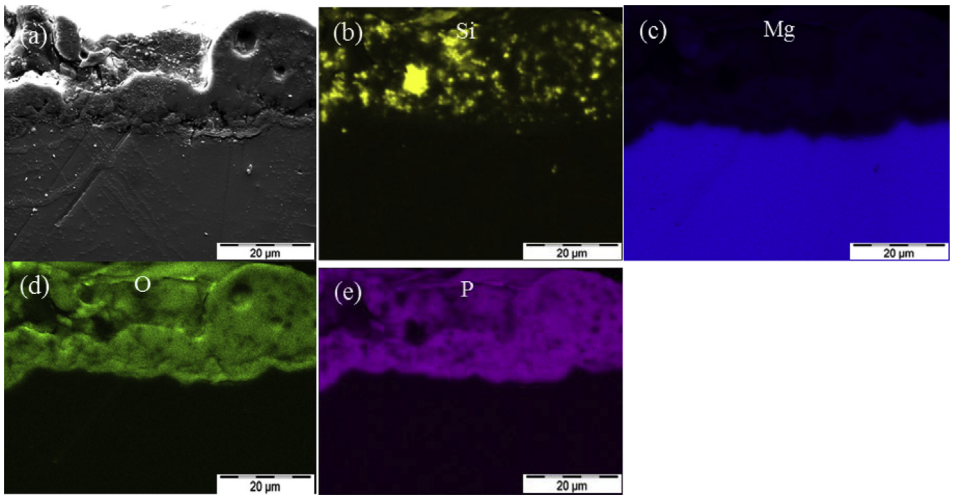

Fig. 4. Elemental mapping of PPEO(M) obtained by EDS (a) SEM image of cross section (b) Si (c) Mg (d) O (e) P.

large volume in specific areas. Phosphorus and oxygen also distribute uniformly in the two PEO coatings. With respect to the magnesium, signal form substrate is stronger than the coating as one would expect.

The PPEO coating is found to be constituted by MgO and $Mg_3(PO_4)_2$ phases, as evidenced from the XRD pattern in Fig. 6. In addition, there are some magnesium peaks, indicating the X-ray could penetrate the layer reaching the magnesium substrate. In PEO coatings achieved from electrolytes with particle addition, many Si_3N_4 peaks and a small peak corresponding to MgO have been found. No crystalline phase containing phosphorus can be detected even though P is seen in EDS analysis, which might be influenced by the addition of particles. As the XRD pattern contains Si_3N_4 peaks and the elemental mapping analysis shows the existence of particles, it confirms that Si_3N_4 particles may have not or not completely reacted to new phases during PEO processing. In other words, the discharge energy cannot melt Si_3N_4 particles, which indicates that the energy of the discharges occurring in these two electrolytes under the applied processing parameters is lower than the melting temperature (1900 °C) of Si_3N_4.

3.4. Corrosion behavior

3.4.1. Potentiodynamic polarization

The corrosion behavior of PEO coatings evaluated by potentiodynamic polarization technique after exposure of 0.5 h in 0.5 wt.% NaCl solution is presented in Fig. 7. The corrosion potential (E_{corr}), corrosion current density (i_{corr}) and the breakdown potential (E_{bd}) derived from potentiodynamic polarization plots are summarized in Table 2.

From Table 2, the free corrosion potentials of PEO coatings are found to be in the active direction to that of the bare alloy, especially for PPEO(M) and PPEO(L). The corrosion potential of AM50 magnesium alloy with a phosphate based PEO coating was found to be slightly active than the magnesium substrate [13]. Interestingly, the corrosion potentials of the PEO coatings with particle addition drift towards more active

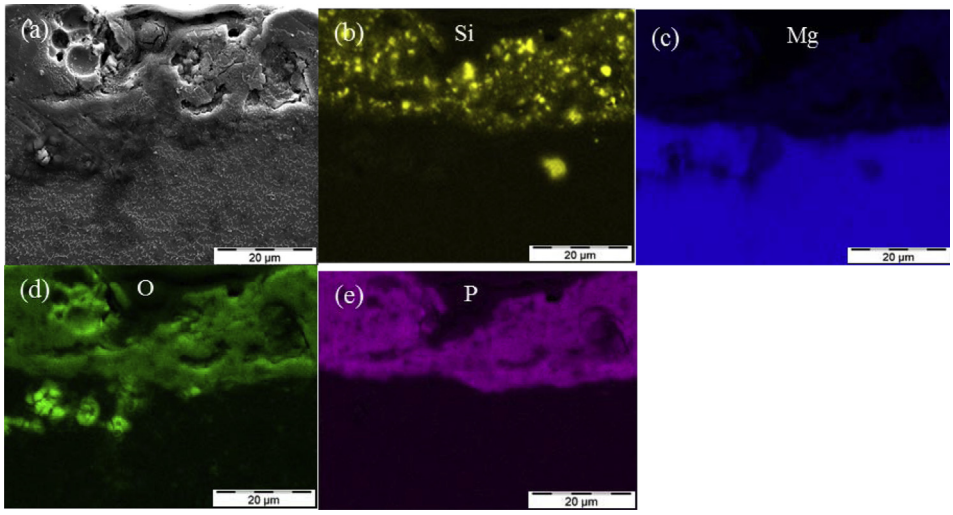

Fig. 5. Elemental mapping of PPEO(L) obtained by EDS (a) SEM image of cross section (b) Si (c) Mg (d) O (e) P.

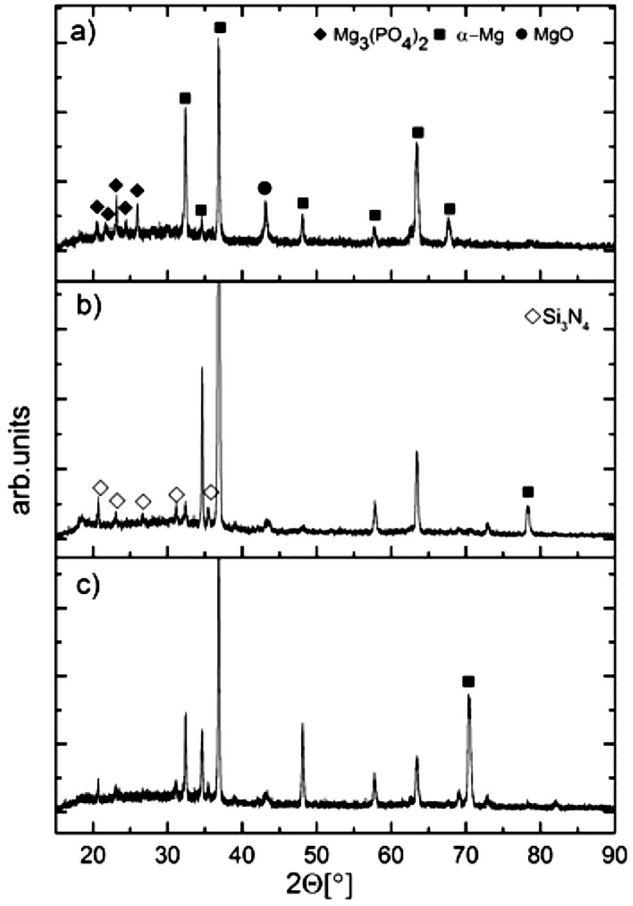

Fig. 6. X-ray diffraction patterns of three PEO coatings (a) PPEO (b) PPEO(M) (c) PPEO(L).

side than PPEO, which might be contributed to the presence of particles containing in the coating. It can also be seen that the i_{corr} values of PPEO(M) and PPEO(L) are in the same order of magnitude in the 0.5 wt. % NaCl solution, whilst the i_{corr} value of PPEO is lower to some extent. The relatively higher corrosion current of PPEO(M) might be caused by the thinner layer and several cracks between the outer layer and the inner

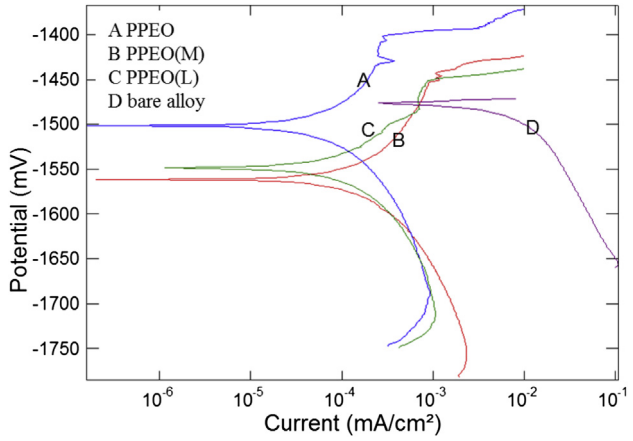

Fig. 7. Potentiodynamic polarization behavior of the specimens PEO coated in electrolytes containing different sized particles (test electrolyte: 0.5 wt.% NaCl).

Table 2
Electrochemical data for PEO coated specimens from potentiodynamic polarization studies.

Coating	E_{corr} (mV)	i_{corr} (mA cm^{-2})	E_{bd} (mV)
PPEO	−1509 ± 9	(9 ± 0.5) × 10^{-5}	−1400 ± 20
PPEO(M)	−1559 ± 2	(1.9 ± 0.2) × 10^{-4}	−1436 ± 16
PPEO(L)	−1575 ± 27	(1.3 ± 0.1) × 10^{-4}	−1445 ± 6
Bare alloy	−1452 ± 10	(3.5 ± 1.1) × 10^{-2}	–

layer. Even though the PPEO(L) is the thinnest layer, its corrosion behavior is not that bad due to fewer defects on the cross section. Generally, the breakdown potential (E_{bd}) of coated alloys in corrosive environments is considered as an indication of the capability of a coating to resist localized corrosion damage [14]. The PPEO seems to be more stable on the basis of higher breakdown potential (−1400 ± 20 mV) in contrast with other two coatings. However, the polarization required to reach breakdown potential from the free corrosion potential is for all the coatings nearly the same.

3.4.2. EIS behavior

The corrosion deterioration of PEO coated specimens in 0.5 wt. % NaCl with prolonged immersion time up to 72 h was examined by EIS measurements. The EIS spectra (Bode plots) of PEO coatings obtained from different electrolytes are presented in Fig. 8.

Based on the impedance plots, taking into account the microstructure of PEO coatings and EIS studies of Liang et al. [15] and Ghasemi et al. [16] on coatings, an appropriate equivalent circuit is given in Fig. 9 and the results are documented in Tables 3–5. The elements in equivalent circuit include R_s (the solution resistance), R_p (resistance of outer porous layer) paralleled with CPE_p (a constant phase element representing the porous outer layer/coating capacitance), R_i (resistance of inner layer) paralleled with constant phase element CPE_i (constant phase element representing the inner layer capacitance).

The Bode plots of PPEO coating after different durations of exposure to the corrosive environment are shown in Fig. 8a and the corresponding electrochemical parameters are presented in Table 3. The resistance of inner layer (R_i) in the EIS test after 0 h of immersion time is 2.35E5 Ω cm^2, with the resistance of the porous layer (R_p) is 63,868 Ω cm^2. The resistance of the R_i and R_p is found to decrease greatly for the tests after 1 h and 3 h immersion, and starts to increase slightly after that until 12 h. The formation of corrosion products and the filling of the pores might be the main reasons for the increase of corrosion resistance. With prolonged exposure the R_p and R_i drop again to lower values. In the case of PEO coatings obtained from electrolyte with particle addition, different trends can be seen from Tables 4 and 5. In the case of PPEO(M), only slight increase of the R_p (from 13,456 Ω cm^2 to 26,097 Ω cm^2) is found after 1 h exposure in 0.5 wt.% NaCl solution. The whole corrosion resistance values decrease rapidly to around 4350 Ω cm^2 after 72 h of exposure. In terms of PPEO(L), no increase of corrosion resistance has been found. However, the R_i after first measurement seems to be

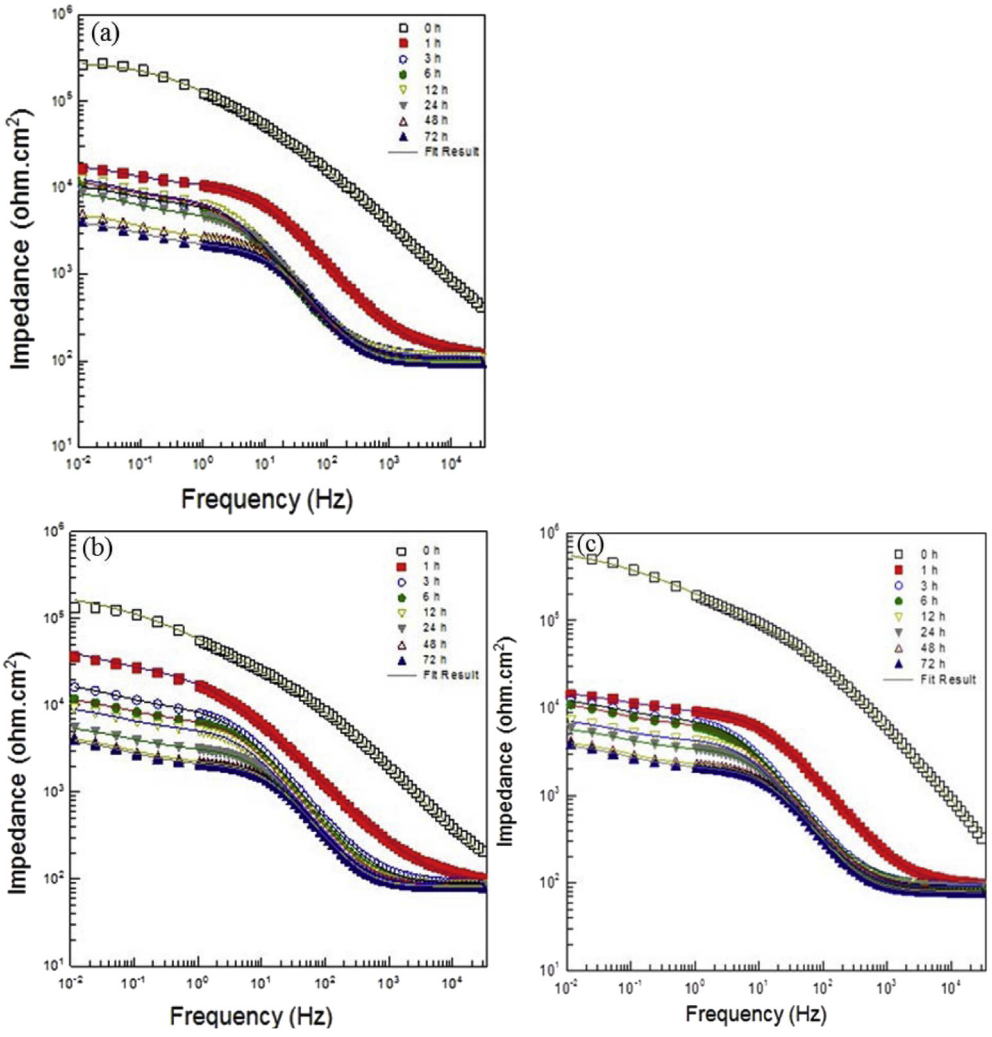

Fig. 8. EIS spectra (Bode plots) of specimens PEO coated obtained from different electrolytes (a) PPEO (b) PPEO(M) (c) PPEO(L) (test electrolyte: 0.5 wt.% NaCl).

larger than other PEO coatings. The R_p and R_i drop continuously to about 2000 Ω cm^2 with the passage of time.

4. Discussions

First of all, it is possible to produce particle-reinforced coatings with addition of relatively large-sized Si_3N_4 particles (0.1–0.8 μm and 1–5 μm). Particles have been found distributed uniformly throughout the cross section of PPEO(M) and PPEO(L). Taking the microstructure and EDS analysis of PEO coatings into consideration, the uniform distribution of particles is caused by two reasons. On the one hand, particles could flow towards the inner coating through discharge channels even reaching the inner layer. On the other hand, Si_3N_4 particles will be pasted on melted material on the surface of the coating and finally the growing coating is embedding them. Pores on the surface of PEO coating have been filled by particles, as can be seen in Fig. 2d anf f. Even though the surface could be optically greatly improved by the particle addition, there is no significant impact on enhancing cross-sectional quality of PEO coatings.

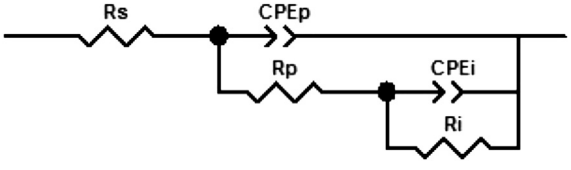

Fig. 9. Equivalent circuits for fitting the impedance data of PEO coatings on AM50 magnesium alloy.

Table 3
Electrochemical fitting data of the PPEO coated specimens from EIS.

Immersion time	R_p, Ω cm^2	(CPE-T)$_p$	(CPE-P)$_p$	R_i, Ω cm^2	(CPE-T)$_i$	(CPE-P)$_i$
0 h	63,868	6.58E-7	0.68	2.35E5	2.15E-6	0.52
1 h	11,224	3.95E-6	0.82	8026	3.27E-4	0.70
3 h	6752	1.21E-5	0.87	4449	7.2E-4	0.75
6 h	7458	1.44E-5	0.87	5353	6.01E-4	0.75
12 h	7620	1.29E-5	0.88	7136	5.46E-4	0.73
24 h	4892	1.15E-5	0.89	4783	6.05E-4	0.72
48 h	2552	1.05E-5	0.91	2965	8.27E-4	0.67
72 h	2035	1.03E-5	0.91	2306	9.1E-4	0.65

Table 4
Electrochemical fitting data of the PPEO(M) coated specimens from EIS.

Immersion time	R_p, Ω cm^2	$(CPE\text{-}T)_p$	$(CPE\text{-}P)_p$	R_i, Ω cm^2	$(CPE\text{-}T)_i$	$(CPE\text{-}P)_i$
0 h	13,456	6.14E-7	0.76	2.02E5	6.37E-6	0.44
1 h	26,097	7.79E-6	0.72	23,526	1.87E-4	0.69
3 h	9547	8.84E-6	0.85	8843	3.45E-4	0.72
6 h	6729	8.74E-6	0.89	6686	4.34E-4	0.66
12 h	5170	9.01E-6	0.91	5415	5.56E-4	0.65
24 h	3016	9.65E-6	0.91	3023	8.19E-4	0.68
48 h	2115	9.59E-6	0.91	2420	9.96E-4	0.68
72 h	1949	9.24E-6	0.92	2401	1.02E-3	0.65

It can also be concluded that mainly an inert incorporation of Si_3N_4 particles (0.1–0.8 μm and 1–5 μm) occurs without reaction with other components of the coating or electrolyte forming new compounds and phases during PEO processing. In other words, the plasma temperature or at least the transferred energy into the coating produced by the discharges during PEO processing from electrolytes with Si_3N_4 particles (0.1–0.8 μm and 1–5 μm) addition is not high enough to reach the melting temperature of Si_3N_4 (1900 °C). The inert particles may be considered as obstacles for coating growth reducing the effective area for formation of conversion products which are finally converted by the discharges into the coating. Furthermore the coating has to grow around the particles thus large-sized particles are bigger obstacles resulting in the observed thinner coatings with increasing particle size. For the electrolyte with the smallest particles (0.02 μm) addition, a normal PEO coating could not be achieved. Coating formation was observed and the breakdown potential was exceeded but a final voltage of 450 V was never reached. The plan view of those specimens revealed severe cracking, with crack opening up to 10 μm and down to the substrate. If this cracking occurs during the processing continuously one can understand that the final voltage cannot be reached because always new substrate is exposed. It might be possible that the nano-sized particles (which are generally known to have lower melting temperatures [17,18]) are being reactive incorporated forming a new and brittle coating phase that cannot withstand the internal stresses generated by the PEO processing. However, this assumption needs further studies to be proven.

In terms of improving corrosion resistance of PEO coating, incorporating Si_3N_4 particles into electrolyte seems to be not effective. Although Si_3N_4 particles are stable and distributed uniformly throughout the cross section, they do not form a dense and thick film. Thus they cannot protect the substrate better than the PPEO coating only. In general, the quality and thickness of the cross section, especially the inner layer, play more important role in the corrosion resistance in contrast with the surface of PEO coating.

Table 5
Electrochemical fitting data of the PPEO(L) coated specimens from EIS.

Immersion time	R_p, Ω cm^2	$(CPE\text{-}T)_p$	$(CPE\text{-}P)_p$	R_i, Ω cm^2	$(CPE\text{-}T)_i$	$(CPE\text{-}P)_i$
0 h	40,641	9.75E-8	0.85	7.21E5	2.04E-6	0.42
1 h	8364	3.12E-6	0.86	8364	2.91E-4	0.56
3 h	7432	8.21E-6	0.89	5899	5.03E-4	0.70
6 h	6757	9.44E-6	0.89	4875	6.56E-4	0.76
12 h	4273	9.36E-6	0.90	3410	8.64E-4	0.72
24 h	3323	9.35E-6	0.91	2895	9.24E-4	0.70
48 h	2193	1.01E-5	0.90	1993	1.16E-3	0.75
72 h	1934	9.30E-6	0.92	2231	1.10E-3	0.65

5. Conclusions

1) No dense PEO coatings can be produced in the electrolyte containing Si_3N_4 particles with average size of 0.02 μm using the same parameters compared to electrolytes with large-sized particles addition.
2) Si_3N_4 particles are filling pores on the surface but do not densify the cross section. The increasing size of the particles has a negative effect on the thickness of PEO coatings.
3) Si_3N_4 particles are mainly inert incorporated into the coating due to their high melting point.
4) The corrosion resistance of PEO coating has not been improved by addition of external Si_3N_4 particles.

Acknowledgments

The author thanks China Scholarship Council for the award of fellowship and funding to Xiaopeng Lu. The technical support of Mr. Volker Heitmann and Mr. Ulrich Burmester during the course of this work is gratefully acknowledged.

References

[1] A.L. Yerokhin, X. Nie, A. Leyland, A. Matthews, S.J. Dowey, Surf. Coat. Technol. 122 (1999) 73.
[2] E. Matykina, R. Arrabal, F. Monfort, P. Skeldon, G.E. Thompson, Appl. Surf. Sci. 255 (2008) 2830.
[3] A. Kuhn, Met. Finish. 101 (2003) 44.
[4] J. Liang, L. Hu, J. Hao, Electrochim. Acta 52 (2007) 4836.
[5] W. Li, L. Zhu, H. Liu, Surf. Coat. Technol. 201 (2006) 2505.
[6] K.M. Lee, K.R. Shin, S. Namgung, B. Yoo, D.H. Shin, Surf. Coat. Technol. 205 (2011) 3779.
[7] K.M. Lee, B.U. Lee, S.I. Yoon, E.S. Lee, B. Yoo, D.H. Shin, Electrochim. Acta 67 (2012) 6.
[8] M. Laleh, A.S. Rouhaghdam, T. Shahrabi, A. Shanghi, J. Alloys Compd. 496 (2010) 548.
[9] R. Arrabal, E. Matykina, P. Skeldon, G.E. Thompson, J. Mater. Sci. 43 (2008) 1532.
[10] M. Aliofkhazraei, A.S. Rouhaghdam, Appl. Surf. Sci. 258 (2012) 2093.
[11] L. Wang, W. Fu, L. Chen, J. Alloys Compd. 509 (2011) 7652.
[12] H. Duan, C. Yan, F. Wang, Electrochim. Acta 52 (2007) 3785.
[13] P.B. Srinivasan, J. Liang, C. Blawert, M. Störmer, W. Dietzel, Appl. Surf. Sci. 256 (2010) 4017.
[14] G.-L. Song, Surf. Coat. Technol. 203 (2009) 3618.
[15] J. Liang, P.B. Srinivasan, C. Blawert, M. Stormer, W. Dietzel, Electrochim. Acta 54 (2009) 3842.
[16] A. Ghasemi, V.S. Raja, C. Blawert, W. Dietzel, K.U. Kainer, Surf. Coat. Technol. 202 (2008) 3513.
[17] A.F. Lopeandía, J. Rodríguez-Viejo, Thermochim. Acta 461 (2007) 82.
[18] W.H. Qi, M.P. Wang, Mater. Chem. Phys. 88 (2004) 280.

5.9 Formation of photocatalytic plasma electrolytic oxidation coatings on magnesium alloy by incorporation of TiO_2 particles *(with permission from Elsevier)*

Surface & Coatings Technology 307 (2016) 287–291

Contents lists available at ScienceDirect

Surface & Coatings Technology

journal homepage: www.elsevier.com/locate/surfcoat

Formation of photocatalytic plasma electrolytic oxidation coatings on magnesium alloy by incorporation of TiO_2 particles

Xiaopeng Lu [a,*], Mauricio Schieda [a], Carsten Blawert [a], Karl Ulrich Kainer [a], Mikhail L. Zheludkevich [a,b]

[a] Institute of Materials Research, Helmholtz-Zentrum Geesthacht, Max-Plank-Str. 1, 21502 Geesthacht, Germany
[b] Department of Materials and Ceramic Engineering, CICECO-Aveiro Institute of Materials, University of Aveiro, 3810-193 Aveiro, Portugal

ARTICLE INFO

Article history:
Received 10 June 2016
Revised 1 September 2016
Accepted in revised form 2 September 2016
Available online 03 September 2016

Keywords:
Magnesium alloy
Plasma electrolytic oxidation
Photocatalytic activity
TiO_2 particles

ABSTRACT

Photocatalytically active plasma electrolytic oxidation coatings on AM50 Mg alloy are reported in the present work. The photocatalytic activity was achieved via introduction of anatase (TiO_2 particles) to the treatment bath. The photocatalytic performance of the coating was evaluated by measuring the degradation rate of aqueous methylene blue solution and was primarily related to the anatase content on the coating surface. Lower treatment voltage and a higher amount of particles in the electrolyte can be used to incorporate more anatase into the layer and generate superior photocatalytic coatings. The tailored and functionalized surface provides new functionality for magnesium alloys.

© 2016 Elsevier B.V. All rights reserved.

1. Introduction

Plasma electrolytic oxidation (PEO) is a promising surface treatment process derived from conventional anodizing to form ceramic-like coatings on light metals, which can be used for industrial (corrosion and wear) and biomedical applications [1–5]. However, it is generally claimed that the coatings have high porosity and limited variations in phase composition. Addition of particles to the PEO electrolytes has been explored as a new strategy to provide a wider range of compositions and enhanced properties for PEO coatings [6–10]. Particles can be incorporated either reactively or inertly into the coatings, depending on the size and melting point of the particles as well as the treatment conditions [11]. Titanium dioxide is a well-known photocatalytic material that exists in two main polymorphs, anatase and rutile [12]. Anatase transforms irreversibly to rutile at elevated temperatures, in the range of 400–1200 °C [13,14]. Anatase generally exhibits higher photocatalytic activity than rutile TiO_2. The phase mixture of different polymorphs is proved to show synergistic effects and better photocatalytic activity is observed compared with pure phases [15]. It can be inferred that inertly incorporated TiO_2 particles via PEO technique may enable Mg alloy surface with photocatalytic properties. It was also reported that TiO_2-based films can provide bioactive and antibacterial ability for steel and nitinol [16,17]. Consequently, TiO_2 doped PEO coatings may provide Mg-based biodegradable implants with bioactivity and antibacterial properties. Such coatings can offer enhanced UV sterilization ability for Mg alloys used in consumer electronics or automotive interiors. Although there are studies about photocatalytic performance of PEO coatings [18–20], the influence of TiO_2 particles on the photocatalytic properties of PEO coated Mg alloy is not yet fully understood. It has been proved that the particle content in the coating increases with the particle concentration in the electrolyte [21,22]. The applied electrical parameters also have a huge effect on the incorporation mode of particles, since electrophoretic force is one of the main driving forces to attract particles to the layer [23,24]. In this study, the effect of TiO_2 particle concentration and the applied voltage on the morphology, composition and photocatalytic performance of the PEO coatings are investigated. The role of the incorporated particles and electrical parameters applied during PEO treatment in the photocatalytic activity of PEO coatings on AM50 Mg alloy is revealed.

2. Experimental

Specimens of AM50 Mg alloy with a size of 15 mm × 15 mm × 4 mm were prepared from gravity cast ingot material. The chemical composition of the alloy in wt%, as measured with an Arc Spark OES (Spark analyser M9, Spectro Ametek, Germany), is 4.74% Al, 0.383% Mn, 0.065% Zn, 0.063% Si, 0.002% Fe, 0.002% Cu and Mg balance. The specimens were ground using emery papers up to 1200 grit and then air-dried prior to PEO treatment. The PEO process was performed by using a pulsed DC power source with a pulse ratio of t_{on}: t_{off} = 0.4 ms: 3.6 ms. The specimen and a stainless steel tube were used as the anode and cathode, respectively. Different amounts of anatase particles (5 g/L, 10 g/L and 20 g/L) were added to hexametaphosphate based electrolyte (5 g/L KOH and 20 g/L $Na_6P_6O_{18}$). The morphology and XRD pattern of the anatase powder (average particle size of

* Corresponding author.
E-mail address: xiaopeng.lu@hzg.de (X. Lu).

http://dx.doi.org/10.1016/j.surfcoat.2016.09.006
0257-8972/© 2016 Elsevier B.V. All rights reserved.

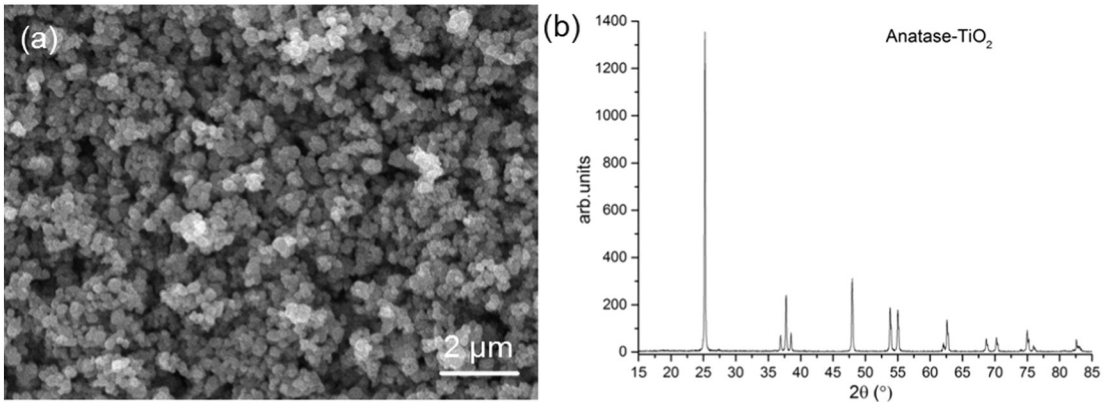

Fig. 1. Morphology and XRD pattern of the anatase powder.

200 nm) is shown Fig. 1. Reference coatings were also produced from electrolyte free of particles. Constant voltage of 400 V and 500 V for 10 min was used for the PEO treatments and the maximum average current density was limited to 300 mA/cm^2. The corresponding coatings are named as PPEO (no-400 V), PPEO (no-500 V), PPEO (5 g-400 V), PPEO (5 g-500 V), PPEO (10 g-400 V), PPEO (10 g-500 V), PPEO (20 g-400 V), and PPEO (20 g-500 V), respectively. A scanning electron microscope (TESCAN Vega3 SB) combined with an energy dispersive spectrometer (EDS) system from eumeX (XRFSystems) was used to examine the surface morphology and composition of the coatings. The phase composition of the coatings was measured by a Bruker X-ray diffractometer using Cu Kα radiation.

The photocatalytic activity of the PEO coatings was evaluated by measuring the degradation rate of aqueous methylene blue (MB) solution. The solution was exposed to light emitted from an incandescent light bulb (OSRAM ULTRA-VITALUX 300 W) for 8 h. The concentration of the MB solution was 5.6 mg/L and the solution volume was 20 mL. An UV–Vis spectrophotometer (Shimadzu UV-1240) was used to measure the concentration change of the MB solution, based on the Beer–Lambert equation stating $A = \varepsilon \times l \times C$ where A, ε, l, and C are absorption of the solution, molar absorptivity, path length, and solution

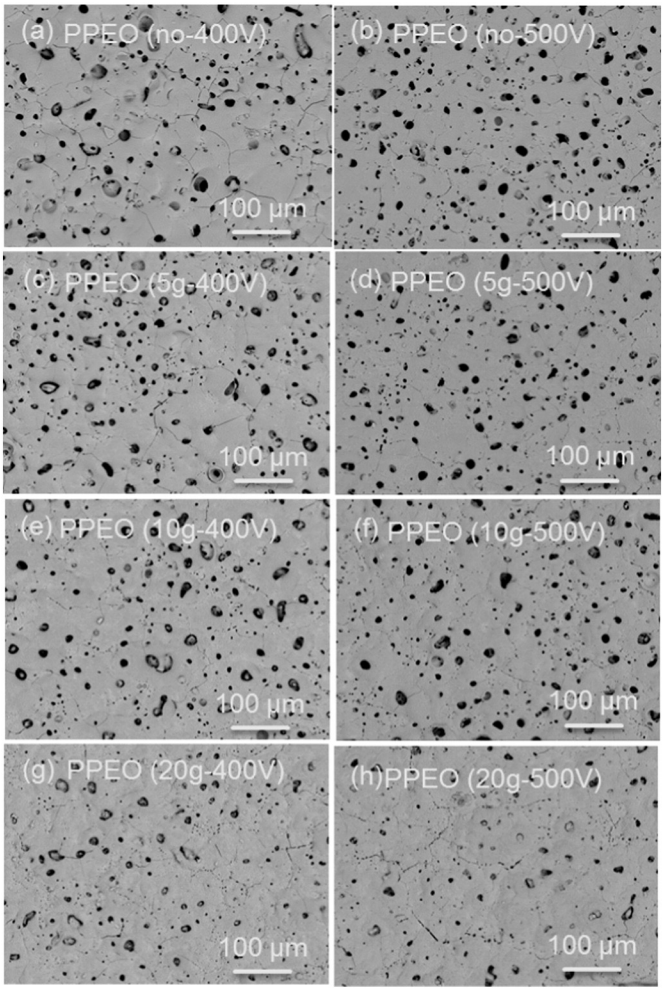

Fig. 2. Surface morphology of different coatings (a) PPEO (no-400 V), (b) PPEO (no-500 V), (c) PPEO (5 g-400 V), (d) PPEO (5 g-500 V), (e) PPEO (10 g-400 V), (f) PPEO (10 g-500 V), (g) PPEO (20 g-400 V) and (h) PPEO (20 g-500 V).

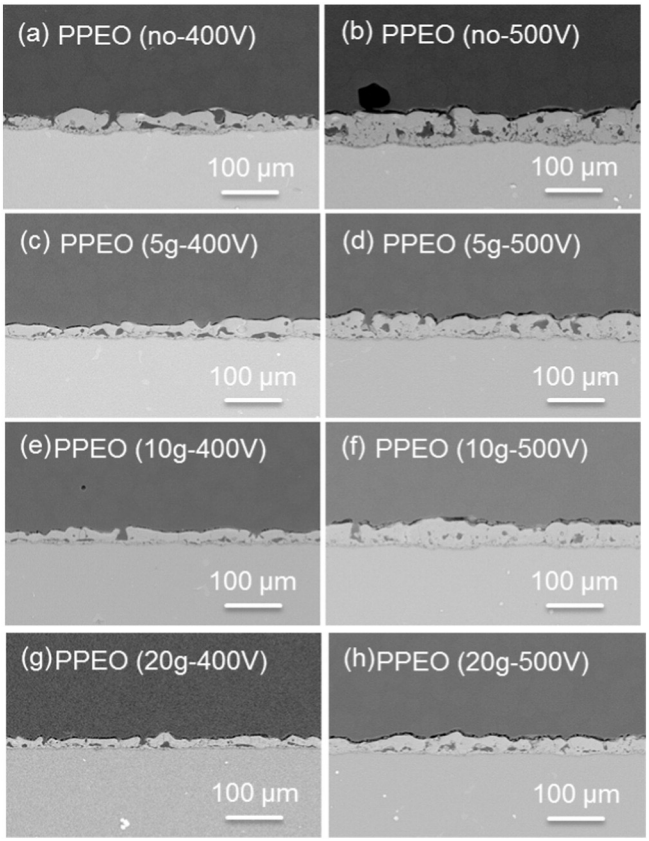

Fig. 3. Cross section of different coatings (a) PPEO (no-400 V), (b) PPEO (no-500 V), (c) PPEO (5 g-400 V), (d) PPEO (5 g-500 V), (e) PPEO (10 g-400 V), (f) PPEO (10 g-500 V), (g) PPEO (20 g-400 V) and (h) PPEO (20 g-500 V).

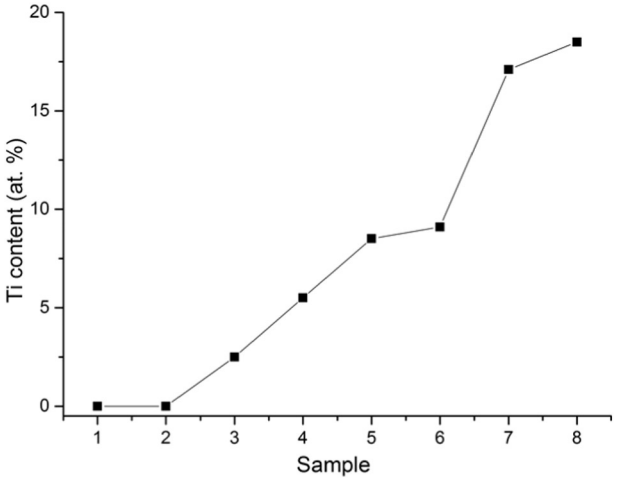

Fig. 4. Ti content on the surface of the coatings (1) PPEO (no-400 V), (2) PPEO (no-500 V), (3) PPEO (5 g-400 V), (4) PPEO (5 g-500 V), (5) PPEO (10 g-400 V), (6) PPEO (10 g-500 V), (7) PPEO (20 g-400 V) and (8) PPEO (20 g-500 V).

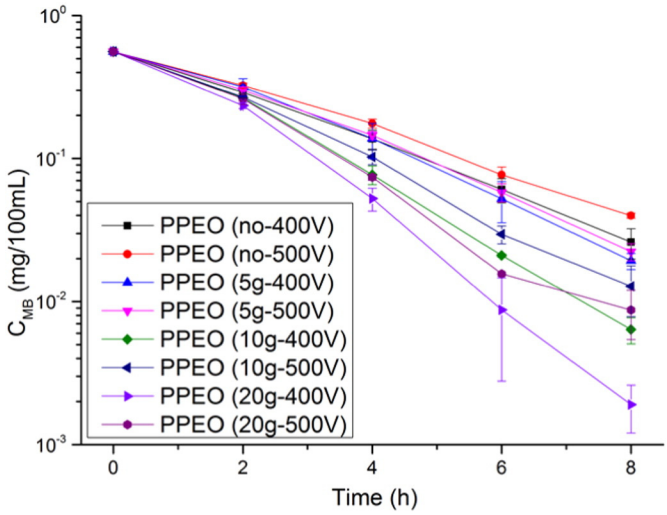

Fig. 6. Photocatalytic activity of the PEO coatings.

concentration, respectively. Since l and ε are constant, the parameter C is linearly proportional to the absorption. The evolution of absorption of MB solution at $\lambda = 663$ nm was measured every 2 h.

3. Results and discussion

3.1. Microstructure

The surface morphology of the PEO coatings is shown in Fig. 2. The coating surface is dominated by pores and is not significantly influenced either by the additional particles in the electrolyte or by the applied voltage during PEO treatment, except for the coatings with addition of 20 g/L particles (Fig. 2g and h) which reveal a lower number and smaller size of pores. Fig. 3 shows the cross sections of the different coatings. It is apparent that the thickness of the coating has been reduced significantly when utilizing particle-containing electrolytes. A higher amount of particles in the electrolyte is evidently detrimental to the coating growth. However, the coatings become thicker at the same amount of particles with the increase of applied voltage from 400 V to 500 V.

3.2. Coating composition

EDS analysis (Fig. 4) of the coating surface was performed to investigate the uptake of the particles into the layer. The Ti content increases

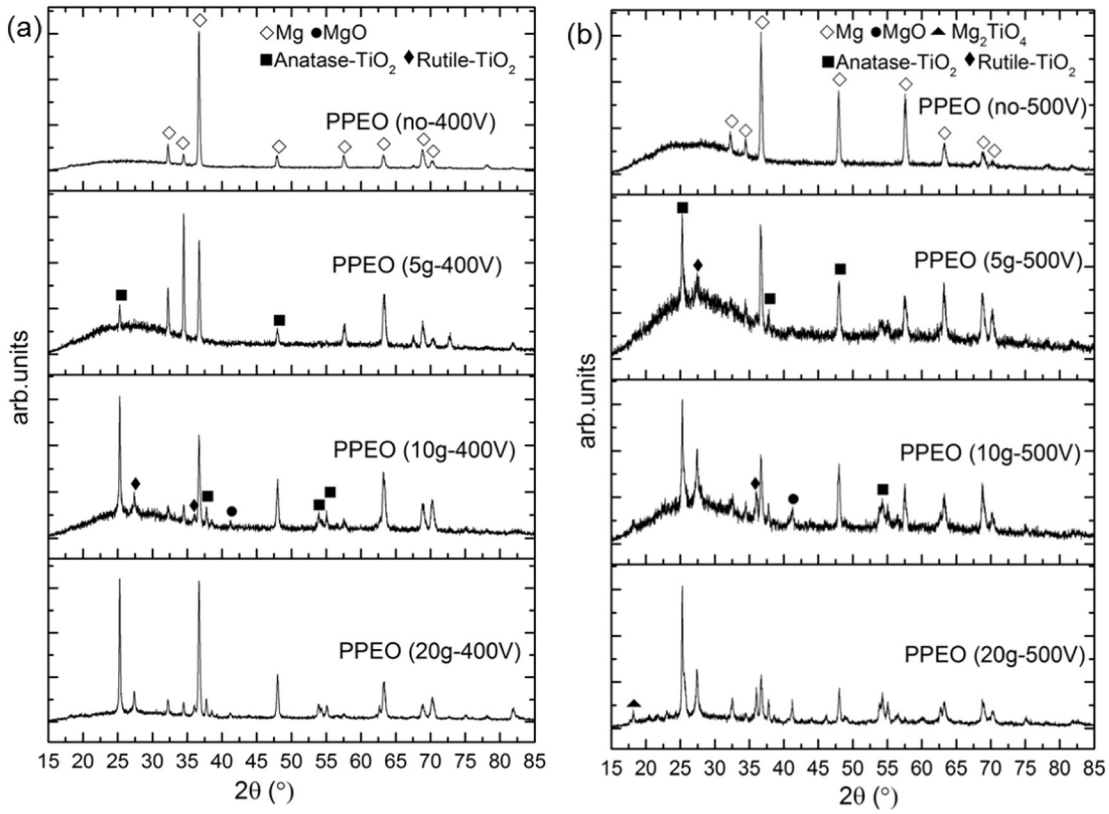

Fig. 5. XRD patterns of the different coatings (a) coatings produced under 400 V, (b) coatings produced under 500 V.

significantly with the particle concentration in the electrolyte and applied voltage during PEO treatment. For instance, the Ti content in coating with 5 g/L particle addition increases from approximately 2.5 at.% to 5.2 at.% with the increase of applied voltage. The particle amount in PPEO (20 g-400 V) is seven times higher than PPEO (5 g-400 V). The X-ray diffraction patterns of the coatings are depicted in Fig. 5. It can be seen that all the coatings are composed of amorphous phase in the 2θ range of 20–35°, possibly containing phosphorus. The appearance of Mg peaks in all conditions is due to the penetration of the X-ray through the whole layer and reaching the substrate. Anatase peaks are visible for all the particle-containing coatings, indicating that the particles are inertly incorporated into the PEO layer. MgO peak only occurs in the layers with addition of 10 and 20 g/L particles, suggesting that the trapped particles might act as nucleation sites for crystallization of the coating. It is worthwhile to note that some of the original anatase was transformed to rutile when applying higher voltage and increasing the particle concentration. In particular, small amount of reactive phase (Mg_2TiO_4) was detected for coatings with 20 g/L particle addition under 500 V, suggesting that different incorporation modes (inert and partly reactive incorporation) can be achieved for anatase under various treatment parameters.

3.3. Photocatalytic activity

The photocatalytic activity of the PEO coatings is shown in Fig. 6. The concentration of the methylene blue decreases slightly without huge difference for all the coatings after 2 h immersion. Afterwards, the degradation rate of MB solution speeds up, especially for the coatings with

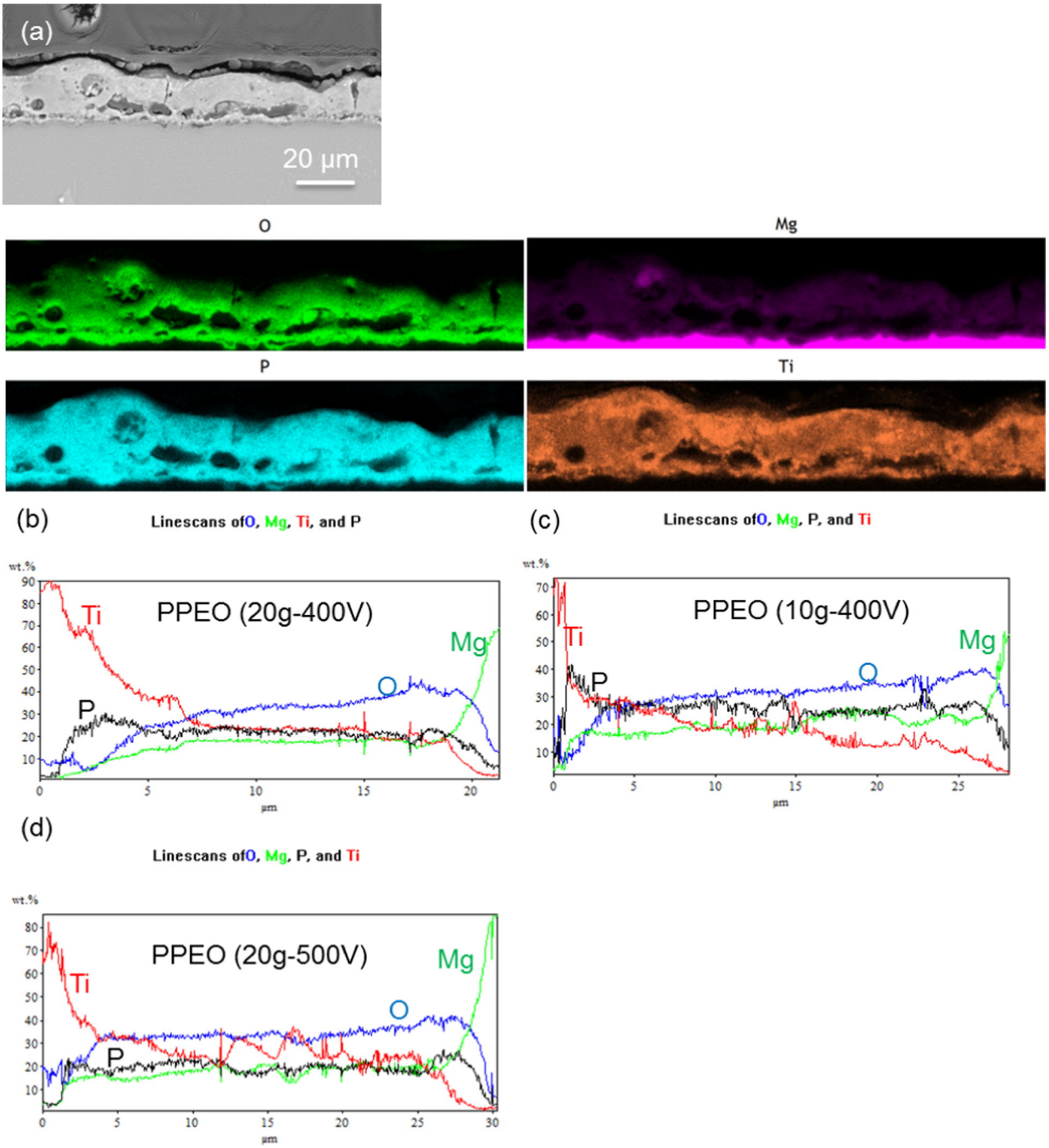

Fig. 7. Mapping (a) PPEO (20 g-400 V); Line scan (b) PPEO (20 g-400 V), (c) PPEO (10 g-400 V) and (d) PPEO (20 g-500 V).

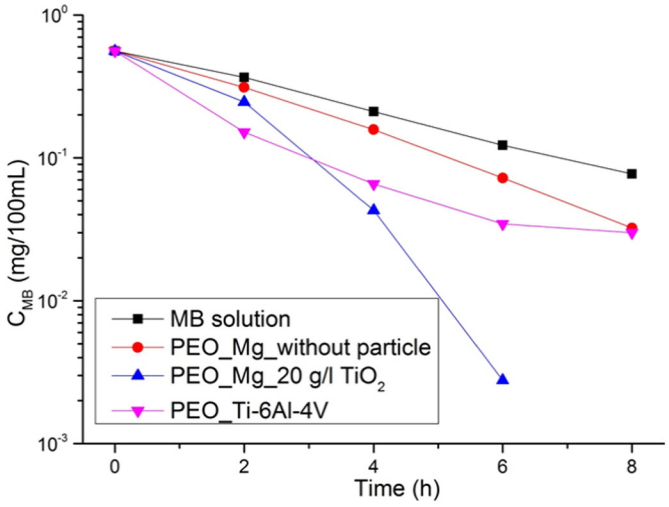

Fig. 8. Comparison of the photocatalytic activity of PEO coatings on Mg alloy and Ti alloy.

higher content of particles. It was found that the coatings synthesized under 400 V with addition of 20 g/L particles demonstrated the optimum photoactivity. Although higher voltage leads to incorporation of more particles into the coating, it is detrimental to the photocatalytic activity of the coatings. This is probably due to the transformation of anatase to rutile and/or Mg_2TiO_4. Moreover, particles that are enriched on the coating surface are more effective to the photocatalytic performance compared with the particles existing in the internal layer, since the Ti content of PPEO (20 g-400 V) is much higher than that of the other coatings (Fig. 7). Therefore, the amount of the inertly incorporated anatase close to the surface plays a dominant role in the photocatalytic properties of PEO coatings on Mg alloy. Additionally, the photocatalytic activity (Fig. 8) of PPEO (20 g-400 V) is even superior to PEO coating formed directly on Ti alloy using parameters according to [25]. It has been reported that the photocatalytic property of TiO_2 decreases with an increase of the particles size [26]. It can be inferred that addition of TiO_2 nanoparticles is more effective in improving the photocatalytic performance of the layer in comparison to the bulk material (TiO_2) in PEO coated Ti alloy.

4. Conclusions

Introduction of anatase (TiO_2 particles) into PEO coatings enables new photocatalytic functionality for Mg and its alloy. Anatase was partially transformed to rutile as well as small amount of Mg_2TiO_4, which can be controlled by the treatment parameters. The photocatalytic performance of the coating is primarily related to the anatase content on the coating surface. Lower treatment voltage and a higher amount of particles in the electrolyte can be used to generate superior photocatalytic PEO coatings. Such coatings may offer improved UV sterilization ability to degradable Mg implants or potential *anti*-bacterial properties for Mg alloys used in consumer electronics or automotive interiors.

Acknowledgements

The technical support of Mr. Volker Heitmann and Mr. Ulrich Burmester during this work is gratefully acknowledged. X. Lu thanks China Scholarship Council (201207090010) for the award of fellowship and funding.

References

[1] A.L. Yerokhin, X. Nie, A. Leyland, A. Matthews, S.J. Dowey, Plasma electrolysis for surface engineering, Surf. Coat. Technol. 122 (1999) 73–93.
[2] J.A. Curran, T.W. Clyne, The thermal conductivity of plasma electrolytic oxide coatings on aluminium and magnesium, Surf. Coat. Technol. 199 (2005) 177–183.
[3] M.P. Staiger, A.M. Pietak, J. Huadmai, G. Dias, Magnesium and its alloys as orthopedic biomaterials: a review, Biomaterials 27 (2006) 1728–1734.
[4] R. Arrabal, E. Matykina, T. Hashimoto, P. Skeldon, G.E. Thompson, Characterization of AC PEO coatings on magnesium alloys, Surf. Coat. Technol. 203 (2009) 2207–2220.
[5] G. Wu, J.M. Ibrahim, P.K. Chu, Surface design of biodegradable magnesium alloys — a review, Surf. Coat. Technol. 233 (2013) 2–12.
[6] T.S. Lim, H.S. Ryu, S.-H. Hong, Electrochemical corrosion properties of CeO_2-containing coatings on AZ31 magnesium alloys prepared by plasma electrolytic oxidation, Corros. Sci. 62 (2012) 104–111.
[7] K.M. Lee, B.U. Lee, S.I. Yoon, E.S. Lee, B. Yoo, D.H. Shin, Evaluation of plasma temperature during plasma oxidation processing of AZ91 Mg alloy through analysis of the melting behavior of incorporated particles, Electrochim. Acta 67 (2012) 6–11.
[8] M. Mohedano, C. Blawert, M.L. Zheludkevich, Silicate-based Plasma Electrolytic Oxidation (PEO) coatings with incorporated CeO_2 particles on AM50 magnesium alloy, Mater. Des. 86 (2015) 735–744.
[9] R. Arrabal, M. Mohedano, E. Matykina, A. Pardo, B. Mingo, M.C. Merino, Characterization and wear behaviour of PEO coatings on 6082-T6 aluminium alloy with incorporated α-Al2O3 particles, Surf. Coat. Technol. 269 (2015) 64–73.
[10] S. Stojadinović, N. Tadić, N. Radić, B. Stojadinović, B. Grbić, R. Vasilić, Synthesis and characterization of Al2O3/ZnO coatings formed by plasma electrolytic oxidation, Surf. Coat. Technol. 276 (2015) 573–579.
[11] X. Lu, C. Blawert, Y. Huang, H. Ovri, M.L. Zheludkevich, K.U. Kainer, Plasma electrolytic oxidation coatings on Mg alloy with addition of SiO_2 particles, Electrochim. Acta 187 (2016) 20–33.
[12] D.H. Hanaor, C. Sorrell, Review of the anatase to rutile phase transformation, J. Mater. Sci. 46 (2011) 855–874.
[13] P.I. Gouma, M.J. Mills, Anatase-to-rutile transformation in titania powders, J. Am. Ceram. Soc. 84 (2001) 619–622.
[14] J. Kim, K.C. Song, S. Foncillas, S.E. Pratsinis, Dopants for synthesis of stable bimodally porous titania, J. Eur. Ceram. Soc. 21 (2001) 2863–2872.
[15] D.O. Scanlon, C.W. Dunnill, J. Buckeridge, S.A. Shevlin, A.J. Logsdail, S.M. Woodley, C.R.A. Catlow, M.J. Powell, R.G. Palgrave, I.P. Parkin, G.W. Watson, T.W. Keal, P. Sherwood, A. Walsh, A.A. Sokol, Band alignment of rutile and anatase TiO_2, Nat. Mater. 12 (2013) 798–801.
[16] P. Evans, D.W. Sheel, Photoactive and antibacterial TiO_2 thin films on stainless steel, Surf. Coat. Technol. 201 (2007) 9319–9324.
[17] H.T. Siu, H.C. Man, Fabrication of bioactive titania coating on nitinol by plasma electrolytic oxidation, Appl. Surf. Sci. 274 (2013) 181–187.
[18] Y.-K. Shin, W.-S. Chae, Y.-W. Song, Y.-M. Sung, Formation of titania photocatalyst films by microarc oxidation of Ti and Ti–6Al–4V alloys, Electrochem. Commun. 8 (2006) 465–470.
[19] X. Jiang, Y. Wang, C. Pan, Micro-arc oxidation of TC4 substrates to fabricate TiO_2/YAG:Ce^{3+} compound films with enhanced photocatalytic activity, J. Alloys Compd. 509 (2011) L137–L141.
[20] W. Li, M. Tang, L. Zhu, H. Liu, Formation of microarc oxidation coatings on magnesium alloy with photocatalytic performance, Appl. Surf. Sci. 258 (2012) 10017–10021.
[21] M. Tang, W. Li, H. Liu, L. Zhu, Influence of titania sol in the electrolyte on characteristics of the microarc oxidation coating formed on 2A70 aluminum alloy, Surf. Coat. Technol. 205 (2011) 4135–4140.
[22] X. Lu, C. Blawert, M.L. Zheludkevich, K.U. Kainer, Insights into plasma electrolytic oxidation treatment with particle addition, Corros. Sci. 101 (2015) 201–207.
[23] D.-Y. Kim, M. Kim, H.-E. Kim, Y.-H. Koh, H.-W. Kim, J.-H. Jang, Formation of hydroxyapatite within porous TiO_2 layer by micro-arc oxidation coupled with electrophoretic deposition, Acta Biomater. 5 (2009) 2196–2205.
[24] K.M. Lee, K.R. Shin, S. Namgung, B. Yoo, D.H. Shin, Electrochemical response of ZrO_2-incorporated oxide layer on AZ91 Mg alloy processed by plasma electrolytic oxidation, Surf. Coat. Technol. 205 (2011) 3779–3784.
[25] R. Kumari, C. Blawert, J.D. Majumdar, Microstructures and properties of plasma electrolytic oxidized Ti alloy (Ti-6Al-4V) for bio-implant application, Metall. Mater. Trans. A 47 (2015) 788–800.
[26] H. Lin, C.P. Huang, W. Li, C. Ni, S.I. Shah, Y.-H. Tseng, Size dependency of nanocrystalline TiO_2 on its optical property and photocatalytic reactivity exemplified by 2-chlorophenol, Appl. Catal., B 68 (2006) 1–11.

6 Discussion of published results

6.1 Influence of particle addition on PEO processing

Generally, current or voltage control is used for PEO treatment. As a result, the voltage increases or the current decreases proportionally as a function of the treatment time because the insulating property of the dielectric ceramic layer is continuously strengthened. Since alkaline electrolytes are commonly used, particles become negatively charged and are moving towards the anode (Mg alloy) together with anions under the applied electrical potential. Subsequently, the particles can be involved in PEO processing and coating formation process.

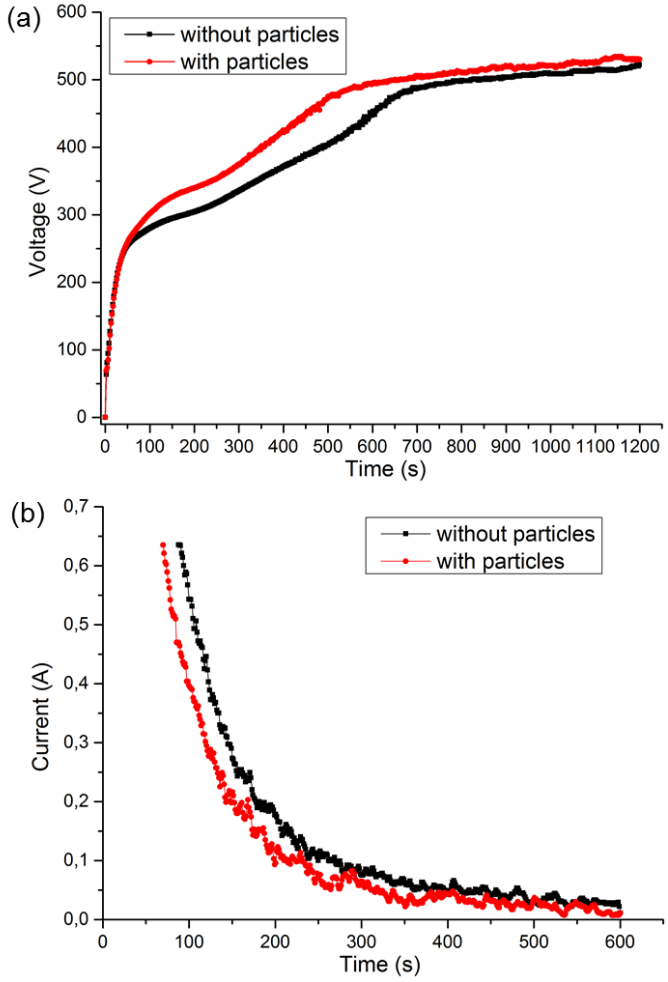

Figure 6-1 (a) voltage evolution under current control (27 mA/cm^2), and (b) current evolution under voltage control (450 V) during PEO processing in electrolytes with and without SiO_2 particles.

Addition of particles into the electrolyte generally has an effect on the PEO process. This is associated with the change of the composition and conductivity of the electrolyte, which plays an important role in the PEO process [82, 83]. As shown in Figure 6-1 (Paper 2), it is evident that the addition of particles influences the PEO process e.g. the evolution of voltage and current during the treatment. In the case of constant current regime, the voltage increases more quickly after the breakdown potential and reaches higher values with particles addition. The current decreases earlier and faster in the presence of particles under constant voltage mode.

Moreover, it was found that SiO_2 nanoparticles have a more remarkable effect on the PEO process in comparison to micro-sized SiO_2 particles, resulting in faster evolution of the voltage or current [84]. This size effect was also confirmed in Paper 2 by optical emission spectroscopy (OES) measurements. Detectable discharges with higher intensity occur first for coatings with SiO_2 nanoparticles, followed by micro-sized SiO_2 particles and the particle-free coatings, indicating that PEO coatings loaded with particles might have higher barrier properties. At the final stage of the treatment, the discharge intensity measured by OES for coatings with SiO_2 nanoparticles in the electrolyte is the strongest among all three coatings. The intensity level of the discharges for treatment in the presence of SiO_2 micro-particles is also higher than that of particle-free electrolyte. In addition, it was found that the emission of the discharges essentially comes from the electrolyte and substrate, i.e., excited species of Na, OH, K and Mg. SiO_2 particles are not directly involved in the plasma discharges, since no excited states of Si are observed by OES. The size effect of the particles is probably caused by the different uptake mechanisms (see 6.2). In short, addition of particles into the electrolyte has an effect on the PEO processing, as reflected by the faster evlution of the current/voltage response. The coating formation is influenced by the particles via modification of the electrolyte composition.

6.2 Influence of treatment parameters on particle uptake

It is well-known that the formation of PEO coatings depends on the treatment parameters, including the electrolyte composition and the electrical parameters applied during PEO processing. Thus the uptake of particles from the electrolyte to the layer is also related to the treatment parameters. However, the change of the composition of the phosphate-based electrolyte has only a slight effect on the particle uptake. In Paper 3, 5 g/L clay particles were added to electrolytes with different concentrations of KOH and Na_3PO_4 [85]. The conductivity of the

electrolyte has increased greatly with the increase of the concentration of KOH and Na_3PO_4, while the pH value is above 12 for all the electrolytes. The Si content on the coating surface is nearly the same for all the coatings, suggesting that the uptake of particles is only slightly influenced by the composition of the base electrolyte. This observation was further confirmed in Paper 1 [86]. The content of nano- and micro-sized SiO_2 particles on the coating surface remains unchanged with the increase of KOH in the electrolyte, which might be attributed to similar zeta potential of the particles. It was shown by Lee et al. [16] that the zeta potential of the particles becomes more negative with the increase of pH of the electrolyte and remains in the same level when the pH value is above 12. Therefore the uptake of the particles is not much influenced by the modification of the composition of the base electrolyte. Nevertheless, the uptake of the particles changes along with the concentration of the particles in the electrolyte. In Paper 8 [87], it was found that the Ti content on the surface of coatings with addition of TiO_2 particles increases significantly with the particle concentration in the electrolyte (Table 6-1). It can also be seen that change of the electrical parameters (voltage) is effective to control the uptake of particles, since the electrical field between the negatively charged particles and the anode provides the main driving force for electrophoretic mobility. Besides voltage, the frequency and duty ratio play an important role in uptake of particles as well [88], since change of frequency and duty ratio essentially influences the number and duration of the pulses. In Paper 4, it was found that the uptake of particles is enhanced with lower frequency and higher duty ratio (Figure 6-2), indicating that longer pulse time in a single cycle facilitates uptake of more particles into the coating. The pulse-on and the pulse-off time in one cycle are altered independently to further confirm the effect of pulse time on particle uptake during PEO processing. The particle concentration on the coating surface increases linearly from 5 at. % (0.2 ms) to 6 at. % (0.4 ms) and 7.2 at. % (0.8 ms) with the pulse-on time in one cycle. In terms of pulse-off time, there is no significant effect on the uptake of particle into PEO coating. Thus the pulse time per cycle combined with the particle concentration in the electrolyte and voltage applied during PEO treatment dominate the uptake of particles into the coating. Among which, the concentration of the particles in the electrolyte plays more important role in the particle uptake.

Table 6-1 Uptake of particles as a function of particle concentration in the electrolyte and voltage applied during PEO processing.

Concentration of TiO_2 particles in the electrolyte (g/L)	Ti content on the coating surface under constant 400 V (at. %)	Ti content on the coating surface under constant 500 V (at. %)
5	2.5	5.5
10	8.5	9.1
20	17.1	18.5

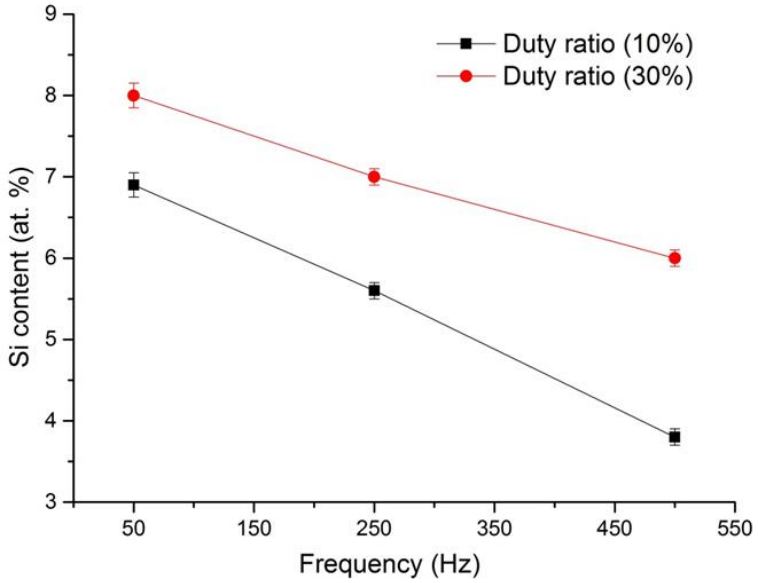

Figure 6-2 Effect of frequency and duty ratio on the uptake of SiO_2 particles.

6.3 Mechanisms of uptake and incorporation of the particles

Like anions, negatively charged particles move towards the anode after the application of voltage, resulting in a particle enriched electrolyte/anode interface. Figure 6-3 is a schematic diagram to demonstrate the growth mechanisms of PEO coatings on Mg alloy. Specifically, the uptake of the particles during different stages of PEO processing is shown in Figure 6-3f. Conversion products grow locally from the area adjacent to Al-Mn intermetallics, which are the typical intermetallics in AM50 alloy. It is probably ascribed to the different properties of the oxides formed on the Al-Mn intermetallics and α-Mg. The potential difference generated during polarization facilitates dissolution of the Mg adjacent the intermetallics and subsequently reacts with the anions from the

electrolyte. Electrochemical and chemical reactions (Eqs. (1)-(3)) occur between the anions from the electrolyte (e.g., phosphate based electrolyte) and dissolution of Mg from the matrix [89].

$$Mg \rightarrow Mg^{2+} + 2e^{-} \quad (1)$$

$$3Mg^{2+} + 2PO_4^{3-} \rightarrow Mg_3(PO_4)_2 \quad (2)$$

$$Mg^{2+} + 2OH^{-} \rightarrow Mg(OH)_2 \quad (3)$$

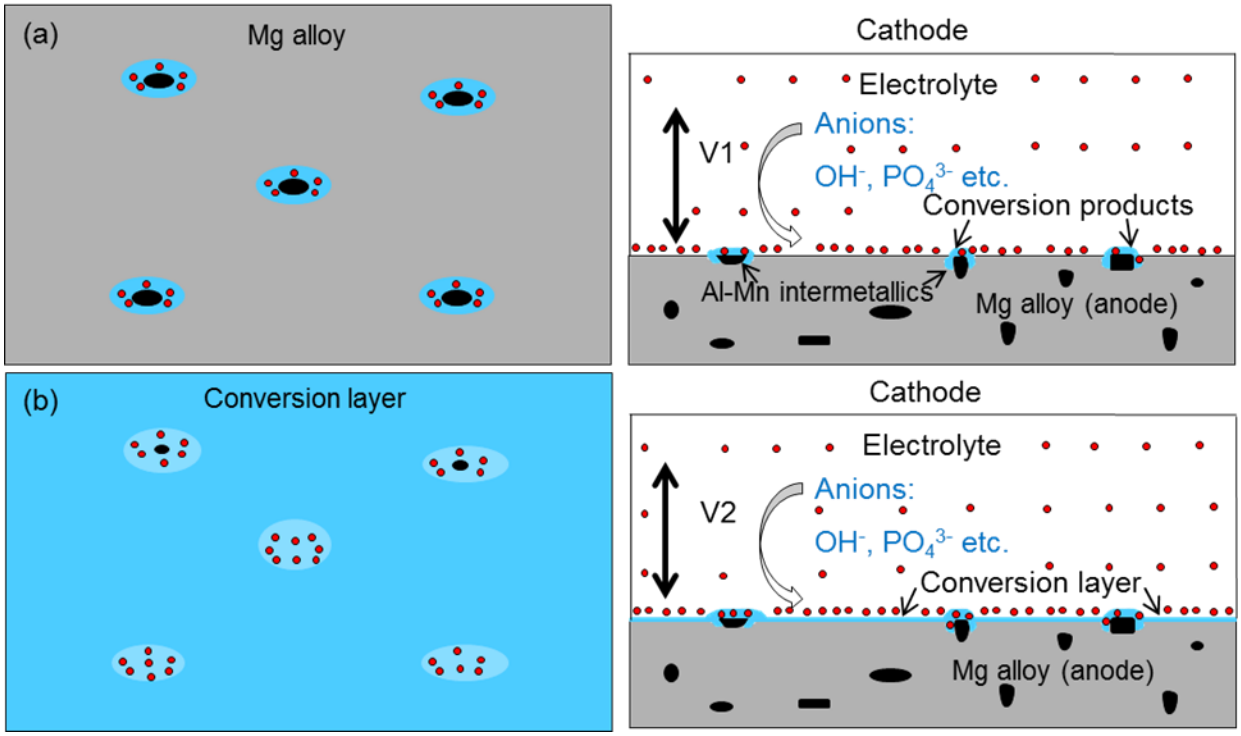

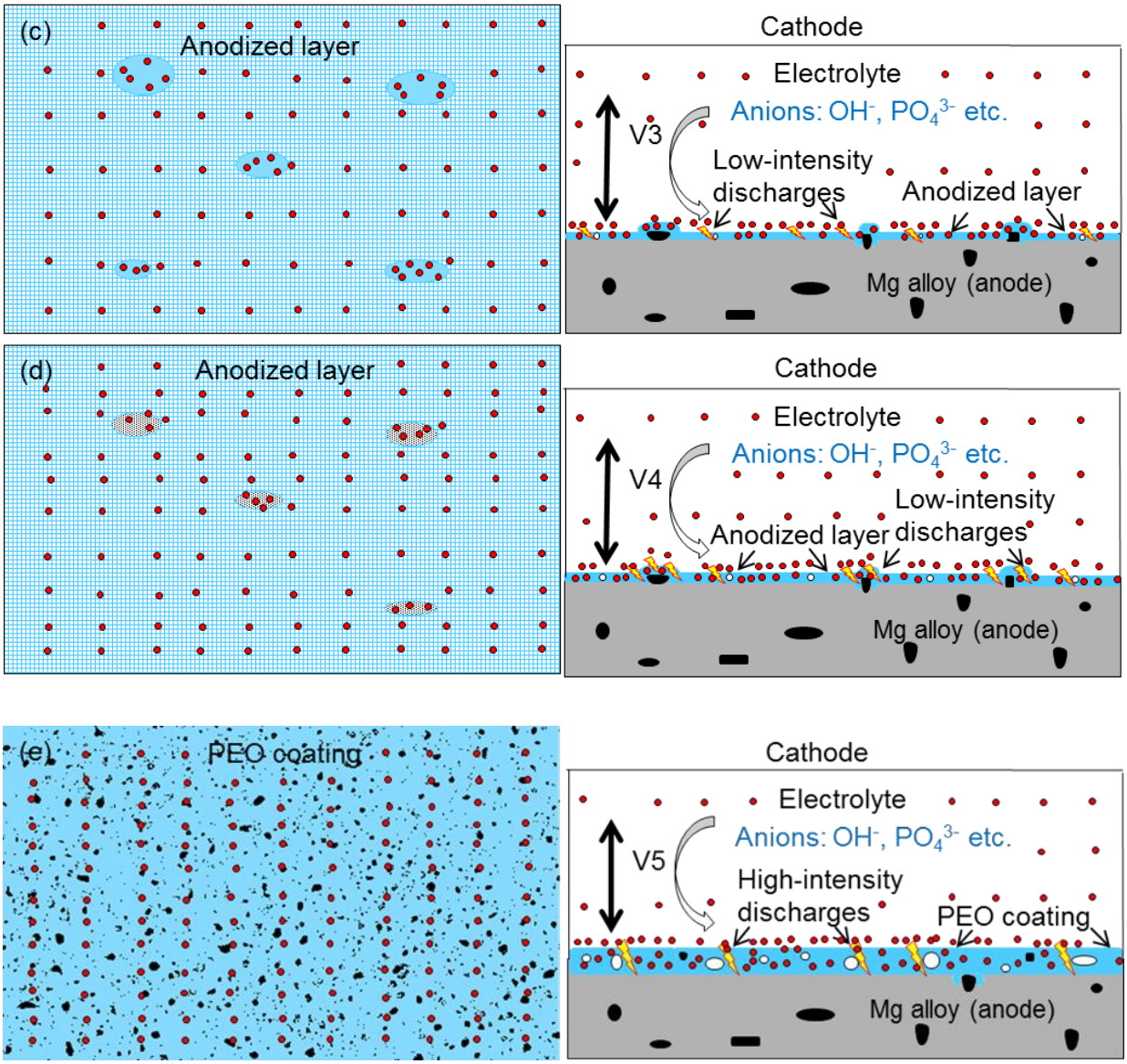
(c)
Anodized layer
Cathode
Electrolyte
Anions: OH^-, PO_4^{3-} etc.
V3
Low-intensity discharges
Anodized layer
Mg alloy (anode)
(d)
Anodized layer
Cathode
Electrolyte
Anions: OH^-, PO_4^{3-} etc.
V4
Low-intensity discharges
Anodized layer
Mg alloy (anode)
(e)
PEO coating
Cathode
Electrolyte
Anions: OH^-, PO_4^{3-} etc.
V5
High-intensity discharges
PEO coating
Mg alloy (anode)

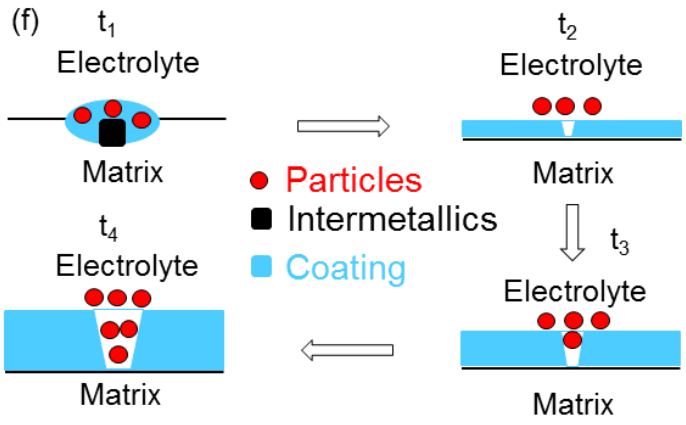

Figure 6-3 Schematic diagram of the coating formation process (a) conversion products formed primarily around the Al-Mn intermetallics, V1 << breakdown potential, (b) conversion layer formed over the entire surface, V2 < breakdown potential, (c) anodized layer formed by low-intensity discharges, V3 > breakdown potential, (d) protruding conversion products: last locations punctured by discharges, V4 > V3, (e) PEO coating formed by high-intensity discharges, V5 > V4, (f) uptake of the particles during different stages ($t_1 < t_2 < t_3 < t_4$).

As discussed in Paper 5, the uptake of particles before the breakdown potential is only via the bulk conversion products (Figure 6-3a and f). An insulating conversion layer is formed in the entire surface with longer treatment time and higher potential (Figure 6-3b). This thin and compact layer is unlikely to absorb the relatively large-sized particles. Besides, it was also found that the preferable growth area of the layer is unaffected with and without particles at the beginning of a treatment (Figure 6-4). After reaching the breakdown potential, discharges appear due to the dielectric breakdown of the insulating conversion layer. Part of the coating material will be melted and ejected outwards, resulting in discharge channels across the coating and melting pools remaining on the coating surface. The appearance of the melting pools results in an easier uptake regime for particles via sticking on the coating surface (Figure 6-3c and f). Owing to the open pores and large discharge channels, some small-sized particles might pass through the outer porous layer and enter into the internal layer directly (Figure 6-3e and f). It is unlikely for particles which are larger than the pores and discharge channels to enter during solidification process, which means that large-sized particles will stay on the coating surface (Figure 6-3f). The pores in the coating can be considered as containers and channels for uptake of the particles.

Therefore, the uptake of the particle depends on the particle size as well as the number and size of the pores on the coating surface, as shown in Figure 6-3f.

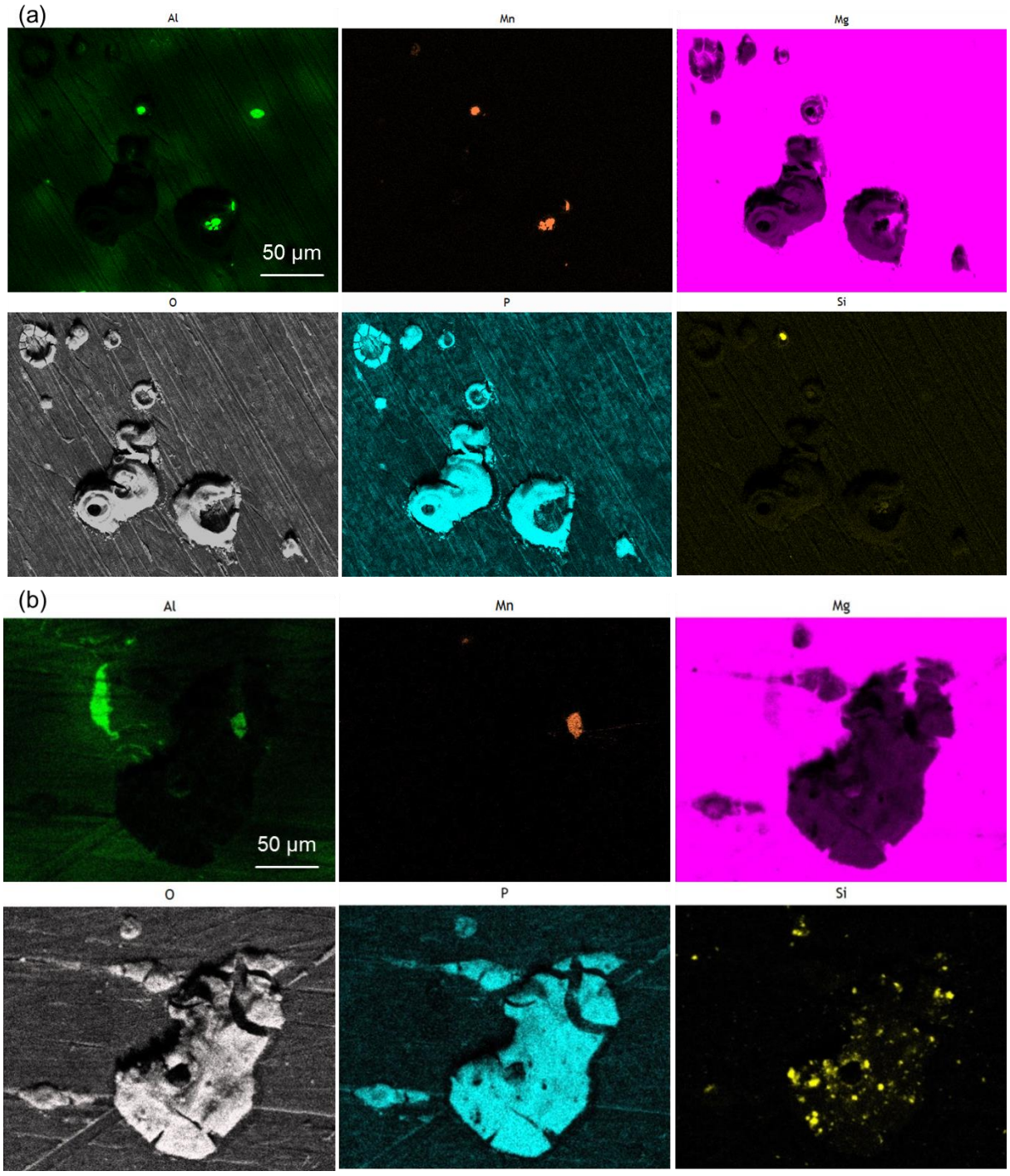

Figure 6-4 Coating formation at the initial stage with and without SiO_2 particles.

In Paper 6, synchrotron-based microtomography was used to generate 3D visualization of the particles and the pores in PEO coatings as a function of treatment time. It was found that the particles are individually distributed in the layer at the beginning of the treatment. Due to the coating growth, the uptake of the particles is continually increased leading to agglomeration in the layer, which results in complex shape and low sphericity of particles. Thus the size and shape of the particles change with the coating growth and a large fraction of large-sized and convex-shaped particles can be detected in the later stage of the treatment. Regarding to the porosity of the coating, it has reduced from 26.25% (30 s) to 10.88% after treated for 10 min. This technique confers more quantitative and precise assessment of the coating porosity compared with the conventional analysis from the surface via SEM investigations.

In general, the incorporation of the particles into the coating can range from fully inert to fully reactive incorporation. The incorporation mode of the particles is mainly related to the possibility of chemical reaction between them and the main metallic oxides (MgO for Mg alloys) generated by the substrate/electrolyte combinations. Hence oxide particles (Paper 1, 2 and 3) can more easily achieve reactive incorporation into the coating in comparison to non-oxide particles (Paper 7). The properties of the particles, i.e., melting point and size (Paper 1, 2 and 3), and the electrical parameters (Paper 5 and 8) play important roles in the incorporation of the particles as well. Size is an important factor since larger particles need longer heating-up time to reach the melting point and lifetime of the discharges might not be sufficiently long. Furthermore, the nanoparticles from the same material have lower melting point compared with the bulk or larger particles. Thus the small-sized and low melting point particles can be more easily melted than large-sized and high melting point particles leading to reactive incorporation into the coating. In the present study, the small-sized particles (SiO_2 nanoparticles in Paper 1 and 2) and low melting point particles (clay particles in Paper 3) have been reactively incorporated into the layer resulting in new amorphous phase. It was found that they can work as sintering additives to promote the coating formation by increasing the liquid phase fraction and lowering the sintering temperature. The liquid phase can react rapidly with the remaining solid compounds to form more fractions of melt and new compounds. Liquid phase sintering can occur to a larger extent if the right amount and type of oxides form on the surface and if the additional elements and compounds provided by the electrolyte together give phase mixtures with lower fusion point. This phenomenon cannot be observed for the relatively high melting point and large-sized particles under the same treatment

conditions, as inert incorporation was detected for them, e.g., nano- and micro-sized Si_3N_4 particles, micro-sized SiO_2 and SiC particles (Figure 6-5).

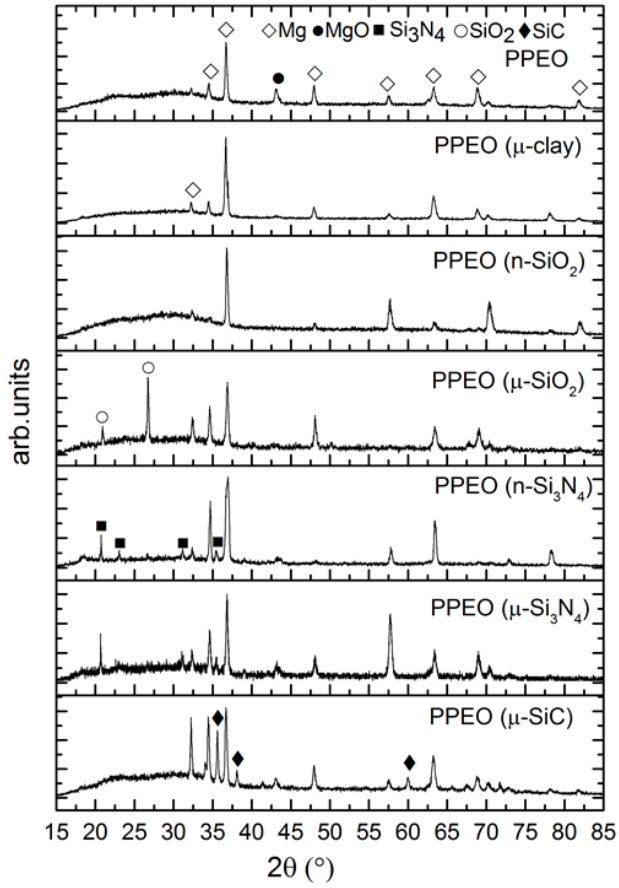

Figure 6-5 XRD patterns of the coatings with and without addition of particles (5 g/L).

Moreover, the applied electrical parameters also play vital role in determining the incorporation mode of particles, since the intensity and lifetime of the discharges are directly related to the voltage and current density during PEO treatment (Paper 5 and 8). Inertly incorporated particles can be melted and achieve reactive incorporation with the appearance of high-intensity discharges when further increasing the energy input. For instance, new reactive phase (Mg_2SiO_4) stemming from the micro-sized SiO_2 particles and MgO was detected in the coating treated for longer treatment time [89], suggesting that the amorphous layer can be transformed to crystalline coating with the increase of voltage. In Paper 8, the transformation of anatase particles under different voltages has further corroborated that the incorporation mode of particles relies on the electrical parameters during PEO treatment (Figure 6-6). Some of the original anatase was transformed to rutile when applying higher voltage. In particular, small amount of reactive phase

(Mg_2TiO_4) was detected for coatings with 20 g/L particle addition under 500 V, indicating that incorporation of particles can be controlled and changed from inert to partly reactive incorporation using different electrical parameters to increase energy input.

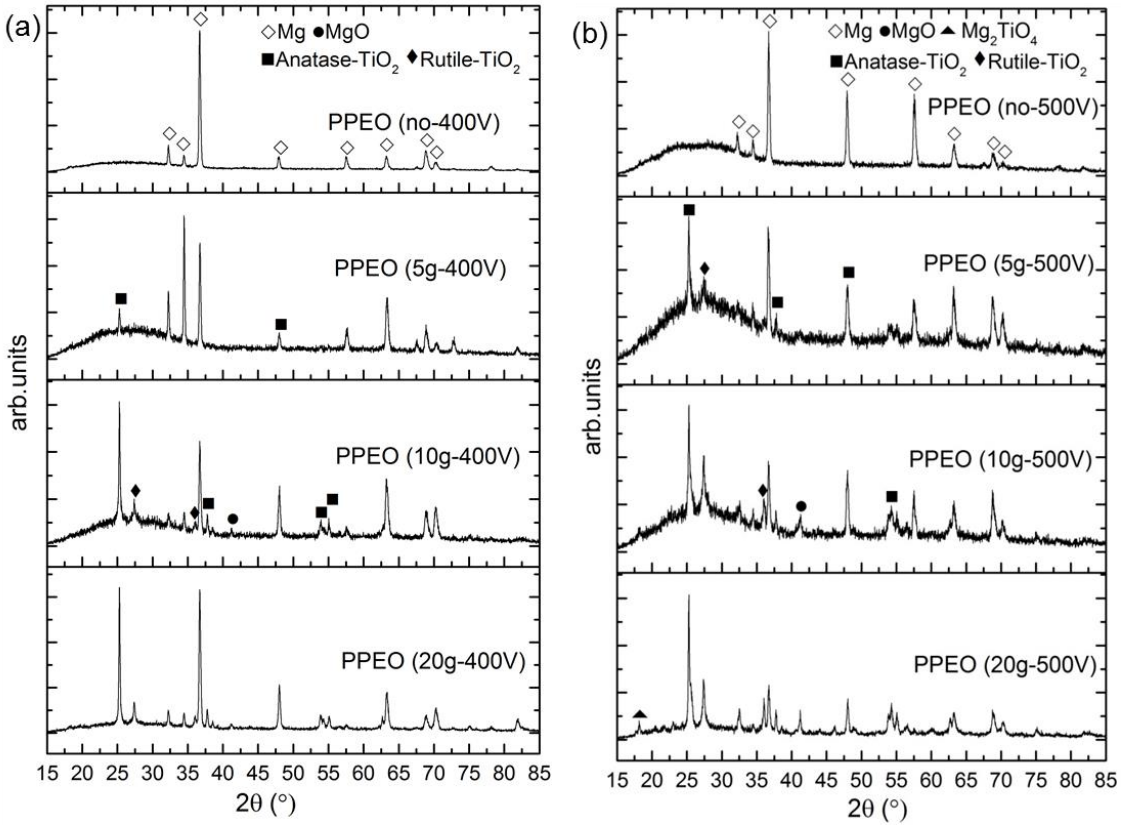

Figure 6-6 XRD patterns of the different coatings obtained from 20 g/L $Na_6P_6O_{18}$ + 8 g/L KOH + 5 g/L, 10 g/L and 20 g/L anatase under constant voltage regime (a) coatings produced under 400V, (b) coatings produced under 500V.

In summary, the uptake and incorporation of particles is primarily related to the coating formation process including dielectric breakdown, sintering and deposition process. The uptake of the negatively charged particles before the breakdown potential can be regarded as an adsorption/deposition process in regions with enhanced anodic dissolution and redeposition of conversion products. After dielectric breakdown, uptake of the particles is associated with the formation of the new coating material via the open pores and discharge channels. The incorporation mode of the particles is related to their reactivity, which depends on the other phases in the surrounding of the particles, the melting point and size of the particle itself and the energy available in the discharges dominated by the processing parameters. Particularly,

interfacial chemical reactions and sintering are likely to occur when the particles mix and interact with other coating material with the aid of the discharges. Thus high-intensity discharges enable coatings with more crystalline and high-temperature phases. The properties of the particles (melting point and size) and the electrical parameters applied during PEO treatment determine the way and mode of the uptake and incorporation of the particles into the layer.

6.4 Change of coating morphology, microstructure and phase composition

It is apparent that the morphology, microstructure and composition of the coatings loaded with particles are different in comparison to the particle-free coatings, as the introduced particles have an effect on PEO processing and participate in the coating formation process. As a matter of fact, the addition of particles is not effective to increase the coating thickness/growth rate, since the layer is generally thinner in the presence of particles (Table 6-2). It was found that the internal layer is still unavoidably porous, although the surface of the coating can be sealed in some cases (Paper 1, 2, 3, 7 and 8). Therefore introduction of particles cannot be used as a strategy to seal the porosity of PEO coatings. Nevertheless, the coatings are likely to demonstrate enhanced barrier property, as indicated by the faster transition of the current/voltage during PEO treatment as well as better corrosion performance at the early stage of corrosion test (see. 6.5.1).

Introduction of particles can open up new ranges of phase composition of PEO coatings (Table 6-2). The particles contribute to the coating composition either as additionally independent phase or formation of new reactive phases, which is related to the incorporation mode of the particles. Mg_2SiO_4 phase is normally observed for PEO coatings produced from silicate-based electrolyte, while Si-containing amorphous phase, unreacted SiO_2 particles and even with a mixture of Mg_2SiO_4 phase have been detected for the coatings loaded with clay and SiO_2 particles (Paper 1, 2, 3, 4 and 5). The composition of the coatings with addition of particles is dominated by the applied electrical parameters, as the incorporation of the particles can range from inert to reactive incorporation under various electrical parameters (Paper 5 and 8). Therefore, addition of particles is more effective to change the composition rather than improve the morphology of the coating. The wider range of phase composition provided by the particles may confer new and/or enhanced functionalities to PEO coatings.

Table 6-2 Phase composition of the coatings with particle addition.

Particle type	Coating morphology	Coating phase composition
SiO_2 nanoparticles (Paper 1 and 2)	Sealed surface and reduced thickness (45 ± 5 μm to 25 ± 4 μm)	Single amorphous phase
Micro-sized SiO_2 particles (Paper 1, 2 and 4)	Reduced thickness (45 ± 5 μm to 33 ± 3 μm)	Amorphous phase, SiO_2 and Mg_2SiO_4 (under higher voltage)
Clay (Paper 3)	Sealed surface (produced from low concentration of KOH and Na_3PO_4)	Single amorphous; mixture of MgO, Mg_2SiO_4 and $Mg_3(PO_4)_2$
Si_3N_4 (Paper 7)	Sealed surface and reduced thickness (35 ± 4 μm to 20 ± 5 μm)	Amorphous phase and Si_3N_4
Anatase (Paper 8)	Reduced thickness (50 ± 5 μm to 40 ± 5 μm)	Mixture of MgO, anatase and rutile, Mg_2TiO_4 (under higher voltage)

6.5 Influence of particle addition on coating functionality

6.5.1 Corrosion protection properties

Owing to the altered morphology and phase composition, the properties of PEO coating have been changed and/or enhanced in the presence of particles. Nevertheless, introduction of particles by itself is not effective to improve the corrosion resistance of PEO coatings in NaCl solution. The corrosion resistance of PEO coating is related to the barrier properties of the outer porous layer together with the resistance of the inner barrier layer. The variation of the phase composition, thickness as well as the porosity of the outer layer determines the degradation process of the coating. Figure 6-7 aims to elucidate the degradation kinetics of the PEO coatings. Equivalent circuits with various RC elements are used to describe appropriate components of the layer. The elements in the equivalent circuit include R_s (the solution resistance), R_o (resistance of the outer layer) paralleled with CPE_o (a constant phase element representing the outer layer/coating capacitance), R_i (resistance of the inner layer) paralleled with a constant phase element CPE_i (representing the inner layer), CPE_{dl} is the capacitance of electrochemical double layer at the metal/electrolyte interface and R_{polar} is the polarization resistance of the corrosion

process. At the very beginning, R_{polar} and CPE_{dl} are removed as the layer is intact without corrosion (Figure 6-7a). It was found that the initial corrosion performance can be improved with addition of particles. In Paper 2, introduction of SiO_2 particles has enhanced the corrosion resistance of the outer layer after short immersion in NaCl solution, indicating that the barrier properties of the outer layer are improved as the coating becomes thinner with particles [84]. Further immersion in NaCl solution results in migration of corrosive species through the outer layer towards the inner layer. The unstable coating materials in the outer layer start to dissolve and the open pores become bigger. The degraded inner barrier layer is replaced by a new corrosion product layer mainly composed of $Mg(OH)_2$ as long as the outer layer still exhibits protective ability. Consequently, dissolution of the magnesium substrate begins due to the degradation of the outer and the inner layer, as indicated by the appearance of R_{polar} and CPE_{dl} (Figure 6-7b). The corrosion resistance of the coatings loaded with particles is generally inferior to particle-free layers during this stage. This is because the layer is generally thinner and the new formed phases are prone to degrade in NaCl solution as well. For instance, coatings with addition of SiO_2 and Si_3N_4 particles demonstrate a faster degradation rate although they can improve the short-term resistance of the coating (Paper 2 and 7). Addition of nanoparticles is even more detrimental to the corrosion performance of the coating in comparison to the large-sized particles [84, 90]. After longer immersion time, the barrier property of the outer layer has strongly decreased due to the continually decreased coating thickness and higher open porosity. Hence R_o and CPE_o are removed at the final stage of the corrosion test (Figure 6-7c). Although addition of particles cannot significantly improve the corrosion resistance of the coating, the degradation process of the layer can be altered and controlled via modification of the coating phase composition. In Paper 3, the coatings with addition of clay particles range from amorphous layer to crystalline layer with the change of the concentration of Na_3PO_4 and KOH in the electrolytes [85]. The crystalline coatings demonstrate higher corrosion performance and degradation stability than the amorphous layers because of the superior thermodynamic stability of the crystalline phases (Mg_2SiO_4, $Mg_3(PO_4)_2$ and MgO). In summary, the degradation process of the coating is primarily controlled by the phase composition, thickness and porosity of the outer layer. Introduction of particles to the coating is not capable of formation of sufficient stable phase with good chemical stability and preventing the high porosity. It is not effective to enhance the corrosion performance of the coating in NaCl solution via addition of particles.

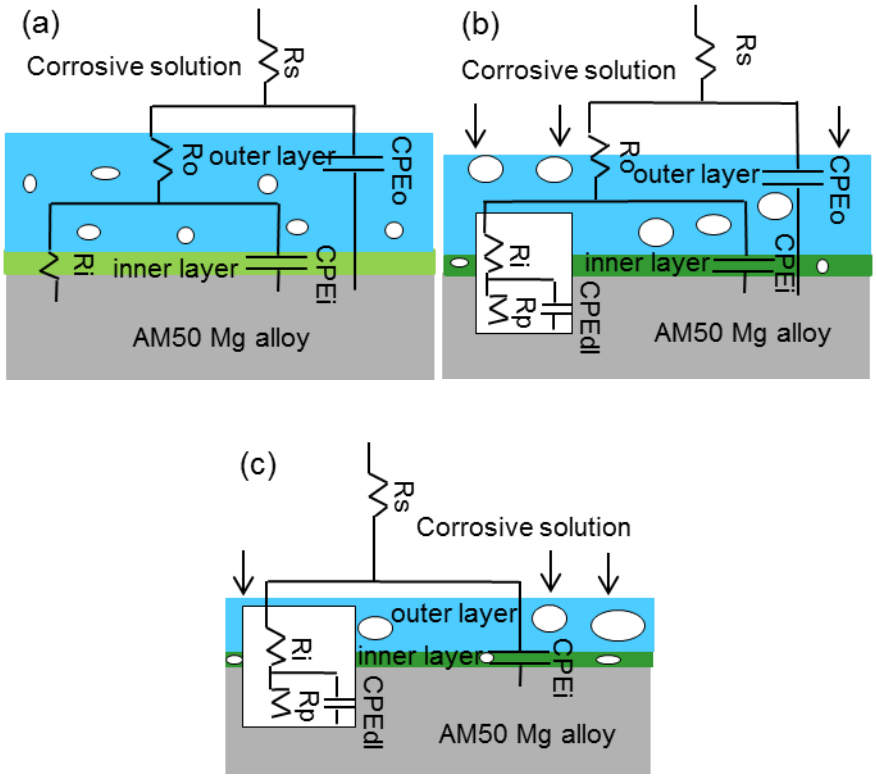

Figure 6-7 Schematic diagram of the degradation of PEO coating (a) initial stage (uncorroded layer), (b) mid-term stage (corroded outer and inner layer), (c) final stage (unprotected outer layer and corroded inner layer).

6.5.2 Bio-degradability

Even if PEO coating is prone to degrade in NaCl solution, stable corrosion products can be formed and redeposited in the layer using specific corrosion medium (Hank's solution), which provide potential possibility for bio-application. This is associated with the reaction between the calcium ions from the corrosion solution and the dissolved phosphate from the amorphous material or hydroxide ions from the substrate. Particularly, addition of SiO_2 nanoparticles has demonstrated remarkable effect on the degradation process of the coating in Hank's solution (Figure 6-8). Owing to the reactive incorporation of the SiO_2 nanoparticles, the coating has been changed from crystalline layer to amorphous layer leading to different degradation processes. Calcium containing corrosion products are mainly deposited in the internal region (coating/substrate interface) of the particle-free coating because of the relatively stable crystalline phases in the outer layer (Figure 6-8b). The large amount of hydroxide from the dissolution of the

Mg substrate facilitate an alkaline environment in the pore band, which can be considered as reservoir for the corrosion products, mainly $Ca(OH)_2$. In terms of the particle-containing coatings, the phosphate containing amorphous phase dissolves rapidly under the attack of the corrosion medium. The dissolved phosphate ions can react with the calcium ions from the Hank's solution resulting in redeposition of corrosion products in the outer layer (Figure 6-8c). The sealed outer layer prevents the coating from further degradation, and thus provides significantly enhanced corrosion performance for the coating (Figure 6-8d). Therefore, it might be feasible to control the degradation process of the PEO coatings in bio-medium via addition of reactive SiO_2 nanoparticles.

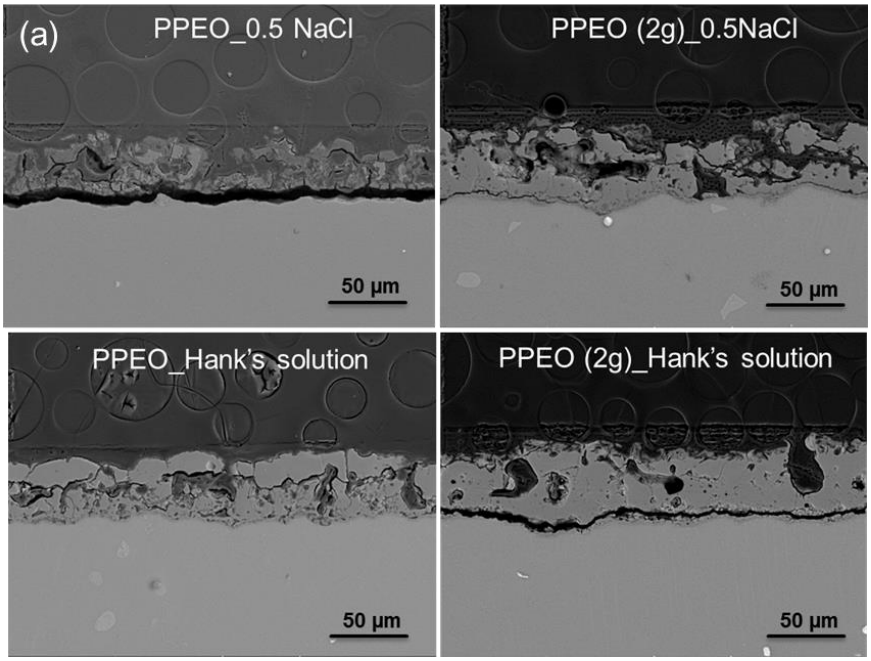

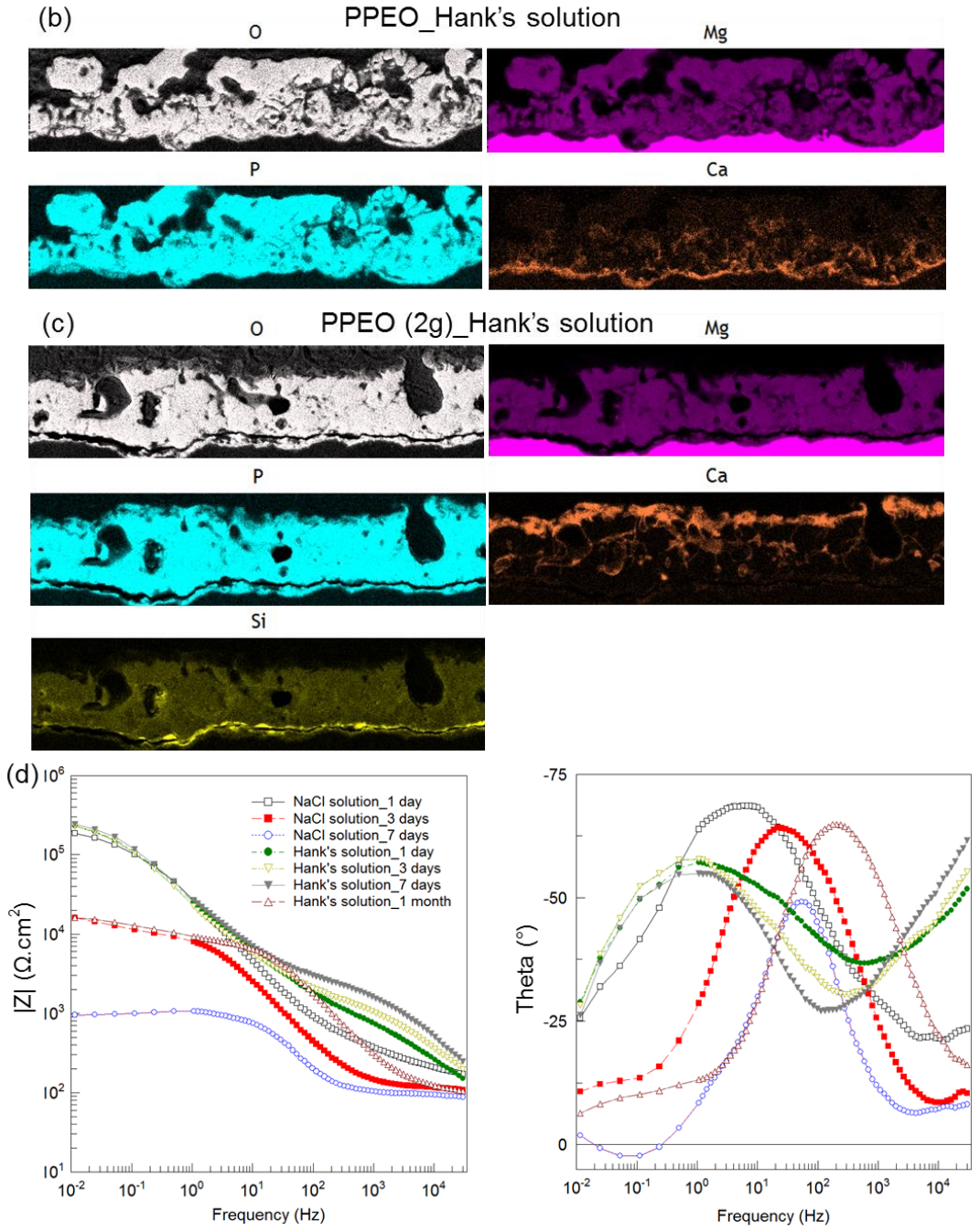

Figure 6-8 (a) cross section morphology of the PEO coatings after corrosion test in different corrosion media cross section morphology, (b) mapping of particle-free coating after corrosion in Hank's solution, (c) mapping of particle containing coating after corrosion in Hank's solution, (d) degradation behavior of the coatings with addition of particles in 0.5 % NaCl and Hank's solution.

6.5.3 Wear resistance

Particles can be used to enhance the wear performance of PEO coatings. For instance, the reactively incorporated SiO_2 nanoparticles result in formation of new amorphous phase in the coating (Paper 2). Due to the superior mechanical properties of the amorphous material [91], the wear rate of the coating and its counterpart is significantly reduced during sliding wear test. Inert incorporation of SiO_2 and Si_3N_4 particles can enhance the wear resistance of PEO coatings as well (Figure 6-9). However, the reinforcement effect is weakened if the inertly incorporated particles (e.g., SiC particles) are beyond a certain limit. It is likely that the reduced coating thickness and porous layer cannot withstand the load resulting in removal of coating and three-body-abrasive wear. It is worthwhile to note that the friction coefficient (Figure 6-9b) is generally high under dry sliding test, which is detrimental for practical applications. The high friction coefficient can lead not only to the wear of the slider, but also to the wear damage of the counter material. For cases like this, lubricant might be used to reduce the friction coefficient.

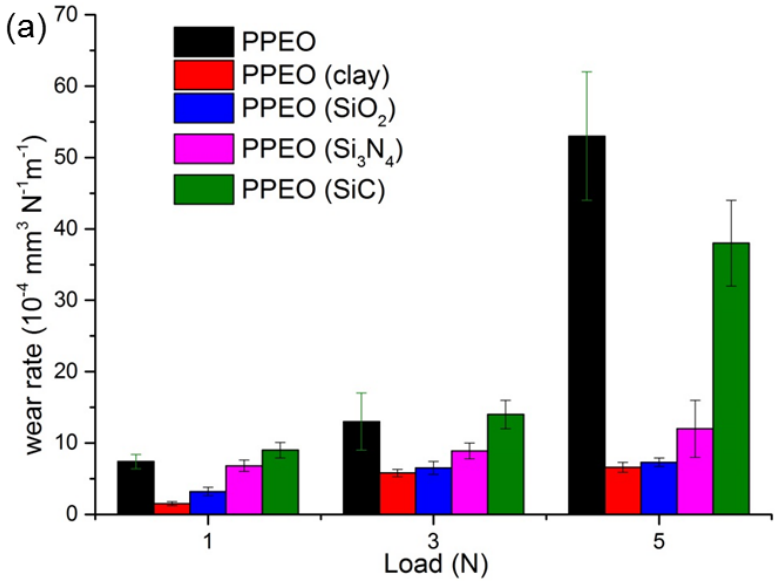

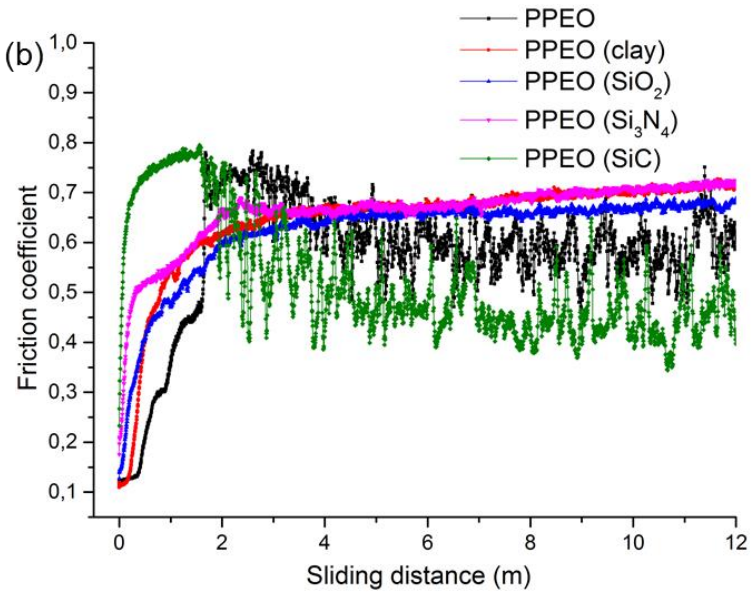

Figure 6-9 (a) Wear rate of PEO coatings with and without addition of 5 g/L particles under different loads, (b) Variation of the friction coefficient during 12 m sliding in the oscillating wear tests under a load of 5 N.

6.5.4 Photocatalytic activity

In some cases, inert incorporation of particles is preferable because they can provide PEO coatings with new functionalities. Owing to the good photocatalytic property of TiO_2 particles [76], anatase particles have been added to PEO coating to confer photocatalytic activity for Mg alloy (Paper 8). Higher amount of particles in the electrolyte and higher voltage applied during PEO treatment can lead to incorporation of higher amount of particles into the layer. The anatase particles have been converted into high temperature phases (rutile and Mg_2TiO_4) under high voltage. It was found that the photocatalytic performance of the coating is primarily related to the anatase content on the coating surface, since the anatase particles can effectively accelerate the decomposition rate of the methylene blue solution. Thus coatings produced from particle-concentrated electrolyte under relatively low voltage demonstrate superior photocatalytic activity. Such coatings may provide Mg-based biodegradable implants with bioactivity and antibacterial properties.

6.6 Summary

Based on the aforementioned results, it is proved that the uptake and incorporation of particles depend on the numerous factors, e.g., properties of the particles (size and melting point), particle

concentration in the PEO electrolyte, processing parameters (frequency, duty ratio and voltage). Uptake of the particles is primarily via the pores in the coating surface. Thus uptake of the small-sized particles can be more easily achieved via the open pores and discharge channels in comparison to the relatively large-sized particles. The particle uptake is also related to the particle concentration in the electrolyte, since the particle content in the coating increases proportionally with the concentration of the particles in the electrolyte. In terms of processing parameters, the pulse duration and the voltage applied during PEO treatment dominate the uptake of particles into the coating. Longer and more pulse combined with higher voltage facilitate uptake of more amount of particles. Besides, the composition of the base electrolyte has slight effect on the uptake of particles. The incorporation mode of the particles is related to the particle reactivity, which relies on the other phases adjacent to the particles, the size and melting point of the particle itself and the energy obtained from the discharges. Small-sized and low melting point particles can more easily achieve reactive incorporation than large-sized and high melting point particles. The incorporation mode can be controlled by modification of the processing parameters. High voltage is an effective approach to convert the inert particles into new reactive phases. Therefore, the incorporation mode of the particles in turn has an effect on the coating phase composition.

The PEO processing is affected by the particles, as reflected by faster transition of the current/voltage response. It is due to the enhanced barrier properties of the coating after incorporation of particles, which has also been confirmed by the improved corrosion performance at the early stage during corrosion test. However, addition of particles is not effective to improve the morphology of PEO coatings, especially the high porosity and coating thickness. The porous layer remains an issue to achieve long-term protection for industrial applications without post treatment. The coating composition can be modified in the presence of particles and controlled by the processing parameters. Owing to the altered composition and morphology, the properties of the coating have been modified and/or enhanced to some extent. It is feasible to control the degradation process of PEO coatings in bio-medium by formation of amorphous layer via addition of particles. The wear resistance of the coating can be improved in the presence of particles, although the friction coefficient is generally high under unlubricated conditions. Moreover, introduction of particles with specific properties to PEO coatings may confer Mg alloys with wider range of applications. For instance, TiO_2 doped coatings can provide improved

UV sterilization ability to degradable Mg implants or potential anti-bacterial properties for Mg alloys used in consumer electronics or automotive interiors.

7 Conclusions and outlook

This work has shown that introduction of particles is an effective approach to modify and optimize the morphology, microstructure, composition and properties of PEO coatings. The main findings are listed below:

- Introduction of particles influence the evolution of current/voltage during PEO treatment. It promotes the ramp rate of the current or voltage under voltage- or current-control regime.
- Uptake of the particles is primarily via the pores in the coating surface. The size of the particles has an effect on the uptake mode. Uptake of the small-sized particles can more easily occur via the open pores and discharge channels in comparison to the relatively large-sized particles.
- Uptake of the particles depends on the electrical parameters applied during the treatment. Longer pulse duration and higher voltage applied during PEO treatment result in uptake of more particles into the coating.
- The change of the base electrolyte has slight influence on the particle uptake. However, the uptake of the particles increases significantly with the particle concentration in the PEO electrolyte.
- The incorporation mode of the particles is related to the particle reactivity, which depends on the other phases adjacent to the particles, the size and melting point of the particle itself and processing parameters. The phase composition of the coating relies on the incorporation mode of the particles. Inert incorporation results in unreacted particles in the coating, while reactive incorporation promotes formation of new phases.
- Addition of particles cannot avoid/seal the high porosity of PEO coatings. The thickness of the coating is reduced in the presence of particles.
- The corrosion resistance of the coating in NaCl solution cannot be improved by the particles, while it is feasible to control and modify the biodegradability of the coating via addition of particles.
- Introduction of particles can improve the wear performance and photocatalytic activity of PEO coatings.

It must be stated that none of the coatings formed in electrolytes with particle additions is used commercially in an industrial application up to now, which might be related to the fact that keeping the particles uniformly dispersed is a challenge especially in large industrial treatment baths. Research of effective surfactants stabilizing dispersions is needed for the future. Repeated use of the electrolyte may weaken it due to the consumption of the particles. However, no quantitative information appears to be available regarding the effective ampere-hours of the electrolyte, particle consumption rate, degree of the deterioration of the coating quality, frequency of the electrolyte correction and associated costs etc. Therefore future work should be dedicated to systematic applied studies required for up-scaling of the particle-based PEO processes. Use of small-sized particles can cause health problems, such as respiratory disease, during preparation and disposal of the electrolytes. Although there are remaining issues and challenges, new research field can be opened regarding the introduction of particles to PEO coatings. For instance, particles can be regarded as perspective containers for loading corrosion inhibitors and be subsequently incorporated into the coating to confer self-sealing functionality during corrosion process. The metallic surface can be tuned and functionalized by PEO technique via addition of particles for a wider range of applications.

8 Bibliography

[1] A.L. Yerokhin, X. Nie, A. Leyland, A. Matthews, S.J. Dowey, Plasma electrolysis for surface engineering, Surface and Coatings Technology, 122 (1999) 73-93.
[2] J.A. Curran, T.W. Clyne, Thermo-physical properties of plasma electrolytic oxide coatings on aluminium, Surface and Coatings Technology, 199 (2005) 168-176.
[3] R. Arrabal, E. Matykina, T. Hashimoto, P. Skeldon, G.E. Thompson, Characterization of AC PEO coatings on magnesium alloys, Surface and Coatings Technology, 203 (2009) 2207-2220.
[4] Y. Song, K. Dong, D. Shan, E.-H. Han, Investigation of a novel self-sealing pore micro-arc oxidation film on AM60 magnesium alloy, Journal of Magnesium and Alloys, 1 (2013) 82-87.
[5] S. Yagi, K. Kuwabara, Y. Fukuta, K. Kubota, E. Matsubara, Formation of self-repairing anodized film on ACM522 magnesium alloy by plasma electrolytic oxidation, Corrosion Science, 73 (2013) 188-195.
[6] Y. Cheng, F. Wu, E. Matykina, P. Skeldon, G.E. Thompson, The influences of microdischarge types and silicate on the morphologies and phase compositions of plasma electrolytic oxidation coatings on Zircaloy-2, Corrosion Science, 59 (2012) 307-315.
[7] R.O. Hussein, D.O. Northwood, X. Nie, The effect of processing parameters and substrate composition on the corrosion resistance of plasma electrolytic oxidation (PEO) coated magnesium alloys, Surface and Coatings Technology, 237 (2013) 357-368.
[8] A. Ghasemi, Contribution to understanding the formation process and corrosion protection of the PEO coating on AM50 magnesium alloy, PhD thesis, Technische Universität Clausthal, Germany, (2011).
[9] C.E. Barchiche, E. Rocca, C. Juers, J. Hazan, J. Steinmetz, Corrosion resistance of plasma-anodized AZ91D magnesium alloy by electrochemical methods, Electrochimica Acta, 53 (2007) 417-425.
[10] P. Bala Srinivasan, J. Liang, C. Blawert, M. Störmer, W. Dietzel, Effect of current density on the microstructure and corrosion behaviour of plasma electrolytic oxidation treated AM50 magnesium alloy, Applied Surface Science, 255 (2009) 4212-4218.
[11] R.O. Hussein, P. Zhang, X. Nie, Y. Xia, D.O. Northwood, The effect of current mode and discharge type on the corrosion resistance of plasma electrolytic oxidation (PEO) coated magnesium alloy AJ62, Surface and Coatings Technology, 206 (2011) 1990-1997.
[12] C. Blawert, V. Heitmann, W. Dietzel, H.M. Nykyforchyn, M.D. Klapkiv, Influence of electrolyte on corrosion properties of plasma electrolytic conversion coated magnesium alloys, Surf Coat Tech, 201 (2007) 8709-8714.
[13] A. Ghasemi, V.S. Raja, C. Blawert, W. Dietzel, K.U. Kainer, The role of anions in the formation and corrosion resistance of the plasma electrolytic oxidation coatings, Surface and Coatings Technology, 204 (2010) 1469-1478.
[14] B.S. Necula, L.E. Fratila-Apachitei, A. Berkani, I. Apachitei, J. Duszczyk, Enrichment of anodic MgO layers with Ag nanoparticles for biomedical applications, J Mater Sci: Mater Med, 20 (2009) 339-345.
[15] D. Hanaor, M. Michelazzi, C. Leonelli, C.C. Sorrell, The effects of carboxylic acids on the aqueous dispersion and electrophoretic deposition of ZrO2, J Eur Ceram Soc, 32 (2012) 235-244.
[16] K.M. Lee, B.U. Lee, S.I. Yoon, E.S. Lee, B. Yoo, D.H. Shin, Evaluation of plasma temperature during plasma oxidation processing of AZ91 Mg alloy through analysis of the melting behavior of incorporated particles, Electrochimica Acta, 67 (2012) 6-11.

[17] K.M. Lee, Y.G. Ko, D.H. Shin, Incorporation of multi-walled carbon nanotubes into the oxide layer on a 7075 Al alloy coated by plasma electrolytic oxidation: Coating structure and corrosion properties, Curr. Appl. Phys., 11 (2011) S55-S59.
[18] J. Guo, L. Wang, S.C. Wang, J. Liang, Q. Xue, F. Yan, Preparation and performance of a novel multifunctional plasma electrolytic oxidation composite coating formed on magnesium alloy, J Mater Sci, 44 (2009) 1998-2006.
[19] M.S. Vasilyeva, V.S. Rudnev, I.A. Korotenko, P.M. Nedozorov, Producing and studying oxide coatings containing manganese and nickel compounds on titanium from electrolyte suspensions, Prot Met Phys Chem Surf, 48 (2012) 106-115.
[20] J. Liang, L. Hu, J. Hao, Preparation and characterization of oxide films containing crystalline TiO2 on magnesium alloy by plasma electrolytic oxidation, Electrochimica Acta, 52 (2007) 4836-4840.
[21] M. Laleh, A.S. Rouhaghdam, T. Shahrabi, A. Shanghi, Effect of alumina sol addition to micro-arc oxidation electrolyte on the properties of MAO coatings formed on magnesium alloy AZ91D, Journal of Alloys and Compounds, 496 (2010) 548-552.
[22] M. Tang, W. Li, H. Liu, L. Zhu, Influence of titania sol in the electrolyte on characteristics of the microarc oxidation coating formed on 2A70 aluminum alloy, Surface and Coatings Technology, 205 (2011) 4135-4140.
[23] R. Balaji, M. Pushpavanam, K.Y. Kumar, K. Subramanian, Electrodeposition of bronze-PTFE composite coatings and study on their tribological characteristics, Surf Coat Tech, 201 (2006) 3205-3211.
[24] B.S. Atiyeh, M. Costagliola, S.N. Hayek, S.A. Dibo, Effect of silver on burn wound infection control and healing: Review of the literature, Burns, 33 (2007) 139-148.
[25] K.J.L. Burg, S. Porter, J.F. Kellam, Biomaterial developments for bone tissue engineering, Biomaterials, 21 (2000) 2347-2359.
[26] C. Blawert, S.P. Sah, J. Liang, Y. Huang, D. Höche, Role of sintering and clay particle additions on coating formation during PEO processing of AM50 magnesium alloy, Surface and Coatings Technology, 213 (2012) 48-58.
[27] R.H.J. Hannink, Microstructural Development of Sub-Eutectoid Aged Mgo-Zro2 Alloys, J Mater Sci, 18 (1983) 457-470.
[28] O. Fukumasa, R. Tagashira, K. Tachino, H. Mukunoki, Spraying of MgO films with a well-controlled plasma jet, Surf Coat Tech, 169 (2003) 579-582.
[29] P. Galliano, J.J. De Damborenea, M.J. Pascual, A. Duran, Sol-gel coatings on 316L steel for clinical applications, J Sol-Gel Sci Techn, 13 (1998) 723-727.
[30] D.C.L. Vasconcelos, J.A.N. Carvalho, M. Mantel, W.L. Vasconcelos, Corrosion resistance of stainless steel coated with sol-gel silica, J Non-Cryst Solids, 273 (2000) 135-139.
[31] D. Wang, G.P. Bierwagen, Sol–gel coatings on metals for corrosion protection, Progress in Organic Coatings, 64 (2009) 327-338.
[32] A. Pepe, M. Aparicio, A. Durán, S. Ceré, Cerium hybrid silica coatings on stainless steel AISI 304 substrate, J Sol-Gel Sci Techn, 39 (2006) 131-138.
[33] M. Schem, T. Schmidt, J. Gerwann, M. Wittmar, M. Veith, G.E. Thompson, I.S. Molchan, T. Hashimoto, P. Skeldon, A.R. Phani, S. Santucci, M.L. Zheludkevich, CeO2-filled sol–gel coatings for corrosion protection of AA2024-T3 aluminium alloy, Corrosion Science, 51 (2009) 2304-2315.
[34] R.T. Bhatt, S.R. Choi, L.M. Cosgriff, D.S. Fox, K.N. Lee, Impact resistance of environmental barrier coated SiC/SiC composites, Materials Science and Engineering: A, 476 (2008) 8-19.

[35] C. Czosnek, M.M. Bućko, J.F. Janik, Z. Olejniczak, M. Bystrzejewski, O. Łabędź, A. Huczko, Preparation of silicon carbide SiC-based nanopowders by the aerosol-assisted synthesis and the DC thermal plasma synthesis methods, Materials Research Bulletin, 63 (2015) 164-172.
[36] X. Li, B.L. Luan, Discovery of Al2O3 particles incorporation mechanism in plasma electrolytic oxidation of AM60B magnesium alloy, Materials Letters, 86 (2012) 88-91.
[37] T.S. Lim, H.S. Ryu, S.-H. Hong, Electrochemical corrosion properties of CeO2-containing coatings on AZ31 magnesium alloys prepared by plasma electrolytic oxidation, Corrosion Science, 62 (2012) 104-111.
[38] W. Li, M. Tang, L. Zhu, H. Liu, Formation of microarc oxidation coatings on magnesium alloy with photocatalytic performance, Applied Surface Science, 258 (2012) 10017-10021.
[39] Y. Wang, D. Wei, J. Yu, S. Di, Effects of Al2O3 Nano-additive on Performance of Micro-arc Oxidation Coatings Formed on AZ91D Mg Alloy, Journal of Materials Science & Technology, 30 (2014) 984-990.
[40] R. Arrabal, E. Matykina, F. Viejo, P. Skeldon, G.E. Thompson, M.C. Merino, AC plasma electrolytic oxidation of magnesium with zirconia nanoparticles, Applied Surface Science, 254 (2008) 6937-6942.
[41] K.M. Lee, K.R. Shin, S. Namgung, B. Yoo, D.H. Shin, Electrochemical response of ZrO2-incorporated oxide layer on AZ91 Mg alloy processed by plasma electrolytic oxidation, Surface and Coatings Technology, 205 (2011) 3779-3784.
[42] H. Nasiri Vatan, R. Ebrahimi-kahrizsangi, M. Kasiri-asgarani, Structural, tribological and electrochemical behavior of SiC nanocomposite oxide coatings fabricated by plasma electrolytic oxidation (PEO) on AZ31 magnesium alloy, Journal of Alloys and Compounds, 683 (2016) 241-255.
[43] M. Sun, A. Yerokhin, M.Y. Bychkova, D.V. Shtansky, E.A. Levashov, A. Matthews, Self-healing plasma electrolytic oxidation coatings doped with benzotriazole loaded halloysite nanotubes on AM50 magnesium alloy, Corrosion Science.
[44] E. Matykina, R. Arrabal, P. Skeldon, G.E. Thompson, Incorporation of zirconia nanoparticles into coatings formed on aluminium by AC plasma electrolytic oxidation, J Appl Electrochem, 38 (2008) 1375-1383.
[45] E. Matykina, R. Arrabal, F. Monfort, P. Skeldon, G.E. Thompson, Incorporation of zirconia into coatings formed by DC plasma electrolytic oxidation of aluminium in nanoparticle suspensions, Applied Surface Science, 255 (2008) 2830-2839.
[46] W.P. Li, L.Q. Zhu, Y.H. Li, Electrochemical oxidation characteristic of AZ91D magnesium alloy under the action of silica sol, Surf Coat Tech, 201 (2006) 1085-1092.
[47] G. Yan, W. Guixiang, D. Guojun, G. Fan, Z. Lili, Z. Milin, Corrosion resistance of anodized AZ31 Mg alloy in borate solution containing titania sol, Journal of Alloys and Compounds, 463 (2008) 458-461.
[48] W.P. Li, L.Q. Zhu, H.C. Liu, Preparation of hydrophobic anodic film on AZ91D magnesium alloy in silicate solution containing silica sol, Surf Coat Tech, 201 (2006) 2573-2577.
[49] L.Q. Zhu, Y.H. Li, W.P. Li, Influence of silica sol particle behavior on the magnesium anodizing process with different anions addition, Surf Coat Tech, 202 (2008) 5853-5857.
[50] W. Li, L. Zhu, H. Liu, Effects of silicate concentration on anodic films formed on AZ91D magnesium alloy in solution containing silica sol, Surface and Coatings Technology, 201 (2006) 2505-2511.
[51] J. Liu, Y. Lu, X. Jing, Y. Yuan, M. Zhang, Characterization of plasma electrolytic oxidation coatings formed on Mg–Li alloy in an alkaline silicate electrolyte containing silica sol, Materials and Corrosion, 60 (2009) 865-870.

[52] A. Seyfoori, S. Mirdamadi, Z.S. Seyedraoufi, A. Khavandi, M. Aliofkhazraei, Synthesis of biphasic calcium phosphate containing nanostructured films by micro arc oxidation on magnesium alloy, Materials Chemistry and Physics, 142 (2013) 87-94.
[53] R. Arrabal, E. Matykina, P. Skeldon, G.E. Thompson, Incorporation of zirconia particles into coatings formed on magnesium by plasma electrolytic oxidation, J Mater Sci, 43 (2008) 1532-1538.
[54] B.S. Necula, I. Apachitei, F.D. Tichelaar, L.E. Fratila-Apachitei, J. Duszczyk, An electron microscopical study on the growth of TiO2–Ag antibacterial coatings on Ti6Al7Nb biomedical alloy, Acta Biomaterialia, 7 (2011) 2751-2757.
[55] G. Rapheal, S. Kumar, N. Scharnagl, C. Blawert, Effect of current density on the microstructure and corrosion properties of plasma electrolytic oxidation (PEO) coatings on AM50 Mg alloy produced in an electrolyte containing clay additives, Surface and Coatings Technology, 289 (2016) 150-164.
[56] R. Arrabal, M. Mohedano, E. Matykina, A. Pardo, B. Mingo, M.C. Merino, Characterization and wear behaviour of PEO coatings on 6082-T6 aluminium alloy with incorporated α-Al2O3 particles, Surface and Coatings Technology, 269 (2015) 64-73.
[57] M. Tang, H. Liu, W. Li, L. Zhu, Effect of zirconia sol in electrolyte on the characteristics of microarc oxidation coating on AZ91D magnesium, Materials Letters, 65 (2011) 413-415.
[58] D. Zhang, Y. Gou, Y. Liu, X. Guo, A composite anodizing coating containing superfine Al2O3 particles on AZ31 magnesium alloy, Surface and Coatings Technology, 236 (2013) 52-57.
[59] C. Ma, M. Zhang, Y. Yuan, X. Jing, X. Bai, Tribological behavior of plasma electrolytic oxidation coatings on the surface of Mg8Li1Al alloy, Tribology International, 47 (2012) 62-68.
[60] Y.M. Wang, F.H. Wang, M.J. Xu, B. Zhao, L.X. Guo, J.H. Ouyang, Microstructure and corrosion behavior of coated AZ91 alloy by microarc oxidation for biomedical application, Applied Surface Science, 255 (2009) 9124-9131.
[61] M. Daroonparvar, M.A.M. Yajid, N.M. Yusof, H.R. Bakhsheshi-Rad, Preparation and corrosion resistance of a nanocomposite plasma electrolytic oxidation coating on Mg-1%Ca alloy formed in aluminate electrolyte containing titania nano-additives, Journal of Alloys and Compounds, 688, Part A (2016) 841-857.
[62] Y. Yang, H. Wu, Effects of Current Frequency on the Microstructure and Wear Resistance of Ceramic Coatings Embedded with SiC Nano-particles Produced by Micro-arc Oxidation on AZ91D Magnesium Alloy, Journal of Materials Science & Technology, 26 (2010) 865-871.
[63] L. Yu, J. Cao, Y. Cheng, An improvement of the wear and corrosion resistances of AZ31 magnesium alloy by plasma electrolytic oxidation in a silicate–hexametaphosphate electrolyte with the suspension of SiC nanoparticles, Surface and Coatings Technology, 276 (2015) 266-278.
[64] Y.Q. Wang, M.Y. Zheng, K. Wu, Microarc oxidation coating formed on SiCw/AZ91 magnesium matrix composite and its corrosion resistance, Materials Letters, 59 (2005) 1727-1731.
[65] W. Xue, Q. Jin, Q. Zhu, M. Hua, Y. Ma, Anti-corrosion microarc oxidation coatings on SiCP/AZ31 magnesium matrix composite, Journal of Alloys and Compounds, 482 (2009) 208-212.
[66] R. Arrabal, E. Matykina, P. Skeldon, G.E. Thompson, Coating formation by plasma electrolytic oxidation on ZC71/SiC/12p-T6 magnesium metal matrix composite, Applied Surface Science, 255 (2009) 5071-5078.
[67] M. Mohedano, C. Blawert, M.L. Zheludkevich, Silicate-based Plasma Electrolytic Oxidation (PEO) coatings with incorporated CeO2 particles on AM50 magnesium alloy, Materials & Design, 86 (2015) 735-744.

[68] D. Sreekanth, N. Rameshbabu, Development and characterization of MgO/hydroxyapatite composite coating on AZ31 magnesium alloy by plasma electrolytic oxidation coupled with electrophoretic deposition, Materials Letters, 68 (2012) 439-442.
[69] X. Lin, X. Wang, L. Tan, P. Wan, X. Yu, Q. Li, K. Yang, Effect of preparation parameters on the properties of hydroxyapatite containing micro-arc oxidation coating on biodegradable ZK60 magnesium alloy, Ceramics International, 40 (2014) 10043-10051.
[70] X. Ma, S. Zhu, L. Wang, C. Ji, C. Ren, S. Guan, Synthesis and properties of a bio-composite coating formed on magnesium alloy by one-step method of micro-arc oxidation, Journal of Alloys and Compounds, 590 (2014) 247-253.
[71] M. Daroonparvar, M.A.M. Yajid, N.M. Yusof, H.R. Bakhsheshi-Rad, Preparation and corrosion resistance of a nanocomposite plasma electrolytic oxidation coating on Mg-1%Ca alloy formed in aluminate electrolyte containing titania nano-additives, Journal of Alloys and Compounds.
[72] Y.L. Song, X.Y. Sun, Y.H. Liu, Effect of TiO2 nanoparticles on the microstructure and corrosion behavior of MAO coatings on magnesium alloy, Materials and Corrosion, 63 (2012) 813-818.
[73] P.B. Srinivasan, J. Liang, C. Blawert, M. Störmer, W. Dietzel, Development of decorative and corrosion resistant plasma electrolytic oxidation coatings on AM50 magnesium alloy, Surf Eng, 26 (2010) 367-370.
[74] R. Arrabal, A. Pardo, M.C. Merino, M. Mohedano, P. Casajús, E. Matykina, P. Skeldon, G.E. Thompson, Corrosion behaviour of a magnesium matrix composite with a silicate plasma electrolytic oxidation coating, Corrosion Science, 52 (2010) 3738-3749.
[75] G. Rapheal, S. Kumar, C. Blawert, N.B. Dahotre, Wear behavior of plasma electrolytic oxidation (PEO) and hybrid coatings of PEO and laser on MRI 230D magnesium alloy, Wear, 271 (2011) 1987-1997.
[76] Y.-K. Shin, W.-S. Chae, Y.-W. Song, Y.-M. Sung, Formation of titania photocatalyst films by microarc oxidation of Ti and Ti–6Al–4V alloys, Electrochemistry Communications, 8 (2006) 465-470.
[77] P. Shi, W.F. Ng, M.H. Wong, F.T. Cheng, Improvement of corrosion resistance of pure magnesium in Hanks' solution by microarc oxidation with sol-gel TiO2 sealing, Journal of Alloys and Compounds, 469 (2009) 286-292.
[78] X.N. Gu, N. Li, W.R. Zhou, Y.F. Zheng, X. Zhao, Q.Z. Cai, L. Ruan, Corrosion resistance and surface biocompatibility of a microarc oxidation coating on a Mg–Ca alloy, Acta Biomaterialia, 7 (2011) 1880-1889.
[79] Z. Shi, M. Liu, A. Atrens, Measurement of the corrosion rate of magnesium alloys using Tafel extrapolation, Corrosion Science, 52 (2010) 579-588.
[80] N. Birbilis, A.D. King, S. Thomas, G.S. Frankel, J.R. Scully, Evidence for enhanced catalytic activity of magnesium arising from anodic dissolution, Electrochimica Acta, 132 (2014) 277-283.
[81] D. Hoche, C. Blawert, S.V. Lamaka, N. Scharnagl, C. Mendis, M.L. Zheludkevich, The effect of iron re-deposition on the corrosion of impurity-containing magnesium, Physical Chemistry Chemical Physics, 18 (2016) 1279-1291.
[82] H. Duan, C. Yan, F. Wang, Effect of electrolyte additives on performance of plasma electrolytic oxidation films formed on magnesium alloy AZ91D, Electrochimica Acta, 52 (2007) 3785-3793.

[83] Y. Mori, A. Koshi, J. Liao, H. Asoh, S. Ono, Characteristics and corrosion resistance of plasma electrolytic oxidation coatings on AZ31B Mg alloy formed in phosphate – Silicate mixture electrolytes, Corrosion Science, 88 (2014) 254-262.
[84] X. Lu, C. Blawert, Y. Huang, H. Ovri, M.L. Zheludkevich, K.U. Kainer, Plasma electrolytic oxidation coatings on Mg alloy with addition of SiO2 particles, Electrochimica Acta, 187 (2016) 20-33.
[85] X. Lu, S.P. Sah, N. Scharnagl, M. Störmer, M. Starykevich, M. Mohedano, C. Blawert, M.L. Zheludkevich, K.U. Kainer, Degradation behavior of PEO coating on AM50 magnesium alloy produced from electrolytes with clay particle addition, Surface and Coatings Technology, 269 (2015) 155-169.
[86] X. Lu, C. Blawert, M.L. Zheludkevich, K.U. Kainer, Insights into plasma electrolytic oxidation treatment with particle addition, Corrosion Science, 101 (2015) 201-207.
[87] X. Lu, M. Schieda, C. Blawert, K.U. Kainer, M.L. Zheludkevich, Formation of photocatalytic plasma electrolytic oxidation coatings on magnesium alloy by incorporation of TiO2 particles, Surface and Coatings Technology, 307, Part A (2016) 287-291.
[88] X. Lu, C. Blawert, M. Mohedano, N. Scharnagl, M.L. Zheludkevich, K.U. Kainer, Influence of electrical parameters on particle uptake during plasma electrolytic oxidation processing of AM50 Mg alloy, Surface and Coatings Technology, 289 (2016) 179-185.
[89] X. Lu, C. Blawert, K.U. Kainer, M.L. Zheludkevich, Investigation of the formation mechanisms of plasma electrolytic oxidation coatings on Mg alloy AM50 using particles, Electrochimica Acta, 196 (2016) 680-691.
[90] X. Lu, C. Blawert, N. Scharnagl, K.U. Kainer, Influence of incorporating Si3N4 particles into the oxide layer produced by plasma electrolytic oxidation on AM50 Mg alloy on coating morphology and corrosion properties, Journal of Magnesium and Alloys, 1 (2013) 267-274.
[91] Z.H. Stachurski, On Structure and Properties of Amorphous Materials, Materials, 4 (2011) 1564-1598.

Appendix

1. List of symbols and abbreviations

AC	Alternating current
Al	Aluminum
AM50	Mg-5Al-0.4Mn (wt.%)
BSE	Back scattered electrons
$\mathbf{C_{inner\ layer}}$	Capacitance of the inner layer
$\mathbf{C_{outer\ layer}}$	Capacitance of the outer layer
$\mathbf{C_{polar}}$	Capacitance pf the double layer
CPE	Constant phase element
DC	Direct current
$\mathbf{E_{corr}}$	Corrosion potential
EIS	Electrochemical impedance spectroscopy
EDS	Energy dispersive X-rays spectroscopy
FIB	Focused ion beam
MAO	Microarc oxidation
MB	Methylene blue
Mg	Magnesium
NDE	Negative difference effect
OCP	Open circuit potential
OES	Optical emission spectroscopy
PEO	Plasma electrolytic oxidation
$\mathbf{R_{inner\ layer}}$	Resistance of the inner layer
$\mathbf{R_{outer\ layer}}$	Resistance of the outer layer
$\mathbf{R_{polar}}$	Polarization resistance
$\mathbf{R_s}$	Solution resistance
SBF	Simulated body fluid
SCE	Saturated calomel electrode
SEM	Scanning electron microscopy
SiC	Silicon carbide
$\mathbf{Si_3N_4}$	Silicon nitride
$\mathbf{SiO_2}$	Silicon dioxide

TEM	Transmission electron microscopy
Ti	Titanium
TiO_2	Titanium dioxide
XRD	X-Ray diffraction
Z	Impedance
Zr	Zirconium
Ψ	Sphericity of pores/particles

2. Publications during candidature

Peer-reviewed papers:

1) **X. Lu**, C. Blawert, N. Scharnagl, K.U. Kainer, Influence of incorporating Si_3N_4 particles into the oxide layer produced by plasma electrolytic oxidation on AM50 Mg alloy on coating morphology and corrosion properties, Journal of Magnesium and Alloys, 1 (2013) 267-274.
2) **X. Lu**, S.P. Sah, N. Scharnagl, M. Störmer, M. Starykevich, M. Mohedano, C. Blawert, M.L. Zheludkevich, K.U. Kainer, Degradation behavior of PEO coating on AM50 magnesium alloy produced from electrolytes with clay particle addition, Surface and Coatings Technology, 269 (2015) 155-169.
3) **X. Lu**, C. Blawert, M.L. Zheludkevich, K.U. Kainer, Insights into plasma electrolytic oxidation treatment with particle addition, Corrosion Science, 101 (2015) 201-207.
4) **X. Lu**, C. Blawert, Y. Huang, H. Ovri, M.L. Zheludkevich, K.U. Kainer, Plasma electrolytic oxidation coatings on Mg alloy with addition of SiO_2 particles, Electrochimica Acta, 187 (2016) 20-33.
5) **X. Lu**, C. Blawert, M. Mohedano, N. Scharnagl, M.L. Zheludkevich, K.U. Kainer, Influence of electrical parameters on particle uptake during plasma electrolytic oxidation processing of AM50 Mg alloy, Surface and Coatings Technology, 289 (2016) 179-185.
6) **X. Lu**, C. Blawert, K.U. Kainer, M.L. Zheludkevich, Investigation of the formation mechanisms of plasma electrolytic oxidation coatings on Mg alloy AM50 using particles, Electrochimica Acta, 196 (2016) 680-691.
7) **X. Lu**, M. Schieda, C. Blawert, K.U. Kainer, M.L. Zheludkevich. Formation of photocatalytic plasma electrolytic oxidation coatings on magnesium alloy by incorporation of TiO_2 particles, Surface and Coatings Technology, 307 (2016) 287-291.
8) M. Klein, **X. Lu**, C. Blawert, K.U. Kainer, M.L. Zheludkevich, F. Walther, Influence of plasma electrolytic oxidation coatings on fatigue performance of AZ31 Mg alloy, accepted by Materials and Corrosion.
9) **X. Lu**, M. Mohedano, C. Blawert, E. Matykina, R. Arrabal, K.U. Kainer, M.L. Zheludkevich. Plasma electrolytic oxidation coatings with particle additions - A review, accepted by Surface and Coatings Technology.
10) Y. Chen, Y. Yang, T. Zhang, W. Zhang, F. Wang, **X. Lu**, C. Blawert, M.L. Zheludkevich. Interaction effect between different constituents in silicate-containing electrolyte on PEO coatings on Mg alloy, accepted by Surface and Coatings Technology.
11) **X. Lu**, C. Blawert, D. Tolnai, T. Subroto, K.U. Kainer, M.L. Zheludkevich. 3D reconstruction of plasma electrolytic oxidation coatings on Mg alloy via synchrotron tomography, submitted for publication.
12) M. Atapour, C. Blawert, **X. Lu**, M.L. Zheludkevich. Dry sliding wear behavior of plasma electrolytic oxidation coatings on Mg alloy formed in an aluminate electrolyte, submitted for publication.

3. Publications included in this thesis

1) **X. Lu**, C. Blawert, M.L. Zheludkevich, K.U. Kainer, Insights into plasma electrolytic oxidation treatment with particle addition, Corrosion Science, 101 (2015) 201-207. - incorporated as **Paper 1** in **Chapter 5.2**.

X. Lu conceived and designed the study in discussion with C. Blawert. X. Lu carried out the experimental work. C. Blawert, M.L. Zheludkevich and K.U. Kainer gave constructive comments on data analysis. All the authors contributed to the interpretation of the results and to writing of the paper.

2) **X. Lu**, C. Blawert, Y. Huang, H. Ovri, M.L. Zheludkevich, K.U. Kainer, Plasma electrolytic oxidation coatings on Mg alloy with addition of SiO_2 particles, Electrochimica Acta, 187 (2016) 20-33. - incorporated as **Paper 2** in **Chapter 5.3**.

X. Lu conceived and designed the study in discussion with C. Blawert. X. Lu Y. Huang and H. Ovri carried out the experimental work. C. Blawert, Y. Huang, M.L. Zheludkevich and K.U. Kainer gave constructive comments on data analysis. All the authors contributed to the interpretation of the results and to writing of the paper.

3) **X. Lu**, S.P. Sah, N. Scharnagl, M. Störmer, M. Starykevich, M. Mohedano, C. Blawert, M.L. Zheludkevich, K.U. Kainer, Degradation behavior of PEO coating on AM50 magnesium alloy produced from electrolytes with clay particle addition, Surface and Coatings Technology, 269 (2015) 155-169. - incorporated as **Paper 3** in **Chapter 5.4**.

X. Lu conceived and designed the study in discussion with S.P. Sah and C. Blawert. X. Lu, M. Störmer, M. Starykevich and M. Mohedano carried out the experimental work. C. Blawert, N. Scharnagl, M.L. Zheludkevich and K.U. Kainer gave constructive comments on data analysis. All the authors contributed to the interpretation of the results and to writing of the paper.

4) **X. Lu**, C. Blawert, M. Mohedano, N. Scharnagl, M.L. Zheludkevich, K.U. Kainer, Influence of electrical parameters on particle uptake during plasma electrolytic oxidation processing of AM50 Mg alloy, Surface and Coatings Technology, 289 (2016) 179-185. - incorporated as **Paper 4** in **Chapter 5.5**.

X. Lu conceived and designed the study in discussion with C. Blawert. X. Lu carried out the experimental work. C. Blawert, M. Mohedano, N. Scharnagl, M.L. Zheludkevich and K.U. Kainer gave constructive comments on data analysis. All the authors contributed to the interpretation of the results and to writing of the paper.

5) **X. Lu**, C. Blawert, K.U. Kainer, M.L. Zheludkevich, Investigation of the formation mechanisms of plasma electrolytic oxidation coatings on Mg alloy AM50 using particles, Electrochimica Acta, 196 (2016) 680-691. - incorporated as **Paper 5** in **Chapter 5.6**.

X. Lu conceived and designed the study in discussion with C. Blawert. X. Lu carried out the experimental work. C. Blawert, K.U. Kainer and M.L. Zheludkevich gave constructive comments on data analysis. All the authors contributed to the interpretation of the results and to writing of the paper.

6) **X. Lu**, C. Blawert, D. Tolnai, T. Subroto, K.U. Kainer, M.L. Zheludkevich. 3D reconstruction of plasma electrolytic oxidation coatings on Mg alloy via synchrotron tomography, submitted for publication. - incorporated as **Paper 6** in **Chapter 5.7**.

X. Lu conceived and designed the study in discussion with C. Blawert and D. Tolnai. X. Lu and D. Tolnai carried out the experimental work. D. Tolnai, T. A. Sosro Subroto, K.U. Kainer and M.L. Zheludkevich gave constructive comments on data analysis. All the authors contributed to the interpretation of the results and to writing of the paper.

7) **X. Lu**, C. Blawert, N. Scharnagl, K.U. Kainer, Influence of incorporating Si_3N_4 particles into the oxide layer produced by plasma electrolytic oxidation on AM50 Mg alloy on coating morphology and corrosion properties, Journal of Magnesium and Alloys, 1 (2013) 267-274. - incorporated as **Paper 7** in **Chapter 5.8**.

X. Lu conceived and designed the study in discussion with C. Blawert. X. Lu carried out the experimental work. C. Blawert, N. Scharnagl and K.U. Kainer gave constructive comments on data analysis. All the authors contributed to the interpretation of the results and to writing of the paper.

8) **X. Lu**, M. Schieda, C. Blawert, K.U. Kainer, M.L. Zheludkevich. Formation of photocatalytic plasma electrolytic oxidation coatings on magnesium alloy by incorporation of TiO_2 particles, Surface and Coatings Technology, 307 (2016) 287-291.- incorporated as **Paper 8** in **Chapter 5.9**.

X. Lu conceived and designed the study in discussion with M. Schieda and C. Blawert. X. Lu and M. Schieda carried out the experimental work. C. Blawert, K.U. Kainer and M.L. Zheludkevich gave constructive comments on data analysis. All the authors contributed to the interpretation of the results and to writing of the paper.

Acknowledgement

After living and working fifty months in Geesthacht, it is a precious opportunity here to express my sincere gratitude to those who have contributed in various ways to this thesis. The thesis would never be possible without the support and encouragement of them.

First and foremost, I would like to thank my supervisors, Prof. Dr. Karl Ulrich Kainer and Prof. Dr. Mikhail Zheludkevich, who have given me the great opportunity to study and learn at such a MagIC center in Helmholtz Zentrum Geesthacht. Their great support, guidance and encouragement essentially contribute to the progress of my work. It is an honor to be Prof. Zheludkevich's first Ph.D. student in the University of Kiel. I appreciate all his contributions of time and ideas to make my study productive and stimulating. I would also like to thank Prof. Dr. Franz Faupel, Chair for Multicomponent Materials within the Faculty of Engineering at the University of Kiel, for being my second academic supervisor and for his valuable suggestions to the dissertation. I am sincerely grateful to Prof. Dr. Daniela Zander for her timely answer and kindness to be the third reviewer of this thesis.

I would like to send my sincerest thanks to my daily supervisor, Dr. Carsten Blawert. The joy and enthusiasm he has shown when working in the labs was contagious and motivational for me on the road to becoming a scientist. His patience and encouragement have been the main motivations during my Ph.D. study. Owing to his wisdom and indefatigable spirit in the pursuit of science, I have learned knowledge and gained experience in the area of PEO.

I am very grateful to Mr. Ulrich Burmester, Mr. Volker Heitmann and Mr. Gert Wiese for their professional technical assistance. Each time they were able to solve all my problems, which allowed me to easily survive in the laboratories.

I would like to thank Dr. Marta Mohedano for all her help and insightful discussions. Many thanks to Dr. Yuanding Huang, Dr. Nico Scharnagl, Dr. Chamini Mendis, Dr. Daniel Höche, Dr. Sviatlana Lamaka, Dr. Maria Serdechnova and Dr. Wolfgang Dietzel for their help in experiments and fruitful discussions on my research project. I warmly thank Dr. Henry Ovri, Dr. Mauricio Schieda and Dr. Domonkos Tolnai for their support in some novel experiments as well as the valuable help during the writing and corrections of scientific papers. My deep gratitude goes to my roommate, Dr. Silva Campos (Rosario), for sharing happiness and sorrows. Many

thanks to Anissa, Damla, and all the staffs of WZK group, for their assistance, cordial and friendly atmosphere provided during my stay.

I would like to acknowledge my Chinese Community, including HZG group (Dr. Jin Lu, Mr. Jian Gu, Dr. Jiangfeng Song, Dr. Kaixiong Hu, Dr. Delei Li, Dr. Jie Liu, Dr. Junjun Shen, Dr. Li Wang, Dr. Zhengye Zhong, Dr. Zhiyong Xie, Ms. Wenying Mi, Mr. Zhidan Liu, Dr. Jie Cheng, Mr. Ben Ma, Dr. Zhi Wang, Ms. Yiyi Lu, Dr. Feifan Wang, Ms. Yan Chen, Ms. Xun Ma, Mr. Junjie Yang, Ms. Yufen Zhang, Ms. Yuling Xu, Mr. Sihang You, Dr. Hongwei Shi, Ms. Meng Zhang, Mr. Yuantao Zhao, Mr. Di Mei), DESY group (Dr. Ge Yang, Ms. Jing Zhang, Mr. Chao Yang, Dr. Jiaguo Zhang, Dr. Yuancun Nie, Dr. Rong Gao) and all the team members of the football club in Hamburg. Not only for the help they provided, but also and more importantly for the fun they brought into my life. My sincere thanks also go to Dr. Xing Yi for accompanying me for coffee break after lunch and catching Pokemons together.

I gratefully acknowledge the funding source from China Scholarship Council (CSC) for the financial support for my PhD study in Germany.

Lastly, I would like to thank my parents for raising me up, unconditionally loving, supporting and encouraging me in every part of my life. To my Father: you are and will always be the first one I would share my sorrow, happiness, failure and success. You have appeared many times on my dreams but never talking with me. At the night after the defense, I saw you again in my dream and suddenly said something. I know this means that you are happy. To my Mother: thank you for taking care of our family for the countless days and nights. I should have accompanied you and taken all the responsibilities. Your son has grown up and is ready to start next journey. I will never let you alone any more. To my uncles, aunts, grandparents, cousins and all my friends: I am sincerely grateful to your love, encouragement and support, which motivate and give me strength to go further in my life. I am so proud of being a part of our big family. To my fiancée (Kun): Thank you for appearing, accompanying and helping me to get through the toughest time in my life. We will go through the rest of the life.